KnE Materials Science

FibEnTech21
1st International FibEnTech Congress (FibEnTech21) New opportunities for fibrous materials in the ecological transition
Volume 2022

Knowledge E
enriching | engaging | empowering

Research article

Efficient Recovery of Lignin and Hemicelluloses from Kraft Black Liquor

Manorma Sharma*, André Simões, Patrícia Alves, and Licínio M. Gando-Ferreira

University of Coimbra, CIEPQPF, Department of Chemical Engineering, Faculty of Sciences and Technology, Pólo II, Rua Sílvio Lima, 3030-790 Coimbra, Portugal

Abstract.

Black liquor (BL) from kraft pulping industries contains a large fraction of lignin and hemicelluloses and their efficient separation can open up new possibilities for integrated biorefineries. In this work, lignin and hemicelluloses were separated from BL and concentrated BL (obtained by ultrafiltration), which was performed using acid precipitation and antisolvent precipitation, respectively. For lignin precipitation, different organic acids, namely acetic, lactic and citric acid, were used and the yield and purity of the extracted lignin were compared with the lignin precipitated using inorganic acids, namely sulphuric and phosphoric acid. Among the organic acids, the highest yield of lignin (57.2%) was obtained by lactic acid, but the extract also contained the highest levels of inorganic impurities (9.2%). The extract obtained from acetic acid contained lower inorganic impurities and the lignin yield was 48.1%. The hemicellulose was extracted from BL liquor and was concentrated using the ultrafiltration process, which was started by first separating lignin (at pH 3.5, 4 and 4.5) from it. The supernatants from the lignin precipitation process were used as a source of hemicellulose and this was precipitated by using acetone as an antisolvent. The highest hemicellulose yield (54.4%) was obtained from the supernatant with the lowest lignin content and highest acetone to supernatant ratio.

Keywords: acidification, antisolvent precipitation, hemicelluloses, kraft black liquor, lignin

Corresponding Author: Manorma Sharma; email: manorma@eq.uc.pt

Dates

?????

Publishing services provided by Knowledge E

© Manorma Sharma et al. This article is distributed under the terms of the Creative Commons Attribution License, which permits unrestricted use and redistribution provided that the original author and source are credited.

Selection and Peer-review under the responsibility of the FibEnTech21 Conference Committee.

OPEN ACCESS

1. Introduction

Kraft black liquor (BL) contains inorganic (pulping chemicals) and organic (mainly lignin and hemicelluloses) components. Pulping chemicals are majorly recovered and reused while its organic part often undergoes for energy conversion process to make the pulping process economically viable. Such components, rather going for energy conversion process, require efficient separation methods as these have great potential to transform into high value-added products [1]. The most studied process for separation of lignin from BL are the precipitation by acidification and the membranes filtration [2,3]. For the acidification process commonly, sulfuric acid is considered in spite of its inorganic nature and difficulties of special handling, therefore the focus is shifting towards the use of greener acidifying agents.

The hemicelluloses are second most abundant organic component of BL, but its is challenging to recover it from BL due to less efficient recovery processes and its lower concentration in BL than lignin. So, sequential recovery of lignin from BL and hemicelluloses from the leftover of lignin recovery process was seen a better solution. Also, prior to recovery process, concentrating these organic components in lower volume of BL can lead in reduction of chemicals consumption in recovery process [4]. It can further improve the efficiency of separation processes by increasing purity or higher separation yield of organic components; also least possible imbalance of inorganic components of BL to maintain the conventional process of chemical recovery in paper industries [5–7]. In light of the aforementioned findings, we studied the separation of lignin by acidification of BL using various organic acids and compared with the precipitate obtained using inorganic acids. Further, a sequential recovery of both lignin and hemicelluloses was carried out, to exploit the full potential of BL, through the acidification and antisolvent precipitation methods. To enhance the efficiency of separation processes BL was pre-filtered by ultrafiltration (UF) membranes to concentrate the lignin and hemicelluloses in the retentate stream and this UF retentate was referred as concentrated BL.

2. Material and methods

Industrial BL—with a total dissolved solid (TDS) content of ~17%—was used as a source for lignin and hemicelluloses. The composition of BL and concentrated BL (UF retentate) is shown in Table 1. The lignin separation by acidification was performed using various acids namely sulfuric acid (SA), phosphoric acid (FA), sulfuric acid + acetic acid (SA+AA), acetic acid (AA), lactic acid (LA) and citric acid (CA). For that purpose, the pH of BL was reduced to 3 - 3.5 using sulfuric acid and sulfuric acid + acetic acid whereas it was reduced to 4 - 4.5 for other acids. The precipitated lignin was separated by centrifugation followed by three times washing with acidic water (pH ~3). The precipitates were dried at 100 °C and analyzed for organic and inorganic contents by thermogravimetric analysis at 650 °C. The lignin content was measured using UV-Vis spectroscopy by measuring the absorption at 295 nm wavelength.

As an improvement in the recovery process, hemicelluloses were separated from supernatant of lignin separation process and concentrated BL was used instead of BL. Prior to separation process, BL was prefiltered by using UF membranes (~10 kDa MWCO) for the reduction of volume upto 70%. The pre-filtration step increased the concentration of lignin and hemicelluloses in retentate stream (see table 1), which

TABLE 1: Composition of BL samples used for lignin and hemicelluloses recovery.

Sample	TDS (g/L)	*Inorganic content (%)	*Organic content (%)	Lignin conc. (g/L)	Hemicellulose conc. (g/L)
Black liquor	187 ± 1.42	48.26 ± 0.55	51.74 ± 0.55	84-92	8-13
Concentrated BL	267 ± 2.12	37.10 ± 0.16	62.89 ± 0.16	135-142	19-23

*Organic and inorganic contents comprise the composition of TDS content.

facilitated the desirable recovery of organic components with comparatively less acid consumption. First, lignin was separated from retentate using acetic acid followed by the separation of hemicellulose from lignin-lean supernatant by antisolvent precipitation using acetone (90% v/v to BL). The process of lignin and hemicellulose separation from concentrated BL is shown in Fig.1. First lignin was precipitated by at pH 3.5, 4 and 4.5 and the supernatants with different concentration of lignin were used for hemicellulose recovery. The yield of hemicellulose as function of lignin concentration in supernatant and the ratio of acetone to supernatant was analysed. The precipitate was analysed for organic and inorganic content similarly to lignin precipitates and hemicellulose content was analysed by HPLC analysis. The yield of TDS was measured as amount of precipitate separated per litre of BL whereas, the yield of lignin or hemicellulose was determined as the amount of lignin or hemicellulose extracted to the amount of lignin or hemicellulose present in BL.

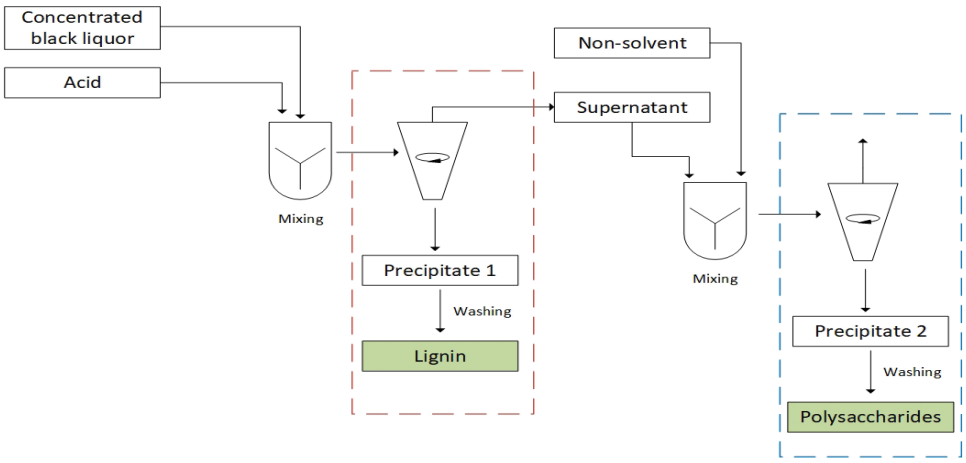

Figure 1: Schematic representation of process for separation of lignin and hemicelluloses from black liquor.

3. Results and discussion

In lignin separation process, the highest yield of separated solids (approx. 56 g/L) was obtained when a combination of sulfuric acid and acetic acid was used as acidification

agent. But the organic content of these solids where lower than the solids separated using organic acids, except for lactic acid, and phosphoric acid, see Fig. 1. In terms of purity of lignin, it was higher for the fractions with high organic content and the highest purity was obtained by acetic acid, citric acid and phosphoric acid. When the recovery performance of different organic acids was compared, the highest yield of lignin was obtained with lactic acid (~57%) however, the separated solid had the highest amount—around 10%—of inorganic impurities in it.

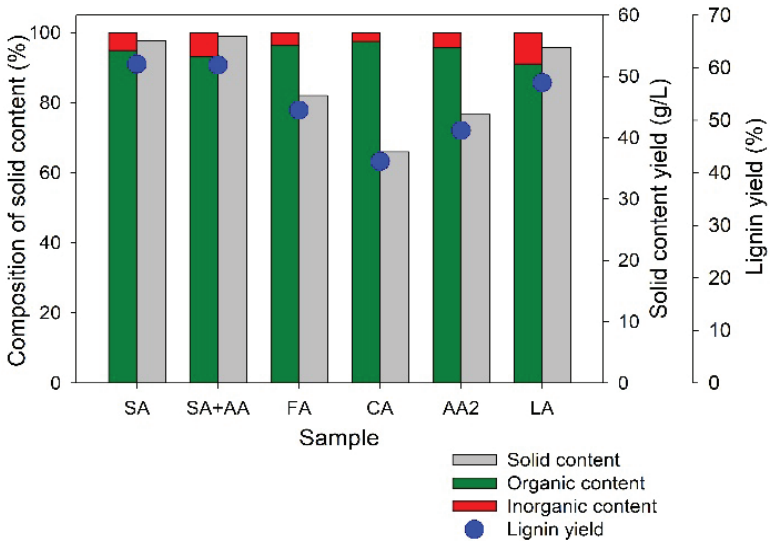

Figure 2: Composition and yield of solid content and the yield of lignin from various acids.

Further for the recovery of both lignin and hemicelluloses from concentrated BL, the acetic acid was used for first acidification step for two reasons: (a) high purity and (b) satisfactory yield of lignin among all organic acids. The highest lignin yield from concentrated BL was 32.7% at pH 4. However, this yield was ~10% lower (with the same acid and same level of pH reduction) from concentrated BL compared with yield from BL. This reduction can be due to the presence of less amount of lower molecular weight lignin in concentrated BL. As a benefit of prefiltration step, separated lignin from concentrated BL has the narrower molecular weight distribution (not shown here). Also, despite of lower yield, the total amount of lignin separated from concentrated BL was similar to the total amount separated from unfiltered BL. Further, the second precipitate, precipitated from the supernatant using acetone, contained mainly polysaccharides, particularly hemicelluloses. The organic and inorganic content of the second precipitate was with respect to lignin concentration in supernatant and acetone to supernatant ratio is shown in Fig. 3. It can be seen that the highest yield of organic content 75.8% with 24.2% inorganic content was obtained from the supernatant with lowest concentration of lignin in it and highest acetone to supernatant ratio.. As the BL came from kraft pulping

of Eucalyptus species, the major portion of hemicelluloses was composed of xylans, therefore hemicelluloses yield and purity was determined considering arabinose, xylose, uronic acids and acetic acid monomer units. The lignin and other polysaccharides mainly glucose were considered as the organic impurities in the extracted hemicellulose. The yield of hemicelluloses at different conditions is shown in Fig 4. It can be observed that the highest yield was ~50% which was also obtained from same sample having highest organic content. However, the precipitates contained some lignin and other organic impurities which still remained challenging to obtain high purity hemicelluloses.

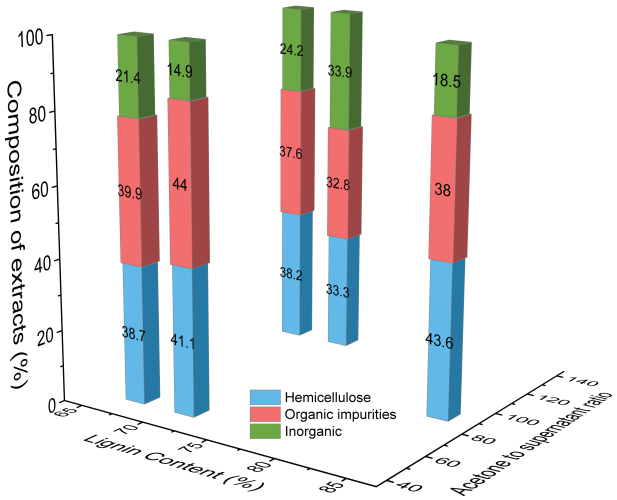

Figure 3: Composition of hemicellulose extracted from concentrated black liquor.

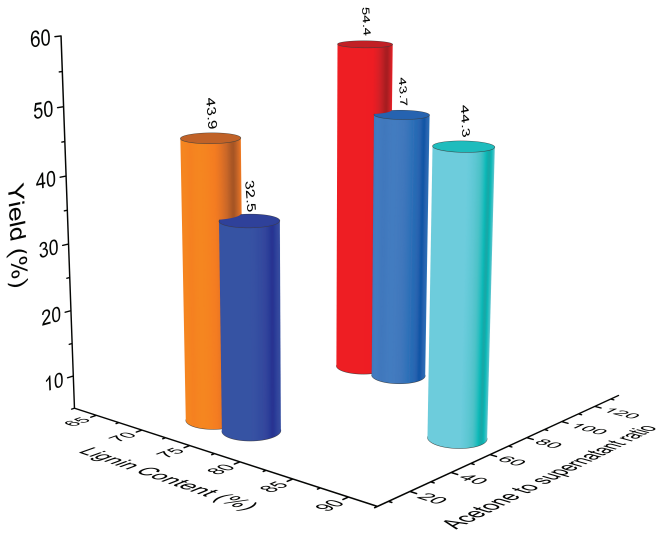

Figure 4: Yield of hemicellulose extracted from concentrated black liquor.

4. Conclusions

In this study the comparative separation of lignin from BL using organic and inorganic acids was shown and observed that the precipitation by organic acids resulted into lower yield of lignin but with higher purity. Therefore, organic acids can be considered greener alternative for separation of high purity lignin from BL. Further, it was observed that combining membrane filtration with recovery processes can lead to higher recovery with less chemical consumptions. In this sense, 35% lignin and 50% hemicelluloses were recovered from the BL concentrated using membranes filtration.

Acknowledgments

This work was carried out under the Project inpactus – innovative products and technologies from eucalyptus, Project N.º 21874 funded by Portugal 2020 through European Regional Development Fund (ERDF) in the frame of COMPETE 2020 nº246/AXIS II/2017.

References

[1] Özdenkçi K, de Blasio C, Muddassar HR et al. A novel biorefinery integration concept for lignocellulosic biomass. Energy Conversion and Management. 2017;149:974–987. https://doi.org/10.1016/j.enconman.2017.04.034

[2] Hubbe MA, Alén R, Paleologou M, Kannangara, Kihlman J. Recovery from spent alkaline pulping liquors using acidification, membrane separation, and related processing steps: A review. Bioresources. 2019;14:2300–2351.

[3] Manorma, Ferreira I, Alves P, Gil MH, Gando-Ferreira LM. Lignin separation from black liquor by mixed matrix polysulfone nanofiltration membrane filled with multiwalled carbon nanotubes, Separation and Purification Technology. 2021;260. https://doi.org/10.1016/j.seppur.2020.118231

[4] Kevlich NS, Shofner ML, Nair S. Membranes for kraft black liquor concentration and chemical recovery: Current progress, challenges, and opportunities. Separation Science and Technology. 2017;52:1070–1094. https://doi.org/10.1080/01496395.2017.1279180

[5] da Silva SHF, Gordobil O, Labidi J. Organic acids as a greener alternative for the precipitation of hardwood kraft lignins from the industrial black liquor. International Journal of Biological Macromolecules. 2020;142:583–591. https://doi.org/10.1016/j.ijbiomac.2019.09.133

[6] Al-Rudainy B, Galbe M, Schagerlöf H, Wallberg O. Antisolvent precipitation of hemicelluloses, lignosulfonates and their complexes from ultrafiltrated spent sulfite liquor (SSL). Holzforschung. 2018;72:839–850. https://doi.org/10.1515/hf-2017-0218

[7] Ren H, Omori S. Comparison of hemicelluloses isolated from soda cooking black liquor with commercial and bacterial xylan. Cellulose Chemistry and Technology. 2014;48:675–681.

KnE Materials Science

FibEnTech21
1st International FibEnTech Congress (FibEnTech21) New opportunities for fibrous materials in the ecological transition
Volume 2022

Knowledge E
enriching | engaging | empowering

Research article

Effect of Pre-Hydrolysis Reaction Conditions on Xylooligosaccharides Extraction in Eucalyptus Globulus

André E.P. Cunha*, and Rogério M. S. Simões

Department of Chemistry, Fiber Materials and Environmental Technologies (FibEnTech-UBI), University of Beira Interior, R. Marques de Ávila e Bolama, 6200-01 Covilhã, Portugal.

Abstract.

Pre-hydrolysis-kraft of *Eucalyptus globulus* by autohydrolysis (batch) and with dilute acid hydrolysis (flow-through reactor) were explored in this study, to examine the recovery of xylooligosaccharides (XOs) from the pre-hydrolysis treatment. The results of this work support the potential reuse of the hydrolysate to increase the recovery yield of added value compounds. The pH of the dilute acid hydrolysis was maintained at 3.5 with acetic acid, to mimic the conditions of the batch reactor medium (autohydrolysis). An increase of XOs recovered was evident when the pre-treatment was in the flow-through reactor instead of the batch reactor. In the latter, a high concentration of furfural was recovered, showing the influence of time in XO conversion through hydrolysis. The total yield of pulp was higher in the flow-through reactor (36.4%) in comparison with the batch system (34.5%) after kraft pulping, which was expected, given the increasing time that the hydrolysate was present in the reactor; however, the difference was small and could have been the result of precipitated compounds in the latter, so this needs further analysis.

Keywords: cellulose, *Eucalyptus globulus*, pre-hydrolysis kraft, xylooligosaccharides

Corresponding Author: André E.P. Cunha; email: aepcunha@gmail.com

Dates

?????

Publishing services provided by Knowledge E

© André E.P. Cunha et al.. This article is distributed under the terms of the Creative Commons Attribution License, which permits unrestricted use and redistribution provided that the original author and source are credited.

Selection and Peer-review under the responsibility of the FibEnTech21 Conference Committee.

OPEN ACCESS

1. Introduction.

Kraft pulping represents the major fraction of the chemical pulping industry; in this process the wood is cooked at high temperatures with an alkaline solution aiming the removal of lignin [1]. However, the harsh reaction conditions induce carbohydrate degradation, including cellulose depolymerisation and hemicelluloses extraction, together with other compounds released in the black liquor [2]. The kraft process provides a pulp mostly composed of cellulose but with significant amount of hemicelluloses suitable to paper production. However, in the last decade, a global increase in the demand of dissolving pulps established the growth of pre-hydrolysis kraft process [3]. This process is similar with kraft pulping, but it's merged with a pre-treatment with hot water or dilute acid before cooking, targeting an higher hemicellulose extraction (cellulose content

>95%), lower viscosity and higher reactivity when comparing with pulp obtained from previous method [4]. The two steps treatment allows not only a pulp production with high cellulose content but also the extraction and valorisation of compounds released in the pre-hydrolyse phase. Cellulose is the most abundant polysaccharide in the plant cell, followed by hemicellulose, being the later, predominantly composed of xylans in hardwoods [5]. Xylans are a heteropolysaccharide which can be converted into different value-added products, such as xylose and xylooligosaccharides (XOs). XOs are sugar molecules made up of several xylose units (X1-X10) with different properties based on their different degree of polymerization (DP). In recent studies [6],[7], the probiotic potential of XOs, particularly xylobiose (x2) and xylotriose (x3), was evidenced based on the digestibility of these compounds by different bacteria present in the digestion system, increasing the interest in recovering these added value compounds. Nevertheless, although xylobiose and xylotriose offer a higher probiotic potential, others XOs extracts can also be used in other applications; for example, XOs can be used to enhance beer brewing or in the formulation of health promoting cereal based food [8].

In this work, a flow-through reactor was used to study the influence of pre-hydrolysis reaction conditions on the extraction of the XOs, including xylobiose and xylotriose; the effect of the pre-hydrolysis conditions on the pulp composition was also evaluated.

2. Methods.

40 grams (oven dry base) of *Eucalyptus globulus* wood chips (3-5 mm thickness) were used for each pre-hydrolysis assay in the flow-through reactor (FTR) while 25 grams were used in the batch system. Different flow rates and reaction times were used in the flow-through system. The hydrolysate from pre-treatment was analysed by using high performance liquid chromatography (HPLC) to allow the characterization of the different compounds released during the procedure. The pre-hydrolysis solid residue was submitted to the kraft process, and the pulp obtained characterized.

3. Results

Table1 resumes the total amount of XOs, and furfural recovered in the different assays. Considering the XOs and furfural recovered and the yield loss (estimated based on the solid residues) in the PH stage, the results indicate that a significant amount of other compounds (including other sugars) were extracted in the PH stage. Regarding xylan (estimated based on xylose), *Eucalyptus globulus* chips have about 15.2% (oven dry

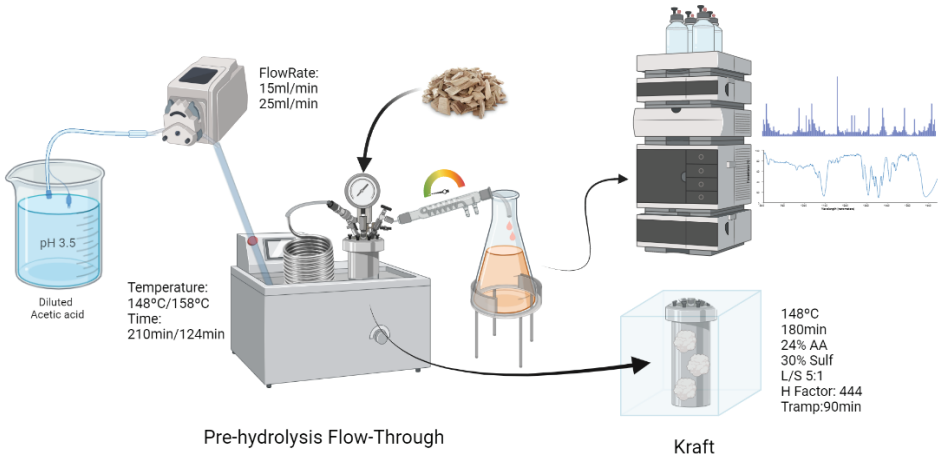

Figure 1: Flow-through reactor system and analysis.

TABLE 1: Total xylooligosaccharides removed in pre-hydrolysis (PH) (See Table 2 for PH conditions).

Total	Yield Loss, gram	XOs + furfural recovered, gram	X1 %	X2 %	X3 %	X4 %	X5 %	x6 %	>X6 %	Furfural %
FTR-1 PH	12.6 (40)	5.0	15.2	11.6	8.8	5.4	2.9	2.1	33.6	20.5
FTR-2 PH	11.4 (40)	3.7	2.9	18.5	10.5	6.6	5.4	4.4	28.0	23.7
FTR-3 PH	13.7 (40)	4.4	1.4	9.6	7.1	3.1	2.0	0.2	32.9	43.7
Batch	4.8 (25)	2.2	6.8	3.3	2.0	1.6	0.4	0.4	1.5	82.3

TABLE 2: Composition of the pulp from the PHK.

Pulp	FTR-1-PHK	FTR-2-PHK	FTR-3-PHK	Batch-PHK
PH Conditions	148°C/210min/15ml.min	148°C/210min/25ml.min	158°C/124min/25ml.min	148°C 210min
Yield, %	35.7	36.4	34.6	34.5
Compositi				
Lignin	1.3 %	1.1 %	1.2%	2.6%
Glucan	91.0 %	95.3 %	95.9%	86.9 %
X/M/G	3.0 %	2.0 %	1.5%	5.4%
Arabinose	2.2 %	1.6%	1.4%	7.7%
Kappa number	7.50	6.32	6.89	8.56
Pulp viscosity	871	800	788	1120

wood) of xylose. In this work, the FTR assays enabled to recover between 6% and 10% of the total biomass as XOs. In addition, the reaction conditions in the PH stage affect the distribution XOs and furfural; within the FTR assays, the increase in temperature provokes a very significant increase in furfural conversion (20.5% vs 43.7%). Considering

that in the batch treatment the wood extracted compounds are exposed during all the reaction time to the reaction conditions, it is expected that the furfural would be even higher, as it is the case (82.3%). In accordance with this result, the percentage of xylooligomers recovered are the lowest in the batch process. In addition, the lowest yield loss recorded for the batch assay deserves further analysis, in order to evaluate the possible contribution of precipitated compounds for these results. In resume, these results confirm the positive effect of the low retention time provided by the FTR on the xylooligosaccharides recovered.

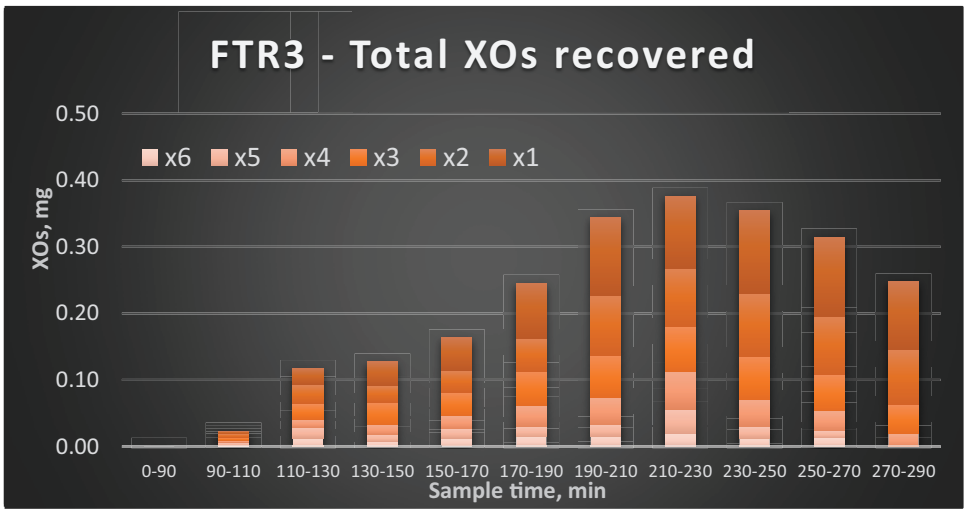

Figure 2: Time profile of the xylooligosaccharides for the FTR1 assay.

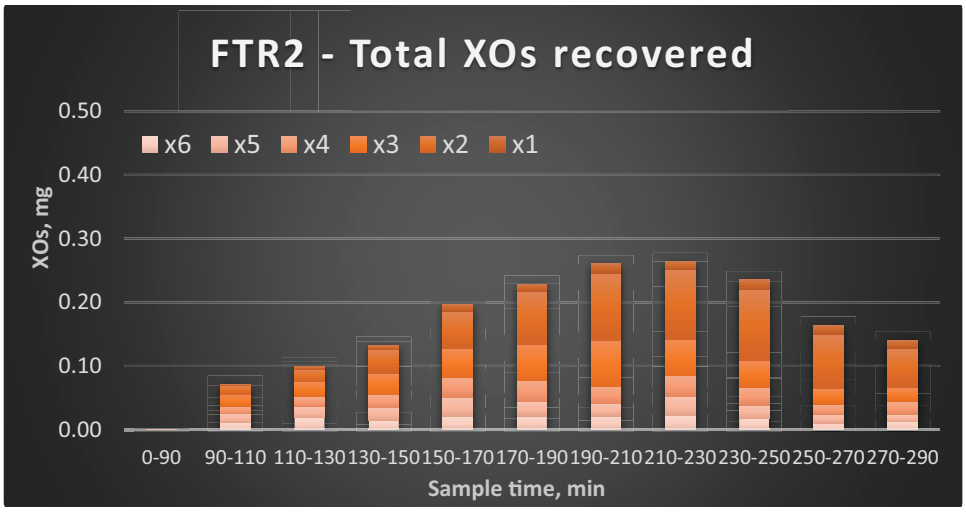

Figure 3: Time profile of the xylooligosaccharides for the FTR2 assay.

Figures 2-4 show the time profile of the the xylooligosaccharides extracted in different time intervals of the pre-hydrolysis treatments, carried out under different reaction conditions, namely different temperatures. Comparing the results show in Figure 3 and 4, it is clear the decrease of XOs recovered with increasing temperature from 148°C to

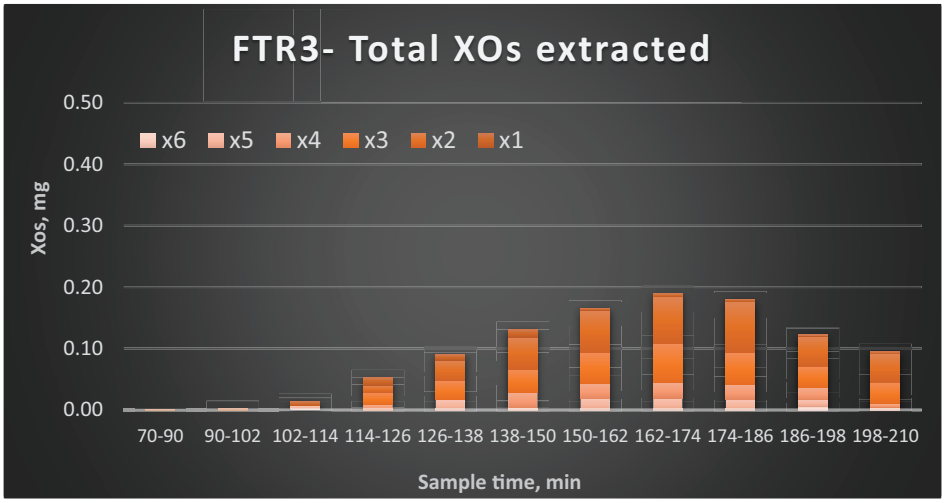

Figure 4: Time profile of the xylooligosaccharides for the FTR3 assay.

158°C. This decrease is due to the degradation of the XOs to furfural (see Table 1). On the other hand, higher recovered yield of XOs and furfural (Table 1 and Figure 2) observed for the FTR-1 essays, where the flow rate is lower deserves further investigation. In addition, the results suggest that the X2-X6 oligomers are more preserved at higher flow rate than at lower flow rate. These results are in accordance with the higher xylan depolymerisation expected at higher mean retention time inside the FTR, when operated at lower flow rate. Contrasting the FTR and batch results (Table 1) the effect of the retention time (in batch operation correspond to the pre-hydrolysis time) is drastic; the amount of X2-X6 fraction is extremely low.

Regarding the xylooligosaccharides with the highest probiotic potential (X2 and X3), the FTR system provides much better reaction conditions than the batch reactor. Within the FTR assays, that carried out with the lowest temperature and the highest flow rate (lowest retention time) provide the best results, in accordance with lowest reaction time for X2 and X3 degradation.

FTR-2 allowed a recover of 1.07 grams of X2 and X3, corresponding to 38% of the XOs recovery and 9.4% of the total biomass recovered in added value compounds. The ratio of XOs conversion is similar with results from Patricia et al [8], using acid hydrolysis of an alkaline extraction filtrate of *Eucalyptus globulus* where 41% of XOs produced were as X2 and X3 when the reaction took 30minutes at pH 1 and 100°C.

However, the flow through process allows fewer steps for XOs production and permits the control of DP by changing the flow rate and temperature.

The effect of the different pre-hydrolysis conditions on the pulp composition was also evaluated. The pulp yield for all assays is relatively low, as expected considering

the deep hemicellulose extraction. The pulps produced after PH in the FTR system exhibit higher cellulose content than the corresponding pulp produced after the PH batch treatment. From among the materials produced by FTR, those produced under higher flow rate in the FTR, and higher temperature provide the dissolving pulps with the highest cellulose content (>95%). The pulp with the highest viscosity was that submitted to the batch pre-hydrolysis. For dissolving pulps, the pulp viscosity should be adjusted to much lower values.

4. Conclusions

The highest quantity of XOs recovered was obtained for the pre-hydrolysis carried out at the

lower temperature and the lower retention time of the extracted compounds in the reactor. In addition, about 40% of the total XOs extracted are X2 and X3. The pre-hydrolysis carried out in batch mode led to much lower XOs recover. Dissolving pulp with cellulose content higher than 95% was obtained by the FTR pre-hydrolysis treatment.

References

[1] Ahlbom A. Kraft cooking of *Eucalyptus urograndis*. An investigation of the delignification kinetics of eucalyptus wood [Master ⊠ thesis]. Sweden: Chalmers University of Technology; 2018. Available from: https://hdl.handle.net/20.500.12380/255573

[2] Gladyshko Y. Extraction of hemicelluloses by acid catalyzed hydrolysis [Bachelor's thesis]. Finland: Saimia University of Applied Sciences Technology; 2011.

[3] Wu C. Dissolving pulp process as recovery source of xylooligosaccharide - A mini-review. BioResources. 2016;11(3):7917–7927.

[4] Borrega M, Sixta H. Purification of cellulosic pulp by hot water extraction. Cellulose. 2013;20(6):2803–2812. https://doi.org/10.1007/s10570-013-0086-1

[5] Neiva D, Fernandes L, Araújo S, Lourenço A, Gominho J, Simões R, Pereira H. Chemical composition and kraft pulping potential of 12 eucalypt species. Industrial Crops and Products. 2015; 66:30–30. https://doi.org/10.1016/j.indcrop.2014.12.016

[6] Singh RD, Muir J, Arora A. Concentration of xylooligosaccharides with a low degree of polymerization using membranes and their effect on bacterial fermentation. Biofuels, Bioprod. Biorefining. 2021;15(1):61–73. https://doi.org/10.1002/bbb.2145

[7] Ding XM, Li DD, Bai SP et al. Effect of dietary xylooligosaccharides on intestinal characteristics, gut microbiota, cecal short-chain fatty acids, and

plasma immune parameters of laying hens. Poultry Science. 2018;97(3):874–881. https://doi.org/10.3382/ps/pex372

[8] Henriques P, Martinho M, de L Serrano M, de Sousa APM, Alves AMB. Xylooligosaccharides production by acid hydrolysis of an alkaline extraction filtrate from *Eucalyptus globulus* bleached kraft pulp. Industrial Crops and Products. 2021;159 :1–7. https://doi.org/10.1016/j.indcrop.2020.113066

[9] Grootaert C, Verstraete W, de Wiele TV. Microbial metabolism and prebiotic potency of arabinoxylan oligosaccharides in the human intestine. Trends in Food Science and Technology. 2007;18(2):64–71. https://doi.org/10.1016/j.tifs.2006.08.004

KnE Materials Science

FibEnTech21
1st International FibEnTech Congress (FibEnTech21) New opportunities for fibrous materials in the ecological transition
Volume 2022

Knowledge E
enriching | engaging | empowering

Research article

Assessment of Autofocus Techniques for Isolated Cellulose Microfiber 3D Imaging by Digital Holography

Francisca Silva[1], Paulo Fiadeiro[2], and Elsa Fonseca[2]*

[1]University of Beira Interior, Covilhã, Portugal
[2]Fiber Materials and Environmental Technologies (FibEnTech-UBI) and University of Beira Interior, Covilhã, Portugal

Abstract.
Studying the three-dimensional structure of paper fibrous networks is an important step towards understanding the relationship between manufacturing conditions and the resulting microstructural and mechanical properties. Digital holography is a promising three-dimensional imaging technique enabling quantitative phase evaluation of micro and nano-fibres. One of the advantages of this high-resolution method is the ability to perform numerical refocusing at several depths from a single shot acquisition. In this work, the suitability of 22 focusing functions to accurately identify the positions of cellulose microfibers, using digital holography, was inspected. The best performing metrics were identified and the trade-off between metric accuracy and robustness to variable conditions and their computational complexity were discussed.

Keywords: digital holography, autofocus, cellulose microfibre, morphology, tomography

Corresponding Author: Elsa Fonseca; email: efonseca@ubi.pt

Dates
?????

Publishing services provided by Knowledge E

© Francisca Silva et al.. This article is distributed under the terms of the Creative Commons Attribution License, which permits unrestricted use and redistribution provided that the original author and source are credited.

Selection and Peer-review under the responsibility of the FibEnTech21 Conference Committee.

OPEN ACCESS

1. Introduction

Digital Holography (DH) is a powerful 3D imaging methodology that is particularly suited to microscopy applications [1]. This is achieved by encoding the wave field transmitted or scattered by an object in the form of an interference pattern with a reference beam. While in conventional imaging systems it is almost impossible to retrieve the correct focused image from a blur, with digital holography the image can be retrieved numerically at any distance from the hologram. DH also allows the reconstruction of various objects at different depths, beyond the depth of field limits of the system, through a technique called extended focus imaging [2]. Digital holographic microscopy (DHM) offers several significant advantages, such as the ability to acquire holograms quickly, availability of full amplitude, optical field phase information, and versatility of interferometric and image processing techniques [3]. Despite all the recognized advantages of this technique

over other more classic ones, there are also some disadvantages such as sensitivity to vibrations, depending on the optical setup used, existence of speckle noise due to the use of coherent light sources and the existence of reconstruction artifacts when using digital plane-wave holography in the in-line Gabor technique [4].

Getting three-dimensional and tomographic information on paper microstructures improves the understanding of the links between the manufacturing conditions and the consequent microstructural and mechanical properties of the paper fibrous networks [5]. In-line DH is characterized by its ability to image intensity and amplitude of objects with sub-micrometre resolution. Hologram reconstruction transforms also provide access to phase information and images of the spatial variations of phase changes of wavefronts in the optical field are easily created. Quantitative determination of phase changes is an integral part of in-line DHM so that, unlike the situation in conventional optical phase microscopy, a quantitative determination of the optical path through an object is easily performed. Classic interferometric phase shift measurements are capable of very high sensitivity but are often difficult to employ. The simplicity of this technique makes it of great interest to determine the extent to which accurate optical path measurements on micrometre-sized objects are possible [6]. Furthermore, the in-line configuration of DH enables highly compact setups, with digital autofocus capabilities. These features allow to overcome typical *runout* and *jitter* constraints inherent to conventional optical tomography [7]. These phenomena result from misalignments and vibrations in the signal acquisition phase due to sample rotation. The multi-view or phase reconstruction capability has the potential to allow the reduction of the number of acquisitions, making the recording process faster. It has recently proved to be possible to apply digital tomography techniques to microscopic plant fibres [7] and to single-mode optical fibres [8] with DH based on the Mach–Zehnder configuration. Also, the application of DHM to the (non-tomographic) study of cellulose nano-whisker aggregates revealed to be promising [9].

Aiming at developing a DH based microtomographic technique for isolated cellulose microfiber characterization, a set of optimization tasks are currently in process, were the selection of the most suitable autofocus technique is of critical importance. The pursued metric should be computationally simple while remaining effective and sufficiently precise for the correct localization of small objects immersed in a liquid or gel matrix medium. A special attention is devoted to sparsity metrics due to their small computational cost and potential to incorporate an advanced reconstruction procedure targeted at simultaneously reconstructing and focusing the complex object field by employing compressive sensing methods [10].

2. Material and methods

To test the selected focusing criteria, digital holograms of a set of objects including a USAF 1951 standard resolution target and two types of plant microfibers (eucalyptus and pine tree) were selected. An in-line Gabor DH setup with a He-Ne laser with $5\ mW$ and $632.8\ nm$ wavelength for sample illumination was used, as shown in Fig.1. The interference patterns were digitized by a Guppy Pro F-503 camera, having a CMOS sensor with a $2.2\ \mu m \times 2.2\ \mu m$ pixel size, using an acquisition mode with 2588×1940 pixels of resolution and 8-bit depth. Each hologram results from a pair of interference patterns, were the first is the test hologram, recorded with the sample in place, and the second is a reference hologram recorded without the sample. The first is then divided by the second to yield the so-called contrast hologram where the influence of illumination inhomogeneities and noise is minimized. To obtain the reconstructed complex object field $E_O(x, y)$, two main groups of numerical reconstruction methods can be applied, according to the distance scales involved, namely, the Rayleigh–Sommerfeld (RS) approximation, for short to intermediate propagation distances, and the Fresnel or paraxial approach, for the long propagation regime. In this case, the propagation distances are of the order of tens of millimetre, which is comparable to the recording sensor size. Therefore, the RS approximation is used in the form of an algorithm consisting of a Fourier Transform (FT) of the digital hologram, the result of which is multiplied by a transfer function, followed by an inverse FT. This is called the Angular Spectrum Method (ASM) [4] and has the advantage of keeping the pixel size independent of the reconstruction distance. After retrieving $E_O(x, y)$, the absolute amplitude $U(x, y) = |E_O(x, y)|$ and the phase $\gamma(x, y) = tan^{-1}\left[\frac{Im\{E_O(x,y)\}}{Re\{E_O(x,y)\}}\right]$ can be computed. For focus evaluation, the absolute amplitude, or alternatively, the intensity $I(x, y) = |E_O(x, y)|^2$ are more often used.

Twenty-two metrics were selected from a preliminary set of focusing metrics that performed well in phase-shifting digital holograms [2] and a study concerning sparsity metrics [11]. Furthermore, these metrics were grouped in four categories according to their mathematical similarities: group A - image statistical/spatial properties-based metrics; group B – wavelet/spectral-based metrics, group C - sparsity metrics, and group D - $l_p - norm$ based sparsity metrics. A detailed description of the focus metrics used in DH and presented herein can be found in recent works [2] [11] [12]. The first group of metrics comprises de following criteria: normalized variance (VAR), the correlation related metrics Vollath's F4 and F5 (VOLF4, VOLF5), the standard deviation correlation function (STDCORR), the differentiation based Tenengrad algorithm (TEN)

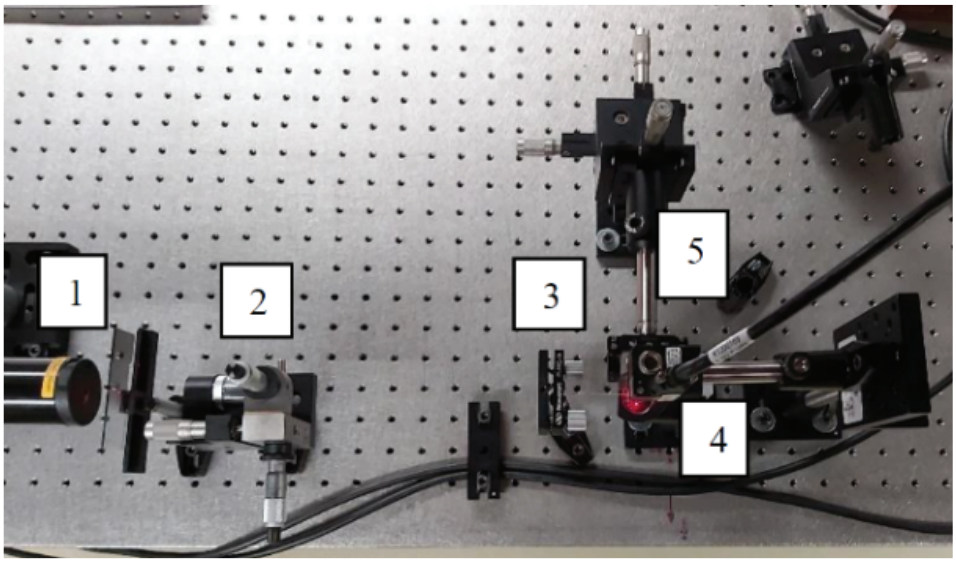

Figure 1: Top view of the inline digital holography setup with vertical camera position. **1**-He-Ne laser ($\lambda = 632.8\ nm$); **2**-Spatial Filter; **3**-Collimating lens; **4**-CMOS camera; **5**-Sample holder.

and Gaussian filter (GF), and finally the energy of the image Laplacian (LAP). The second group includes the wavelets-based focus measures include a decomposition with Daubechies wavelets (WAVRDB6) or with dyadic wavelet using smooth filtering (WAVFILT), the transform-based metrics midfrequency DCT transform metric (MDCT), and the weighted Fourier spectral focus measure (FSL). The third group includes the sparsity related criterion Gini index (GINI), Gaussian entropy (GENTR), Shannon entropy (SHENTR), modified Shannon entropy (MSE), -log (LOG), Kurtosis (KURT) and Hoyer. Finally, in the fourth group are the sparsity-based focus measures l_p (LPNORM), l_1 (L1NORM), $l_{\boxtimes}^0$ (L0EPSNORM), l_2/l_1(L2L1NORM). To compare the results of different focus measures, a set of performance criteria related to unimodality, accuracy (AM), resolution (RM) and range was used. Since only amplitude or mixed amplitude/phase holograms were tested in this study, the above-mentioned metrics, all should yield a maximum at the in-focus position z_f, after proper normalization of the focus curves. The trade-off between performance metrics and computational burthen is also inspected using the mean computation time, at a given step of the search interval, for each of the 22 focus algorithms.

3. Results and discussion

Twenty-two focusing metrics were tested on a calibration object (Fig.2A, USAF 1951 target) and several types of plant fibres from which two were selected: a sample of eucalyptus microfibers (Fig.2B) and a sample of pine tree microfibers (Fig.2C). Since

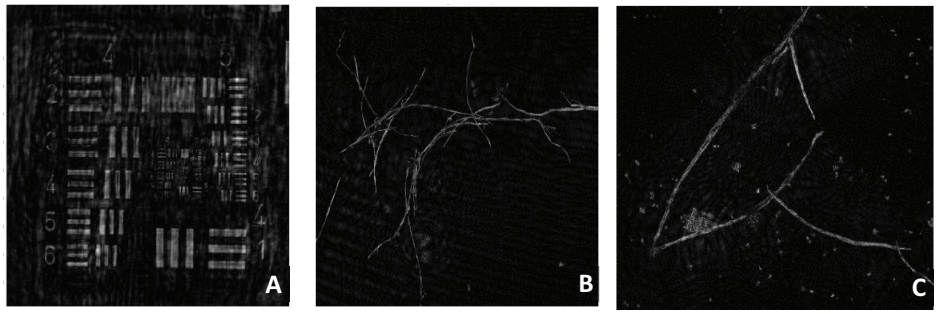

Figure 2: Cropped areas from reconstructed holograms at best focus distances obtained from the average results of the set of focus metrics. (A) USAF1951 (542 ×545 pixels); (B) Eucalyptus microfibers (1232 ×947 pixels); and (C) Pine tree microfibers (1403 ×1070 pixels). Indicated values are the tested resolutions. The displayed resolutions have been squared down to the lowest dimension.

the distances from the camera to the sample holder where small (less than 20 mm), the amplitude spectrum method was used for numerical reconstruction of the acquired holograms. Small distances are recommended for best spatial resolution. The focusing functions were applied to two main sets of data: one using the absolute value of the amplitude of the reconstructed complex fields, $U(x,y) = |E_O(x,y)|$, and another using the corresponding intensity $I(x,y) = |E_O(x,y)|^2$, as this choice has an important influence on the focus performance, as suggested in [11]. The results were compared for each sample, and the amplitude input proved itself a more reliable option, with less cases of failure to identify a peak value. The two sets of data were further divided in two cases regarding reconstruction resolution: one set comprised full-sized reconstructions with square resolutions of 1940 ×1940 pixels; and a set of interactively selected cropped reconstructions with lower resolutions (in number of pixels) about surrounding de region of interested (ROI) in each case. In the latter case, the idea was to promote a much faster focusing procedure without sacrificing the focusing performance. The second approach, not only revealed to be faster, but also more effective in most cases. Thus, the following presented results relate mainly to the case of cropped ROIs of amplitude inputs to the tested focus functions.

Table 1 was selected from a set of results to illustrate the behaviour of the tested metrics when using an object with different scales of resolution such as the USAF 1951 target, ranging from 1 to 645 pair of lines per mm. The focusing criteria outcomes for the Eucalyptus microfibers sample are also shown for comparison. Using the USAF 1951 target also allowed an appraisal of the resolution capability of the setup used in this work. Figures 3 to 5 show the behaviour of the focus metrics, grouped as previously described, for the resolution target and the two types of microfibers presented in Fig. 2. The focusing curves obtained from Eucalyptus microfibres samples showed a smoother behaviour except for the GINI index and the $l_{\boxtimes}^{0}$ norm. This is likely due to less abrupt

Table 1: Performance of focusing criteria for the cropped areas of a USAF 1951 target and Eucalyptus microfibers shown in Fig.2A and Fig.2B, respectively. The three most performing metrics values in terms of accuracy (AM- accuracy metric), fidelity to the true value and resolution (RM-resolution metric), while identifying the correct z_f, are highlighted. All values in millimetres.

Metrics	USAF 1951			Eucalyptus microfibers			Pine tree microfibers		
	AM	z_f	RM	AM	z_f	RM	AM	z_f	RM
VAR	0.050	17.67	0.121	0.044	18.36	0.099	0.104	17.73	0.148
VOLF4	0.026	17.71	0.076	0.032	18.37	0.088	0.034	17.71	0.123
VOLF5	0.037	17.66	0.127	0.053	18.36	0.102	0.100	17.75	0.147
STDCORR	0.054	17.67	0.124	0.046	18.36	0.102	0.103	17.78	0.148
TEN	0.025	17.67	0.090	0.028	18.36	0.082	0.036	17.71	0.129
GF	0.126	17.72	0.123	0.082	18.38	0.114	0.091	17.78	0.145
LAP	0.004	17.65	0.114	0.015	18.35	0.059	0.106	17.79	0.170
WAVRDB6	0.050	17.68	0.108	0.035	18.36	0.087	0.040	17.72	0.121
WAVRFILT	0.015	17.66	0.127	0.010	18.35	0.068	0.009	17.80	0.135
MDCT	0.016	17.67	0.046	0.022	18.36	0.064	0.025	17.71	0.135
FSL	0.004	17.65	0.121	0.017	18.36	0.056	0.050	17.68	0.161
GINI	0.039	17.66	0.121	0.025	18.41	0.157	0.098	17.79	0.155
GENTR	0.048	17.67	0.119	0.051	18.36	0.101	0.096	17.79	0.150
SHENTR	0.049	17.67	0.119	0.044	18.36	0.098	0.102	17.73	0.145
MSHENTR	0.044	17.67	0.118	0.043	18.36	0.100	0.103	17.79	0.149
LOG	0.054	17.70	0.121	0.048	18.36	0.103	0.000	17.77	0.147
KURT	0.050	17.70	0.122	0.051	18.36	0.101	0.103	17.73	0.147
HOYER	0.049	17.67	0.119	0.044	18.36	0.098	0.102	17.73	0.145
L0EPSNORM	0.007	17.67	0.120	0.002	18.11	0.290	0.000	18.10	0.406
LPNORM	0.050	17.70	0.121	0.046	18.36	0.101	0.103	17.79	0.149
L1NORM	0.053	17.70	0.124	0.045	18.36	0.102	0.102	17.78	0.148
L2L1NORM	0.051	17.67	0.121	0.044	18.36	0.099	0.105	17.73	0.149

refractive index changes and consequent absence of speckle noise, as shown in Fig. 2. The LAP and the FSL metrics yield the best accuracy value (AM) for all the tested samples. However, they fail to fulfil the unimodality criterion over most of the samples. Wider metrics such as the VAR, or sparsity based l_p and l_1 norms, tend to be more reliable, although they may not be so useful when the separation of different layers with individual particles or features is intended, such as in particle tracking applications.

Another important aspect of a focus metric's performance is its computational complexity. Thus, to assess the efficiency of each algorithm, the mean and standard deviation of the computation time for the calculation each focus measure for a given step of the search interval was computed. The tests were performed on the USAF 1951 reconstructions with 1940×1940 pixels. All codes were developed with MATLAB R2018b, using a Pentium core i7 – 4720HQ at 2.6 GHz (four cores. eight logical processors). It can be

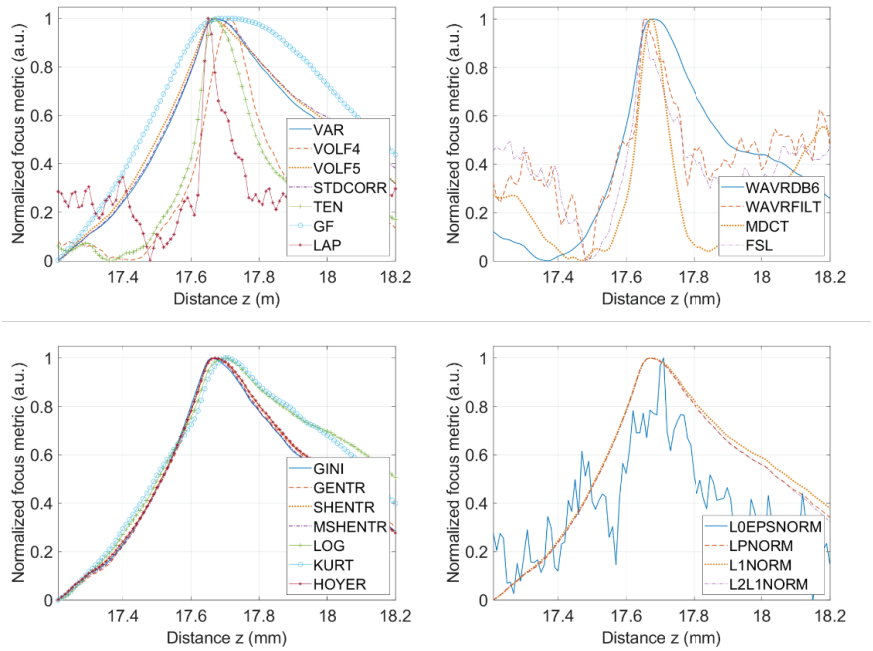

Figure 3: Comparative assessment of focusing metrics from group A to group D using the cropped area of the USAF 1951 target. All the represented metrics were able to identify a sharp peak near the true value determined by visual inspection. The search interval contained 100 points with a step size 20 µm over a range of $[17.2.\ 18.2]$ mm.

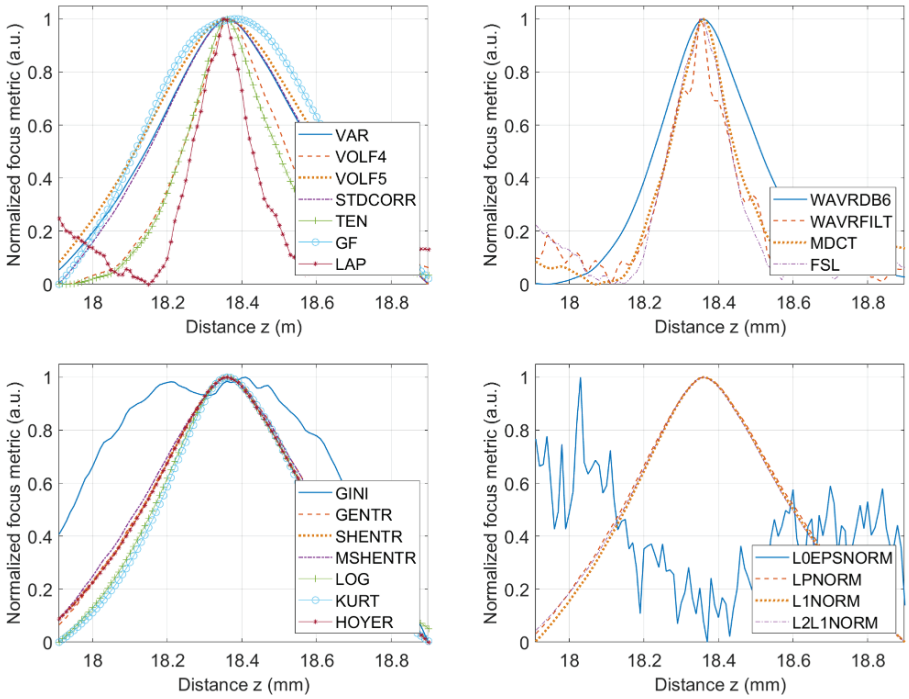

Figure 4: Comparative assessment of focusing metrics from group A to group D using the cropped area of Eucalyptus microfibers. The search interval contained 100 points. with a step size of 10 μm. over a range of [17.8.18.8] mm. All the represented metrics were able to identify a sharp peak near the true value, except for the $l_{\square}^{0}$ norm.

observed that among the most performing metrics in terms of correct identification of the

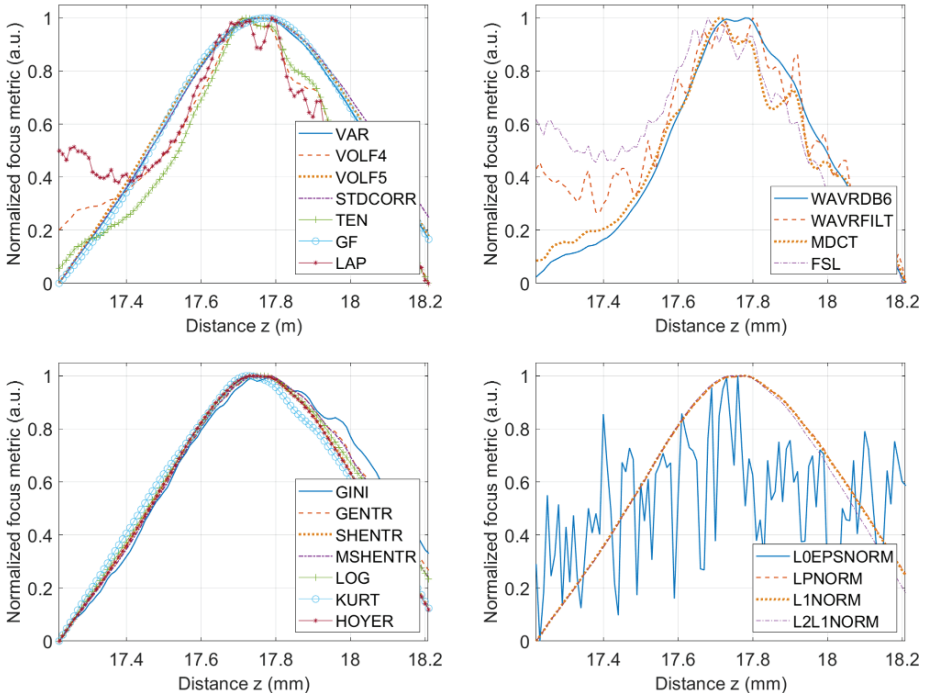

Figure 5: Focus curves comparison for the sample of Pine tree microfibers. The search interval contained 100 points. with a step size of 10 μm. over a range of [17.2.18.2] mm. As in the previous sample, all but the $l_{\square}^{0}$ norm have successfully identified the focus distance.

focus distance, the sparsity-based metrics l_p and l_1, and l_2/l_1 norms have the additional advantage of being very fast. Furthermore, as pointed out earlier, these metrics are widely employed in compressive sensing methods, thus showing a promising value in the development of a new simultaneous reconstruction/focusing method for improved resolution and noise reduction.

4. Conclusions

The present results illustrate the importance of choosing a highly performing autofocus method for in-line digital holography of plant microfibers. The nature of each tested sample has an impact in this choice. with diversity of feature size and axial location of different objects within the sample leading to stronger differences between focus criteria. For a coarse initial location of a given microstructure, faster and more robust, but less precise metrics such as the VAR, or sparsity based l_p and l_1 norms, tend to be more reliable and can be embedded in compressive sensing algorithms. The Laplacian (LAP) and the Fourier spectral focus measure (FSL) metrics yield the best accuracy value, but can only be applied to narrow range intervals, due to the lack of unimodality. More elaborated metrics, such as the dyadic wavelet using smooth filtering (WAVRFILT), help

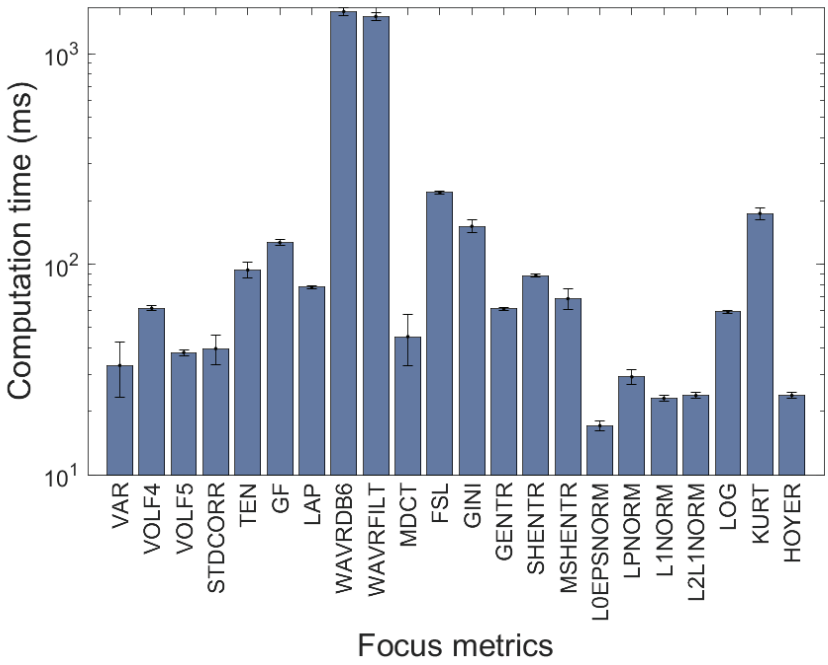

Figure 6: Mean and standard deviation of the computation time, at a given step of the search interval, for each of the 22 focus measures when applied to the reconstruction of the USAF 1951 target.

distinguishing structures buried at distinct depths, at the cost of a high computation complexity. Regarding future work, a comparative study of autofocus methods using an in-line digital holographic microscopy setup is in progress. Preliminary results show that magnified holograms are more demanding in terms of autofocus robustness to misalignment and noise issues. In this case, the statistically based metrics such as the variance (VAR) and Vollath's F5 (VOLF5), and the sparsity-based metrics such as the Gini Index (GINI) have shown better performance, so far.

References

[1] Hong XYJ, Liu C, Kim MK. Review of digital holographic microscopy for three-dimensional profiling and tracking. Optical Engineering, 2014, 53.11:112306-1.

[2] Fonseca ES, Fiadeiro PT, Pereira M, Pinheiro A. Comparative analysis of autofocus functions in digital in-line phase-shifting holography. Applied Optics, 2016, 55.27: 7663-7674.

[3] Kim MK. Applications of digital holography in biomedical microscopy. Journal of the Optical Society of Korea, 2010, 14.2: 77-89.

[4] Ting-Chung O, Jung-Poon L. Introduction to modern digital holography. UK: Cambridge University Press; 2014.

[5] Marulier C, Dumont P, Orgéas L, Roscoat SR. Towards 3D analysis of pulp fibre networks at the fibre and bond levels. Nordic Pulp and Paper Research Journal, 2012, 27.2: 245-255.

[6] Chhaniwal V, Singh AS. Leitgeb RA, Javidi B, Anand A. Quantitative phase-contrast imaging with compact digital holographic microscope employing Lloyd's mirror. Optics letters, 2012, 37.24: 5127-5129.

[7] Malek M, Khelfa H, Picart P, Mounier D, Poilâne C. Microtomography imaging of an isolated plant fiber: A digital holographic approach. Applied Optics, 2016, 55.3:111-121.

[8] Ma X, Xiao W, Pan F. Reconstruction method for samples with refractive index discontinuities in optical diffraction tomography. Optics and Lasers in Engineering, 2017, 94: 58-62.

[9] Wahba H, Sjödahl M, Gren P, Olsson E. High resolution digital holographic microscopy for the study of aggregated natural cellulose nanowhisker fibers. Optics and Lasers in Engineering, 2015, 73: 69-74.

[10] Zhang Y, Huang Z, Jin S, Cao L. Autofocusing of in-line holography based on compressive sensing. Optics and Lasers in Engineering. 2021, 146. 106678-1.

[11] Xin F, Healy J, Hennelly B. Investigation of sparsity metrics for autofocusing in digital holographic microscopy. Optical Engineering, 2017, 56.5: 053112-1.

[12] Mohamed S, Bouamama L, Bahloul D, Picart P. Quality assessment of refocus criteria for particle imaging in digital off-axis holography. Applied Optics, 2017, 56.13: 158-166.

KnE Materials Science

FibEnTech21
1st International FibEnTech Congress (FibEnTech21) New opportunities for fibrous materials in the ecological transition
Volume 2022

Knowledge E
enriching | engaging | empowering

Research article

E. Globulus Vessel and Fibre Chemical Analysis

Álvaro Vaz[1]*, João Coelho[1], Vera Costa[1], Ana Marques[2], Thaddeus Maloney[3], Phiri Josphat[3], Paula Pinto[4], Ricardo Oliveira[4], Rogério Simões[1], and António M. Sousa[2]

[1]FibEnTech, Chemistry Department, University of Beira Interior, R. Marquês de Ávila e Bolama, 6201-001 Covilhã, Portugal.
[2]Department of Chemical Engineering, IST, University of Lisbon, Av. Rovisco Pais, 1, 1049-001 Lisboa, Portugal.
[3]Department of Bioproducts and Biosystems, Aalto University, P.O. Box 11000 (Otakaari 1B), FI-00076 Aalto, Finland.
[4]RAIZ – Forest and Paper Research Institute, Quinta de S. Francisco, 3800-783 Eixo, Aveiro, Portugal.

Abstract.
Hardwood species have a complex cellular structure consisting of fibres, vessel elements and parenchyma cells with different chemical compositions. However, the presence of vessels with significant dimensions in their structure is a recurrent problem in the operation of industrial UWF paper printing. Since the 1980s, vessel picking and ink refusal are problems that paper professionals have tried to solve, but solutions for these have not yet been fully found. If vessels are concentrated in a stream, they can be pre-treated (e.g., by mechanical refining) and reincorporated into the pulp. Other strategies aim at vessel enzymatic and/or chemical passivation and sheet surface chemical treatment, altering the vessel adhesion to the fibre network. This requires vessel concentration at laboratorial level for proper chemical studies, such as FE-SEM, μ-XPS, TOF-SIMS and μFTIR. The main objective of our experimental study was to examine bleached kraft pulp *E. globulus* vessel and fibre composition. For this we performed EDX and μ-FTIR analysis on both fibre and vessel elements, and obtained the carbohydrate composition, the total acids content, the hexenuronic acids content and the zeta potential.

Keywords: *E. globulus*, vessel, EDX, μ-FTIR, sugar content, zeta potential

Corresponding Author: Álvaro Vaz; email: avaz@ubi.pt

Dates
?????

Publishing services provided by Knowledge E

© Álvaro Vaz et al.. This article is distributed under the terms of the Creative Commons Attribution License, which permits unrestricted use and redistribution provided that the original author and source are credited.

Selection and Peer-review under the responsibility of the FibEnTech21 Conference Committee.

OPEN ACCESS

1. Introduction

Vessels represent an important percentage of the volume of eucalyptus wood, 10 to 30%, corresponding to 3 to 5% weight [1]. Vessel elements are weakly bonded to fibres and fines in the paper structure, particularly on its surface. Morphologically, their length can vary between 200 and 600 μm, their width can be greater than 500 μm and the width/length ratio can be between 1:1 and 1:3 [2, 3]. Vessels specific characteristics and their behaviour in the uncoated wood free (UWF) paper production process remains poorly understood [4]. Some of the main problems associated with vessel elements

arise when UWF papers are subjected to offset printing, such as vessel picking and ink refusal. The vessel picking phenomenon manifests itself as some of the of hardwoods vessel elements detachment from the paper surface due to their weak bonding and to the printing ink high viscosity [5]. The ink refusal phenomenon is characterized by white spots in the printing areas; in this case, the vessel is present on the paper surface, but the ink did not adhere to it due to its low surface energy [6]. Preventing problems related to vessel picking and ink refusal during papermaking can be achieved through various operations, namely with pulp suspension refining, paper surface sizing, vessel elements fractionation and vessel surface passivation [7]. Any of the proposed options entails production costs and must be weighed against the obtained benefits. Pulp stock refining has been investigated with the intention of minimizing vessel related problems, but with the negative effect of over refining the pulp for printing papers [8]. In addition to the costs inherent to this operation, the reduction in drainage and the loss of porosity, specific volume, opacity, and dimensional stability are also documented. Pulp refining promotes vessel fragmentation and increases the fibre-vessel cohesion resulting in a greater adhesion to the paper surface and a reduction of vessel picking. Starch sizing is another operation that has been investigated to reduce problems associated with vessels. It is proven that a greater amount of starch on the paper surface promotes vessels adhesion, however with a loss in opacity, in addition to obtaining a paper with greater rigidity. The use of modified starches in the paper surface sizing as well as treatment with carboxymethyl cellulose showed positive results in the vessel picking problems [9]. However, it should be noted that vessels detachment from the paper surface in the sizing operation is also a frequent problem in terms of contamination of the sizing bath. The use of strength agents can have a positive effect in preventing vessel picking, nonetheless, high dosages are required to have a significant impact. The fractionation of the vessels can be carried out using hydrocyclones, flotation followed by sieving, sieving with different sized meshes or flocculation of fibres with subsequent separation of the vessels. Any of these solutions allows fractions rich in vessels to be obtained, nevertheless they are not 100% effective [10,8,11,12]. However, Orblin *et al*. [4] propose a new method using a Britt Jar with greater efficiency in separating vessels. Fractions rich in vessels can be previously subjected to physical (refining) or chemical (passivation) treatments and be later added to the furnish. Adequate refining of the vessels and their reincorporation into the stock seems to be an interesting alternative to approach the problem while avoiding losing a substantial amount of material. Likewise, the chemical modification of the vessels surface, namely their ionic charge and hydrophobicity, is

one of the most attractive and promising alternatives that has not been yet extensively investigated.

2. Material and methods

2.1. Fibres and vessels quantification and morphological characterization

The methodology for the primary fibre and vessel content quantification was based on the use of the Morfi Analyzer - version LB-01 (2002), a prototype implemented by Techpap. The system consists of a measuring cell (connected to a PC), a hydraulic system (pump, tank, solenoid valves) and an electrical system. The measuring cell analyses the suspension at two consistencies: 30 mg / L and 300 mg / L. The optical resolution is 10 µm, but the working resolution reaches 4 µm thanks to specific grey image analysis treatments.

Optical microscopy was also used to estimate vessels length, width, and aspect-ratio, to compare with the values provided by Morfi. A Micros microscope was used, coupled with a MicroVisible 4.0 image capture and data treatment software.

2.2. Separation methodology and optimization

Primary dimension separation was carried out using a Bauer-McNett equipment, fitted with U.S. mesh # 30, # 50 and # 200 screens. The #30 screen retained long vessels, while #200 screen let fines pass.

Laboratory prototypes were developed to apply the Jacquelin method, in which the effect of continuous rotation promotes the consolidation of flakes and the maintenance of suspended vessels. According to Soszynski [13] and the 1972 Jacquelin's patent [14], the estimated value for the peripheral rotation speed would be 30 m/min for hardwoods. Two systems were used to cause this rotational acceleration: a rotary evaporator and a stirring rotor. The rotary evaporator allowed a closer approximation to the scheme idealized by Jacquelin, but only with about one tenth of the required peripheral speed, compensated with a prolonged period of rotating action (about 24 hours). The stirring rotor allowed speed values closer to those suggested in the literature but moving away from the proposed system.

A Britt Dynamic Drainage Jar was also set up according to the method generically described by Orblin *et al.* [15], adapted with a recirculation system. A two-step system

was developed, initially for vessels accumulation within the jar and afterwards for vessels extraction.

2.3. Analytical methods

Microscopy observations were performed UBI Optics Center using a Hitachi S-2700 scanning electron microscope (SEM) operated at 20 kV. Images were formed through secondary electrons. All of the samples were previously gold sputtered by cathodic spraying (Quorum Q150R ES). Elemental analysis of the samples was performed using Energy-dispersive X-ray spectroscopy (EDX) using the same SEM equipmentto estimate silica, carbon and oxygen contents. The most relevant result is the O/C ratio, which may indicate the presence of different functional groups.

Fibre and vessel analysis of *E. globulus* were performed using a Perkin-Elmer μ-FTIR from the Chemical Engineering Department of Instituto Superior Técnico.

The samples neutral carbohydrate composition was determined by ionic chromatography after quantitative saccharification upon acid hydrolysis according to an adaptation of the Tappi T222 om-88 proceeding guidelines for the determination acid-insoluble lignin in wood and pulp. The samples total acidic groups content was determined through a conductimetric titration method, adapted from the standard SCAN-CM 65:02. Hexenuronic acid groups content was determined using a colorimetric method proposed by Chai *et al*. [16]. The Zeta potential of fibre rich and vessel rich aqueous suspensions was measured using a Mütek SZP-06 System Zeta Potential at a 0.2 % consistency. KCl was added to the suspensions to increase the conductivity of the samples.

3. Results and discussion

Fibre and vessel quantification results for *E. globulus* bleached kraft pulp using Morfi Analyser are compiled in Table 1, namely fibres number per gram, vessels number per gram and fibre/vessel ratio, and in Table 2 vessels and fines area percentage. Fibre and vessel microscopic study is shown in Table 3, specifically length (L), width (D), and aspect ratio (L/D). These data are fundamental for any separation process design.

Table 1: *E. globulus* fibre and vessel quantification (Morfi Analyser).

Fibre number (10^6fibers/g)	30.3 ± 0.2
Vessel number (10^6vessels/g)	0.147 ± 0.06
Fibre-Vessel ratio	206.1 ± 9.6

Table 2: *E. globulus* vessel and fines area (Morfi Analyser).

Vessels (%)	0.32 ± 0.01
Fines (%)	6.6 ± 0.8

Table 3: Fibre and vessel morphology by optical microscopy.

	L (µm)	D (µm)	L/D
Fibres	1072 ± 137	15,9 ± 2,6	67 ± 20
Vessels	300 ± 32	154 ± 18	1,95 ± 0,44

Attending to the global purpose of our work a proper vessels and fibres chemical composition analysis is fundamental. So, a proportion of 206 fibres per vessel requires a vessel concentration process. The use of a three stage Bauer-McNett was fundamental for fines and parenchyma removal but was not enough to attain the required vessel concentration. Just a 3% increase in vessel content was attained at this stage. The Jacquelin method was essayed, but it was not the most viable process for a scale-up of vessels removal. As described earlier, a Britt Jar was used to achieve a size exclusion separation in two steps; the first phase retained the vessels and allowed fibres to pass through; the second phase with wider screen holes let vessels pass through and retained long fibres. The results of the first phase may be observed in Fig. 1-a), while in the second phase it was possible to accumulate a practically pure vessel fraction.

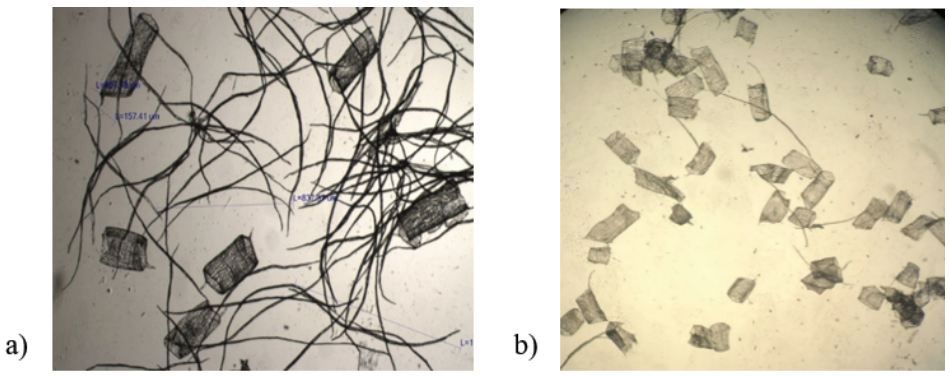

Figure 1: Vessel separation: a) 1st phase enrichment; b) 2nd phase enrichment.

SEM imaging was performed on the surface of a sheet produced from the vessel rich fraction. Fig. 2 depicts two noticeable vessels amongst the fibres The EDX results are presented in Table 4, where the most relevant result is the higher O/C ratio for *E. globulus* fibres (0.9) comparatively to vessels (0.7), suggesting higher lignin and extractives content for the latter.

Fig. 3 shows the µ-FTIR spectra obtained for E. globulus fibres and vessels. The spectra obtained from vessels and fibres are quite similar, but there is mainly a noticeable

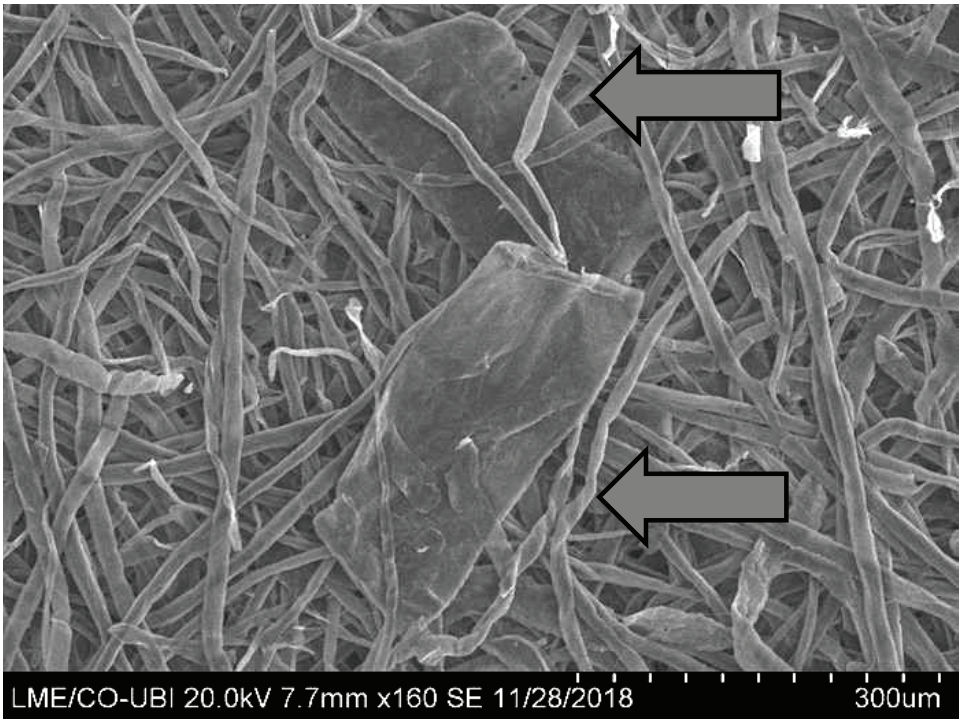

Figure 2: SEM image of a vessel rich sheet surface (the arrows indicate vessels).

Table 4: EDX *E. globulus* elemental composition.

Elemental Composition (%)	Fibre	Vessel
C	48.2	54.6
O	43.4	37.9
O/C Ratio	0.90	0.70

Table 5: Chemical Analysis and Zeta Potential

	XMG (%) *	Hexenuronic Acid (µmol/g)	Total Acids (µmol/g)	Zeta Potential (mV)
Fibres	18.8	7	133	-20.8
Vessels	25.4	12	149	-9.8

* XMG: Xylose, Mannose and Galactose content.

difference in the peaks relative to the CH bonds and to the COC ether group. Vessel spectra have a slightly higher peak at ca. 900 cm^{-1} (CH stretch and COC stretch), 1105 cm^{-1} (COC strain) and 1160 cm^{-1} (aromatic C-H strain in plane, asymmetric C-C stretch). The presence of higher hydrocarbon concentration may be related to the higher vessel hydrophobicity [4]. These results seem to be coherent with the data obtained with EDX.

Table 5 compiles the values for the hemicellulose content (percentage of Xylose, Mannose and Galactose, referred as XMG), hexenuronic and total acids contents (µmol/g) and the pulp suspension Zeta potential (mV). Zeta potential values suggest that fibres are more anionic than vessels. XMG content in vessels is 35% higher than in fibres,

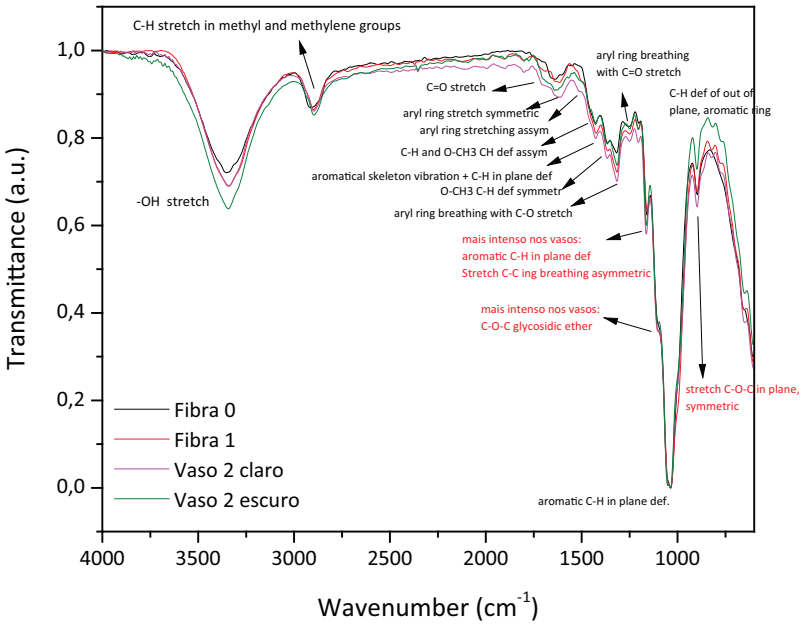

Figure 3: *E. globulus* vessel and fibre spectra obtained by μ-FTIR.

thus having a higher hemicellulose percentage. Concerning the total acids content, this value is also higher in vessels (12%), difference even more evident for the hexenuronic acid content (71%). Considering the higher hexenuronic and total acids content in the vessels it would be expected a higher zeta potential for the vessel, however, this is not the case, and the issue is currently under investigation.

4. Conclusions

The main results compiled in this paper are:

1. **Separation methods:** Size exclusion methodology in two steps, preceded by fines removal with Bauer-McNett has proven to be an effective method for obtaining a vessel rich fraction.
2. **EDX:** Lower O/C ratio observed in vessels suggests a higher lignin and extractives content.
3. **μ-FTIR:** The spectra obtained from the vessels and fibres are in general similar, but there is a noticeable difference in the peaks relative to the CH bonds and to the COC ether group. The possible presence of higher hydrocarbon concentration may be related to the higher hydrophobicity shown by vessels.

4. **Chemical Analysis:** Vessels have a higher hemicellulose content and a higher total and hexenuronic acids content, nevertheless being less anionic than fibres in the zeta potential measurement, which requires further investigation.

This work was carried out under the Project inpactus – innovative products and technologies from eucalyptus, Project N.º 21874 funded by Portugal 2020 through European Regional Development Fund (ERDF) in the frame of COMPETE 2020 nº246/AXIS II/2017.

References

[1] Dadswell H, Wardrop A. Some aspects of wood anatomy in relation to pulping quality and to tree breeding. Appita. 1960;13(5):161-173.

[2] Alén R. Papermaking science and technology. Stenius P, Pakarinen H, editors. Helsinki: FapetOy; 2000.

[3] Chen F, Evans R. A robust approach for vessel identification and quantification in eucalypt pulps woods. Appita. 2005;58(6):442-447.

[4] Orblin E, Lindström N, Fardim P. Probing the chemical and surface chemical modification of vessel cell walls during bleaching of eucalyptus pulp. Holzforschung. 2012;66(8):945-950.

[5] Ohsawa J. Vessel picking in printing papers. Paper presented at: Tropical Wood Pulp Symposium; 1988 Jun 21-23; Singapore.

[6] Jopson N. Coping with hardwood vessels. Pulp & Paper International. 2005;47(11):36-37.

[7] Chen C, Liu H-B. The causes and solutions of the vessel picking. China Pulp and Paper. 2013;32(12):66-69.

[8] Heintze H, Shallhorn P. Hardwood vessel picking and manufacturing process. Pulp and Paper Canada. 1995;96(11):28-30.

[9] Rakkolainen M, Kontturi E, Isogai A, Enomae T, Blomstedt M, Vuorinen T. Carboxymethyl cellulose treatment as a method to inhibit vessel picking tendency in printing of eucalyptus pulp sheets. Industrial & Engineering Chemistry Research. 2009;48(4):1887–1892.

[10] Hardell H, Leary G, Stoll M, Westermark U. Variations in lignin structure in defined morphological parts of spruce. Svensk Papperstidning. 1980;83(2):44-49.

[11] Panula-Ontto S, Fuhrmann A, Kariniemi M, Särkilahti A. Evaluation of vessel picking tendency in printing. Paper presented at ICEP International Colloquium on Eucalyptus Pulp; 2007 Mar 4-7; Belo Horizonte, Brazil.

[12] Backfolk K, Henricson K, Kajanto I, Karjalainen M, Niinimäki J, Rousu P. Wheat straw pulp fractionation part 1. The effect of cells, vessels, and fines on paper properties. Cellulose Chemistry and Technology. 2013;47(5):443-453.

[13] Soszynski R. The formation and properties of coherent flocs in fibre suspension [Ph.D. thesis]. University of British Columbia, Vancouver, Canada; 1987.

[14] Jacquelin G. Methods of treating suspensions of fibres to form fibrous aggregates. United States patent. US 3, 679, 542. 1972 July 25.

[15] Orblin E, Eta V, Fardim P. Surface chemistry of vessel elements by FE-SEM, μ-XPS and ToF-SIMS. Holzforschung. 2011;65:681-688.

[16] Chai XS, Zhu JY, Li J. Simple and rapid method to determine hexeneuronic acid groups in chemical pulps. Paper presented at: 10^{th} International Symposium on Wood and Pulping Chemistry; 1999 June 7-10; Yokohama, Japan.

KnE Materials Science

FibEnTech21
1st International FibEnTech Congress (FibEnTech21) New opportunities for fibrous materials in the ecological transition
Volume 2022

Knowledge E
enriching | engaging | empowering

Research article

Development of Sustainable Cellulose-Based Tissue Materials Using an Innovative Experimental and Computational Methodology

Flávia P. Morais[1]*, Ana M.5M.S. Carta[2], Maria E. Amaral[1], and Joana M.R. Curto[1,3]

[1]Fibre Materials and Environmental Technologies (FibEnTech-UBI), University of Beira Interior, R. Marquês de Ávila e Bolama, 6201-001 Covilhã, Portugal
[2]Forest and Paper Research Institute (RAIZ), R. José Estevão, 3800-783 Eixo, Aveiro, Portugal
[3]Chemical Process Engineering and Forest Products Research Centre (CIEPQPF), University of Coimbra, R. Sílvio Lima, Polo II, 3004-531 Coimbra, Portugal

Abstract.
In recent years, the tissue industry has been exposed to several challenges related to the growing demand for high-quality materials and sustainability. An approach that combined experimental and computational planning was implemented and presented in this work. For this purpose, a simulator that established relationships between the key fibre properties, the process steps that modify them, and the functional properties, named the *SimTissue*, was developed and validated. Different scenarios and a summary of the *SimTissue* research strategy are presented. The experimental planning design consisted of examining the influence of refining, enzymatic treatment, and incorporation of additives such as micro / nanofibrillated cellulose and biopolymers. The correlations between these tissue process inputs, and the softness, strength and absorption properties were established using the *SimTissue*. Overall, the *SimTissue* predicted and optimized several case studies for the management and optimization of sustainability formulations.

Keywords: 3D computational simulation, cellulose-based materials, furnish optimization, tissue materials

Corresponding Author: Flávia P. Morais; email: flavia.morais@ubi.pt

Dates
?????

Publishing services provided by Knowledge E

© Flávia P. Morais et al. This article is distributed under the terms of the Creative Commons Attribution License, which permits unrestricted use and redistribution provided that the original author and source are credited.

Selection and Peer-review under the responsibility of the FibEnTech21 Conference Committee.

OPEN ACCESS

1. Introduction

Sustainable cellulose-based fibrous materials, such as tissue papers, are designed for personal hygiene and utility purposes. Examples of tissue papers include toilet papers, towel papers, napkins, facial tissue papers, among others. These materials are recognized for their creped and embossed structures, with low basis weight, and high porosity. Their key properties include bulk, softness, strength, and absorption, whose contribution and importance differ and depend on the type of final product [1]. Significant global growth in this sector is projected into the next decade, also related to the current outbreak of COVID-19. Consumption of tissue materials was estimated to grow by

around 55% in Eastern Europe and 45% in Western Europe between 2012-2022 [2]. The tissue industry is exposed to several challenges related to the growing demand for sustainable products and furnish, namely the raw materials, process operations steps, and additives incorporation [1]. A commitment to sustainable development is necessary to guide process decisions, as well as to search for simultaneous strategies of economic prosperity, environmental responsibility, and social equity [3]. Raw materials, such as cellulose fibre pulp, are the main factor in tissue paper manufacture, accounting for 45% to 59% of the total manufacturing cost [4]. Therefore, finding strategies to optimize the use of these raw materials on the final product and offset the cost-effectiveness offers substantial opportunities to drive consumer demand for optimized tissue products with innovative functionality and added value.

Eucalyptus fibre pulps are traditionally used in tissue production because of their ability to provide formation and softness to the materials, while softwood fibre pulps are used to ensure strength and paper machine runnability [1]. Eucalyptus fibres present the potential to be optimized to improve their mechanical properties while maintaining existing benefits. A more recent example is the extended impregnation cooking process which has shown the potential to increase tensile strength, reduce refining energy through its physical and chemical properties, increase pulp production yield, with higher product quality, lower consumption of chemical products in cooking, and cost reduction [5]. In addition to these strategies in the pulping process development, fibre modification strategies along the process steps have also been extensively investigated in recent years [1,4,6-12]. Maximizing the *Eucalyptus globulus* fibres incorporation, and the total or partial replacement of softwood pulps consists of a challenge since the required adjustments represent consequences on the runnability of the paper machine and converting lines. Obtaining tissue products with the best combination of fibres, and maximization of *Eucalyptus globulus* fibres, suggests knowledge of the different pulps on the market and the consequences on the finished product properties [6,7]. Due to the fibres' properties, such as high coarseness, the eucalyptus fibre's structure can be modified through enzymatic treatment processes [10], refining, and incorporation of additives such as micro/nanofibrillated cellulose (MFC/NFC) and biopolymers [11,12], minimizing the influence on the strength and stiffness properties that the structure needs for the process operations [13,14].

This entire tissue furnish optimization process requires extensive research and methodologies to overcome the issues, which involves the design and analysis of laboratory and computational experiences. Computational methods for integrating all important variables for analysing the behaviour and modelling of fibre materials, process

modification steps, and functional properties have been increasingly investigated in recent decades [8,9,14-19]. Computational tools allow us to significantly reduce experimental work in the development and optimization of new materials, to present a better synergy between experimental tests and simulation of specific properties. The development of advanced computational tools with predictive capability for furnish is a major milestone soon as it allows us to estimate which raw materials are most promising for a particular tissue product and which process operations allow us to obtain tissue with desired and optimized properties [20].

Therefore, an innovative design approach was implemented to create product differentiation. To develop and optimize these premium materials, we designed a simulator that allows us to compare various scenarios of furnish formulations, the *SimTissue*. This simulator establishes relationships between key fibre properties, the fibre modification process steps, and the tissue structural and functional properties. In this work, we present different scenarios and a summary of all the research that is based on the development of *SimTissue* for the management and optimization of sustainable furnish materials, using experimental and computational methodology approaches.

2. Material and methods

To implement the computational studies, initially, a characterization of the fibre dimensions in the paper structure was carried out, in the three dimensions, through the development of methodologies using SEM image analysis and advanced computational tools for fibre and structure modelling [8,9]. The experimental planning also consisted of the characterization and selection of different cellulosic pulps, obtained from hardwood (HW) and softwood (SW) species and different pulping processes of industrial interest [6,7]. The effect of fibre modification was also investigated, either by mechanical (refining) process, either by enzymatic treatment, or a combination of both [10], and the incorporation of additives such as MFC/NFC and commercial biopolymer (CBA) [11,12]. All experimental conditions used can be found in our referenced and cited publications. The properties of bulk (ISO 12625-3), softness (using Tissue Softness Analyzer (TSA Emtec) equipment), tensile strength index (ISO 12625-4), water absorption capacity (ISO 12625-8 adaptation), and capillary rise (ISO 8787 adaptation) were evaluated on laboratory structures of 20 g/m^2 (ISO 5269-1 adaptation). This was a proposed methodology to mimic the tissue-based sheets. The relationships between these properties were established, using different innovative computational tools, such as Lasso regression, robust multi-linear regressions (MLR), artificial neural networks

(ANN), among others, and using simulation and experimental data, to obtain predictive capacity. Then, the structures were 3D computationally simulated, to calibrate the tissue model and validate its predictive character [8,9,15,16]. This entire process allowed the computational implementation of the *SimTissue* through the calculation engine algorithm programming, database, and user interface integration, to be used in specific cases to support furnish's industrial management.

3. Results and discussion

For the *SimTissue* development, a methodology that combines an experimental and computational approach was designed (Figure 1). *SimTissue* establishes relationships between input variables of fibre properties and output variables of tissue functional properties. Through experimental and computational data, *SimTissue* quantifies the changes that occur due to the use of different pulps and process operations of tissue paper production. The validation of the final end-use properties' prediction was carried out with experimental and simulated structures, to develop this simulator for the fibrous materials and furnish optimization [21]. Different furnish scenarios with industrial interest are investigated including different fibre combinations and the design and optimization of each tissue product. In our previous works, this simulator was also used to obtain predictive capacity for the creping and embossing influence on the softness, strength, and absorption properties of industrial and laboratory structures produced with eucalyptus and softwood fibers [20]. Therefore, the computational implementation of *SimTissue* also supports industrial furnish management considering structures with creping and converting operations. In the present work, we are presenting only a furnish optimization approach, not considering these operations.

The results indicate that *SimTissue* predicts the influence of various types of raw materials used to produce tissue products, process operations, and additives at the micro and nanoscale. An important achievement is the comparison of structures produced with 100% eucalyptus fibres, with different percentages of other fibres, and additives. In this work, we present different comparative scenarios of case studies predicted by *SimTissue* to design new tissue paper formulations, compared to typical industrial formulations (75%HW+25%SW) with typical mill drainability values (≈25°SR). These formulations presented a softness of 59.9 HF, a tensile index of 18.5 Nm/g, a water absorption capacity of 7.5 g/g, and a capillary rise of 121 mm.

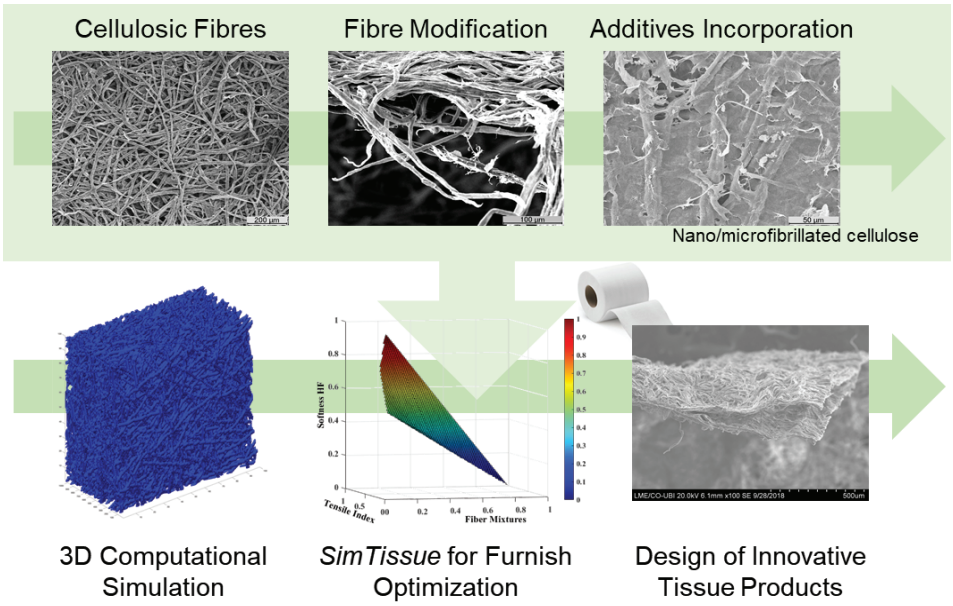

Figure 1: Outline of the methodology approach used in this work to develop the *SimTissue* for furnish management and optimization.

Figure 3 presents the percentage of variation in the final end-use tissue properties for formulations with different fibrous compositions and MFC/NFC incorporation. Formulations were simulated with a eucalyptus pulp (HW), and a softwood pulp (SW) with higher strength properties, in percentages of 1%, 5%, and 10% (Figure 3a). Formulations with MFC/NFC incorporation were also simulated, at the same percentages (Figure 3b). A formulation was further proposed that contained these three fibrous elements, namely, 90%HW+5%MFC/NFC+5%SW (Figure 3b). All formulations with HW and SW presented 25°SR, and formulations with MFC/NFC presented drainability between 26 and 44°SR.

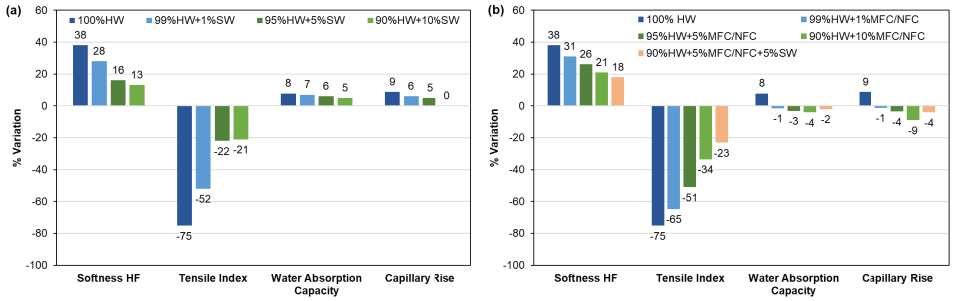

Figure 2: Percentage of variation in the tissue final end-use properties for formulations with (a) HW and SW; and (b) HW and MFC/NFC, compared to the typical industrial structures (75%HW+25%SW), and predicted using the *SimTissue*.

From these scenarios, the results indicated that the production of tissue structures with reduced SW incorporation or its replacement by MFC/NFC promoted an increase in softness properties. Structures with HW and SW contributed positively to the strength

development compared to structures with MFC/NFC. The formulations whose balance between the softness and tensile index properties, and with the highest potential to replace this industrial reference, were 90%HW+10%SW and 95%HW+5%MFC/NFC. This evidence is suggested by comparison with industrial base tissue papers. Despite the 51% loss in the tensile index, structures with 5% MFC/NFC showed strength values in the range of these industrial tissue papers (6.9 - 12.0 Nm/g), and consequently, unsustainable breaks are expected to be unlikely to occur. The results also indicated that SW fibres remain an important element to confer strength and absorption properties, especially in products such as wet strength papers. MFC/NFC presents a good potential to be used in tissue products such as toilet and facial papers, produced with the eucalyptus maximization. The 90%HW+5%MFC/NFC+5%SW formulation also presented a good combination between softness, strength, and absorption, essential to produce premium materials [11].

Regarding fibre modification studies, a kraft eucalyptus pulp with higher tensile index values and a sulphite pulp with higher softness values were separately subjected to enzymatic treatments [10]. The information about fibre flexibility and biometry is determinant to predict tissue paper properties. These two raw materials correspond to the two extremes of eucalyptus pulps, regarding fibre wall thickness, degree of collapse, refining ability, flexibility values, and softness and strength properties. All these fibre properties and dimensions are essential to model them in 3D, resulting in a structure with optimized bulk, for example. Therefore, the results constitute valuable information applicable for other pulps of interest, with fibre dimensions in this range. Through this optimization, the variation of time and enzyme dosage can be predicted, using data-driven statistical mathematical models. Table 1 presents examples of simulated scenarios for the enzymatic treatment of these pulps. First, and regarding kraft pulp, *SimTissue* predicted softness and tensile index values in the same range as typical industrial formulations (softness: 60 HF; tensile index: 19 Nm/g; capillary rise: 121 mm). Therefore, *SimTissue* predicts the formulation properties with variation in these two process variables: reaction time and enzyme dosage. In these simulation studies, similar softness and strength properties are obtained with an enzyme reaction time of 30 minutes, and with a dosage of 50 g/ton, or also with twice the enzyme reaction time, and with a lower dosage of 20 g/ton. The same analysis can also be performed for other pulps of interest.

To obtain new formulations with 100% eucalyptus pulps, it is important to select the process conditions that allow a good trade-off between them, to adjust the furnish for the tissue properties development. A design was proposed that combines 80% of

TABLE 1: Scenarios for the enzymatic treatments of kraft and sulphite pulps, predicted by *SimTissue*.

	Enzyme Dosage (g/ton)	Reaction Time (minutes)	Softness HF	Tensile Index (Nm/g)	Capillary Rise (mm)
Simulation 1 (Kraft pulp)	50	30	53	18	108
Simulation 2 (Kraft pulp)	20	60	53	20	108
Simulation 3 (Sulphite pulp)	100	30	81	7	117
Simulation 4 (Sulphite pulp)	30	60	82	7	116

the enzymatically treated kraft eucalyptus pulp and 20% of the sulphite pulp with and without enzymatic treatment [10]. Figure 4a presents the percentage of variation in the final end-use tissue properties for formulations with different combinations, compared to formulations with 75%HW+25%SW. Overall, the simulated combinations contributed to increased softness with good tensile and absorption properties, ensuring the necessary strength to obtain premium tissue papers. Considering the inverse progression of softness HF and tensile index, the identification of different mixture conditions that allow the best balance between these two properties can be identified for different types of tissue papers. Despite the difference found between the strength of the combinations and the industrial reference, the tensile index values of the combinations (14 – 17 Nm/g) were higher than the range of values for industrial base creped tissue papers (6 – 11 Nm/g) [20].

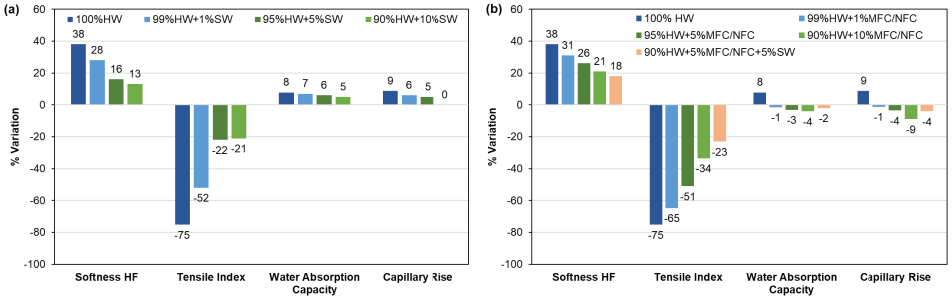

Figure 3: Percentage of variation in the tissue final end-use properties for fibre modification formulations, compared to the typical industrial structures (75%HW+25%SW) and predicted using the *SimTissue*. (a) Combination 1: 80% kraft pulp with 10 g/ton, 30 minutes + 20% sulphite pulp without treatment; Combination 2: 80% kraft pulp with 10 g/ton, 60 minutes + 20% sulphite pulp without treatment; Combination 3: 80% kraft pulp + 20% sulphite pulp, both with 100 g/ton, 30 minutes; Combination 4: 80% kraft pulp + 20% sulphite pulp, both with 100 g/ton, 60 minutes. (b) Simulation 1: kraft pulp treated with 50 g/ton, 120 minutes followed by mechanical treatment (500 PFI revolution); Simulation 2: kraft pulp treated with 350 g/ton, 120 minutes followed by 500 PFI revolution; Simulation 3: kraft pulp with 500 PFI revolution followed by 50 g/ton, 120 minutes; Simulation 4: kraft pulp with 500 PFI revolution followed by 100 g/ton, 120 minutes.

One of *SimTissue*'s features is also to allow the simulation of scenarios that combine different process operations, such as mechanical and enzymatic treatments. To this end, the same kraft pulp was subjected to enzymatic pre-treatment followed by refining, and vice versa. Examples of these simulations, compared to the industrial reference (75%HW+25%SW), are shown in Figure 4b. From this study, *SimTissue* predicted that similar properties were obtained with an enzymatic pre-treatment with an enzyme dosage of 350 g/ton, followed by refining (simulation 2) and a pre-refining followed by enzymatic treatment with an enzyme dosage 7 times less, 50 g/ton (simulation 1). With this approach, several scenarios for enzymatic and mechanical treatments with equivalent energy consumption can be foreseen. Overall, formulations were obtained with improved softness and absorption properties compared to the industrial reference, and with strengths in the commercial tissue paper range. Although a pre-refining followed by an enzymatic treatment presents a negative impact on the fibres, namely the decrease of fibre length and the increase of fines content, this procedure can be advantageous in obtaining pulps with strength characteristics. Therefore, a pulp with this fibre modification process can be used as an additive in pulps with good softness and absorption properties. Consequently, the production of tissue papers with a composition of 100% eucalyptus pulp and with optimized tissue properties can be achievable.

Regarding the incorporation of additives, in addition to MFC/NFC, *SimTissue* also allows the study of other additives such as CBA [12]. This computational platform predicted the tissue properties as a function of the CBA incorporation in eucalyptus pulps and compared with the industrial reference (Figure ??a). Overall, the incorporation of this additive increased the softness and absorption at the expense of decreasing strength, up to 3% incorporation. On the other hand, after the 4% incorporation, the softness and strength properties increased at the expense of absorption. Note also that the 4% CBA incorporation has practically the same tensile index value as the industrial reference. This means that this incorporation can allow the replacement of SW in terms of strength properties compared to 75%HW+25%SW.

Another planning design that included the selection of eucalyptus and softwood pulps, the combination of process operations and incorporation of two additives was carried out and foreseen by *SimTissue*. Two scenarios were simulated on our computational platform and compared to the industrial reference (Figure ??b). The simulations were carried out to study the effect of the conjugation of two additives on tissue properties and to study their implication in softwood pulp reduction [12]. In Simulation 1, the scenario of selecting 75%HW, 25%SW with mechanical refining treatment followed by enzymatic treatment of 30 g/ton for 60 minutes, and incorporation of 2% MFC/NFC

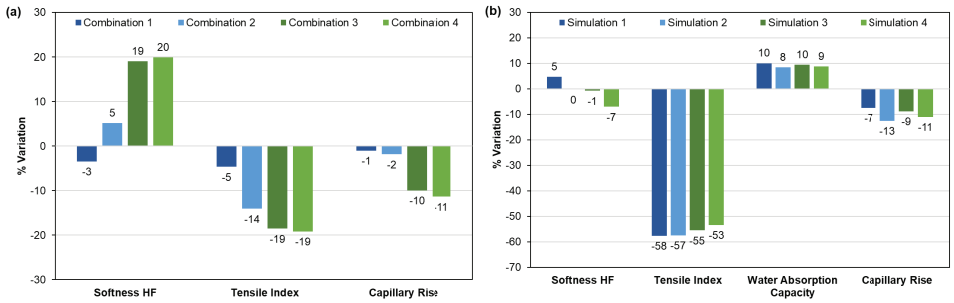

Figure 4: Percentage of variation in the tissue final end-use properties for formulations with (a) HW and CBA; and (b) HW, SW, MFC/NFC, and CBA, compared to the typical industrial structures (75%HW+25%SW), and predicted using the *SimTissue*. Simulation 1: 75%HW+25%+2%MFC/NFC+2%CBA; Simulation 2: 90%HW+10%+2%MFC/NFC+2%CBA.

and 2%CBA, as additives, was proposed. In Simulation 2, the same previous conditions of process operation and additives were proposed, but with a selection of 90%HW and 10%SW. Compared to 100%HW formulations, the addition of both additives improved strength at the expense of decreased softness and absorption. With the softwood pulp reduction, the additives' incorporation promoted an increase in softness and absorption, with good strength properties similar to commercial tissue papers. The understanding of the possibility of producing tissue structures with different additives, softwood pulp reduction, and fibre modification treatments, in the range of industrial drainage, was possible through these simulations.

4. Conclusions

With this research work, we present an experimental and computational methodology to develop sustainable cellulose-based tissue materials. A simulator with predictive capability, the *SimTissue*, was developed and validated to optimize innovative furnish formulations, saving laboratory, and industrial resources. *SimTissue* was applied to identify the more adequate eucalyptus and softwood pulps from a set of raw material pulps. The results indicated the optimized combination of pulps to produce toilet and facial papers, in which softness is the key property, as well as towel papers and napkins, in which strength and absorption are essential. Simulation studies were used to optimize different furnish formulations, predicting different scenarios with enzyme dosages reduction, extending its reaction time, translating into refining energy gains. The effects of incorporating additives, such as MFC/NFC or CBA, were also estimated by *SimTissue*. Several hypotheses of industrial interest were simulated, and the trade-off between softness, strength, and absorption properties was quantified in different

scenarios. In conclusion, the *SimTissue* is a computational tool with predictive capacity useful for furnish management and sustainable process optimization.

Acknowledgments

This research was supported by Project InPaCTus – Innovative Products and Technologies from eucalyptus. Project N° 21 874 funded by Portugal 2020 through European Regional Development Fund (ERDF) in the frame of COMPETE 2020 n° 246/AXIS II/2017. The authors are also very grateful for the support given by research unit Fibre Materials and Environmental Technologies (FibEnTech-UBI), on the extent of the project reference UIDB/00195/2020, funded by the Fundação para a Ciência e a Tecnologia, IP/MCTES through national funds (PIDDAC).

References

[1] de Assis T, Reisinger LW, Pal L, Pawlak J, Jameel H, Gonzalez RW. Understanding the effect of machine technology and cellulosic fibers on tissue properties – A review. BioResources. 2018;13(2):4593-4629. https://doi.org/10.15376/biores.13.2.DeAssis

[2] Tissue Word Magazine. Growth in the European tissue business moving from West to East. 2014, March 13. Available from: https://www.tissueworldmagazine.com/departments/marketissues/growth-in-the-european-tissue-business-moving-from-west-to-east/

[3] The Navigator Company. Sustainability policy. 2021. Available from: http://en.thenavigatorcompany.com/Sustainability/Sustainable-Forest/Sustainability-Policy

[4] Gotera ZFJ. Developing and understanding state-of-the-art technologies at nano- and macroscales to enhance fiber utilization in the hygiene tissue industry [Ph.D. thesis]. Raleigh: North Carolina State University (NCSU); 2021.

[5] Tissue World Magazine. Eucalyptus – Adding tensile strength and keeping formation and softness. 2020, December 3. Available from: https://www.tissueworldmagazine.com/special-features/focus-on/eucalyptus-adding-tensile-strength-and-keeping-formation-and-softness/

[6] Morais FP, Bértolo RAC, Curto JMR, Amaral MECC, Carta AMMS, Evtyugin DV. Comparative characterization of eucalyptus fibers and softwood fibers for tissue papers application. Materials Letter. 2019;10(4):100028. https://doi.org/10.1016/j.mlblux.2019.100028

[7] Morais FP, Bértolo RAC, Curto JMR, Amaral MECC, Carta AMMS, Evtyugin DV. Characterization data of pulp fibres performance in tissue papers applications. Data in Brief. 2020;29:105253. https://doi.org/10.1016/j.dib.2020.105253

[8] Morais FP, Carta AMMS, Amaral ME, Curto JMRC. Experimental 3D fibre data for tissue papers applications. Data in Brief. 2020;30:105479. https://doi.org/10.1016/j.dib.2020.105479

[9] Morais FP, Carta AMMS, Amaral ME, Curto JMRC. 3D Fiber models to simulate and optimize tissue materials. BioResources. 2020;15(4):8833-8848. https://doi.org/10.15376/biores.15.4.8833 8848

[10] Morais FP, Carta AMMS, Amaral ME, Curto JMRC. Cellulose fiber enzymatic modification to improve the softness, strength, and absorption properties of tissue papers. BioResources. 2021;16(1):846-861. https://doi.org/10.15376/biores.16.1.846 861

[11] Morais FP, Carta AMMS, Amaral ME, Curto JMRC. Micro/nano fibrillated cellulose (MFC/NFC) fibers as an additive to maximize eucalyptus fibers on tissue paper production. Cellulose. 2021;28(4):6587-6605. https://doi.org/10.1007/s10570021039129

[12] Morais FP, Carta AMMS, Amaral ME, Curto JMRC. An innovative computational strategy to optimize different furnish compositions of tissue materials using micro/nanofibrillated cellulose and biopolymer as additives. Polymers. 2021;13(15):2397. https://doi.org/10.3390/polym13152397

[13] Ramezani O, Nazhad MM. The effect of coarseness on paper formation. African Pulp and Paper Week; 2004.

[14] Alava M, Niskanen K. The physics of paper. Reports on Progress in Physics. 2006;69(3):669-723. https://doi.org/10.1088/0034-4885/69/3/R03

[15] Conceição ELT, Curto JMR, Simões RMS, Portugal ATG. Computational modeling of objects represented in images. Barneva RP, Brimkov VE, Hauptman HA, Natal Jorge RM, Tavares JM, editors. Heidelberg: Springer; 2010.

[16] Curto JMR, Conceição ELT, Portugal ATG, Simões RMS. Three dimensional modelling of fibrous materials and experimental validation. Materialwissenschaft und Werkstofftechnik. 2011;42(5):370-374. https://doi.org/10.1002/mawe.201100790

[17] Lavrykov S, Lindström SB, Singh KM, Ramarao BV. 3D network simulations of paper structure. Nordic Pulp and Paper Research Journal. 2012;27:256-263. https://doi.org/10.3183/NPPRJ-2012-27-02-p256-263

[18] Raunio J-P, Ritala R. Simulation of creping pattern in tissue paper. Nordic Pulp and Paper Research Journal. 2012;27:375-381. https://doi.org/10.3183/NPPRJ-2012-27-02-p375-381

[19] Simon J-W. A review of recent trends and challenges in computational modeling of paper and paperboard at different scales. Archives of Computational Methods in Engineering. 2021;28:2409-2428. https://doi.org/10.1007/s11831-020-09460-y

[20] Curto JR, Vieira JC, Morais FP et al. Embossing influence on the 3D structure and key properties of tissue paper. Paper presented at: Proceedings of the XXV TECNICELPA Conferência Internacional da Floresta, Pasta e Papel XI CIADICYP 2021; 2021 Mar 9-12; WebConference, Tomar, Portugal.

[21] Morais FP, Curto JMR. Challenges in Computational Materials Modelling and Simulation. A case-study to predict tissue paper properties. Heliyon. 2022 (Accepted).

KnE Materials Science

FibEnTech21
1st International FibEnTech Congress (FibEnTech21) New opportunities for fibrous materials in the ecological transition
Volume 2022

Knowledge E
enriching | engaging | empowering

Research article

Agrimonia Eupatoria L.-Incorporated Electrospun Nanofibers and Cotton Composite for Antibacterial Wound Dressing Applications

Cláudia Mouro[1]*, Raul Fangueiro[2] and Isabel C. Gouveia[1]

[1]Fiber Materials and Environmental Technologies (FibEnTech-UBI), University of Beira Interior, R. Marquês de Ávila e Bolama, 6201-001 Covilhã, Portugal
[2]Centre for Textile Science and Technology (2C2T), University of Minho, Campus de Azurém, 4800-058 Guimarães, Portugal

Abstract.
Composite wound dressings which combine the suitable properties of distinct materials into one dressing are currently being explored, in combination with different types of bioactive compounds, to enhance the healing process and avoid skin infections. In the present work, poly(vinyl alcohol) and chitosan nanofibers containing *Agrimonia eupatoria* L. were fabricated using a needleless electrospinning method (through Nanospider technology) and deposited on top of a 2,2,6,6-tetramethylpiperidine-1-oxyl (TEMPO)-oxidized cotton textile dressing. The negatively charged carboxyl groups on the cotton fibers interacted with the positively charged amino groups of chitosan, which was previously blended with poly(vinyl alcohol) and *Agrimonia eupatoria* L. to produce the nanofiber layer. The properties of the produced composite materials were analyzed to determine the dressing's potential for antimicrobial wound dressing applications.

Keywords: cotton, textile dressing, electrospun nanofibers, *Agrimonia eupatoria* L., antibacterial composite wound dressings

Corresponding Author: Cláudia Mouro; email: d1684@ubi.pt

Dates
?????

Publishing services provided by Knowledge E

© Cláudia Mouro et al.. This article is distributed under the terms of the Creative Commons Attribution License, which permits unrestricted use and redistribution provided that the original author and source are credited.

Selection and Peer-review under the responsibility of the FibEnTech21 Conference Committee.

OPEN ACCESS

1. Introduction

Nowadays, a wide a range of wound dressings has been fabricated using different materials and physical forms from several techniques in order to cover the wound site, provide protection against external agents, and efficiently support the healing process [1,2]. However, wound dressings from natural textile materials, like cotton, remain one of the most used due to their low cost, limited side effects, easy handling and fabrication, as well as a suitable mechanical support and robust protection against external threats [3]. Furthermore, cotton textile materials are non-toxic, haemostatic, non-allergic, biocompatible, biodegradable, and easily tailored to the wound [3]. Nevertheless, cotton wound dressings can lead to maceration of the wound and cause trauma and pain when

removed, delaying the healing process and making skin more susceptible to infection [3,4]. To overcome such limitations and improve their application as wound dressings, different surface modifications have been reported. Among the various techniques, the chemical modification of cotton using 2,2,6,6-tetramethylpiperidine-1-oxyl (TEMPO) has received considerable attention due to its ability to increase the negative charge density onto the cotton surface [5,6]. This enables the cotton fibers to be functionalized with other materials, namely with electrospun nanofibers which exhibit structural features similar to those presented by the native skin's extracellular matrix (ECM). Moreover, electrospun nanofibers present a high surface area to volume ratio and high porosity which help to maintain an appropriate wound environment for healing, and allow the delivery of the bioactive compounds that are effective in wound healing, improving their therapeutic performance [4,7]. As such, composite wound dressings that combine the benefits of different materials have been highlighted as a promising alternative [1,3].

Concerning that, in the present work, Poly(vinyl alcohol) (PVA) and Chitosan (CS) nanofibers containing *Agrimonia eupatoria* L. (AG), a medicinal plant widely known for its traditional bioactive properties, non-toxicity, limited side effects, and low price acquisition, were electrospun using a needleless electrospinning method onto a cotton dressing to both protect the wound from infections and enhance the healing process.

2. Material and methods

Preparation of Crude AG Extract. The AG extraction was carried out by maceration using ethanol solvent in a ratio of 1:20 (w/v).

Production of the TEMPO-oxidized cotton-electrospun nanofibers composite materials. Firstly, the surface of cotton dressing was oxidized using the 0.0125% (w/v) TEMPO/0.125% (w/v) NaBr/ 3.2% (v/v) NaClO system at pH 10.5, one of the most common surface chemical modification methods of cotton fibers, which directly oxidizes the primary alcohol of cellulose to negatively-charged carboxyl groups, increasing the cotton negative surface charge density [5,6].

In turn, PVA and CS solutions were prepared separately by dissolving 10% (w/v) PVA powder in distilled water and 2% (w/v) CS in 0.1 M glacial acetic acid, respectively. Subsequently, the pH of CS solution was adjusted to 5 using 0.1 M HCl, producing a positive charge, and then added to the PVA solution in a ratio of 30:70. Lastly, AG (5.0 wt.%) was added to the PVA_CS blend before the electrospinning process. The PVA_CS and PVA_AG_CS blends were electrospun on top of the previously TEMPO-activated cotton using the Nanospider needleless system (Nanospider laboratory machine NS

LAB 500S from Elmarco S.R.O., Liberec, Czech Republic) by applying a voltage of 75 kV, an electrode rotation of 55 Hz, and a working distance of 13 cm, at room temperature.

Evaluation of the properties of the produced TEMPO-oxidized cotton-electrospun nanofibers composite materials.

Characterization of the composite materials' morphology. The produced TEMPO-oxidized cotton-electrospun nanofibers composite materials and the electrospun PVA_CS and PVA_AG_CS nanofibers were analyzed by Scanning electron microscopy (SEM) (SEM, S-3400N, Hitachi, Tokyo, Japan) at an accelerating voltage of 20 kV to characterize their morphology and the electrospun fibers' diameter were examined using an image analysis software (Image J, National Institutes of Health, Bethesda, MD, USA).

Determination of the composite materials' porosity. The porosity of each material of the produced TEMPO-oxidized cotton-electrospun nanofibers composites was measured by the liquid displacement method using ethanol as displacement liquid, according to the method described in [7].

Evaluation of the composite materials' wettability. The wettability of each material of the produced TEMPO-oxidized cotton-electrospun nanofibers composites was evaluated by determining the water contact angle (WCA) at their surfaces using the Dataphysics Contact Angle System OCAH-200, operating in static mode, at room temperature.

Evaluation of the composite materials' swelling capacity. The sweeling capacity of the dried TEMPO-oxidized cotton-electrospun nanofibers composite materials (W_0) was determined by immersing them in PBS (pH = 5.5) at 37°C and removed from the media at predetermined time points. Excess water on the surface was removed with a filter paper, and the swollen samples weighed (W_t) immediately. The swelling ratio was calculated according to the equation described in [7].

Evaluation of the composite materials' antibacterial activity. The TEMPO-oxidized cotton-electrospun nanofibers composite materials' antibacterial performance was studied through the Standard Test Method for Determining the Activity of Incorporated Antimicrobial Agent(s) in Polymeric or Hydrophobic Materials (ASTM E2180-07 standard) by using *Staphylococcus aureus* (*S. aureus*) (gram-positive bacterium) and *Pseudomonas aeruginosa* (*P. aeruginosa*) (gram-negative bacterium) as models. A filter paper control (pore size of 0.22 µm) was used as control and the log (CFU/mL) was calculated for each material.

Evaluation of the composite materials' cytotoxicity. The cytotoxicity of the produced TEMPO-oxidized cotton-electrospun nanofibers composite materials was analyzed through an MTT assay, according to the ISO 10993-5:2009 guidelines (Biological evaluation of medical devices—Part 5: Tests for in vitro cytotoxicity). To accomplish that, the produced materials were sterilized by UV irradiation (254 nm, ≈ 7 mW cm^{-2}) for 1 hour, and then placed into 24-well plates in direct contact with normal human dermal fibroblasts (NHDF) cells during 1, 3, and 7 days.

3. Results and discussion

The obtained results demonstrated that from cross-section of produced TEMPO-oxidized cotton-electrospun nanofibers composite materials (TEMPO-oxidized cotton/PVA_CS and TEMPO-oxidized cotton/PVA_AG_CS) it is possible to identify the two different materials' layers, Fig. 1A. In addition, the electrospun nanofibers' layers (PVA_CS and PVA_AG_CS) presented uniform and homogeneous fibers with average diameters of 280.20 ± 82.65 nm and 208.11 ± 57.92 nm, respectively, similar to those found at the collagen fibers in the native skin's extracellular matrix (ECM) (50–500 nm) [8], increasing its structural similarity with the native skin tissue, Fig. 1B.

Moreover, the electrospun PVA_AG_CS nanofibers' layer of the produced composite materials displayed a greater porosity (92.77 ± 6.01%), a moderate hydrophilic character (42.37 ± 7.52º), and a desired swelling capacity (~400%), confirming the nanofibers ability to ensure a moist wound environment and exudate absorption, as well as to improve cell adhesion and proliferation, Fig. 2.

Besides, AG-incorporated into PVA_CS's nanofibers layer showed an inhibitory effect against *S. aureus* (99.17 ± 4.05%) and *P. aeruginosa* growth (98.13 ± 0.88%), Fig. 3, while the *in vitro* cytotoxicity assay on normal human fibroblast (NHDF) cells demonstrated more than 80% cell viability, even after 7 days, confirming its biocompatibility, Fig. 4.

4. Conclusions

These findings highlight that the TEMPO-oxidized cotton/PVA_CS composite dressing material containing AG extract represents a promising approach to be used as an antibacterial wound dressing due to the potential benefits of AG, particularly its excellent antibacterial activity against pathogenic bacteria and low tendency to develop bacterial resistance, as well as the enhanced properties regarding the combination of two distinct materials, like the mechanical protection, wettability, porosity, and swelling ratio.

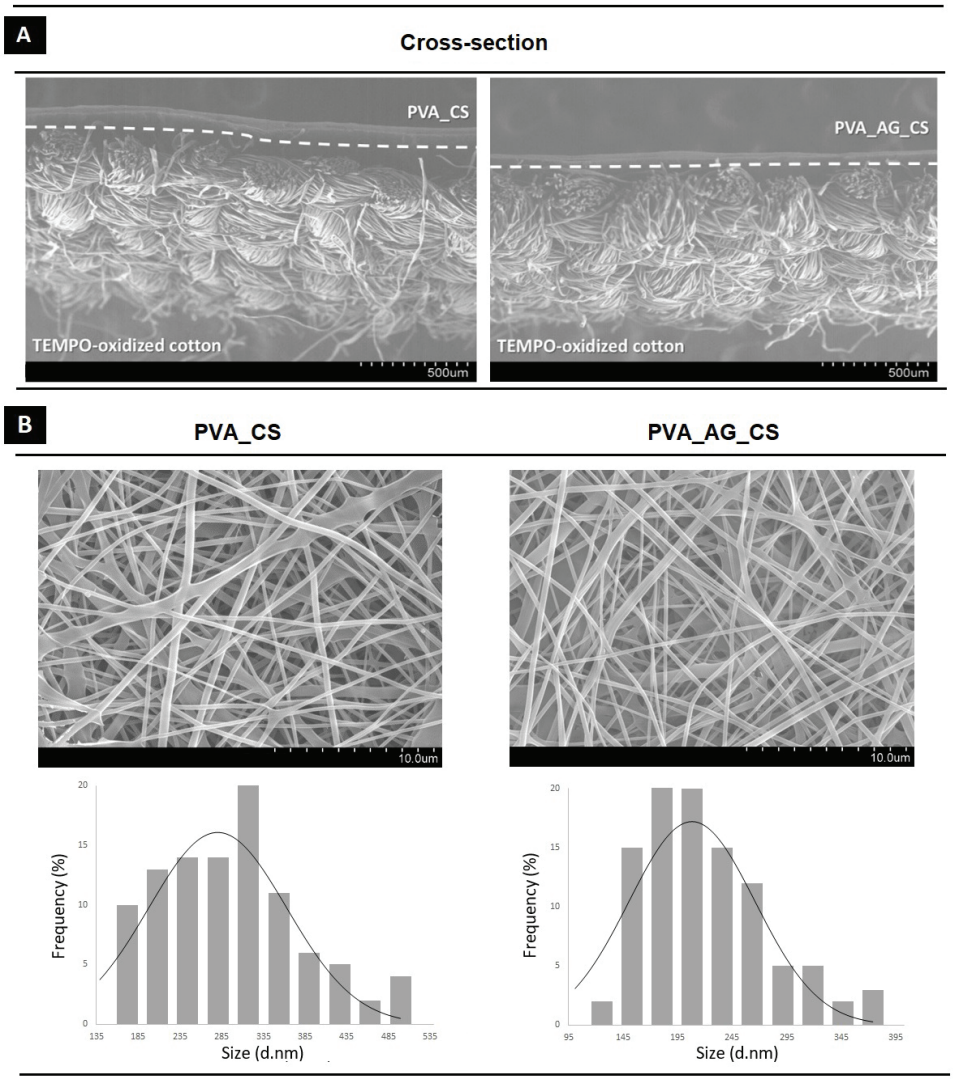

Figure 1: Morphological characterization of the produced 2,2,6,6-tetramethylpiperidine-1-oxyl radical (TEMPO)-oxidized cotton/ Poly(vinyl alcohol) (PVA)_Chitosan (CS) materials with and without crude *Agrimonia eupatoria L.* (AG) extract. Cross-sections of the produced composite materials (**A**); surface morphologies and respective diameter distribution of the electrospun nanofibers' layers (PVA_CS and PVA_AG_CS) (**B**).

Acknowledgments

The authors are grateful for the support provided by FibEnTech Research Unit, in the scope of the FibEnTech Research Unit project (UIDB/00195/2020), funded by the Portuguese Foundation for Science and Technology (FCT), I.P./MCTES through national funds (PIDDAC). Cláudia Mouro also acknowledges a PhD fellowship from FCT (PD/BD/113550/2015).

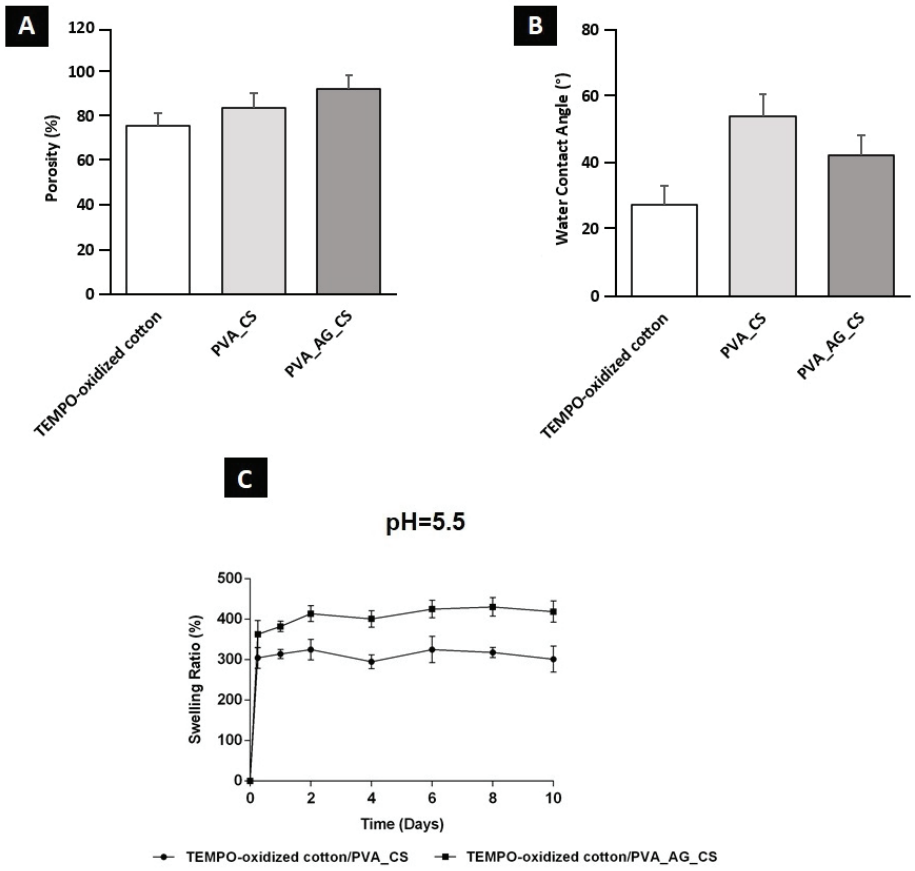

Figure 2: Characterization of the porosity (**A**), wettability features by the water contact angle (WCA) (**B**), and the swelling profile at pH=5.5 (**C**) of the produced composite materials.

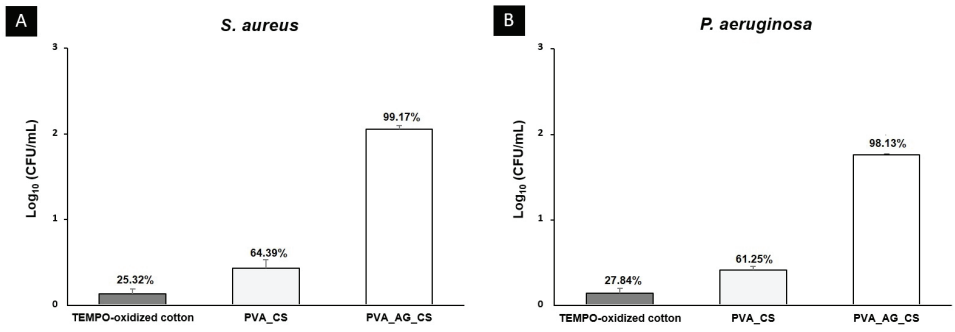

Figure 3: Evaluation of the TEMPO-oxidized cotton, PVA_CS and PVA_AG_CS' antibacterial properties against *S. aureus* (**A**) and *P. aeruginosa* (**B**).

References

[1] Adamu BF, Gao J, Jhatial AK, Kumelachew DM. A review of medicinal plant-based bioactive electrospun nano fibrous wound dressings. Materials & Design. 2021;209:1-9. https://doi.org/10.1016/j.matdes.2021.109942

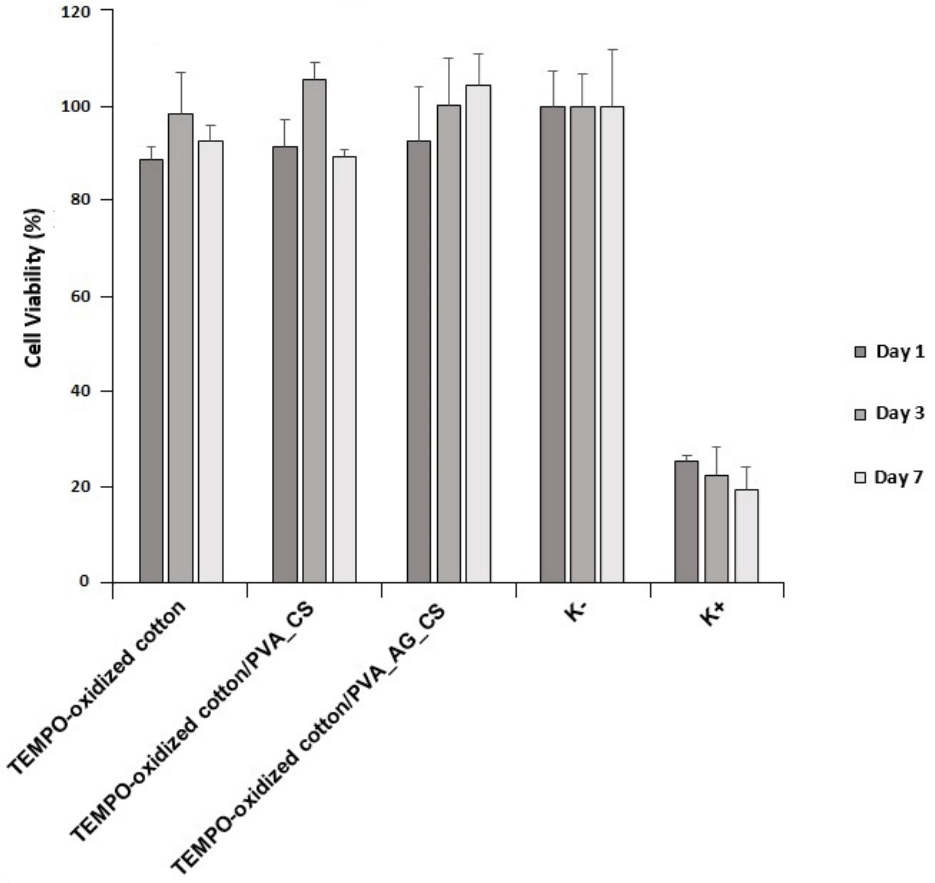

Figure 4: Evaluation of the normal human dermal fibroblast (NHDF) cell viability after 1, 3, and 7 days in contact with the TEMPO-oxidized cotton and the produced composite materials.

[2] Simões D, Miguel SP, Ribeiro MP, Coutinho P, Mendonça AG, Correia IJ. Recent advances on antimicrobial wound dressing: A review. European Journal of Pharmaceutics and Biopharmaceutics. 2018;127:130–141. https://doi.org/10.1016/j.ejpb.2018.02.022

[3] Pinho E, Soares G. Functionalization of cotton cellulose for improved wound healing. Journal of Materials Chemistry. 2018;6:1887-1898. https://doi.org/10.1039/c8tb00052b

[4] Wang F, Hu S, Jia Q, Zhang L. Advances in electrospinning of natural biomaterials for wound dressing. Journal of Nanomaterials. 2020;2020:1-14. https://doi.org/10.1155/2020/8719859

[5] Nikolic T, Korica M, Milanovic J, Kramar A, Petronijevic Z, Kostic M. TEMPO-oxidized cotton as a substrate for trypsin immobilization: impact of functional groups on proteolytic activity and stability. Cellulose. 2017;24:1863-1875. https://doi.org/10.1007/s10570-017-1221-1

[6] Gomes AP, Mano JF, Queiroz JA, Gouveia IC. New biomaterial based on cotton with incorporated biomolecules. Journal of Applied Polymer Science. 2014;131:1-9. https://doi.org/10.1002/app.40519

[7] Mouro C, Gomes AP, Ahonen M, Fangueiro R, Gouveia IC. *Chelidonium majus* L. Incorporated emulsion electrospun PCL/PVA_PEC nanofibrous meshes for antibacterial wound dressing applications. Nanomaterials. 2021;11:1-17. https://doi.org/10.3390/nano11071785

[8] Bombin ADJ, Dunne NJ, McCarthy HO. Electrospinning of natural polymers for the production of nanofibres for wound healing applications. Materials Science and Engineering. 2020;114:1-14. https://doi.org/10.1016/j.msec.2020.110994

KnE Materials Science

FibEnTech21
1st International FibEnTech Congress (FibEnTech21) New opportunities for fibrous materials in the ecological transition
Volume 2022

Knowledge E
enriching | engaging | empowering

Research article

Functionalization of Bacterial Cellulose With Bacterial Pigments: Optimization Using a Full Factorial Design Approach

Lúcia F.A. Amorim[1]*, Raul Fangueiro[2], and Isabel C. Gouveia[1]

[1]FibEnTech Research Unit, Faculty of Engineering University of Beira Interior, Covilhã, Portugal
[2]Centre for Textile Science and Technology (2C2T), University of Minho, Guimarães, Portugal

Abstract.
Pigments from natural sources, such as bacterial pigments, have gained increased attention in recent years due to their biodegradability, non-toxicity, and non-carcinogenicity. The intention to replace synthetic and oil-derived compounds is not restricted to synthetic dyes; other applications include the replacement of oil-derived polymers for more environmentally friendly options, such as biopolymers. In this work, the functionalization of a bacterial cellulose (BC) biopolymer with bacterial pigments was explored using a full factorial design methodology to evaluate the best functionalization conditions to produce colored BC. From the factors and interactions evaluated, it was possible to conclude that the variable duration of the functionalization procedure could be reduced to a low level without significantly affecting the functionalization of the BC samples with bacterial pigments. Moreover, BC is a product with high industrial applicability, versatility, and sustainability. Hence, the multifunctional colored BC can be applied in the packaging, paper, and textile industries, among others.

Keywords: bacterial pigments, bacterial cellulose, full-factorial design, optimization

Corresponding Author: Lúcia F.A. Amorim; email: ?????

Dates
?????

Publishing services provided by Knowledge E

© Lúcia F.A. Amorim et al. This article is distributed under the terms of the Creative Commons Attribution License, which permits unrestricted use and redistribution provided that the original author and source are credited.

Selection and Peer-review under the responsibility of the FibEnTech21 Conference Committee.

OPEN ACCESS

1. Introduction

The adverse side effects ensued from the extensive use of synthetic dyes in food, pharmaceutical, textile, and cosmetic industries pushes research towards their replacement with safer and more sustainable alternatives [1–3]. Moreover, high concentrations of natural, biodegradable, non-toxic, and non-carcinogenic pigments can be obtained from microorganisms, as an alternative to chemically produced dyes. These pigments exhibit a wide range of colors as well as interesting biological activities [4]. Additionally, microorganisms are also able to produce non-toxic and biodegradable biopolymers, such as Bacterial Cellulose (BC), which exhibits noteworthy intrinsic properties, with high industrial applicability [5,6] Employing microbial resources for BC production simplifies the downstream and upstream processes, due to the capacity of production regardless climatic or environmental conditions, in a controlled environment, and also owing to the

absence of undesirable compounds (such as lignin, pectin, and hemicellulose, contained in vegetable cellulose) [5,6]. Furthermore, factorial designs are commonly used to investigate how one or more responses are affected by the effects of experimental factors (variables evaluated) and the interactions between those factors, using a reduced number of experiments, and at the same time increasing the possibilities to evaluate interactions among the variables, which ultimately may reduce the process evaluation costs [7]. Thus, the aim of the present work is to investigate the functionalization of BC pellicles with the bacterial pigments prodigiosin, violacein and flexirubin-type pigment and improve the functionalization process using full factorial design methodology.

2. Material and methods

Biosynthesis and recovery of bacterial pigments: Prodigiosin was produced by *Serratia plymuthica*, in Peptone Glycerol Phosphate medium, at 20□C, with no light exposure [8]. Violacein production was accomplished using *Chromobacterium violaceum*, in Tryptic Soy Broth, at 30□C [9]. Flexirubin-type pigment was produced by bacteria *Chryseobacterium shigense*, also at 30□C, in nutrient medium [10]. The pigments recovery was achieved using previously established methods with acidified ethanol, ethanol, and acetone, for prodigiosin) [11], violacein [12], and flexirubin-type pigment [10], respectively.

Biosynthesis and recovery of BC : A commercial Kombucha beverage was used as inoculum 10% (v/v) for BC production. The fermentation was carried out for 7 days, at 30 □C, using a mixture of 16.5 g/L of black and green tea, and 70 g/L of glucose. The recovered BC pellicles were subjected to an alkaline treatment to remove impurities and possible cellular debris [13].

Functionalization conditions optimization : Experimental runs were designed by Design Expert software, version 7.0.0 (Stat-Ease, Minneapolis), using the full factorial method. The two-level three-factor full factorial experimental design approach was applied for the evaluation of three variables at two levels, for each pigment tested, in order to evaluate the optimal conditions for BC functionalization with violacein, prodigiosin, and flexirubin-type pigment. The variables evaluated in this work were temperature (A), duration of functionalization (B), and pigment concentration (C). Temperature was kept at 40 □C (low level) and 90 □C (high level), the duration of BC-functionalization was 20 min or 60 min, for low (-1) and high level (+1), respectively, and pigment solutions were prepared at 5 and 30% over the weight of the fiber (owf). In addition, triplicate mid-level of variables, center points, were also included. The Statistical software was also used to establish the validity of the models on the basis

of analysis of variance (ANOVA) and evaluate the effects of process variables (A, B, C) and their interactions on the response variable, BC functionalization, by measuring the color strength (K/S) of the samples produced.

Functionalization procedure and samples' evaluation: A Datacolor AHIBA IR equipment (Datacolor company, USA) was used for BC functionalization with each pigment solution. The pigment solutions were prepared at 30% owf, 17.5% owf, and 5% owf. The functionalization temperatures evaluated were 40, 65, 90 ⁰C, and the functionalization duration was 20, 40 and 60 min. A liquor ratio of 1:30, 20 rpm, and a 2 ⁰C/min raise velocity were maintained constant during the entire full factorial experimental design study. A Datacolor 110 spectrophotometer (Datacolor company, USA) was used to evaluate the response variable by determining the K/S values of the functionalized samples. The Kubelka–Munk equation was used to determine the K/S values.

3. Results and discussion

Table 1, 2 and 3 summarize the randomized set of the experiments with actual factors and the measured K/S response for BC functionalized with violacein, prodigiosin and flexirubin-type pigment.

ANOVA was performed to statistically evaluate the significance of the factors (data not shown) and the Pareto charts (Figure 1) illustrate the relative importance of the main effects and their interactions. Pareto charts are composed of columns that represent the values obtained from a student's t-test to determine whether the calculated effects (factors and interactions between factors) were significantly different from zero [14]. The charts also show two limits, the Bonferroni and the t-limit, that aid in the evaluation of significant factors and interactions. Significant effects appear above the threshold given by the Bonferroni limit, insignificant factors appear below the t-limit, and in between both limits the effects may be significant [15]. As can be observed in Figure 1, significant factors and interactions, for violacein and prodigiosin pigments (Figure 1 (a) e (b)), were temperature, duration of functionalization, pigment concentration, and the interaction between temperature and concentration. Whereas, for flexirubin-type pigment, the temperature, and the pigment concentration were the only two significant factors (Figure 1 (c)).

TABLE 1: Summary of the randomized set of the experiments with actual factors and the measured K/S response, for the 2^3full factorial design with violacein pigment.

Violacein					
Std	Run	Factor A: Temperature (⊠C)	Factor B: Duration(Minut	Factor C: Concentration	Response: K/S
26	1	65	40	0.175	3.35
16	2	90	20	0.300	6.40
27	3	65	40	0.175	3.36
13	4	40	20	0.300	3.61
22	5	90	60	0.300	6.47
7	6	40	60	0.005	1.63
19	7	40	60	0.300	4.35
25	8	65	40	0.175	3.33
4	9	90	20	0.005	1.36
1	10	40	20	0.005	1.55
10	11	90	60	0.005	2.15
14	12	40	20	0.300	3.59
29	13	65	40	0.175	3.41
20	14	40	60	0.300	4.07
11	15	90	60	0.005	2.05
23	16	90	60	0.300	6.46
30	17	65	40	0.175	3.34
2	18	40	20	0.005	1.22
5	19	90	20	0.005	1.49
8	20	40	60	0.005	1.61
28	21	65	40	0.175	3.67
17	22	90	20	0.300	5.79
32	23	65	40	0.175	3.53
15	24	40	20	0.300	4.05
9	25	40	60	0.005	1.62
12	26	90	60	0.005	2.30
33	27	65	40	0.175	3.96
18	28	90	20	0.300	5.71
3	29	40	20	0.005	1.55
21	30	40	60	0.300	4.42
6	31	90	20	0.005	1.71
24	32	90	60	0.300	6.62
31	33	65	40	0.175	3.60

TABLE 2: Summary of the randomized set of the experiments with actual factors and the measured K/S response, for the 2^3full factorial design with prodigiosin pigment.

Prodigiosin					
Std	Run	Factor A: Temperature (°C)	Factor B: Duration(Minut	Factor C: Concentration	Response: K/S
26	1	65	40	0.175	1.97
13	2	40	20	0.300	1.15
19	3	40	60	0.300	1.83
10	4	90	60	0.005	0.67
1	5	40	20	0.005	0.3
25	6	65	40	0.175	1.78
16	7	90	20	0.300	2.74
22	8	90	60	0.300	2.94
7	9	40	60	0.005	0.45
27	10	65	40	0.175	1.57
4	11	90	20	0.005	0.7
23	12	90	60	0.300	2.98
5	13	90	20	0.005	0.78
20	14	40	60	0.300	1.62
29	15	65	40	0.175	1.61
8	16	40	60	0.005	0.49
14	17	40	20	0.300	1.69
30	18	65	40	0.175	1.64
17	19	90	20	0.300	2.61
11	20	90	60	0.005	0.94
2	21	40	20	0.005	0.29
28	22	65	40	0.175	1.24
6	23	90	20	0.005	0.86
15	24	40	20	0.300	1.34
9	25	40	60	0.005	0.44
3	26	40	20	0.005	0.48
24	27	90	60	0.300	2.97
18	28	90	20	0.300	2.76
32	29	65	40	0.175	1.45
21	30	40	60	0.300	1.96
12	31	90	60	0.005	0.87
31	32	65	40	0.175	1.48
33	33	65	40	0.175	1.2

TABLE 3: Summary of the randomized set of the experiments with actual factors and the measured K/S response, for the 2^3full factorial design with flexirubin-type pigment.

Flexirubin-type pigment					
Std	Run	Factor A: Temperature (°C)	Factor B: Duration(Minutes)	Factor C: Concentration	Response: K/S
26	1	65	40	0.175	0.28
4	2	90	20	0.005	0.55
16	3	90	20	0.300	1.50
27	4	65	40	0.175	0.40
10	5	90	60	0.005	0.51
25	6	65	40	0.175	0.44
1	7	40	20	0.005	0.10
7	8	40	60	0.005	0.13
13	9	40	20	0.300	0.24
19	10	40	60	0.300	0.23
22	11	90	60	0.300	1.40
14	12	40	20	0.300	0.21
5	13	90	20	0.005	0.56
28	14	65	40	0.175	0.25
11	15	90	60	0.005	0.45
23	16	90	60	0.300	1.13
2	17	40	20	0.005	0.11
8	18	40	60	0.005	0.12
29	19	65	40	0.175	0.38
20	20	40	60	0.300	0.24
30	21	65	40	0.175	0.39
17	22	90	20	0.300	1.06
21	23	40	60	0.300	0.20
32	24	65	40	0.175	0.27
6	25	90	20	0.005	0.47
24	26	90	60	0.300	1.02
3	27	40	20	0.005	0.11
33	28	65	40	0.175	0.35
31	29	65	40	0.175	0.44
12	30	90	60	0.005	0.60
9	31	40	60	0.005	0.13
15	32	40	20	0.300	0.20
18	33	90	20	0.300	1.43

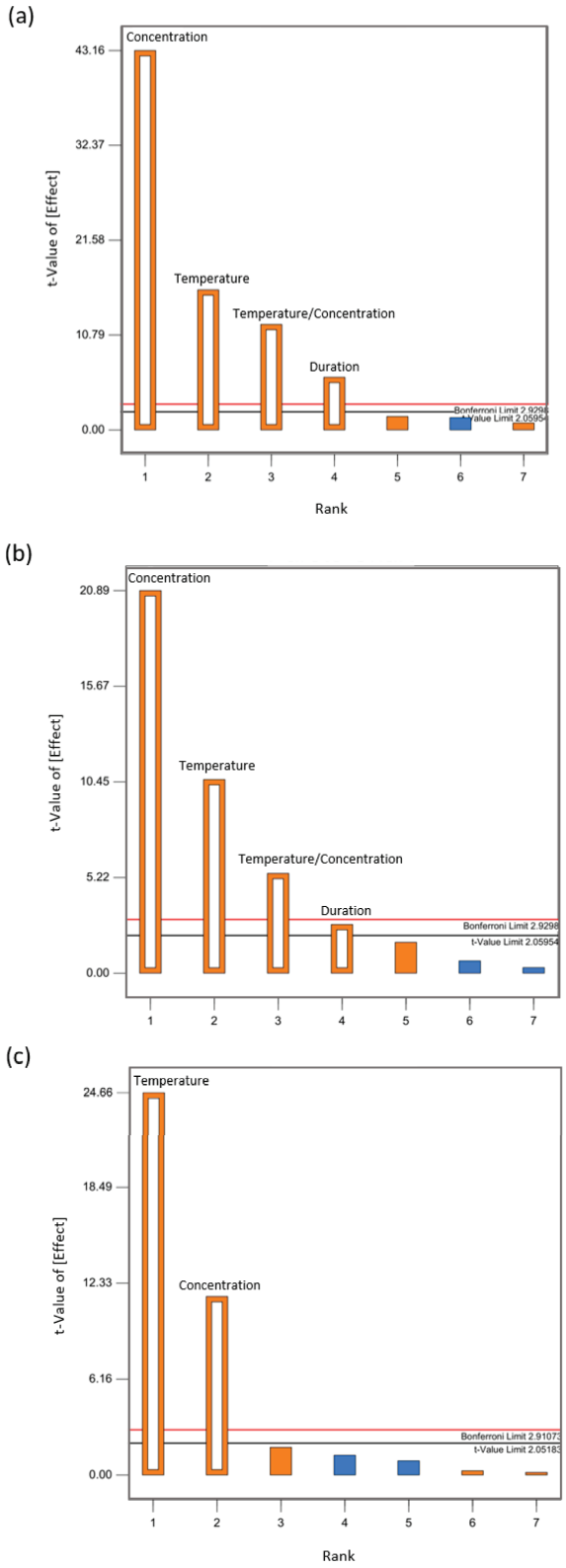

Figure 1: Pareto charts for the models of each pigment, violacein (a), prodigiosin (b), and Flexirubin-type pigment (c), presenting graphically the statistical significance of the factors and interactions.

4. Conclusions

The results indicated that the variable duration was the least significant, for BC functionalized with violacein and prodigiosin pigments, and not even a significant factor, for flexirubin-type pigment-BC functionalization. Moreover, the K/S obtained for the BC functionalization, with the three pigments, under best dyeing conditions would be similar to the K/S achieved if the variable duration was reduced to its low level.

5. Acknowledgements

The authors are grateful for the support provided by FibEnTech Research Unit, in the scope of the FibEnTech Research Unit project (UIDB/00195/2020), funded by the Portuguese Foundation for Science and Technology (FCT), I.P./MCTES through national funds (PIDDAC). Lúcia Amorim also acknowledges a PhD fellowship from Foundation for Science and Technology (FCT) (PD/BD/128417/2017), co-financed by the European SocialFund (FSE), through the Regional Operational Program of the Center (Centro2020).

References

[1] Slama HB, Bouket AC, Pourhassan Z et al. Diversity of synthetic dyes from textile industries, discharge impacts and treatment methods. Applied Sciences. 2021;11:6255-6276. https://doi.org/10.3390/APP11146255

[2] Oliveira MEP, Silva WMB, Alves DR, Neto JBA, Morais SM, Pinheiro SO. Dyes and pigments used in foods: An integrative literature review. Research, Society and Development. 2021;10:e316101018925-316101018949. https://doi.org/10.33448/rsd-v10i10.18925

[3] Gičević A, Hindija L, Karačić A. Toxicity of azo dyes in pharmaceutical industry. IFMBE Proceedings. 2019;73:581–587. https://doi.org/10.1007/978-3-030-17971-7_88

[4] Ramesh C, Vinithkumar NB, Kirubagaran R, Venil CK, Dufossé L. Multifaceted applications of microbial pigments: Current knowledge, challenges and future directions for public health implications. Microorganisms. 2019;7:186-232. https://doi.org/10.3390/microorganisms7070186

[5] Mona S, Bajar S, Deepak B, Kiran B, Kaushik A. Materials for biomedical engineering. Grumezescu V, Grumezescu AM, editors. Elsevier; Amsterdam, Netherlands, 2019.

[6] Seddiqi H, Oliaei E, Honarkar H et al. Cellulose and its derivatives: Towards biomedical applications. Cellulose. 2021;28:1893–1931. https://doi.org/10.1007/S10570-020-03674-W

[7] Emmanuel E, Yong LL, Asadi A, Anggraini V. Full-factorial two-level design in optimizing the contents of olivine and coir fiber for improving the strength property of a soft marine clay. Journal of Natural Fibers. 2020:19(2):1–16. https://doi.org/10.1080/15440478.2020.1751373

[8] Giacomelli F. Avaliação das condições de crescimento da serratia plymuthica para produção de prodigiosina. University of Beira Interior; Covilhã, Portugal, 2018.

[9] Ahmad WA, Yusof NZ, Nordin N, Zakaria ZA, Rezali MF. Production and characterization of violacein by locally isolated *Chromobacterium violaceum* grown in agricultural wastes. Applied Biochemistry and Biotechnology. 2012;167:1220–1234. https://doi.org/10.1007/s12010-012-9553-7

[10] Venil CK, Zakaria ZA, Usha R, Ahmad WA. Isolation and characterization of flexirubin type pigment from *Chryseobacterium* sp. UTM-3T. Biocatalysis and Agricultural Biotechnology. 2014;3:103–107. https://doi.org/10.1016/j.bcab.2014.02.006

[11] Elkenawy NM, Yassin AS, Elhifnawy HN, Amin MA. Optimization of prodigiosin production by serratia marcescens using crude glycerol and enhancing production using gamma radiation. Biotechnology Reports Journal. 2017;14:47–53. https://doi.org/10.1016/j.btre.2017.04.001

[12] Mendes A, Carvalho J, Duarte M. Factorial design and response surface optimization of crude violacein for *Chromobacterium violaceum* production. Biotechnology Letters. 2001:23(23):1963–1969. https://doi.org/10.1023/A:1013734315525

[13] Cheng K-C, Catchmark JM, Demirci A. Effect of different additives on bacterial cellulose production by *Acetobacter xylinum* and analysis of material property. Cellulose. 2009;16:1033–1045. https://doi.org/10.1007/s10570-009-9346-5

[14] Bingol D, Tekin N, Alkan M. Brilliant yellow dye adsorption onto sepiolite using a full factorial design. Applied Clay Science. 2010;50:315–321. https://doi.org/10.1016/j.clay.2010.08.015

[15] Hu X, Wang H, Liu Y. Statistical analysis of main and interaction effects on Cu(II) and Cr(VI) decontamination by nitrogen–doped magnetic graphene oxide. Scientific Reports. 2016;6:34378-34389. https://doi.org/10.1038/srep34378

KnE Materials Science

FibEnTech21
1st International FibEnTech Congress (FibEnTech21) New opportunities for fibrous materials in the ecological transition
Volume 2022

Knowledge E
enriching | engaging | empowering

Research article

Development of Biodegradable, Cellulose-Based, Essential Oil and Chitosan Drug Delivery Systems for Cosmetic Mask Applications

Joana Moreira[1]*, Catarina Lopes[1], Manuel-José Lis Arias[2], Lúcia Silva[1], and Joana M.R. Curto[1]

[1]FibEnTech, Chemistry Department, University of Beira Interior, Covilhã, Portugal
[2]POLQUITEX, Chemical Engineering Department, Universitat Politècnica de Catalunya, Terrassa, Spain

Abstract.

The goal of this research was the development of cellulose-based biodegradable drug delivery systems solutions for cosmetic mask applications. Cellulose-based materials derived from natural renewable sources provide a sustainable alternative to nonwoven cosmetic masks derived from nondegradable fossil-based raw materials. An experimental design was executed to assemble the 3D cellulose fibres matrix and the water in oil emulsion comprising the active molecules from *Mentha piperita* L. Two types of biopolymeric additives were used, one derived from a nano/micro fibrillated cellulose pulp and another one including chitosan. A 3D computational simulation study was performed to enhance porosity and strength properties. The results indicated that the cosmetic face mask optimized prototypes, made from a biodegradable 3D matrix of cellulose fibres and active molecules, are suitable for dermic use.

Keywords: biopolymers, dermic application, drug delivery systems (DDS), essential oil, *Mentha piperita*

Corresponding Author: Joana Moreira; email: joana.maria.moreira@ubi.pt

Dates

?????

Publishing services provided by Knowledge E

© Joana Moreira et al. This article is distributed under the terms of the Creative Commons Attribution License, which permits unrestricted use and redistribution provided that the original author and source are credited.

Selection and Peer-review under the responsibility of the FibEnTech21 Conference Committee.

OPEN ACCESS

1. Introduction

Cellulose is a polymer, consisting of long chains of glucose anhydride, also known as anhydridoglucose (AGU), which has three hydroxyl groups. These groups give cellulose the ability to make hydrogen bonds, which allows for great stability and resistance [1,2].It is produced by the biosynthesis of plants, animals and bacteria in the Eubacteria domain, it leads to many variations of it [3]. Cellulose is properly structured, as it has crystalline and amorphous areas. Cellulose from plants requires processes to remove lignin and hemicelluloses, which can be tricky to solve experimentally [4]. Cellulose is a renewable source of bio-polymers, being produced by several species, such as plants,

animals and bacteria. Cellulose is the structural unit of plants, and is therefore one of the most abundant natural materials [4].

Chitosan is a polysaccharide, vastly abundant like cellulose, becoming an inexpensive resource. Chitosan is derived from organisms such as crustaceans and fungus, and since its common in nature it presents the benefits of being biodegradable, biocompatible and innocuous [5]. Essential oils are multifaceted as they are used in various industries, such as the cosmetic, pharmaceutical and food industries [6]. These are produced by plants and extracted from them, in which many extracts have been recognized as GRAS (Generally Recognized as Safe) [7]. These by-products have anti-inflammatory, antimicrobial and even antiviral properties [8]. Essential oils can be extracted from various parts of the plant such as flowers, fruits, seeds and leaves. Other extractions can be done in a variety of ways, such as solvent extraction and cold pressing [9]. The extraction product's consistency, quantity, and composition can differ depending on environment, soil composition, plant organ, age, and vegetative cycle stage [10]. To obtain the same composition of EOs, they must be harvested under the same conditions, i.e., from the same organ of the plant, which must be growing in the same soil, atmosphere, and season [11]. Each essential oil is a complex sample, composed by many volatile compounds, mostly terpenes [12]. Monoterpenes are present in all essential oils. They are made up of 10 carbon atoms that are derived from two isoprene units. Monoterpenes may have a straight-chain or a single ring backbone. Because of their smaller size, they respond easily to air and heat, and they degrade faster than their more complex molecules [7]. Due to the high volatility of essential oils, the dermal application in the form of masks has the advantage of storing the therapeutic molecules, prolonging their period of action [13]. The innovation of this project is the development of a cosmetic face mask prototype, made from an optimized 3D matrix, containing micro and nano cellulose fibres, obtained by a combination of mechanical and enzymatic processes, to achieve the desired porosity and strength [14-16]. The biopolymer chitosan is also being investigated as an additive, to promote the controlled release of peppermint active molecules [5].

2. Material and methods

Bleached and unbleached *Pinus pinaster* and Eucalyptus pulps from FibEnTech (University of Beira Interior) Research Laboratory were used.

In this study hardwood and softwood industrial Kraft pulps processes were disintegrated according to the ISO 5263/1. The fibres' morphological properties were

determined automatically by image analysis of a diluted suspension (20 mg/L and 30 mg/L 145 to hardwood and softwood samples, respectively) in a flow chamber in MorFi Fiber Analyzer (TECHPAP, Grenoble, France). After their characterization, the hardwood and soft wood pulps were mixed in different ratios.

The cellulose fibres were modified using enzymatic and mechanical treatments. The mechanical treatment was applied to the kraft pulp using a PFI mill at 500-7500 revolutions, under an intensity of 3,33 N/mm. Enzimatyc treatments were performed using an enzyme dosages of 10 g per ton of pulp, for 30 and 60 minutes. The assays were carried out at a consistency of 4%, pH 7, and 40ºC, with continuous mechanical agitation. To stop the reaction sodium hypochlorite was added to the pulp suspension. After these enzymatic treatments, the pulps were mixed in a ratio of 80:20. A more detailed description of this study can be found in the work of Morais et al. [13-15,18].

Different mixtures with additives were made to understand their influence. The micro/nanofibrillated cellulose (MFC/NFC) was incorporated in a never-dry (slush) bleached eucalyptus kraft pulp, according to loads of 1%, 5%, and 10%. A chistosan additive was also incorporated in the same fiber pulp slurry, at the same dosages. A more detailed description of this study can be found in the master thesis document of the author Moreira, J.

The tissue structures were produced in a batch laboratory sheet former according to an adaptation of ISO 5269/1. The adjustments consisted of the production of structures with a basis weight of 20 g/m^2 and of 60 g/m^2 and suppression of the pressing operation.

The prototype mask samples were conditioned at 22±1ºC, with a relative humidity of 50±2%, according to ISO 187. For all assays, the tissue properties for handsheets were measured in terms of structural and functional properties. The basis weight (ISO 12625-6) was obtained by the ratio between the average mass of each structure and the respective area (0,02138 m^2). The thickness (ISO 12625-3) was obtained using a Frank-PTI micrometer. The bulk (ISO 12625- 3) was obtained by the quotient between the structure thickness and the basis weight. A water in oil emulsion was prepared using a ratio of 1:4 (w/w) and 3700 rpm. The water phase is a peppermint infusion, and the oil phase is made using a carrier sunflower oil and the *Mentha piperita L*. essential oil. The emulsion was incorporated in the fibre mixture bulk, and the mask prototype was stored between 0ºC and 4ºC [18]. The fibres length, width, coarseness and fine content were characterized using an automated analyser. The essential oil was analysed using Gas Chromatography–Mass Spectrometry (GC-MS). The Gas Chromatography was performed using an Agilent technologies 7890A GC A.01.13 with Agilent Technologies

5975 inert XL MSD with Triple-Axis Detector. SEM images were performed using Hitachi S-2700 (Tokyo, Japan). The structures were cross-sectioned were covered with gold using a Sputter Quorum Q 15 OR ES (Laughton, East Sussex, UK) and analysed at different magnifications. FTIR-ATR was used to analyse the face mask prototypes without and with peppermint essential oil active molecules. The equipment used was a FTIR-ATR Thermo-Nicolet IS10.

The 3D fibrous matrix computational simulation was performed using Matlab®, according to a previously validated model [18,19]. The fibrous material simulation model was used to simulate the deposition of fibres and the assembly of the mask structure prototype.

3. Results and discussion

The assembly of the mask prototype and its structural hierarchy is presented in Figure 1. Cellulose microcrystalline and chitosan molecular structures are represented in Fig1.b) and c).

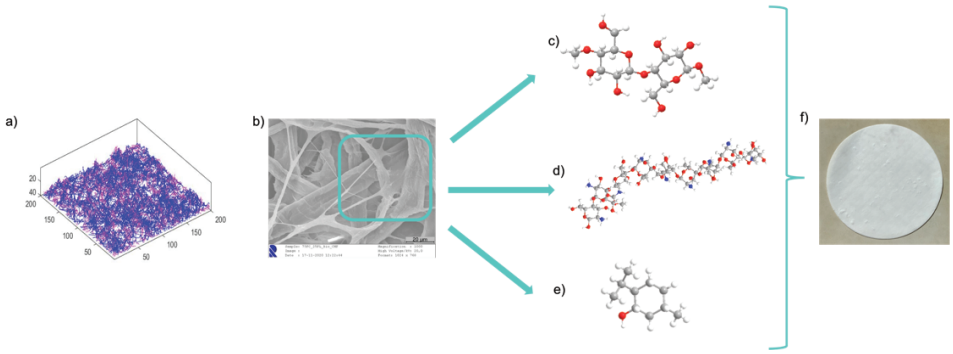

Figure 1: Visual representation of the mask prototype structural hierarchy. a) Structures obtained by Computational Simulation, representing fibres at the end of their deposition, b) SEM image of the fibrous matrix, c) cellulose, d) chitosan, e) menthol and f) laboratory made mask prototype. Molecules made using ChemDraw ® Professional 16.0 by Moreira, J. Model and computational Simulation by Curto, J.

The fibres morphology and biometry changes with the type of raw-material and the mechanical and enzymatic processes are presented in table 1 and table 2.

To identify the components of *Mentha piperita* essential oil, a Gas Chromatography–Mass Spectrometry (GC-MS) analysis was performed. The results (table 3 and fig.2) indicate that the major component is menthol (35.31%).

With this result, we can conclude that after nine months there's still some molecules of peppermint essential oil in the structure, due to the wavelength interval within 2700-3000 cm $^{-1}$.

Table 1: Biometry of different raw materials and mechanical and enzymatic operations.

	Hardwood Fibre	Softwood Fibre	Softwood Fibre + Enzymatic treatment	Softwood Fibre + Mechanical treatment (4000 rev. PFI)	Softwood Fibre + Enzymatic + Mechanical treatment (4000 rev. PFI)
Fibres (million/g)	21,269±0,010	4,742±0,538	5,542±0,265	6,714±0,058	6,704±0,067
Length weighted in length (mm)	0,793±0,003	1,858±0,047	1,889±0,052	1,693±0,026	1,745±0,009
Width (µm)	19,3±0,1	30,1±0,2	30,6±0,4	32,3±0,3	32,2±0,1
Coarseness (mg/100 m)	0,0692±0,0002	0,2052±0,0323	0,1692±0,0065	0,1581±0,0021	0,1509±0,0017
Fine elements (% in length)	36,8±0,2	24,4±21,3	37,9±1,7	42,7±2,2	37,8±1,5

Table 2: Characterization of different raw materials and mechanical and enzymatic operations

	Hardwood Fibre	Softwood Fibre	Softwood Fibre+ Enzymatic treatment	Softwood Fibre + Mechanical treatment(4000 rev. PFI)	Softwood Fibre+ Enzymatic+Mechanical treatment(4000 rev. PFI)	Softwood Fibre +Microcrystalline cellulose+Chitosan
Porosity (%)	84,710±1,96	90,376±1,22	86,847±2,1	72,926±19,46	80,736±4,19	81,964±0,45
Tissue Thickness (µm)	135,378±43,46	138,854±0,18	146,462±0,031	91,710±38,195	93,919±32,00	230,800±7,085
Sheet Density (g/cm^3)	0,229±0,039	0,144±19,64	0,197±64,662	0,406±0,291	0,289±0,063	0,271±0,006
Bulk (cm^3/g)	4,432±0,58	7,066±1,15	5,181±0,72	2,945±0,921	3,593±0,64	3,698±0,091
Grammage (g/m^2)	31,845±13,24	20,080±4,06	30,583±19,15	36,220±24,19	28,815±17,48	62,404±0,56

Table 3: a) Relative chemical composition (%) of *Mentha piperita L.* essential oil b) Menthol Molecular structure in 2D and 3D. Molecules made using ChemDraw ® Professional 16.0 by Moreira, J.

a)

Compound	**RI**	
β-pinene	978	1,0
Limonene	1030	2,0
1,8-Cineole	1032	5,5
Menthone	1151	20,8
Menthofuran	1164	7,3
Neomenthol	1167	3,2
Menthol	1177	35,3
Terpinen-4-ol	1177	1,3
Pulegone	1234	1,7
Menthyl acetate	1296	7,1
β-Caryophyllene	1420	2,9
Germacrene D	1481	2,0

b)

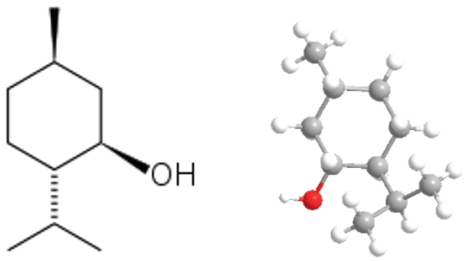

The results indicate that *Mentha piperita* active molecules are retained in the cellulose fibres porous structure.

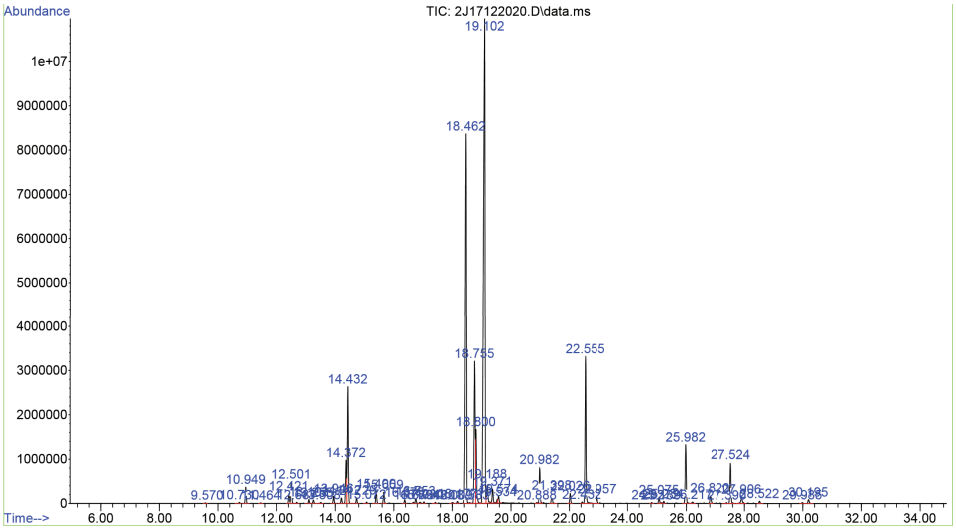

Figure 2: Chromatogram representing the relative chemical composition (%) of *Mentha piperita L.* essential oil

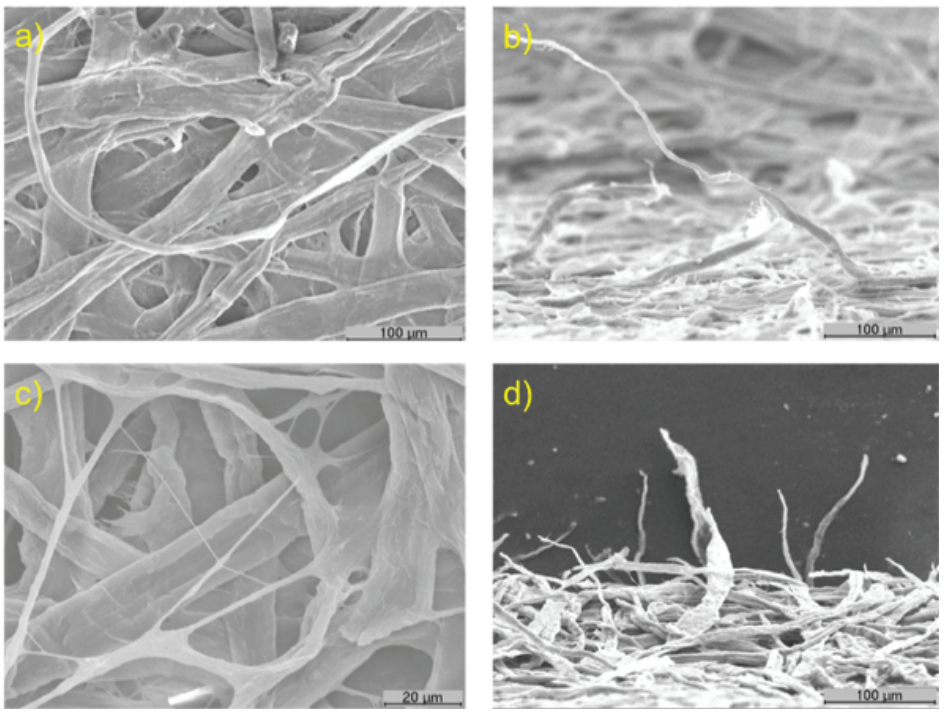

Figure 3: SEM image of the structures of cellulose that went through enzymatic and mechanical treatment, where it can be visualized (a) how the cellulose fibres deposit (magnification of x300), (b) fibrilization of the fibre (magnification of x300), (c) diversity of pore dimensions (magnification of x1000) and (d) fibre in a z axis (magnification of x300).

4. Conclusions

A 3D cellulose fibres matrix was used to make a biodegradable *Mentha piperita* Delivery System, suitable for dermic application. With the mechanic and enzymatic treatment is it possible to see many changes, including in porosity and bulk. With SEM images it was

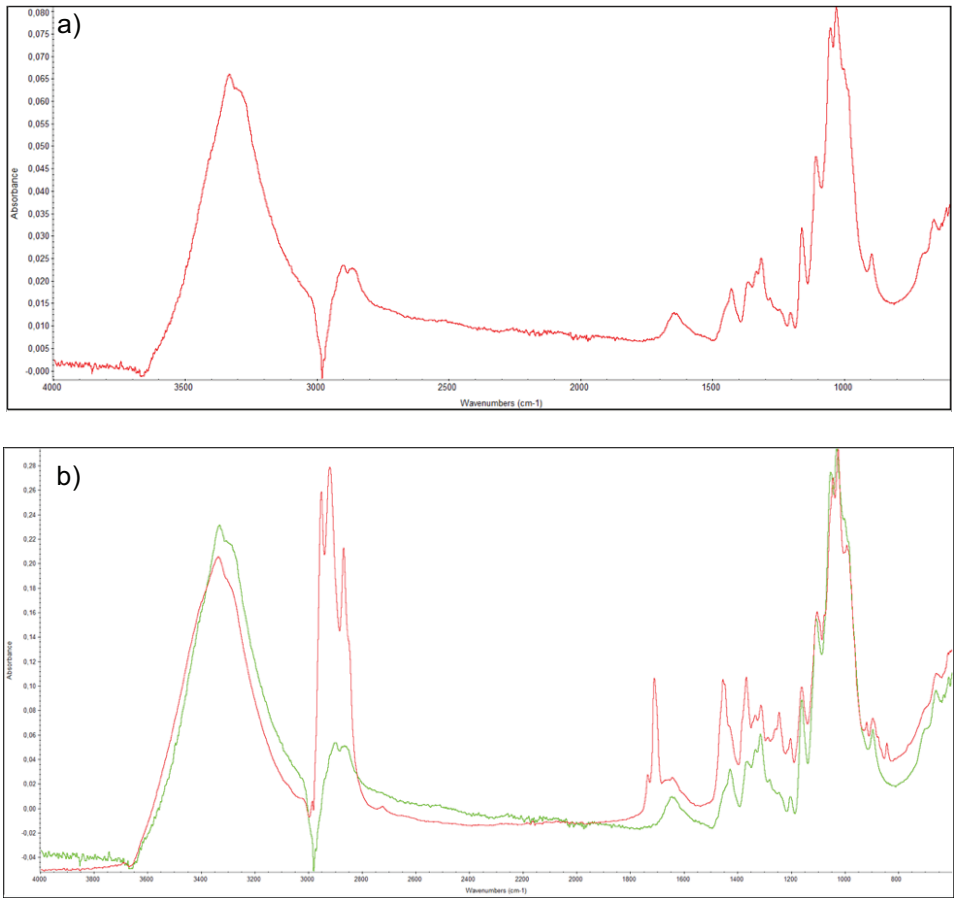

Figure 4: FTIR-ATR spectrum of fibrous matrix without essential oil **b)** FTIR-ATR spectrum of fibre refined containing *Mentha piperita L.* essential oil (red) compared with the fibrous matrix without essential oil (Green).

possible to visualize the pore diversity that is present in every structure and also the fibrilization of cellulose fibres that occur with mechanical and enzymatical treatment. FTIR-ATR results indicate that the peppermint essential oil is retained in the fibrous structure, as is possible to visualize the peak in the wavelength 2700-3000 cm $^{-1}$ that represent the OH groups, since the main component of the essential oil is menthol.

References

[1] Lavoine N, Desloges I, Dufresne A, Bras J. Microfibrillated cellulose - Its barrier properties and applications in cellulosic materials: A review. Carbohydrate Polymers. 2012;90(2):735–764. https://doi.org/10.1016/j.carbpol.2012.05.026

[2] Jorfi M, Foster EJ. Recent advances in nanocellulose for biomedical applications. Journal of Applied Polymer Science. 2015;132(14):1–19. https://doi.org/10.1002/app.41719

[3] Abeer MM, Mohd Amin MCI, Martin C. A review of bacterial cellulose-based drug delivery systems: Their biochemistry, current approaches and future prospects. Journal of Pharmacy and Pharmacology. 2014;66(8):1047–1061. https://doi.org/10.1111/jphp.12234

[4] Abitbol T, Rivkin A, Cao Y et al. Nanocellulose, a tiny fiber with huge applications. Current Opinion in Biotechnology. 2016 ;39(I):76–88. https://doi.org/10.1016/j.copbio.2016.01.002

[5] Arias M, López A, Vilaseca M et al. Influence of chitosan characteristics in the microencapsulation of essential oils. Journal of Biomedical Science and Engineering. 2021;14:119-129. https://doi.org/10.4236/jbise.2021.143012

[6] Klimek-Szczykutowicz M, Szopa A, Ekiert H. Citrus limon (lemon) phenomenon — A review of the chemistry, pharmacological properties, applications in the modern pharmaceutical, food, and cosmetics industries, and biotechnological studies. Plants. 2020;9(1). https://doi.org/10.3390/plants9010119

[7] Pavoni L, Perinelli DR, Bonacucina G, Cespi M, Palmieri GF. An overview of micro- and nanoemulsions as vehicles for essential oils: Formulation, preparation and stability. Nanomaterials. 2020;10(1):135. https://doi.org/10.3390/nano10010135

[8] Mutlu-Ingok A, Devecioglu D, Dikmetas DN, Karbancioglu-Guler F, Capanoglu E. Antibacterial, antifungal, antimycotoxigenic, and antioxidant activities of essential oils: An updated review. Molecules. 2020;25(20). https://doi.org/10.3390/molecules25204711

[9] Turek C, Stintzing FC. Stability of essential oils: A review. Comprehensive Reviews in Food Science and Food Safety. 2013;12(1):40–53. https://doi.org/10.1111/1541-4337.12006

[10] Angioni A, Barra A, Coroneo V, Dessi S, Cabras P. Chemical composition, seasonal variability, and antifungal activity of *Lavandula stoechas* L. ssp. stoechas essential oils from stem/leaves and flowers. Journal of Agricultural and Food Chemistry. 2006;54(12):4364–4370. https://doi.org/10.1021/jf0603329

[11] Baptista-Silva S, Borges S, Ramos OL, Pintado M, Sarmento B. The progress of essential oils as potential therapeutic agents: A review. Journal of Essential Oil Research. 2020;32(4):279–295. https://doi.org/10.1080/10412905.2020.1746698

[12] Shaaban HAE, El-Ghorab AH, Shibamoto T. Bioactivity of essential oils and their volatile aroma components: Review. Journal of Essential Oil Research. 2012;24(2):203–212. https://doi.org/10.1080/10412905.2012.659528

[13] Morais FM, Simões RMS, Curto JM. Biopolymeric delivery systems for cosmetic applications using *Chlorella vulgaris* algae and tea tree essential oil. Polymers.

2020;12(11). https://doi.org/10.3390/polym12112689

[14] Morais FP, Carta AMMS, Amaral ME, Curto JMR. Micro/nano-fibrillated cellulose (MFC/NFC) fibers as an additive to maximize eucalyptus fibers on tissue paper production. Cellulose. 2021;28**:**6587–6605. https://doi.org/10.1007/s10570-021-03912-9

[15] Morais FP, Carta AMMS, Amaral ME, Curto JMR. Cellulose fiber enzymatic modification to improve the softness, strength, and absorption properties of tissue papers. BioResources. 2021;16:846-861.

[16] Spiridon I, Duarte AP, Curto J. Influence of xilanase treatment on *Pinus pinaster* kraft pulp. Cellulose Chemistry and Technology. 2003;37(3-4):497-504.

[17] Mota AS, Martins RM, Arantes S et al. Antimicrobial activity and chemical composition of the essential oils of Portuguese *Foeniculum vulgare* fruits. Natural Product Communications. 2015;10(4):673-676.

[18] Morais FP, Carta AMMS, Amaral ME, Curto JMR. 3D fiber models to simulate and optimize tissue materials. BioResources. 2020;15:8833-8848.

[19] Curto JMR, Conceição ELT, Portugal ATG, Simões RMS. Three-dimensional modelling of fibrous materials and experimental validation. Materialwissenschaft Und Werkstofftechnik. 2011;42(5):370–374. https://doi.org/10.1002/mawe.201100790

KnE Materials Science

FibEnTech21
1st International FibEnTech Congress (FibEnTech21) New opportunities for fibrous materials in the ecological transition
Volume 2022

Knowledge E
enriching | engaging | empowering

Research article

Chemical Composition of the Essential Oils in Portuguese Daucus Carota Subspecies

Sofia J. Silva[1]*, Jasmine Barata[2], Violeta R. Lopes[3], Ana M. Barata[3], Arlindo Gomes[1,4], Lúcia Silva[1,4], and Ana Luísa Fernando[5]

[1]Departament of Chemistry, University of Beira Interior, Rua Marquês d'Ávila e Bolama, 6201-001, Covilhã, Portugal
[2]Chemical and Engineer Department, Universidad de Lorraine, 54601 Villers Les Nancy Cedex, France
[3]Banco Português de Germoplasma Vegetal, INIAV, I.P., Quinta de S. José, S. Pedro de Merelim, 4700-859, Braga, Portugal
[4]FibEnTech, University of Beira Interior, Rua Marquês d'Ávila e Bolama, 6201-001, Covilhã, Portugal
[5]MEtRICs, Department of Science and Technology of Biomass (DCTB), NOVA School of Science and Technology, New University of Lisbon, Campus de Caparica, 2829-516 Caparica, Portugal

Abstract.
This study focused on five different subspecies of Portuguese *Daucus carota* L., to identify the main compounds in the essential oils of umbels from each subspecies. The isolation of the essential oils was performed by hydrodistillation methods followed by further composition analysis by gas chromatography-mass spectrometry, ultimately demonstrating that each subspecies had different major compounds. This study concluded that the main compounds found in *Daucus carota* subsp. *maritimus* were geranyl acetate, followed by trans-methyl-isoeugenol, α-pinene, cis-asarone and elemicin. *Daucus carota* subsp. *hispidus* presented with the major compounds as geranyl acetate, caryophyllene oxide, trans-methyl-isoeugenol and sabinene. For *Daucus carota* subsp. *maximus*, the major compounds were cis-asarone, geranyl acetate and elemicin, which was similar to *Daucus carota* subsp. *carota* which presented with the major compounds as geranyl acetate, cis-asarone, trans-methyl-isoeugenol and α-pinene. Finally, the major components of *Daucus carota* subsp. *sativus* were carotol and daucol.

Keywords: essential oils, chemical composition, *Daucus carota*, hydrodistillation, GC-MS

Corresponding Author: Sofia J. Silva; email: sofia.joia.silva@ubi.pt

Dates
?????

Publishing services provided by Knowledge E

© Sofia J. Silva et al. This article is distributed under the terms of the Creative Commons Attribution License, which permits unrestricted use and redistribution provided that the original author and source are credited.

Selection and Peer-review under the responsibility of the FibEnTech21 Conference Committee.

OPEN ACCESS

1. Introduction

Essential oils from aromatic plants are used for hundreds of years ago, as they are composed by volatile secondary metabolites that rapidly are absorbed through the skin and further provide notorious therapeutic benefits of high importance in Human life [1]. Essential oils are complex mixtures and researchers aim to know their composition, to allow practical application and understand which beneficial and adverse effects these oils might have [2]. The Apiaceae family is one of the most studied related to essential oils, not only for being one of the most consumed worldwide, but also because they

are used as food, flavoring agents, medical purposes and for being nutraceutical plants [1,2]. One of the species of this family is *Daucus carota*, or as it is commonly called, carrot. *D. carota* is a biannual plant with its flowering seasons from June to August. The umbels appear white and round in full blossom. Before the domestication, the carrot root appeared white, but after intensive breeding, orange carrot became carotenoid-rich existing still other root colours like purple [3]. This specie has some subspecies like *Daucus carota* supbsp. *sativus* and *Daucus carota* subsp. *carota* that are presented worldwide, being the first one the only cultivated and assumed to be originated by selective breeding of the ancestral wild form of the second one [4,5]. According with Heywood study in 1968, there were recognized eleven wild subspecies of *Daucus carota*. In previous studies, a great variety of compounds with different proportions were described in essential oils from umbels. In Tunisia, *Daucus carota* subsp. *maritimus* presented as major components elemicin, geranyl acetate, α-pinene, myrcene and cubenol [1]. *Daucus carota* subsp. *hispidus*, presented as major components α-cadinol, *trans*-methyl-isoeugenol, premnaspirodiene and carotol [6]. As in the chemical analysis of *Daucus carota* subsp. *maximus*, in Italy, it appears that the major compounds are carotol and β-bisabolene, however, a previous Portuguese study presented as major components α-pinene, geranyl acetate, *cis*-asarone, *trans*-methyl-isoeugenol and elemicin [7,5]. For *Daucus carota* subsp. *carota*, a German study compared Polish, French and Moroccan essential oils and it has reported as main component in all of them carotol. The one collected in Poland had higher amounts of verbenol, caryophyllene oxide, -pinene and *trans*-pinocarveol. French oil presented -pinene, caryophyllene oxide and caryophyllene. Finally, Moroccan oil presented caryophyllene oxide and β-bisabolene as major components [8]. Accordingly with the same Portuguese study α-pinene and geranyl acetate are the higher percentage components [5], which differs from the ones observed in *Daucus carota* subsp. *sativus*, in India, where the major components are carotol α-pinene, myrcene and limonene [9].

2. Material and methods

2.1. Plant Material

Plant material was provided and maintained in *ex situ* by the *Banco Português de Germoplasma Vegetal* (BPGV). Flowering and mature umbels were preserved at dry place and room temperature.

2.2. Essential oil isolation

All the subspecies were submitted to hydrodistillation, where essential oils from the plant umbels were extracted. First 10 g of plant materials are packed in a distillation flask and then is added 200 mL of water and brought to boil and maintain for 2 h [10]. For this method, we used a Clevenger apparatus.

2.3. Essential oil analysis and chemical composition

Essential oils analysis and chemical composition were proceeded by GC-MS chromatography using an Agilent 7890A GC coupled with an Agilent 5975C inert XL mass selective detector. For the separation of the volatile compounds was used an DB-5 J&W GC capillary column (5% phenylmethylpolysiloxane, 30m length, 0,25mm diameter and 0,25µm film), being helium the mobile phase, at 1mL/min. The components identification were obtained by comparison of the retention times and mass spectra, which were also compared with the ones at the data system library NIST and Wiley.

3. Results and discussion

The yields obtained in our hydro-distillation extractions are present in table 1 and they are very small in all subspecies.

After the oil extraction, we proceeded to analyse the compounds present in our oils. The main compounds found in *Daucus carota* subsp. *maritimus* were geranyl acetate (33.9%), followed by *trans*-methyl-isoeugenol (9.3%), α-pinene (7.2%), *cis*-asarone (6.9%) and elemicin (6.0%). *Daucus carota* subsp. *hispidus* presented as major compounds geranyl acetate (41.1%), caryophyllene oxide (9.1%), *trans*-methyl-isoeugenol (7.0%) and sabinene (4.3%). For *Daucus carota* subsp. *maximus*, the major compounds were *cis*-asarone (47.1%), geranyl acetate (14.8%) and elemicin (13.1%), similar with *Daucus carota* subsp. *carota* that presented as major compounds geranyl acetate (32.2%), *cis*-asarone (29.6%), *trans*-methyl-isoeugenol (9.8%) and α-pinene (6.5%). Finally, *Daucus carota* subsp. *sativus* has presented as major components carotol (53.8%) and daucol (26.7%). All subspecies presented, even though at some small percentage in some of them, geranyl acetate, *trans*-methyl-isoeugenol, *β*-bisabolene, caryophyllene oxide and *cis*-asarone, as shown in **Table 2.**

It has been reported that some variations occurred in comparison with the previous studies of different countries. Focussing on *Daucus carota* subsp. *maritimus* results

TABLE 1: Yield percentage (v/w)

Subspecies	Yield (%)
D. carota subsp. *maritimus*	0.39
D. carota subsp. *hispidus*	0.33
D. carota subsp. *maximus*	0.45
D. carota subsp. *carota*	0.23
D. carota subsp. *sativus*	0.06

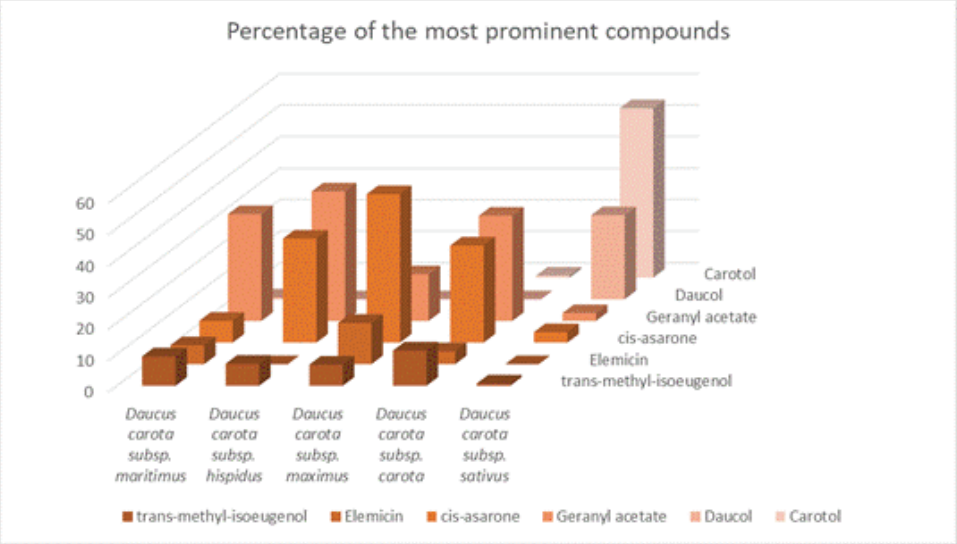

Figure 1: Percentage of the most prominent compounds in *Daucus carota* subspecies.

has shown that major components were geranyl acetate, *trans*-methyl-isoeugenol, α-pinene, *cis*-asarone and elemicin. Geranyl acetate and α-pinene as expected represented most of the compounds, such as elemicin, reported by Majdoub in [1], however, the concentrations of *trans*-methyl-isoeugenol and *cis*-asarone were higher than the ones in other countries. For *Daucus carota* subsp. *hispidus*, geranyl acetate was the major component, followed by caryophyllene oxide, *trans*-methyl-isoeugenol and sabinene. From the previous studies, *trans*-methyl-isoeugenol was the one who kept the most similar quantity compared to the Tunisian study. *Daucus carota* subsp. *maximus* appears to have as major components *cis*-asarone, geranyl acetate and elemicin, a very diverse constitution compared to the Italian oil, by Gaglio in [7], that presented as major component carotol, that was not traced in our oil and *β*-bisabolene, that only presented 3.9% of our oil. Comparing to the Portuguese study, geranyl acetate presented similar percentage, however *cis*-asarone presented a much higher quantity

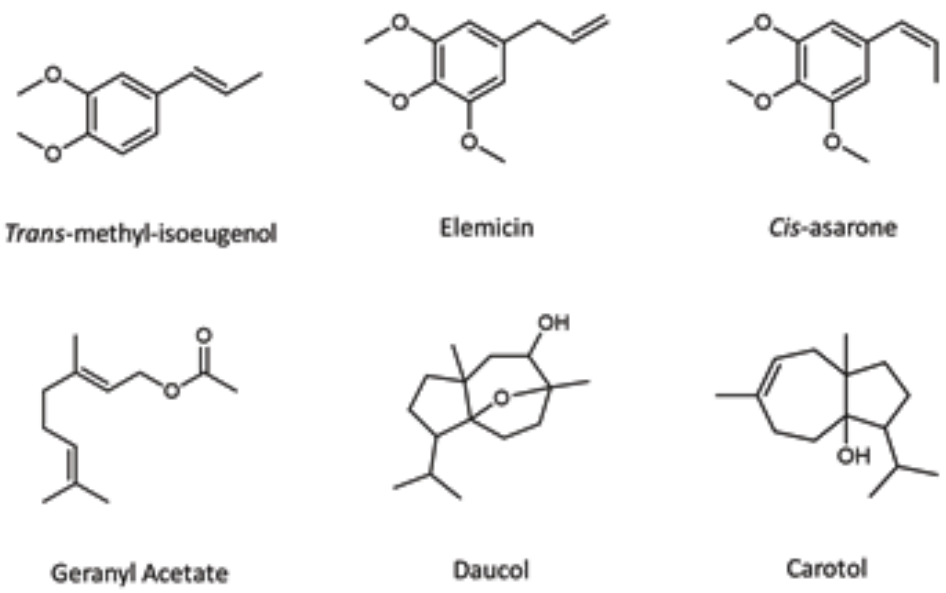

Figure 2: Structures of the most prominent compounds in *Daucus carota* subspecies.

and *trans*-methyl-isoeugenol a smaller percentage than the one referred, like α-pinene. *Daucus carota* subsp. *carota* presented as major components, geranyl acetate, *cis*-asarone, *trans*-methyl-isoeugenol and α-pinene. Comparing to the German study, by Sieniawska in [8], our oil percentage of carotol was significantly lower, not even being in the major components, being only similar the quantity of α-pinene. However, the previous Portuguese study presented a similar percentage of geranyl acetate, being the only concordance among the studies, since α-pinene in our oil presented a much smaller percentage and *cis*-asarone, the second most prominent component in our oil was not traced in the previous study. Finally, *Daucus carota* subsp. *sativus*, also presented different results, being carotol and daucol the most prominent components. According with the Indian study, carotol is the major component, however, it hasn't been described daucol as a major component in previous studies, and α-pinene, myrcene and limonene were not traced in our study.

Many outcomes indicate these variations in the percentage of the major components depend on the location, if they are wild or cultivated and stage of flowering, and for that reason, some diversity was observed to other studies. As stated for Snene [6], due to its nutritional and therapeutic values, the essential oil combination from *Daucus carota* subspecies from different countries all over the world show considerable quantitative and qualitative variability [6]. It is also considerable as a possible variation reason the harvesting stage. The extraction method can also be one of the causes of variety

		% *Daucus carota* subspecies				
Compounds	RI	*maritimus*	*hispidus*	*maximus*	*carota*	*sativus*
α - pinene	936	7.2	2.0	1.0	6.5	-
Camphene	950	0.5	-	-	-	-
Sabinene	973	1.5	4.3	2.3	1.2	-
β - pinene	978	5.5	1.7	1.9	4.2	-
β - myrcene	989	1.1	0.5	-	0.7	-
α -terpinene	1017	-	-	-	-	-
p - cymene	1024	0.3	0.4	-	-	-
Limonene	1029	2.0	1.3	0.9	1.1	-
γ-terpinene	1059	-	0.5	-	-	-
cis - Linalool Oxide (furanoid)	1075	0.5	-	-	0.7	-
trans - Linalool Oxide (furanoid)	1083	0.3	-	-	-	-
α - terpinolene	1086	-	-	-	-	-
Linalol	1099	2.2	1.7	-	1.2	-
α - campholenol	1124	0.3	0.7	-	-	-
trans - Pinocarveol	1140	1.2	3.3	0.8	0.9	-
trans - Verbenol	1144	0.3	3.3	-	-	-
cis - Verbenol	1145	1.7	2.3	-	1.3	-
Sabina ketone	1157	-	0.7	-	-	-
Pinocarvone	1160	0.6	1.0	-	-	-
p-mentha-1,5-dien-8-ol	1166	0.5	0.5	-	-	-
4-Terpineol	1177	0.4	2.4	1.5	-	1.3
α - terpineol	1189	0.5	-	-	-	-
Myrtenal	1192	1.3	3.2	-	-	-
Verbenone	1206	0.6	-	-	-	-
Carvone	1242	-	0.4	-	-	-
Linalyl acetate	1255	1.9	-	-	-	-
Bornyl acetate	1283	-	0.9	-	-	-
α - terpinenyl acetate	1347	0.4	-	-	-	-
Geranyl acetate	1379	33.9	41.1	14.8	32.2	2.5
β - selinene	1486	0.3	-	-	0.8	-
trans - methyl - isoeugenol	1495	9.3	7.0	6.8	9.8	0.7
β - bisabolene	1508	3.4	4.0	3.9	2.2	0.5
Elemicin	1553	6.0	-	13.1	4.1	-
Spathulenol	1576	-	0.4	-	-	0.3
Caryophyllene oxide	1581	1.9	9.1	4.5	2.5	1.2
Carotol	1595	2.2	-	-	0.7	53.8
Daucol	1639	0.6	-	-	-	26.7
cis - asarone	1679	6.9	3.3	47.1	29.6	3.3

Figure 3: Main components found in the analysed Daucus carota subspecies.

in these components, as we can see in Madjdoub study, different percentage of the components were presented, depending on the extraction method used [1].

The percentage of some of the most prominent compounds and its distribution per each subspecies are present as visual representation in **Figure 1** and in **Figure 2** their structures.

4. Conclusions

Essential oils obtained by hydrodistillation of umbels from five subspecies of Portuguese *Daucus carota* L. were analysed by gas chromatography-mass spectrometry (GC-MS). A total of 38 compounds were identified. For three subspecies (*maritimus*; *hispidus* and *carota*), high levels of geranyl acetate are found. *Daucus carota* subsp. *maximus* presented *cis*-asarone as main compound but geranyl acetate is the second main component and elemicin the third. *Daucus carota* subsp. *sativus* has more than 50% of carotol and daucol as second main compound. Knowing the amount of geranyl acetate present in these oils, and considering the therapeutic value of monoterpenes like it, we could use these oils due to its pharmacological properties, in cases off inflammation, pain-related and antioxidant effects [11]. Previous studies also demonstrated that both carotol and daucol present high antifungal activity, probably due to its polar groups, which can be a good indicator that *Daucus carota* subsp. *sativus* essential oil might be a good antifungal oil [12].

Acknowledgments

We acknowledge *the Banco Português de Germoplasma Vegetal* for providing our plant samples. This research was funded by Fundação para a Ciência e a Tecnologia, FCT, through the funding of the UID Fiber Materials and Environmental Technologies (FibEnTech-UBI), project UIDB/00195/2020.

References

[1] Majdoub S, El Mokni R, Muradalievich AA, Piras A, Porcedda S, Hammami S. Effect of pressure variation on the efficiency of supercritical fluid extraction of wild carrot (*Daucus carota* subsp. maritimus) extracts. Journal of Chromatography B: Analytical Technologies in the Biomedical and Life Sciences. 2019;1125:121713;1-6. https://doi.org/10.1016/j.jchromb.2019.121713

[2] Khalil N, Ashour M, Fikry S, Singab AN, Salama O. Chemical composition and antimicrobial activity of the essential oils of selected apiaceous fruits. Future Journal of Pharmaceutical Sciences. 2018;4(1):88–92. https://doi.org/10.1016/j.fjps.2017.10.004

[3] Ng TB, Fang EF, Li X, Lu Q, Wong JH, Guo H. Essential oils in food preservation, flavor and safety. *In Essential Oils in Food Preservation, Flavor and Safety*. Elsevier Inc; 2015;34;303-308 https://doi.org/10.1016/B978-0-12-416641-7.00034-1

[4] Spooner, DM. Daucus : Taxonomy, Phylogeny, Distribution. in *The Carrot Genome* 2019 ; 9–26. https://doi:10.1007/978-3-030-03389-7_2.

[5] Tavares AC, Loureiro J, Castro S et al. Assessment of *Daucus carota* L. (apiaceae) subspecies by chemotaxonomic and DNA content analyses. Biochemical Systematics and Ecology. 2014;55 :222–230. https://doi.org/10.1016/j.bse.2014.03.031

[6] Snene A, Mokni R, El Mahdhi A, Joshi RK, Hammami S. Comparative study of essential oils composition and in vitro antibacterial effects of two subspecies of *Daucus carota* growing in Tunisia. South African Journal of Botany. 2020;130:366–370. https://doi.org/10.1016/j.sajb.2020.01.028

[7] Gaglio R, Barbera M, Aleo A, Lommatzsch I, La Mantia T, Settanni L. Inhibitory activity and chemical characterization of *Daucus carota* subsp. maximus essential oils. Chemistry and Biodiversity. 2017;14(5);1-6. https://doi.org/10.1002/cbdv.201600477

[8] Sieniawska E, Świątek Ł, Rajtar B, Kozioł E, Polz-Dacewicz M, Skalicka-Woźniak K. Carrot seed essential oil—Source of carotol and cytotoxicity study. Industrial Crops and Products. 2016;92:109–115. https://doi.org/10.1016/j.indcrop.2016.08.001

[9] Verma RS, Padalia RC, Chauhan A. Chemical composition variability of essential oil during ontogenesis of *Daucus carota* L. subsp. sativus (Hoffm.) Arcang. Industrial Crops and Products. 2014;52:809–814. https://doi.org/10.1016/j.indcrop.2013.12.012

[10] Azmir J, Zaidul ISM, Rahman MM et al. Techniques for extraction of bioactive compounds from plant materials: A review. Journal of Food Engineering. 2013;117(4):426–436. https://doi.org/10.1016/j.jfoodeng.2013.01.014

[11] Khayyat SA, Sameeh MY. Bioactive epoxides and hydroperoxides derived from naturally monoterpene geranyl acetate. Saudi Pharmaceutical Journal. 2018;26(1):14–19. https://doi.org/10.1016/j.jsps.2017.11.005

[12] Sharma M, Chahal KK, Kaur R, Singh R, Kataria D. Antifungal potential and structure activity relationship of carrot seed constituents. Journal of Food Biochemistry. 2019;43(9):1–9. https://doi.org/10.1111/jfbc.12971

KnE Materials Science

FibEnTech21
1st International FibEnTech Congress (FibEnTech21) New opportunities for fibrous materials in the ecological transition
Volume 2022

Knowledge E
enriching | engaging | empowering

Research article

Chemical Characterization of Essential Oils With a Biocide Base for Conservation and Restoration

Cecília Baptista[1,2]*, Luís Santos[2,3], Maria Emília Amaral[4,5], and Lúcia Silva[4,5]

[1]Engineering Unit, PolytechnicInstitute of Tomar, Campus da Quinta do Contador, 2300-313 Tomar, Portugal
[2]Techn&Art Research Centre, PolytechnicInstitute of Tomar, Campus da Quinta do Contador, 2300-313 Tomar, Portugal
[3]Archaeology, Conservation and Restoration and Heritage Unit, PolytechnicInstitute of Tomar, Campus da Quinta do Contador, 2300-313 Tomar, Portugal
[4]Department of Chemistry, University of Beira Interior, Rua Marquês d'Ávila e Bolama, 6201-001 Covilhã, Portugal
[5]Fiber Materials and Environmetal Technologies (FibEnTech), University of Beira Interior, Rua Marquês d'Ávila e Bolama, 6201-001 Covilhã, Portugal

Abstract.
Essential oils (EOs) are acclaimed for their antimicrobial properties, leading to their multiple applications in various fields. In this work, four aromatic plants were used, namely thyme (*Thymus mastichina)*, everlasting (*Helychrysum stoechas* Moench*)*, European pennyroyal (*Mentha pulegium*) and fennel (*Foeniculum vulgare* Mill.*)*. Hydrodistillation was the extraction method used, and the obtained extracts were composed of a variety of volatile molecules, mainly terpenoids and phenylpropenoids. The EO yields were determined, and the chemical composition of these natural products was obtained by gas chromatography-mass spectrometry (GC-MS) analysis. The yields varied greatly, in the range of 0.99 to 4.27% (v/w). The two major chemical constituents of the EOs analysed by GC-MS were as follows: thyme – 1,8-cineole and champhor; everlasting – α-pinene and limonene; European pennyroyal – pulegone and isomenthone; fennel – trans-anethole and limonene. This preliminary study is an important contribution to the understanding of EO bioactive compounds that are under investigation to establish their ability to control the biocolonization of cultural heritage.

Keywords: aromatic plants, chemical characterization, essential oils, green biocides

Corresponding Author: Cecília Baptista; email: cecilia@ipt.pt

Dates
?????

Publishing services provided by Knowledge E

© Cecília Baptista et al. This article is distributed under the terms of the Creative Commons Attribution License, which permits unrestricted use and redistribution provided that the original author and source are credited.

Selection and Peer-review under the responsibility of the FibEnTech21 Conference Committee.

OPEN ACCESS

1. Introduction

Humans since prehistorical times left us a cultural heritage as a legacy, which due, mostly to biodeterioration, requires conservation and, in many cases, restoration. The 21st Century enlightened politicians and scholars alike onto the importance of preserving such a patrimony, resulting on the investment in research and education from which most chemical and mechanical biodeterioration solutions we use nowadays arose. On the other hand, the 21st Century brought, along with a tourism boom, environmental concerns which lead to many studies on the safety and sustainability of chemicals used in

Conservation and Restoration of cultural heritage elements [1]. Cultural asset safeguard combined with the purpose of cultural heritage use and enhancement are mechanisms to value the large Portuguese historical heritage and to promote the Tourism Industry. Following this protective action, various conservation and restoration interventions aim to minimize the degradation of different materials where the artistic expressions are externalised. Biodeterioration, as the unwanted alterations of various materials, mainly caused by microorganisms, can be observed in art and architectural works holding patrimonial value. This phenomenon is primarily attributed to the proliferation of various microorganisms (bacteria, fungi, algae, lichens) that, alone or in association, through their energy-producing metabolisms, lead to the formation of acidic substances that can attack the physicochemical structures of support [2-4]. This structural degradation encompasses mechanical damages through substrate breakage or cohesion decrease, chemical alterations due to metabolites chemical action and aesthetic damages by the breeding of patinas or crusts. These alterations are directly linked to the climatic and environmental conditions to which the artwork is exposed [5].

In conservation and restoration, different compounds of synthetic origin are traditionally used, however they can exhibit human and environmental toxicity, and cause adverse effects on treated materials. The traditional biocides can be divided into four different groups: pesticides, disinfectants, preservatives, and other biocidal products [6]. For instance, quaternary ammonium compounds, phenols, aldehydes, and alcohols are a clear example of disinfectants, with temporary results and long-term damage to the preserved artifacts [2,7,8]. Environmental awareness, side effects of disinfectants and inhibitors led to the need for new materials with biocidal effects. Biocides with a wide spectrum of activity and low cost, favouring natural materials derived from plants, such as essentials oils (EOs) which are generally attributed to easy handling environmental stability and lower toxicities are currently preferred [9-11]. Several plants were already studied with this purpose in different geographies, namely *Origanum vulgare* L., *Thymus vulgaris* L., *Thymus capitatus* L., *Cymbopogon khasans*, *Pimpinella anisum* L., *Syzygium aromaticum* L., *Cuminum cyminum* L., *Allium sativum* L., *Laurus nobilis* L., and *Citrus sinensis* (L.) Osbeck, [12-17]. The EOs contain a wide variety of secondary metabolites able to act against several biological systems. The complex mixture that constitutes essential oils can comprise dozens of compounds, belonging to different families of lipids, including hydrocarbons, alcohols, esters, aldehydes and ketones, phenols, phenolic ethers, and terpenes. The analysis of essential oils shows that terpenes exhibit the highest relative abundance and subgroups such as monoterpenes, sesquiterpenes and diterpenes, among others, can be distinguished. In general, the most abundant

constituent confers the biological activity of the essential oil, although this activity often results from a synergistic action between several constituents [18]. These compounds may be presented as environmentally acceptable pesticides, acting on the microbial cell by different mechanisms such as growth inhibition, cytoplasmic membrane deterioration, metabolism regulation throughout disturbance of enzymatic reactions, affecting the enzyme's synthesis or behaviour. Some isolated chemical components of essential oils have also been studied to prevent biocolonization and improve heritage conservation, such as Thymol, Menthol, Linalool, Eucalyptol, Cinnamaldehyde, Eugenol, Cuminaldehyde, Limonene, Citral, Citronellol, among many others [10,19, 20].

Environmental concerns along with the need to replace synthetic biocides in Conservation, originated the core idea for a global project (NatBio Project – Natural Biocides for Sustainable Heritage Conservation) which primary goal is the development of new natural materials extracted from endemic or naturalized plants that can be used as biocides in the preservation of cultural and artistic heritage. Altogether the project encompasses several phases and diverse activities starting with the collection of plants, extraction, purification, and characterization of extracts (including EOs). Tests to evaluate biocide potential - *in vitro* laboratory tests and *in situ* tests on monuments are foreseen. Ecotoxicological tests will be carried out aiming the determination of extract solutions' toxicity. Two Portuguese iconic heritage sites will also be intervened during this Project. As main results it is intended to study a group of aromatic plants, to select those whose extract will exhibit higher biocide potential, from which it is possible to formulate an ecological biocide with evident results in the preservation of stone and ceramic materials. The Project combines a team of 14 transdisciplinary researchers from multiple Institutions.

The current paper is part of the early stages of NatBio Project, involving the need to study and analyse the biocide potential of several plants. The focus relies on essential oils obtained by hydrodistillation in a Clevenger type-apparatus from four endemic aromatic plants. The yields in EOs extractions were ascertained and the chemical composition of these natural products was established by GC-MS analysis. Subsequent tests on organic solvent extracts and ulterior assessment of biocide potential of all the extracts are being carried out.

2. Material and methods

Raw materials – Four aromatic plants, belonging to different genera, holding different major compounds, and recognised by their antiseptic properties were selected for this

study. From Asteraceae family the *Helichrysum stoechas* (L.) Moench (common name Everlasting; portuguese name Perpétuas-das-areias), from Lamiaceae family the *Thymus mastichina* L. (common name Thyme; portuguese name Bela-luz or Amor-de-Deus) and the *Mentha pulegium* L. (common name European Pennyroyal; portuguese name Poejo), and finally from Apiaceae family the *Foeniculum vulgare* Mill. (common name Fennel; portuguese name Funcho-amargo). These plants are autochthonous in the national territory, and their essential oils (EOs) are already industrially produced for the market with other purposes. These products can be applied in pharmaceutical, cosmetic and food industries, besides the usage in wellness aromatherapy or agricultural disinfestation.

The plants were provided by D'Alenguadiana Company located in Cortes-Sines, Mértola, Alentejo, harvested in Canais do Guadiana. Collecting was performed in their respective flowering seasons, namely: everlasting and thyme – June; european pennyroyal – July; fennel – August. For the essential oil extraction tests, the entire aerial part of the plants was used, cut at about 15 cm from the ground to allow its renewal in the following year.

Extraction method – Aerial parts of the plants were manually cut in small pieces of 2 cm long and 100 g of each sample were extracted with 2 L of distilled water in a Clevenger type-apparatus, during 2 h. After the extraction, the essential oils' volumes were measured for yield determination.

Chemical characterization – A sample of each EO was prepared to gas chromatographic-mass spectral (GC-MS) analysis, dissolving 50 µL of the EO in 2 mL of Dichloromethane. The EOs analysis [21] were performed using an Agilent 7890 CG coupled with an Agilent 5975 C inert XL mass selective detector (MSD) and an Agilent ChemStation data system. The MSD was operated under the following conditions: electron impact EI mode (with an electron energy of 70 eV, scan range of 50-500 amu and a scan rate of 3.99 scans/sec. The separation conditions included a DB-5MS fused silica capillary GC column, constituted by a (5% phenyl)-polymethylsiloxane stationary phase, film thickness of 0.25 µm and an internal diameter of 0.25 mm. The carrier gas was helium, and the column head pressure was 48.7 kPa and a flow rate of 1.0 mL/min. Temperature profile: injector temperature – 250°C, oven initial temperature – 60°C for 5 minutes; temperature rise – 10°C/min until 250°C. The GC was operated with an injection volume of 1 µL and a split ratio of 1:50. The identification of components was ascertained by comparison of the retention times and mass spectra with those of the pure standard compounds. All mass spectra were also compared with those of the data system library NIST and Wiley.

3. Results and discussion

The antimicrobial activity of essential oils is recognized, however, there aren't sufficient studies concerning their usage in conservation of the cultural heritage. For this reason, the present study is dedicated to four Iberian aromatic plants and respective essential oils extracted by hydrodistillation. The yield of the essential oil obtained from *Helichrysum stoechas* was 0.99% (v/w). This value is higher than 0.04%, obtained by Vernin & Poite [22]. For *Thymus mastichina* the obtained yield was 3.76% (v/w) which is in accordance with the yields reported by other authors – from 0.4% to 6.90% (v/w) [23]. The yield obtained from *Mentha pulegium* was 4.27% (v/w). The present result is clearly above 1.6% reported for this species from Turkey [24] and 2.34% for aerial parts of european pennyroyal collected from Algeria [25]. The yield of the EOs of *Foeniculum vulgare* was 1.19% (v/w), which is in accordance with the results showed by Mota *et al.* [21], mainly regarding the species from de Center and South of mainland. Other authors reported an yield of 2.5% (v/w) obtained also by hydrodistillation method [26].

The yield and chemical composition of the EOs can change from plant to plant due to many factors such as abiotic and biotic, location and growing conditions, postharvest treatment, conservation, and extraction conditions [18]. These factors could explain the results presented in this study.

The chemical characterization of the essential oils was performed by GC-MS analysis. The chromatograms are depicted in Figure 1 and the quantitative results are summarized in Table 1. A total of 14 components were identified in the EO of *Thymus mastichina*, which represented 98.13% of the total oil. The main component was 1,8-Cineole (55.72%). The other components present in significant percentage were Camphor (13.29%), Borneol (7.21%) and Camphene (6.19%). These four major compounds correspond to 82.41% of total oil. The chemical composition obtained for the EOs of the analysed thyme is identical to that mentioned by Rodrigues *et al*. [23], mainly for the leaves, leaves and flowers and aerial parts of the plants harvested in the flowering phase, at Algarve, where most of the samples exhibited 1,8-Cineole as the principal compound, representing about 50% of thyme EO composition.

In the case of EO of *Helichrysum stoechas*, three compounds were identified (99.43% of total oil). The main components were ⍁-Pinene (85.65%) and Limonene (13.62%) that constitutes aproximately the entire oil (99.27%). These contents are similar to the reported by Vernin & Poite [22], where the major components were α-Pinene and Limonene, despite the smallest amount reported for the former (63% and 14%, respectively) and the absence of compounds like β-Caryophyllene and α-Humulene.

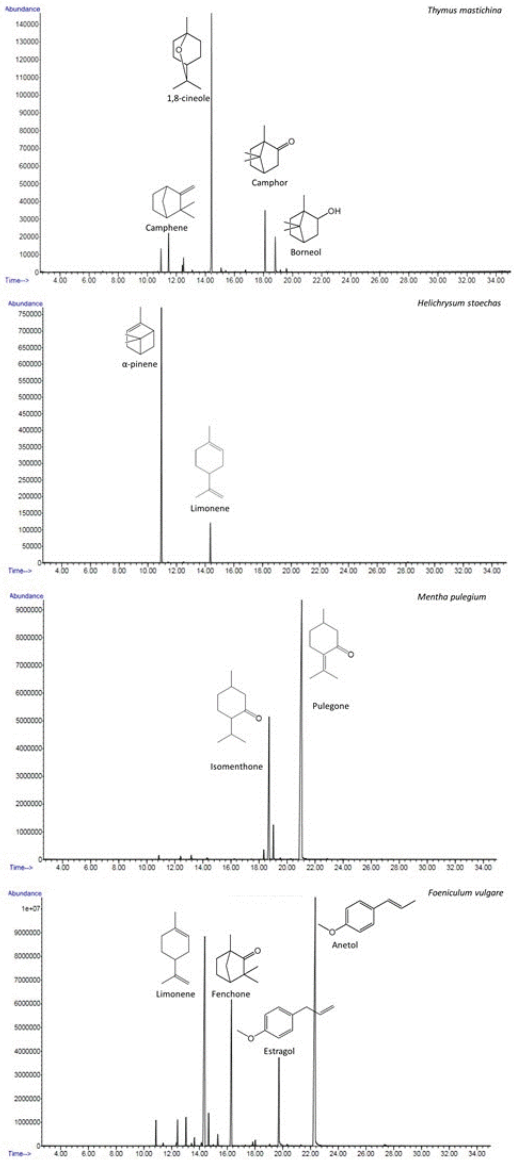

Figure 1: Chromatograms of the Essential Oils of the used aromatic plants.

In *Mentha pulegium* EO a total of 17 components were identified, fulfilling 99.48% of its oil. The main components found were Pulegone (70.02%) and Isomenthone (21.99%), followed by the isomers *trans*-Isopulegone (3.90%) and Menthone (1.10%). These four monoterpenes combined totalize 97.01% of the oil. Previous studies with the same plant harvested in other locations and continents reported Menthone and Pulegone as the major components of the essential oil, although some discrepancies in relative amounts. However, considering the results summarized in [27], there is some consistency between the present results and particular cases of european pennyroyal species of Portugal and Greece.

Table 1: Relative chemical composition (%) of Essential Oils from the used aromatic plants.

		Thymus mastichina L.	Helichrysum stoechas (L.) Moench	Mentha pulegium L.	Foeniculum vulgare Mill.
RI *	**Compound**	%	%	%	%
936	α-Pinene	4.78	85.65	0.44	1.70
950	Camphene	6.19	0.16		0.24
973	Sabinene	1.22		0.08	0.22
978	β-Pinene	2.95		0.36	1.74
989	β-Myrcene			0.04	1.88
993	Octan-3-ol			0.58	
1004	α-Phelandrene				0.19
1011	δ-3-Carene				0.56
1022	m-Cymene				0.34
1030	Limonene		13.62	0.18	26.84
1032	1,8-Cineole	55.72		0.15	
1038	β-*cis*-Ocimene				2.10
1048	β-*trans*-Ocimene	1.29			
1060	γ-Terpinene	1.21			0.82
1088	Fenchone			0.07	14.94
1099	Linalool	1.18			
1138	Limonene oxide				0.31
1143	Camphor	13.29			0.43
1151	Menthone			1.10	
1159	Isomenthone			21.99	
1166	Borneol	7.21			
1176	*trans*-Isopulegone			3.90	
1177	Terpinen-4-ol	1.18			0.16
1190	α-Terpineol	1.47		0.25	
1196	Estragol				7.22
1217	*trans*-Carveol				0.20
1234	Pulegone			70.02	
1284	Bornyl acetate	0.40			
1285	Anethole				40.00
1289	Lavandulyl acetate	0.04			
1341	Piperitenone			0.15	
1420	*trans*-Caryophylene			0.03	
1453	α-Humulene			0.08	
1480	γ-Curcumene				0.09
1481	Germacrene D			0.06	

* RI- retention index on GC column; blank spaces correspond to an absence or compound traces.

Foeniculum vulgare EO presented the higher number of constituents, totalizing 19 different compounds and the amount of 99.98% of the oil. The compound with higher relative abundance is *trans*-Anethole (40.00%), followed by Limonene (26.84%), Fenchone (14.94%) and Estragol (7.22%). All the other constituents are presented in tiny amounts below 2.10%. These results are according to the composition detected by Mota *et al*. [21].

4. Conclusions

The essential oils yields were found to vary greatly in the range of 0.99 to 4.27% (v/w). The two major chemical constituents of the essential oils analysed by GC/ MS were as follows: thyme – 1,8-Cineole and Champhor; everlasting – α-Pinene and Limonene; european pennyroyal – Pulegone and Isomenthone; fennel – *trans*-Anethole and Limonene. Overall yields, somehow differ from literature, allowing some room for in depth research into the most adequate collection sites and later study of viability of production and use. Considering the chemical compounds present in the essential oils of the four analysed plants, the existence of a bactericidal and fungicidal effect is predicted as described in Fidanza & Caneva [20]. For this reason, studies are being carried out to prove its antimicrobial activity in specific case studies. If the biocidal effect is verified, it may be considered that these natural pesticides (green biocides) hold potential as a valid alternative to the currently available methods for the biodeterioration control of cultural heritage.

5. Acknowledgments

The authors wish to thank Techn&Art Research Centre for the NatBio Project financial support, D'Alenguadiana Company for kindly supplying us with the necessary aromatic plants and Maria Inês Girão, a 3^{rd} year Chemical Technology Degree student from IPT, for the help to carry out the extraction essays.

References

[1] Allsopp D. Worldwide wastage: The economics of biodeterioration Applied Microbiology and Biotechnology 2011;38:150–153. https://doi.org/10.1007/s00253-013-5283-1

[2] Meng H, Katayama Y, Gu JD. More wide occurrence and dominance of ammonia-oxidizing archaea than bacteria at three Angkor sandstone temples of Bayon, Phnom Krom and Wat Athvea in Cambodia. International Biodeterioration & Biodegradation. 2017;117:78–88. https://doi.org/10.1016/j.ibiod.2016.11.012

[3] Sterflinger K, Piñar G. Microbial deterioration of cultural heritage and works of art-tilting at windmills. Applied Microbiology and Biotechnology. 2013;97:9637–9646. https://doi.org/10.1007/s00253-013-5283-1

[4] Farooq M, Hassan M, Gull F. Mycobial deterioration of stone monuments of Dharmarajika. Taxila. Journal of Microbiology & Experimentation 2015;2(1):29–33. https://doi.org/10.15406/jmen.2015.02.00036

[5] Liu X, Meng H, Wang Y, Katayama Y, Gu JD. Water is a critical factor in evaluating and assessing microbial colonization and destruction of Angkor sandstone monuments. International Biodeterioration & Biodegradation 2018;133:9–16. https://doi.org/10.1016/j.ibiod.2018.05.011

[6] Ashraf MA, Ullah S, Ahmad I, Qureshi AK, Balkhair KS, Rehman MA. Green biocides, a promising technology: Current and future applications to industry and industrial processes. Journal of the Science of Food and Agriculture 2014;94:388–403. https://doi.org/10.1002/jsfa.6371

[7] Mateus DMR, Silva RB, Costa FMC, Coroado JPF. Microbiological diversity in the Unfinished Sacristy building of the Convent of Christ, Tomar, and evaluation of its biocide-based control. Conservar Património 2013;17:11-20. https://doi.org/10.14568/cp2012005

[8] Zhang X, Ge Q, Zhu Z, Deng Y, Gu JD. Microbiological community of the Royal Palace in AngkorThom and Beng Mealea of Cambodia by illumina sequencing based on 16S rRNA gene. International Biodeterioration & Biodegradation 2018;134:127–135. https://doi.org/10.1016/j.ibiod.2018.06.018

[9] Céspedes CL, Alarcon JE, Aqueveque P, Seigler DS, Kubo I. In the search for new secondary metabolites with biopesticidal properties. Israel Journal of Plant Sciences 2015;62(4):216–228. https://doi.org/10.1080/07929978.2015.1006424

[10] Jeong SH, Lee HJ, Kim DW, Chung YJ. New biocide for eco-friendly biofilm removal on outdoor stone monuments. International Biodeterioration & Biodegradation 2018;131:19–28. https://doi.org/10.1016/j.ibiod.2017.03.004

[11] Kakakhel MA, Wu F, Gu JD, Feng H, Shah K, Wang W. Controlling biodeterioration of cultural heritage objects with biocides: A review. International Biodeterioration & Biodegradation 2019;143:1047721-1047731. https://doi.org/10.1016/j.ibiod.2019.104721

[12] Palla F, Bruno M, Mercurio F, Tantillo A, Rotolo V. Essential oils as natural biocides in conservation of cultural heritage. Molecules. 2020;25 (730): 1-11. https://doi.org/10.3390/molecules25030730

[13] Casiglia S, Bruno M, Scandolera E, Senatore F, Senatore F. Influence of harvesting time on composition of the essential oil of *Thymus capitatus* (L.) Hoffmanns. & Link. Growing wild in northern Sicily and its activity on microorganisms affecting historical art crafts. Arabian Journal of Chemistry 2015;12:2704-2712. http://dx.doi.org/10.1016/j.arabjc.2015.05.017

[14] Mishra PK, Shukla R, Singh P, Prakash B, Kedia A, Dubey NK. Antifungal, anti-aflatoxigenic, and antioxidant efficacy of Jamrosa essential oil for preservation of herbal raw materials. International Biodeterioration & Biodegradation 2012;74:11-16. http://dx.doi.org./10.1016/j.biod.2012.06.026

[15] Walentowska J, Foksowicz-Flaczyk J. Thyme essential oil for antimicrobial protection of natural textiles. International Biodeterioration & Biodegradation 2013;84:407-411. http://dx.doi.org./10.1016/j.biod.2012.06.028

[16] Pietrzak K, Otlewska A, Danielewicz D et al. Disinfection of archival documents using thyme essential oil, silver nanoparticles misting and low temperature plasma. Journal of Cultural Heritage 2017;24:69-77. http://dx.doi.org/10.1016/j.culher.2016.10.011

[17] Borrego S, Valdés O, Vivar I et al. Essential oils of plants as biocides against microorganisms isolated from Cuban and Argentine documentary heritage. International Scholarly Research Network ISRN Microbiology. 2012; 826786: 1-7. https://doi.org/10.5402/2012/826786

[18] da Cunha PA, Roque OR, Nogueira MT. Plantas aromáticas e óleos essenciais - Composição e aplicações. Lisboa: Fundação Calouste Gulbenkian; 2012.

[19] Veneranda M, Blanco-Zubiaguirre L, Roselli G, Di Girolami G, Castro K, Madariaga JM. Evaluating the exploitability of several essential oils constituents as a novel biological treatment against cultural heritage biocolonization. Microchemical Journal 2018;138:1-6. https://doi.org/10.1016/j.microc.2017.12.019

[20] Fidanza MR, Caneva J. Natural biocides for the conservation of stone cultural heritage: A review. Journal of Cultural Heritage 2019;38:271-286. http://doi.org/10.1016/j.culher.2019.01.005

[21] Mota AS, Martins MR, Arantes S et al. Antimicrobial activity and chemical composition of the essential oils of Portuguese *Foeniculum vulgare* fruits. Natural Products and Communication 2015;10(4):673–676. https://doi.org/10.1177/1934578X1501000437

[22] Vernin G, Poite JC. GC/MS analysis of volatile components of everlasting (*Helichrysum stoechas* L.) essential oil. Journal of Essential Oil

Research1998;10(5):553-557. https://doi.org/10.1080/10412905.1998.9700969

[23] Rodrigues M, Lopes AC, Vaz F et al. *Thymus mastichina*: Composition and biological properties with a focus on antimicrobial activity. Pharmaceuticals. 2020;13(479): 1-26. https://doi.org/10.3390/ph13120479

[24] Yasa H, Onar HC, Yusufoglu AS. Chemical composition of the essential oil of *Mentha pulegium* L. from Bodrum, Turkey. Journal of Essential Oil Bearing Plants 2013;15(6):1040-1043. https://doi.org/10.1080/0972060X.2012.10662609

[25] Ouakouak H, Chohra M, Denane M. Chemical composition, antioxidant activities of the essential oil of *Mentha pilegium* L., South East of Algeria. International Letters of Natural Sciences 2015;39:49-55. https://doi.org/10.18052/www.scipress.com/ILNS.39.49

[26] Yamini Y, Sefidkon F, Pourmortazavi SM. Comparison of essential oil composition of Iranian fennel (*Foeniculum vulgare*) obtained by supercritical carbon dioxide extraction and hydrodistillation methods. Flavour and Fragrance Journal 2002;17(5):345-348. https://doi.org/10.1002/ffj.1117

[27] Teixeira B, Marques A, Ramos C et al. European pennyroyal (*Mentha pulegium*) from Portugal: Chemical composition of essential oil and antioxidant and antimicrobial properties of extracts and essential oil. Industrial Crops and Products 2012;36:81-87. https://doi.org/10.1016/j.indcrop.2011.08.011

KnE Materials Science

FibEnTech21
1st International FibEnTech Congress (FibEnTech21) New opportunities for fibrous materials in the ecological transition
Volume 2022

Knowledge E
enriching | engaging | empowering

Research article

Degradation of C. I. Direct Red 80 by the Electro-Fenton Process

Boaventura Borges[1], Ana Baía[1,2]*, Ana Lopes[1,2], Maria José Pacheco[1,2], Lurdes Ciríaco[1,2], and Annabel Fernandes[1,2]

[1]Department of Chemistry, University of Beira Interior, R. Marquês de D'Ávila e Bolama, 6201-001 Covilhã Portugal
[2]Fiber Materials and Environmental Technologies (FibEnTech-UBI), University of Beira Interior, R. Marquês de D'Ávila e Bolama, 6201-001 Covilhã Portugal

Abstract.
Essential oils (EOs) are acclaimed for their antimicrobial properties, leading to their multiple applications in various fields. In this work, four aromatic plants were used, namely thyme (*Thymus mastichina)*, everlasting (*Helychrysum stoechas* Moench*)*, European pennyroyal (*Mentha pulegium*) and fennel (*Foeniculum vulgare* Mill.*)*. Hydrodistillation was the extraction method used, and the obtained extracts were composed of a variety of volatile molecules, mainly terpenoids and phenylpropenoids. The EO yields were determined, and the chemical composition of these natural products was obtained by gas chromatography-mass spectrometry (GC-MS) analysis. The yields varied greatly, in the range of 0.99 to 4.27% (v/w). The two major chemical constituents of the EOs analysed by GC-MS were as follows: thyme – 1,8-cineole and champhor; everlasting – α-pinene and limonene; European pennyroyal – pulegone and isomenthone; fennel – trans-anethole and limonene. This preliminary study is an important contribution to the understanding of EO bioactive compounds that are under investigation to establish their ability to control the biocolonization of cultural heritage.

Keywords: aromatic plants, chemical characterization, essential oils, green biocides

Corresponding Author: Ana Baía
email:
ana.isabel.mota.baia@ubi.pt

Dates
?????

Publishing services provided by Knowledge E

© Boaventura Borges et al.. This article is distributed under the terms of the Creative Commons Attribution License, which permits unrestricted use and redistribution provided that the original author and source are credited.

Selection and Peer-review under the responsibility of the FibEnTech21 Conference Committee.

OPEN ACCESS

1. Introduction

Freshwater contamination by synthetic dyes is a global environmental concern. According to the literature, there are more than 100,000 commercially available dyes, with an estimated annual production of more than 7×10^5 tonnes, which are used by different types of industry, such as textile, papermill, cosmetic, pharmaceutical, food industry, among others [1]. As a result, large volumes of wastewater, containing high concentrations of dyes, are daily produced, being aesthetic and with potential toxicity and carcinogenicity [2].

The degradation of synthetic dyes by conventional wastewater treatment processes is often ineffective, and thus, the development of new treatment technologies, capable of degrading these contaminants into non-toxic and biodegradable products, is required [2]. The application of electrochemical processes to degrade synthetic dyes has

received great attention in the last years, due to the high potential of these processes to eliminate different types of organic compounds, including compounds with recalcitrant properties [1]. Among them, the electro-Fenton (EF) process, an electrochemical process based on Fenton's reaction (Eq. (1)), has stood out due to the promising results achieved [3,4].

$Fe^{2+} + H_2O_2 \rightarrow Fe^{3+} + HO^{\cdot} + HO^{-}$ (1)

In the EF process, the organic compounds are oxidised by the hydroxyl radicals produced in the Fenton reaction, being the H_2O_2 continuously electrogenerated *in situ* through the reduction of oxygen gas injected into a carbon cathode, generally carbon-felt (Eq. (2)). The H_2O_2 formed is decomposed to $HO^{\cdot}$ by the Fenton reaction (Eq. (1)). In this electrochemical process, Fe^{3+} is reduced at the cathode, generating Fe^{2+}, which results in a higher degradation rate of organic pollutants than the traditional Fenton process [5]. Iron sulfate or chloride are the most common iron sources for EF process, but, in the recent years, the use of heterogeneous iron sources, such as pyrite (FeS_2) and chalcopyrite ($CuFeS_2$), have gained significant attention [6].

$O_2 + 2H^{+} + 2e^{-} \rightarrow H_2O_2$ (2)

According to the literature, the efficiency of the EF process can be further enhanced by utilizing a high O_2-overpotential anode, such as boron-doped diamond (BDD) anode, being the organic compounds additionally oxidised through adsorbed hydroxyl radicals (BDD($HO^{\cdot}$)), formed as an intermediate of the anodic water discharge (Eq. (3)) [5,6].

$BDD + H_2O \rightarrow BDD(HO^{\cdot}) + H^{+} + e^{-}$ (3)

The aim of the present work was to evaluate the feasibility of EF process, using a BDD anode, to degrade the azo dye C. I. Direct Red 80 (DR80), and to study the influence of different operational parameters, namely the applied current density (*j*) and the iron source, on the effectiveness of the treatment.

2. Material and methods

The DR80 aqueous solutions were prepared with ultrapure water, using Direct Red 80, dye content 25% (CAS Number 2610-10-8), purchased from Sigma-Aldrich. Iron(III) sulfate pentahydrate, 97% (CAS Number 10028-22-5), ferric chloride hexahydrate, 97% (CAS Number 10025-77-1), and iron(III) oxide, 96% (CAS Number 1309-37-1), were also purchased from Sigma-Aldrich. Chalcopyrite was mined from Jendouba (Tunisia) and presented an iron content of 30.6%. Its preparation and characterization are described elsewhere [6]. The DR80 solutions studied in this work were prepared to contain an

initial concentration of 50 mg L^{-1} of DR80 and 10 mg L^{-1} of iron. The composition of the different solutions is presented in Table 1.

Table 1: Composition of the DR80 aqueous solutions used in the experiments.

Reagent	DR80 + Iron sulfate	DR80 + Ferric chloride	DR80 + Iron oxide	DR80 + Chalcopyrite
Direct Red 80 (mg L^{-1})	201 ± 2	202 ± 3	201 ± 1	200 ± 2
$Fe_2(SO_4)_3.5H_2O$ (mg L^{-1})	45.1 ± 0.4	–	–	–
$FeCl_3.6H_2O$ (mg L^{-1})	–	49.0 ± 0.3	–	–
Fe_2O_3 (mg L^{-1})	–	–	29.0 ± 0.4	–
Chalcopyrite (mg L^{-1})	–	–	–	789 ± 1

The EF experiments were conducted in batch mode, using an undivided and cylindrical glass cell, with a useful volume of 200 mL. During the experiments, the solution was continuously stirred, with a magnetic bar, to enhance the mass transport of reactants/products toward/from the electrodes. A carbon-felt piece (Carbone Loraine) with a thickness of 0.5 cm and an immersed area of 136 cm^2 was used as cathode, and a BDD electrode (Neocoat), with an immersed area of 20 cm^2, was used as anode. The anode was centered in the cell and surrounded by the cathode, which covered the inner wall of the cell. Continuous O_2 saturation at atmospheric pressure was ensured by bubbling compressed air through a fritted glass diffuser at 1 L min^{-1}, starting 10 min before the assay, to reach a steady O_2 concentration that allowed H_2O_2 electrogeneration (Eq. (2)).

The experimental setup utilized a DC power supply GW, Lab DC, model GPS-3030D (0–30 V, 0–3 A), being the anodic current densities studied 12.5, 25, and 50 A m^{-2}. At 12.5 A m^{-2}, experiments were performed with 2, 4, and 8 h duration (180, 360, and 720 C, respectively). To apply the same electric charge (180, 360, and 720 C) to the experiments run at 25 A m^{-2}, these assays had 1, 2, and 4 h duration, respectively, and at 50 A m^{-2} had 0.5, 1, and 2 h duration. The initial and final solutions from each experiment were utilized for DR80, chemical oxygen demand (COD), total carbon (TC), inorganic carbon (IC), total organic carbon (TOC), total dissolved iron (TDI), dissolved Fe^{2+}, H_2O_2, pH, and conductivity determinations.

COD determinations were performed according to the standard methods [7]. TC, IC, and TOC were measured in a Shimadzu TOC-V CPH analyser. DR80 concentration was spectrophotometrically determined at 526.5 nm. TDI and dissolved Fe^{2+} determinations followed the 1,10-phenanthroline method [8]. H_2O_2 concentration was determined by the colorimetric metavanadate method [9].

3. Results and discussion

The characterization of the DR80 aqueous solutions used in this study is presented in Table 2. It can be seen that, although the solutions were prepared to have 10 mg L^{-1} of iron, the initial dissolved Fe^{3+} concentration, in the solutions prepared with the iron salts, was much lower, indicating that the iron salts were not completely solubilized during the initial stage of the solutions preparation. In fact, for the solutions prepared with iron oxide, a solid residue was observed along all the EF experiments duration, corresponding to non-dissolved iron oxide. For the solutions prepared with the heterogeneous iron source, chalcopyrite, a residual Fe^{3+} concentration was detected during the samples characterization, since, in this case, iron is slowly released from the mineral source during the experiments.

The initial pH of the solutions prepared with iron sulfate and ferric chloride was around 3-4, which is the optimum pH for the EF process, due to its influence on iron speciation and on H_2O_2 decomposition [5,6]. However, the solutions prepared with iron oxide and chalcopyrite presented a higher initial pH, especially the solution prepared with iron oxide.

Table 2: Characterization of the DR80 aqueous solutions used in the experiments.

Parameter	DR80 + Iron sulfate	DR80 + Ferric chloride	DR80 + Iron oxide	DR80 + Chalcopyrite
DR 80 (mg L^{-1})	52 ± 3	54 ± 2	52 ± 1	55 ± 3
Fe^{3+} (mg L^{-1})	3.4 ± 0.1	3.3 ± 0.5	0.7 ± 0.1	0.6 ± 0.2
COD (mg L^{-1})	74 ± 1	76 ± 2	75 ± 3	76 ± 2
TC (mg L^{-1})	23.0 ± 0.9	25.9 ± 0.7	25.8 ± 0.4	24.6 ± 0.5
IC (mg L^{-1})	0.4 ± 0.1	0.5 ± 0.1	1.3 ± 0.1	0.6 ± 0.2
TOC (mg L^{-1})	22.6 ± 0.9	25.4 ± 0.6	24.5 ± 0.4	24.0 ± 0.6
pH	3.67 ± 0.04	3.54 ± 0.05	6.74 ± 0.09	4.85 ± 0.05
Conductivity (μS cm^{-1})	372 ± 6	362 ± 9	256 ± 5	297 ± 8

Fig. 1 presents the DR80 relative concentration decay with applied electric charge for the EF experiments performed with different iron sources, at different applied current densities. At the lowest *j* studied, 12.5 A m^{-2}, the experiments performed with iron sulfate and ferric chloride presented the highest DR80 removal rates, being the results of these two iron sources similar. After 2 h of assay (180 C), the DR80 removal was 91% for the solutions prepared with iron sulfate and ferric chloride, being 79% and 54%, respectively, for the solutions prepared with chalcopyrite and iron oxide. After 4 h of

assay (360 C), for all the solutions studied, the DR80 concentration was inferior to 1 mg L^{-1}.

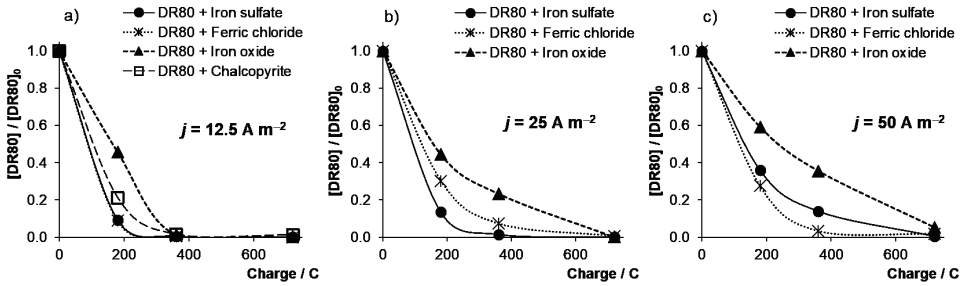

Figure 1: DR80 relative concentration decay with applied electric charge, for the EF experiments performed with different iron sources at: (a) 12.5 A m^{-2}, (b) 25 A m^{-2}, and (c) 50 A m^{-2}.

With the increase in *j* to 25 A m^{-2}, the DR80 removal rate decreased for all the iron sources studied, being this decrease more pronounced in the experiments with ferric chloride than in the experiments with iron sulfate. However, when *j* was further increased to 50 A m^{-2}, an increase in the DR80 removal rate was observed for the experiments performed with ferric chloride, compared to 25 A m^{-2}, although a decrease in the DR80 removal was observed for experiments performed with iron sulfate and iron oxide. These DR80 removal results can be explained by the Fe^{2+} concentration evolution in solution along the experiments (Fig. 2).

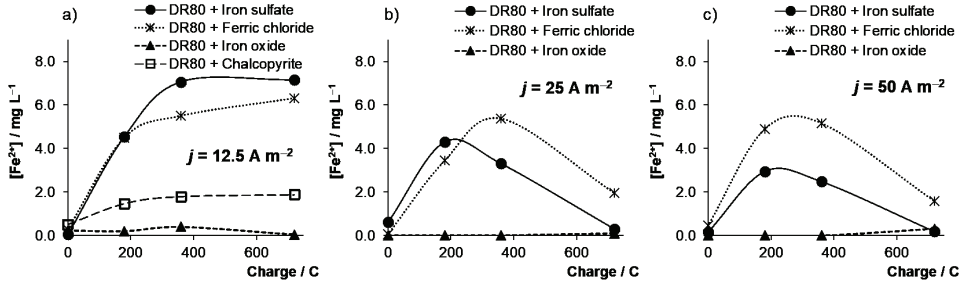

Figure 2: Dissolved Fe^{2+} concentration evolution with applied electric charge, for the EF experiments performed with different iron sources at: (a) 12.5 A m^{-2}, (b) 25 A m^{-2}, and (c) 50 A m^{-2}.

In fact, solutions prepared with iron sulfate and ferric chloride are those with higher concentrations in dissolved Fe^{2+} and, the higher the Fe^{2+} concentration, the larger the extension of the Fenton reaction and, consequently, the higher the concentration of hydroxyl radicals available for oxidation. Focusing on the applied charge of 180 C, where the highest DR80 removal occurs for all the experimental conditions studied, it can be seen that, at 12.5 A m^{-2}, solutions prepared with iron sulphate and ferric chloride present similar Fe^{2+} concentration; at 25 A m^{-2}, Fe^{2+} concentration is higher for the solution with iron sulfate; but at 50 A m^{-2}, the highest Fe^{2+} concentration is presented by the solution with ferric chloride. The Fe^{2+} concentration also explains the lower

DR80 removals obtained with iron oxide, since, in these solutions, Fe^{2+} concentration was practically zero.

At 25 and 50 A m^{-2}, a decrease in Fe^{2+} concentration is observed after a certain point of the experiments performed with iron sulfate and ferric chloride. This can be due to parallel sulfate and chloride oxidation reactions that inhibit the Fe^{2+} regeneration reaction. In fact, analysing the TDI evolution (Fig. 3), no decrease in the TDI concentration is found for these experiments, indicating that the iron in solution is in the form of Fe^{3+}.

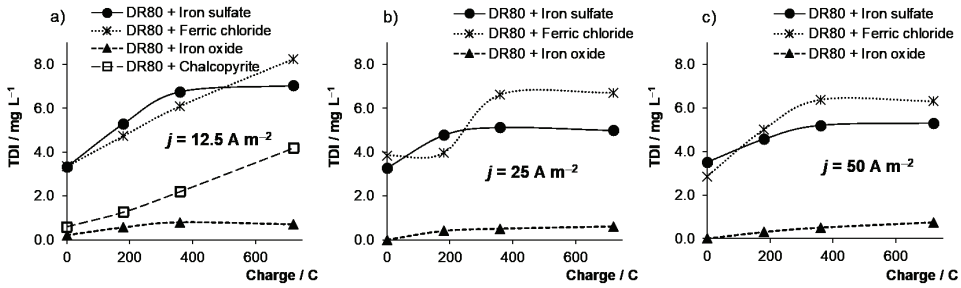

Figure 3: TDI concentration evolution with applied electric charge, for the EF experiments performed with different iron sources at: (a) 12.5 A m^{-2}, (b) 25 A m^{-2}, and (c) 50 A m^{-2}.

In Fig. 3, it can also be seen that TDI concentration was higher in the experiments performed at 12.5 A m^{-2}, which can be explained by the fact that, at this *j*, the experiments had longer duration and therefore the release of iron in solution was enhanced.

Regarding the COD decay (Fig. 4), although the experiments performed with iron sulfate attained the highest COD removals for all the *j* studied, at 50 A m^{-2}, and until an applied electric charge of, approximately, 400 C, the COD removal rate of the experiments performed with ferric chloride was significantly higher than that of the experiments with iron sulfate.

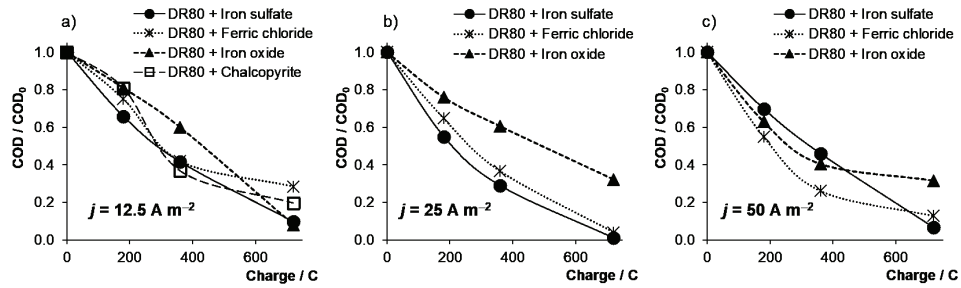

Figure 4: COD relative decay with applied electric charge, for the EF experiments performed with different iron sources at: (a) 12.5 A m^{-2}, (b) 25 A m^{-2}, and (c) 50 A m^{-2}.

This enhanced performance of the experiments run with ferric chloride at 50 A m^{-2}, also observed for the DR80 removal, probably results from the higher Fe^{2+} concentration found in the ferric chloride solution, as described above. Also, the additional

indirect oxidation of the pollutant load by oxidizing species, such as sulfate radical and hypochlorite, resulting from the oxidation of sulfate and chloride, may explain the COD removal in the last period of the experiments run at 25 and 50 A m^{-2}.

Iron oxide was the iron source that led to the lowest COD removals, except for the experiments performed at 12.5 A m^{-2}, where, despite initially presenting the lowest removal rate, it reached a final removal like that obtained with iron sulfate. Given the low dissolved Fe^{2+} concentration in the solutions prepared with iron oxide (Fig. 2), this high COD removal at 12.5 A m^{-2} is probably due to the organics oxidation by hydroxyl radicals formed from water electrolysis. In fact, the solutions prepared with iron oxide and chalcopyrite presented the highest pH values during the first period of assay (Fig. 5) and, according to the literature [1], hydroxyl radical generation from water electrolysis is favoured at higher pH values.

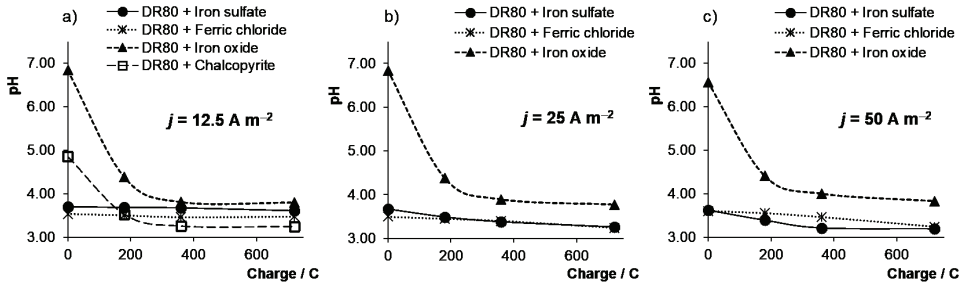

Figure 5: pH evolution with applied electric charge, for the EF experiments performed with different iron sources at: (a) 12.5 A m^{-2}, (b) 25 A m^{-2}, and (c) 50 A m^{-2}.

Fig. 6 presents the TOC relative concentration decay with applied electric charge for the EF experiments performed with different iron sources, at different applied current densities. At 12.5 A m^{-2}, the solution prepared with iron oxide is the one that presents the highest TOC removal, and consequently the one that attained the highest mineralization degree, followed by the solution prepared with chalcopyrite. These results agree with the organics oxidation by hydroxyl radicals produced from water electrolysis, since, according to the literature [1], the organics degradation through hydroxyl radicals, formed on the surface of the BDD anode by water oxidation, leads to higher mineralization degrees. For the highest applied current densities, 25 and 50 A m^{-2}, the iron source that led to the highest DOC removals was iron sulfate.

4. Conclusions

EF process, using a BDD anode and a carbon-felt cathode, is effective in DR80 degradation and in the pollutant load elimination. From the different iron sources studied,

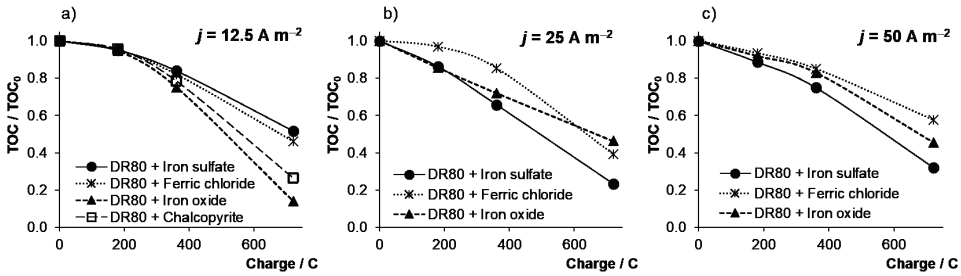

Figure 6: TOC relative decay with applied electric charge, for the EF experiments performed with different iron sources at: (a) 12.5 A m^{-2}, (b) 25 A m^{-2}, and (c) 50 A m^{-2}.

at the experimental conditions assayed, iron sulfate led to the best DR80 degradation results, followed by ferric chloride. Although DR80 removal was more efficient at the lowest applied current density, 12.5 A m^{-2}, attaining DR80 removals of 91% at 180 C, the same was not observed for COD and TOC removals, indicating that, at 12.5 A m^{-2}, the dye is not completely mineralized, but rather transformed into other by-products. Thus, to significantly reduce the solutions organic load it is necessary to increase the applied current density. The highest COD removals, 99% and 96%, were obtained, respectively, with iron sulfate and ferric chloride, at the applied current density of 25 A m^{-2}. Solutions prepared with iron oxide also led to high COD (92%) and TOC (86%) removals, mainly due to the anodic oxidation of the dye and its degradation products, and not to the electro-Fenton process. For this iron source, the solutions initial pH adjustment to pH 3 should increase the effectiveness of the electro-Fenton process. As for chalcopyrite, despite not showing the best results in any of the parameters evaluated, the results obtained with this natural mineral are quite promising. At 12.5 A m^{-2}, complete DR80 removal was attained after 4 h assay, and COD and TOC removals of 80% and 74%, respectively, were achieved after 8 h treatment. Given the observed pH values, these results might be improved if the initial pH of the solution is adjusted to values close to 3, the optimum pH value for the electro-Fenton process.

Acknowledgements

The authors are very grateful for the support given by research unit Fiber Materials and Environmental Technologies (FibEnTech-UBI), on the extent of the project reference UIDB/00195/2020, funded by the Fundação para a Ciência e a Tecnologia, IP/MCTES through national funds (PIDDAC).

References

[1] Brillas E, Martínez-Huitle CA. Decontamination of wastewaters containing synthetic organic dyes by electrochemical methods. An updated review. Applied Catalysis B: Environmental. 2015;166-167:603-643. https://doi.org/10.1016/j.apcatb.2014.11.016

[2] Lopes A, Martins S, Morão A, Magrinho M, Gonçalves I. Degradation of a textile dye C. I. Direct Red 80 by electrochemical processes. Portugaliae Electrochimica Acta. 2004;22:279-294. https://doi.org/10.4152/PEA.200403279

[3] Garcia-Segura S, El-Ghenymy A, Centellas F et al. Comparative degradation of the diazo dye Direct Yellow 4 by electro-Fenton, photoelectro-Fenton and photo-assisted electro-Fenton. Journal of Electroanalytical Chemistry. 2012;681:36-43. https://doi.org/10.1016/j.jelechem.2012.06.002

[4] Labiadh L, Oturan MA, Panizza M, Hamadi NB, Ammar S. Complete removal of AHPS synthetic dye from water using new electro-Fenton oxidation catalyzed by natural pyrite as heterogeneous catalyst. Journal of Hazardous Materials. 2015;297:34-41. https://doi.org/10.1016/j.jhazmat.2015.04.062

[5] Souiad F, Rodrigues AS, Lopes A, et al. Methiocarb degradation by electro-Fenton: Ecotoxicological evaluation. Molecules. 2020;25:5893. https://doi.org/10.3390/molecules25245893

[6] Ltaïef AH, Fernandes A, Nunes MJ et al. WASTES – Solutions, treatments and opportunities III. Selected papers from the 5th edition of the International Conference on Wastes: Solutions, Treatments and Opportunities, Caparica, Portugal, 4-7 September 2019. Vilarinho C, Castro F, Gonçalves M, editors. Leiden: CRC Press/Balkema; 2020. https://doi.org/10.1201/9780429289798

[7] Eaton A, Clesceri L, Rice E, Greenberg A, Franson MA. Standard methods for examination of water and wastewater. 21st ed. Washington, DC: American Public Health Association; 2005.

[8] ISO 6332, 1988. In water quality – Determination of iron – Spectrometric method using 1,10-Phenanthroline.

[9] Nogueira RFP, Oliveira MC, Paterlini WC. Simple and fast spectrophotometric determination of H_2O_2 in photo-Fenton reactions using metavanadate. Talanta. 2005;66:86-91. https://doi.org/10.1016/j.talanta.2004.10.001

[10] Brillas E, Sirés I, Oturan MA. Electro-Fenton process and related electrochemical technologies based on Fenton's reaction chemistry. Chemical Reviews. 2009;109:6570-6631. https://doi.org/10.1021/cr900136g

KnE Materials Science

FibEnTech21
1st International FibEnTech Congress (FibEnTech21) New opportunities for fibrous materials in the ecological transition
Volume 2022

Knowledge E
enriching | engaging | empowering

Research article

Diclofenac Photodegradation Under Visible Light With (La,Ba)(Fe,Ti)O_3 Perovskites

Ana Sofia Rodrigues, Lurdes Ciríaco, Maria José Pacheco, and Ana Lopes

FibEnTech and Departament of Chemistry, University of Beira Interior, Rua Marquês d'Ávila e Bolama, 6201-001, Covilhã, Portugal

Abstract.
Perovskites $BaTiO_3$ and $BaFeO_3$ were prepared by the ceramic and complex polymerization methods and the substituted perovskites $La_{0.2}Ba_{0.8}TiO_3$, $BaFe_{0.8}Ti_{0.2}O_3$, and $BaFe_{0.6}Ti_{0.4}O_3$ were prepared by the ceramic method. All of them were used as photocatalytic material for the degradation of the pharmaceutical diclofenac under visible light. The best diclofenac degradation results were obtained with the substituted perovskite $La_{0.2}Ba_{0.8}TiO_3$ (46%), prepared by the ceramic method, and with the non-substituted perovskite $BaFeO_3$ (43%), prepared by the complex polymerization method.

Keywords: visible light, perovskites, photocatalysis, (La,Ba)(Fe,Ti)O_3, diclofenac

Corresponding Author: Ana Sofia Rodrigues; email: ana.sf.rodrigues@ubi.pt

Dates
?????

Publishing services provided by Knowledge E

© Ana Sofia Rodrigues et al. This article is distributed under the terms of the Creative Commons Attribution License, which permits unrestricted use and redistribution provided that the original author and source are credited.

Selection and Peer-review under the responsibility of the FibEnTech21 Conference Committee.

OPEN ACCESS

1. Introduction

Perovskites are a class of compounds with the general formula ABX_3, where A is an alkali or alkaline earth metal or a member of the lanthanides' family, B is a transition metal, X is an anion, frequently an oxygen ion [1]. Perovskite oxides are characterized by their flexible chemical composition, structural stability, and elemental abundance. Approximately 90% of the Periodic Table metal elements can be accommodate in the perovskite structure, modifying the catalytic properties, without destroying the matrix structure [1,2].

Perovskite-type metal oxides are being increasingly investigated in various areas, namely as photocatalysts for water decontamination [2]. Photocatalysts are semi-conductors with band gap energy (Eg) between 1.4 and 3.8 eV, being activated by UV light for Eg<3 eV and by visible light for Eg>3 eV. However, perovskites optical properties may be changed by doping, inducing visible light absorption, allowing their utilization with visible light or even sunlight, a green, safe, and sustainable energy. Thus, for good-environmental practices, it is important to develop photocatalysts activated by visible light, to use the maximum potential of solar energy.

In this work, perovskites of the family (La,Ba)(Fe,Ti)O_3, namely $BaTiO_3$, $BaFeO_3$, $La_{0.2}Ba_{0.8}TiO_3$, $BaFe_{0.8}Ti_{0.2}O_3$ e $BaFe_{0.6}Ti_{0.4}O_3$ were synthetized and tested as photocatalysts. The influence of the chemical composition and of the preparation method on their

photocatalytic properties was assessed, using synthetic solutions of a model compound – Diclofenac (DIC). This pharmaceutical drug is of great environmental concern due to its occurrence and fate, and also due to the metabolites from its degradation in the human body [3]. Diclofenac was already detected in reservoirs for drinking water, and the European media of diclofenac occurrence in wastewater is 0.174 µg/L [3,4]. Diclofenac can be removed by many ways: biodegradation [5], sorption [6]; solar photo-Fenton reaction [7]; bioaugmentation [8]; ultrasound [9], electro-oxidation using BDD [10], electro-Fenton process [11]; pyrite catalysed Fenton oxidation [12], and activation of peroxymonosulfate by $LaFeO_3$ [13].

2. Material and methods

Perovskites $BaTiO_3$, $BaFeO_3$, $La_{0.2}Ba_{0.8}TiO_3$, $BaFe_{0.8}Ti_{0.2}O_3$ and $BaFe_{0.6}Ti_{0.4}O_3$ were synthetized by the ceramic method (MC) and $BaTiO_3$, $BaFeO_3$ were also synthesized by the complex polymerization method (PC).

For the synthesis using the ceramic method, stoichiometric amounts of commercial La_2O_3 (Acros Organics, +99.9%), $BaCO_3$ (Fluka, +99.0%), Fe_2O_3 (Merk, +99.0%) and TiO_2 (Aldrich, +99.8%) were weighed and milled for 30 min, pre-calcined at 900 °C for 6 h in a tubular furnace and calcined at 1130 °C for 4 h (adapted from [14]).

The perovskites synthesized by the complex polymerization method (adapted from [15,16]) were prepared with stoichiometric amounts of commercial $BaCO_3$ (Fluka, +99%), $C_{12}H_{28}O_4Ti$ (Acros Org., +98%) or $FeN_3O_9{\cdot}9H_2O$ (Sigma-Aldrich, 99.95%). For the preparation, $C_{12}H_{28}O_4Ti$ or $FeN_3O_9{\cdot}9H_2O$ are weighed, dissolved in ethylene glycol (Carlo Erba, +99,5%). After that, citric acid (Aldrich, +99%) is added, being ethylene glycol/ citric acid volumetric ratio 1:4. $BaCO_3$ is then added and the resulting mixture is submitted to successive heating: 50 °C, 90 °C, 150 °C; finally, at 400 °C, for 2 h, in a tubular furnace, with a heating rate of 5 °C/min, for the formation of a black precursor powder. The powder is then calcined at 900 °C, for 3 h (5 °C/min), milled for 15 min, calcined again at 900 °C, for 3 h (5 °C /min), and milled again for 15 min.

All the synthetized perovskites were characterized by X-ray diffraction, XRD, using a Rigaku diffractometer, model DMAX III/C, with automatic data acquisition (MDI, Materials Data), equipped with a monochromatized Cu kα radiation (λ = 0.15406 nm), operating at 40 mA and 30 kV. Dispersive energy spectroscopy (EDS) and scanning electron microscopy (SEM) were done in a Hitachi (S-3400N)/ Bruker system, operating at 20 keV.

In a setup [17] that allows simultaneous assays (Fig. 1), 10 mL diclofenac (25 ppm) aqueous solutions were submitted to photocatalytic degradation assays, performed in batch mode, with orbital stirring, for 6 h, under visible light (OSRAM, 300W).

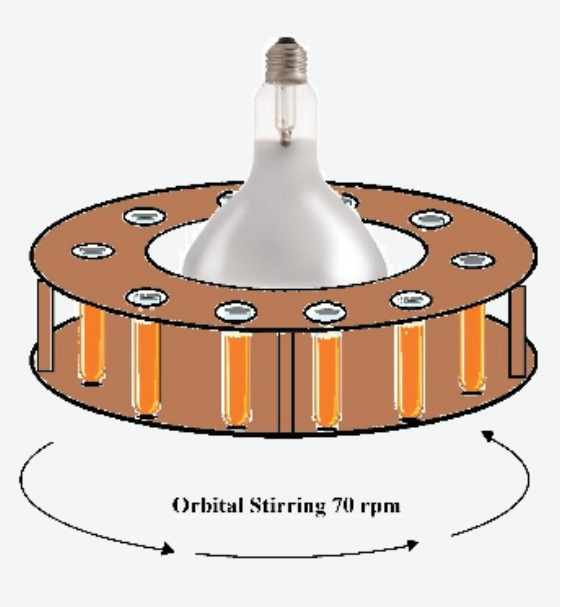

Figure 1: Setup for the photocatalytic assays [17].

The perovskites concentration in suspension was 250 ppm. After the photocatalytic assays, solutions were centrifuged, and the diclofenac degradation was monitored by UV/visible absorption spectrophotometry, with the spectra performed in a Shimadzu UV-1800 spectrophotometer. To determine ban gap energies for the different perovskites, diffuse reflectance spectra of the perovskite films were also obtained, in an UV–vis spectrometer Shimadzu UV-2600PC, equipped with an integrating sphere ISR 2600plus, over the spectral range 200–900 nm. Kubelka–Munk function was used to analyze the diffuse reflectance spectra. $BaSO_4$ was utilized as reflectance standard.

3. Results and discussion

The diffractograms of the prepared perovskite powders are presented in Fig. 2. Both $BaTiO_3$ MC and PC present cubic symmetry in a Pm3m space group. However, for $BaTiO_3$ PC there is evidence of another phase, an orthorhombic secondary phase of Ba_2TiO_4, probably due to the lower synthesis temperature utilized in the PC method.

$BaFeO_3$ MC presents a predominant tetragonal phase, with traces of secondary hexagonal and cubic phases. On the other hand, $BaFeO_3$ PC has a predominance of a cubic structure, although with traces of hexagonal and tetragonal secondary phases.

$La_{0.2}Ba_{0.8}TiO_3$ is the only one that exhibit monoclinic structure, and traces of reagent La_2O_3.

$BaFe_{0.8}Ti_{0.2}O_3$ and $BaFe_{0.6}Ti_{0.4}O_3$have hexagonal structure,but a new phase of $BaO(TiO_2)_2$ can be detected. This perovskite, without Fe may be the responsible for an higher EDS signal in Ti, indicating a higher concentration in Ti in the intended perovskite.

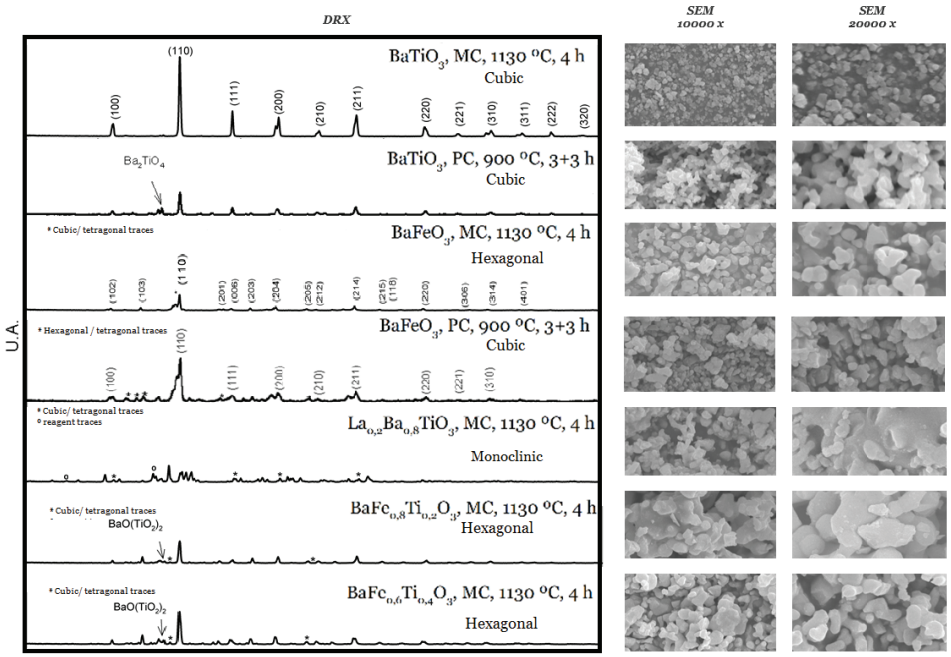

Figure 2: Results of the perovskites powders characterization by DRX and SEM.

Table 1 shows the crystallite size, cell parameters, band-gap energies (Eg) and EDS results for the perovskites prepared. $BaTiO_3$MC and $BaTiO_3$PC present cubic structure, with a cell parameter of approximately 0.4 nm. For this peroveskite, it seems that the preparation method does not to have any influence on the unit cell. Regarding $BaFeO_3$MC and $BaFeO_3$PC, the later perovskite presents a crystallite size of approximately half of the former perovskite. This must be due to the calcination temperature since higher temperature will allow the formation of a more developed crystallite.

Peroveskites presenting Eg<3 eV are $BaFeO_3$ MC, $BaFe_{0.8}Ti_{0.2}O_3$ MC and $BaFe_{0.6}Ti_{0.4}O_3$ MC, being promising for use in photocatalytic assays activated by visible light; the other perovskites present Eg>3 eV, being technically only activated by UV light. However, the existence of secondary phases, forming heterostructures, may someties allow their activation by visible light.

Figure ?? shows the results for DIC photocatalytic degradation tests. $BaFeO_3$ PC, presents the best results for the non-substituted perovskite. Regarding the perovskites

TABLE 1: Physical properties of perovskite powders prepared at different experimental conditions.

Perovskite	Crystallite size /nm	Cell param. / nm*	Eg / eV	EDS
$BaTiO_3$, MC,1130, 4h	55.16	a=4.007	3.24	$Ba_{0.85}Ti_{1.00}O_{3.15}$
$BaTiO_3$, PC 900, 3+3h	55.76	a=4.014	3.24	$Ba_{1.00}Ti_{1.05}O_{2.94}$
$BaFeO_3$, MC,1130, 4h	36.37	a=3.989 c=4.067	2.96	$Ba_{1.14}Fe_{1.07}O_{2.79}$
$BaFeO_3$, PC 900, 3+3h	19.87	a=4.005	3.61	$Ba_{1.04}Fe_1O_{2.96}$
$La_{0.2}Ba_{0.8}TiO_3$, MC,1130, 4h	55.28	a=3.997	3.47	$La_{0.23}Ba_{0.63}Ti_{0.94}O_{3.20}$
$BaFe_{0.8}Ti_{0.2}O_3$, MC,1149.93 4h		a=5.690 c=13.984	2.57	$Ba_{1.18}Fe_{0.64}Ti_{0.37}O_{2.81}$
$BaFe_{0.6}Ti_{0.4}O_3$, MC,1146.60 4h		a= 5.702 c=14.00	2.65	$Ba_{1.10}Fe_{0.36}Ti_{0.70}O_{2.84}$

*Determined using Holland TJB, Redfern SAT. Unicell, computer program, developed at the University of Cambridge, in 1995.

that underwent substitutions, it was found that 20% substitution of Ba by La causes an increase in the photocatalytic activity, surpassing the DIC removal value with $BaTiO_3$ and even with $BaFeO_3$. This perovskite maintained the cubic structure of $BaTiO_3$and the size of the crystallites did not vary significantly.

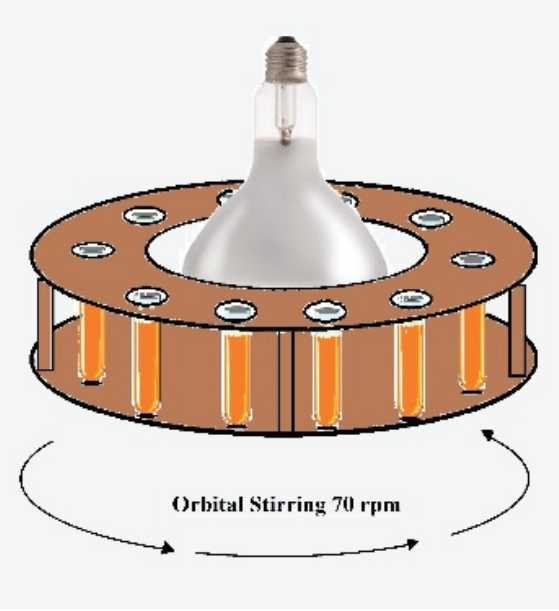

Figure 3: Results of Diclofenac degradation tests, after 6 h in a circular set-up, using different perovskites: (a,c) – UV-Vis absorbance spectra; (b,d) – DIC removal. [perov]=250ppm.

Removal of diclofenac was calculated based on its absorbance at 276 nm, where DIC presents an absorption maximum. The UV-Vis spectra show the formation of by-products that absorb at 240 nm, probably acetophenone [18]. However, this by-product also suffers degradation since the absorbance at this wavelength decreases as the assay proceeds.

4. Conclusions

Results show that perovskites of the family (La,Ba)(Fe,Ti)O_3 can be utilized as visible light-driven photocatalysts for diclofenac degradation, as well as for the degradation of the DIC by-products. The best DIC removal rates were attained with $La_{0.2}Ba_{0.8}TiO_3$ (46%), prepared by the ceramic method, and with $BaFeO_3$ (43%), prepared by the complex polymerization method. The results evidence that synthesized perovesquites are promising for use with natural sunlight for depuration of natural waters.

Acknowledgments

The authors acknowledge the financial support from Fundação para a Ciência e a Tecnologia, FCT, through the funding of the UID Fiber Materials and Environmental Technologies (FibEnTech), project UIDB/00195/2020, and for the grant SFRH/BD/109901/2015 awarded to A.S. Rodrigues.

References

[1] Zhu J, Li H, Zhong L et al. Perovskite oxides: Preparation, characterizations, and applications in heterogeneous catalysis. Acs Catalysis. 2014;4(9):2917-2940. https://doi.org/10.1021/cs500606g

[2] Grabowska E. Selected perovskite oxides: Characterization, preparation and photocatalytic properties - A review. Appl. Catal. B-Environ. 2016;186:97-126. https://doi.org/10.1016/j.apcatb.2015.12.035

[3] Rigobello ES, Dantas ADB, Di Bernardo L, Vieira EM. Removal of diclofenac by conventional drinking water treatment processes and granular activated carbon filtration. Chemosphere. 2013;92(2):184-191. https://doi.org/10.1016/j.chemosphere.2013.03.010

[4] Rabiet M, Togola A, Brissaud F, Seidel JL, Budzinski H, Elbaz-Poulichet F. Consequences of treated water recycling as regards pharmaceuticals and drugs in surface

and ground waters of a medium-sized Mediterranean catchment. Environmental Science & Technology. 2006;40(17):5282-5288. https://doi.org/10.1021/es060528p

[5] Gusmaroli L, Mendoza E, Petrovic M, Buttiglieri G. How do WWTPs operational parameters affect the removal rates of EU watch list compounds? Science of the Total Environment. 2020;714:136773. https://doi.org/10.1016/j.scitotenv.2020.136773

[6] Pérez-Estrada LA, Malato S, Gernjak W et al. Photo-Fenton degradation of diclofenac: Identification of main intermediates and degradation pathway. Environmental Science & Technology. 2005;39(21):8300-8306. https://doi.org/10.1021/es050794n

[7] Vieno N, Sillanpää M. Fate of diclofenac in municipal wastewater treatment plant—A review. Environment International. 2014;69:28-39. https://doi.org/10.1016/j.envint.2014.03.021

[8] Toufexi E, Dailianis S, Vlastos D, Manariotis ID. Mediated effect of ultrasound treated diclofenac on mussel hemocytes: First evidence for the involvement of respiratory burst enzymes in the induction of DCF-mediated unspecific mode of action. Aquatic Toxicology. 2016;175:144-153. https://doi.org/10.1016/j.aquatox.2016.03.017

[9] Zhao X, Hou Y, Liu H, Qiang Z, Qu J. Electro-oxidation of diclofenac at boron doped diamond: Kinetics and mechanism. Electrochimica Acta. 2009;54(17):4172-4179. https://doi.org/10.1016/j.electacta.2009.02.059

[10] Sadeghi M, Mehdinejad MH, Mengelizadeh N et al. Degradation of diclofenac by heterogeneous electro-Fenton process using magnetic single-walled carbon nanotubes as a catalyst. Journal of Water Process Engineering. 2019;31:100852. https://doi.org/10.1016/j.jwpe.2019.100852

[11] Bae S, Kim D, Lee W. Degradation of diclofenac by pyrite catalyzed Fenton oxidation. Applied Catalysis B: Environmental. 2013;134:93-102. https://doi.org/10.1016/j.apcatb.2012.12.031

[12] Rao Y, Zhang Y, Han F et al. Heterogeneous activation of peroxymonosulfate by LaFeO3 for diclofenac degradation: DFT-assisted mechanistic study and degradation pathways. Chemical Engineering Journal. 2018;352:601-611. https://doi.org/10.1016/j.cej.2018.07.062

[13] Han F, Ye X, Chen Q, Long H, Rao Y. The oxidative degradation of diclofenac using the activation of peroxymonosulfate by BiFeO3 microspheres—Kinetics, role of visible light and decay pathways. Separation and Purification Technology. 2020;232:115967. https://doi.org/10.1016/j.seppur.2019.115967

[14] Shao S, Zhang J, Zhang Z et al. High piezoelectric properties and domain configuration in BaTiO3 ceramics obtained through the solid-state reaction route. Journal

of Physics D: Applied Physics. 2008;41(12):125408. https://doi.org/10.1088/0022-3727/42/18/189801

[15] Vinothini V, Singh P, Balasubramanian M. Synthesis of barium titanate nanopowder using polymeric precursor method. Ceramics International. 2006;32(2):99-103. https://doi.org/10.1016/j.ceramint.2004.12.012

[16] Kakihana M, Okubo T, Arima M et al. Polymerized complex synthesis of perovskite lead titanate at reduced temperatures: Possible formation of heterometallic (Pb, Ti)-citric acid complex. Chemistry of Materials. 1997;9(2):451-456. https://doi.org/10.1021/cm9602353

[17] Rodrigues AS, Jorge MEM, Ciríaco L, Pacheco MJ, Lopes A. Perovskites (La,Ba)(Fe,Ti)O3: AO7 photocatalysis under visible light. Reviews on Advanced Materials Science. 2020;59(1):151-159. https://doi.org/10.1515/rams-2020-0012

[18] Silverstein R, Bassler GC, Morrill T. Identificação espectrofotométrica de compostos orgânicos E. LTC. São Paulo: Editora Guanabara Dois; 1994.

KnE Materials Science

FibEnTech21
1st International FibEnTech Congress (FibEnTech21) New opportunities for fibrous materials in the ecological transition
Volume 2022

Knowledge E
enriching | engaging | empowering

Research article

Photocatalytic Activity of $LaTi_{1-x}Fe_xO_3$ Perovskite-Type Oxides Under UV and Visible Light

Maria João Nunes[1*], André Rodrigues[2], Paulo Fiadeiro[3], Ana Lopes[1], Maria José Pacheco[1], and Lurdes Ciríaco[1]

[1]FibEnTech-UBI and Departament of Chemistry, Universidade da Beira Interior, Rua Marquês d'Ávila e Bolama, 6201-001, Covilhã, Portugal
[2]Departament of Chemistry, Universidade da Beira Interior, Rua Marquês d'Ávila e Bolama, 6201-001, Covilhã, Portugal
[3]FibEnTech-UBI and Departament of Physics, Universidade da Beira Interior, Rua Marquês d'Ávila e Bolama, 6201-001, Covilhã, Portugal

Abstract.
$LaTi_{1-x}Fe_xO_3$ (x = 0, 0.2, 0.4, 0.6, 0.8 and 1) perovskite-type oxide samples were synthesized by the solid state reaction method and characterized, and their photocatalytic activity was tested in the degradation of Acid Orange 7 under ultraviolet and visible light. The oxides were successfully synthesized and the XRD results showed a phase change from monoclinic to orthorhombic, with an increase in Fe content (x), with $LaTi_{0.8}Fe_{0.2}O_3$ and $LaTi_{0.6}Fe_{0.4}O_3$ samples presenting both phases. All samples presented low photocatalytic activity under visible light radiation, with a maximum Abs_{484nm} removal of 2.9% for $LaFeO_3$ after one hour. The best results were obtained under ultraviolet radiation, for all samples, with the best photocatalytic activity exhibited by the $La_2Ti_2O_7$ perovskite, with 44.6% Abs_{484nm} removal after one hour.

Keywords: perovskites, $LaTi_{1-x}Fe_xO_3$, photocatalysis, Acid Orange 7

Corresponding Author: Maria João Nunes; email: ?????

Dates
?????

Publishing services provided by Knowledge E

© Maria João Nunes et al. This article is distributed under the terms of the Creative Commons Attribution License, which permits unrestricted use and redistribution provided that the original author and source are credited.

Selection and Peer-review under the responsibility of the FibEnTech21 Conference Committee.

OPEN ACCESS

1. Introduction

Perovskite-type oxides belong to a family of ceramic compounds with a general formula ABO_3, where A and B are metallic inorganic cations, with $r_A > r_B$ [1,2]. They can occur in many structures, from triclinic to cubic, and are well-known for their versatile and flexible structure, capable of accommodating many cationic combinations without collapsing. This characteristic results in a large variety of properties and applications, such as photocatalysts in the degradation of organic pollutants [3]. The partial substitution of the metallic cations in the $LaFeO_3$ structure, with other elements, was found to improve its photocatalytic activity [4,5]. Hou et al [4] tested the influence of the partial substitution of La with Li, on the photocatalytic activity degradation of Methyl Blue under UV-Vis radiation. The substitution was found to increase the degradation rate of the dye, with

an optimum amount of Li of $La_{0.97}Li_{0.03}FeO_3$. Similarly, the presence of Ti, in the double-perovskite La_2FeTiO_6 was assumed to be responsible for the higher p-chlorophenol degradation under visible light, when compared with the results obtained with $LaFeO_3$ [5]. The aim of this work was to synthesize $LaTi_{1-x}Fe_xO_3$ perovskite-type oxides and test their photocatalytic activity in the degradation of the dye Acid Orange 7 (AO7), under UV and visible light.

2. Material and methods

$LaTi_{1-x}Fe_xO_3$ (x = 0, 0.2, 0.4, 0.6, 0.8 and 1) sample powders were synthesized by solid-state reaction. Stoichiometric amounts of La_2O_3 (Acros Organics, 99.9 %), TiO_2 (Aldrich, 99.5 %) and Fe_2O_3 (Merck, 99 %) were mechanically grinded in an agate mortar for 30 min, and heated at 900 °C, for 24 h. Followed by intermediate regrinding and another heating procedure at 1200 °C, for 24 h. All heating procedures were performed in a tubular furnace (Carbolite, model STF) with a Carbolite 3216 temperature controller. All powder samples were structurally characterized by X-ray diffraction (XRD), on a Rigaku, model DMAX II/C with automatic data acquisition (APD Philips v3.5B), equipped with a monochromatized Cu k_α radiation (λ = 0.15406 nm), operating at 40 mA and 30 kV. The recording conditions were 2θ between 10 and 90° at a scanning rate of 1.2°/min. The morphological characterization was performed by scanning electron microscopy (SEM), using a Hitachi S2700, operating at 20 keV. Diffuse reflectance spectra (DRS) were measured with a SPEC STD spectrometer (Sarspec), configured with a 25 µm slit, light source, reflectance probe, and reflectance standard, operating in the Ultraviolet/Visible range using a Deuterium Tungsten High Power. The band gap energies (E_g) were calculated from the diffuse reflectance values through the Kubelka-Munk function.

The powders photocatalytic activity was tested under UV and visible light, on the degradation of 10 mg L^{-1} aqueous solutions of AO7 dye (Sigma, 85 %), with radiation provided by a 7 W TUV PL-S lamp (Phillips), emitting at 254 nm, and a 300 W Ultra-Vitalux lamp (Osram), respectively. The 300 W lamp spectrum is shown in Fig.1. The AO7 dye solution volume used was of 10 mL and 160 mL for the photocatalytic assays performed under visible and UV light, respectively. The photocatalytic assays were performed with 0.5 g L^{-1} photocatalyst powder suspensions during 1 h. Prior to both radiation type assays, all suspensions were sonicated for 15 min and stirred, in the dark, for 45 min, to achieve the adsorption-desorption equilibrium between the photocatalyst's surface and AO7 molecules. The dye concentration was monitored by UV-visible absorption spectrophotometry (Shimadzu UV-1800).

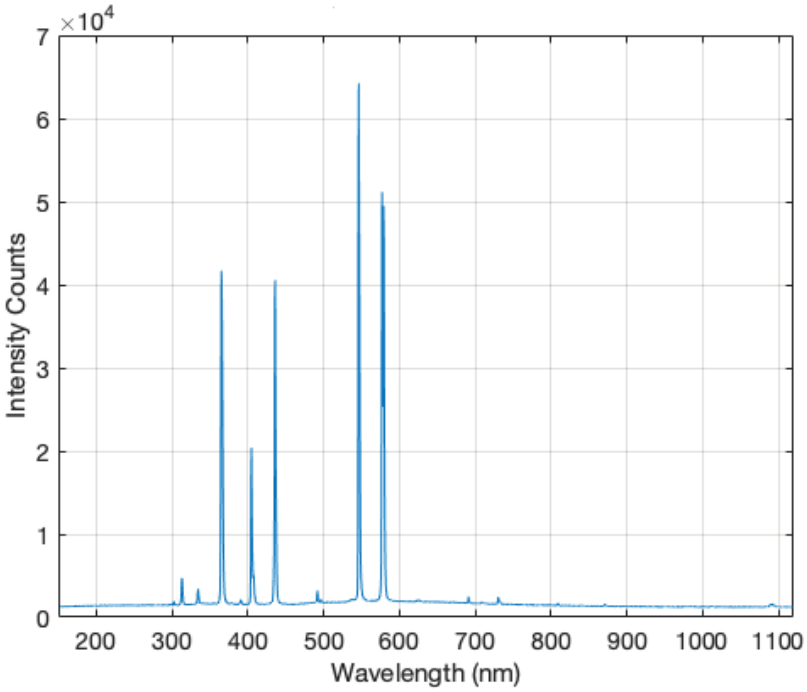

Figure 1: Emission spectrum of the 300 W Ultra-Vitalux UV-visible lamp.

3. Results and discussion

The XRD patterns for all synthesized powders are presented in Fig. 2. The diffractogram corresponding to the x = 0 exhibited a well crystallized phase belonging to the $La_2Ti_2O_7$ monoclinic structure, *P21/** space group (ICDD file PDF#28-0517). For the x = 1 oxide a single well-crystalized phase belonging to the $LaFeO_3$ orthorhombic structure, *Pbnm* space group (ICDD file PDF#74-2203) was obtained. With the increase of Fe content (x) a phase change is observed, from a monoclinic to an orthorhombic symmetry, as it can be observed in Fig. 2, through the change of peaks intensity and position. For some samples, such as x =0.2 and 0.4, both phases were present, but no extra phases were identified.

The morphological characterization results, done by SEM, are in Fig. 3. In these, it is possible to observe a heterogeneous morphology, with the occurrence of different sizes and shapes throughout all samples, with a tendency to agglomerate. It is also evident that the samples corresponding to $La_2Ti_2O_7$ and $LaFeO_3$ exhibit a bigger average grain size.

The E_g values were obtained through the application of the Kubelka-Munk function on the diffuse reflectance values. This procedure is represented in Fig. 4, with the extrapolation of the linear region of the $(F_{KM}h\nu)^2$ vs. hν plot to the abscissa axis for the

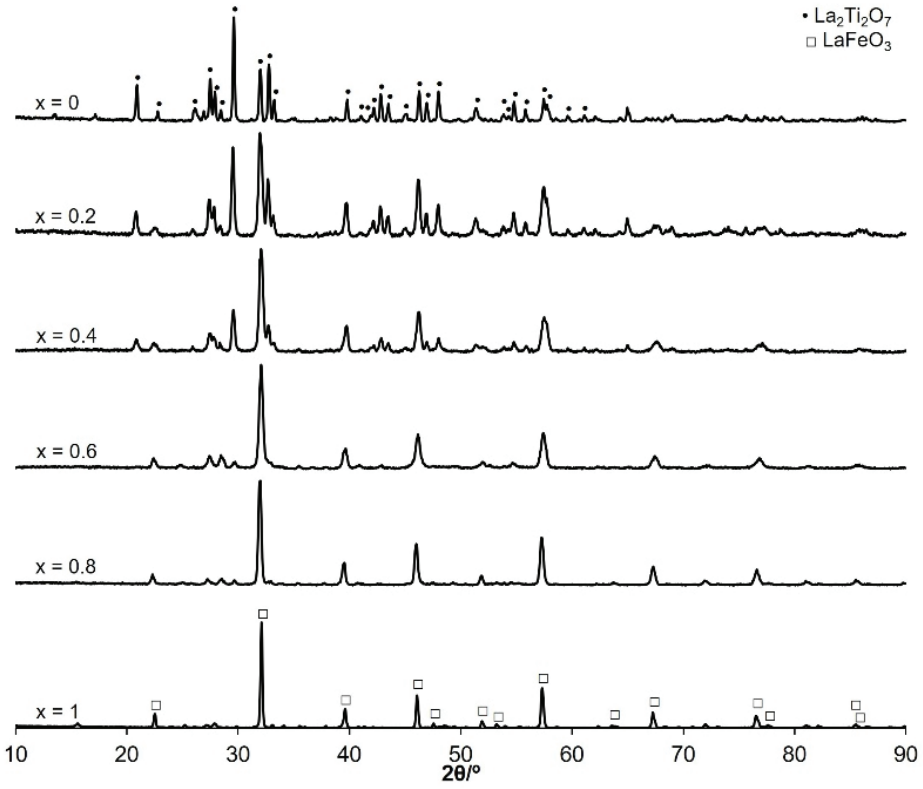

Figure 2: XRD patterns for the $LaTi_{1-x}Fe_xO_3$ oxides.

$La_2Ti_2O_7$ sample, obtaining the E_g value of 3.97 eV. The same procedure was applied for all samples, and all E_g values were obtained (Table 1). For the $LaTi_{0.8}Fe_{0.2}O_3$ and $LaTi_{0.6}Fe_{0.4}O_3$ samples two E_g values were obtained, this could be associated with the presence of two phases in both samples, one predominant, belonging to the monoclinic phase of the $La_2Ti_2O_7$, and one secondary, belonging to the orthorhombic phase of the $LaFeO_3$. For the rest of the samples, the E_g values decreases with the increase in Fe content. Regarding the color of the obtained powders, Table 1, the introduction of iron in the perovskite structure results in an orange-like coloration, that gets darker with the increase in Fe content.

The results from the photocatalytic degradation of AO7, under UV and visible light, are presented in Fig. 5. These results show that all synthesized samples do not exhibit favorable photocatalytic activity under visible light, with the best results obtained by the $LaFeO_3$ (x = 1) sample, with an Abs_{484nm} removal of 3%, after 1h. These results are in accordance with the high E_g values calculated, for most samples, with the best photocatalytic activity obtained for the oxide with the lowest E_g value. Regarding the results obtained under UV light irradiation, an improvement was observed for all samples, with Abs_{484nm} removals from 8% to 45%, the latter obtained by the $La_2Ti_2O_7$ (x = 0) perovskite. Further increase in assay time (data not shown) resulted in an

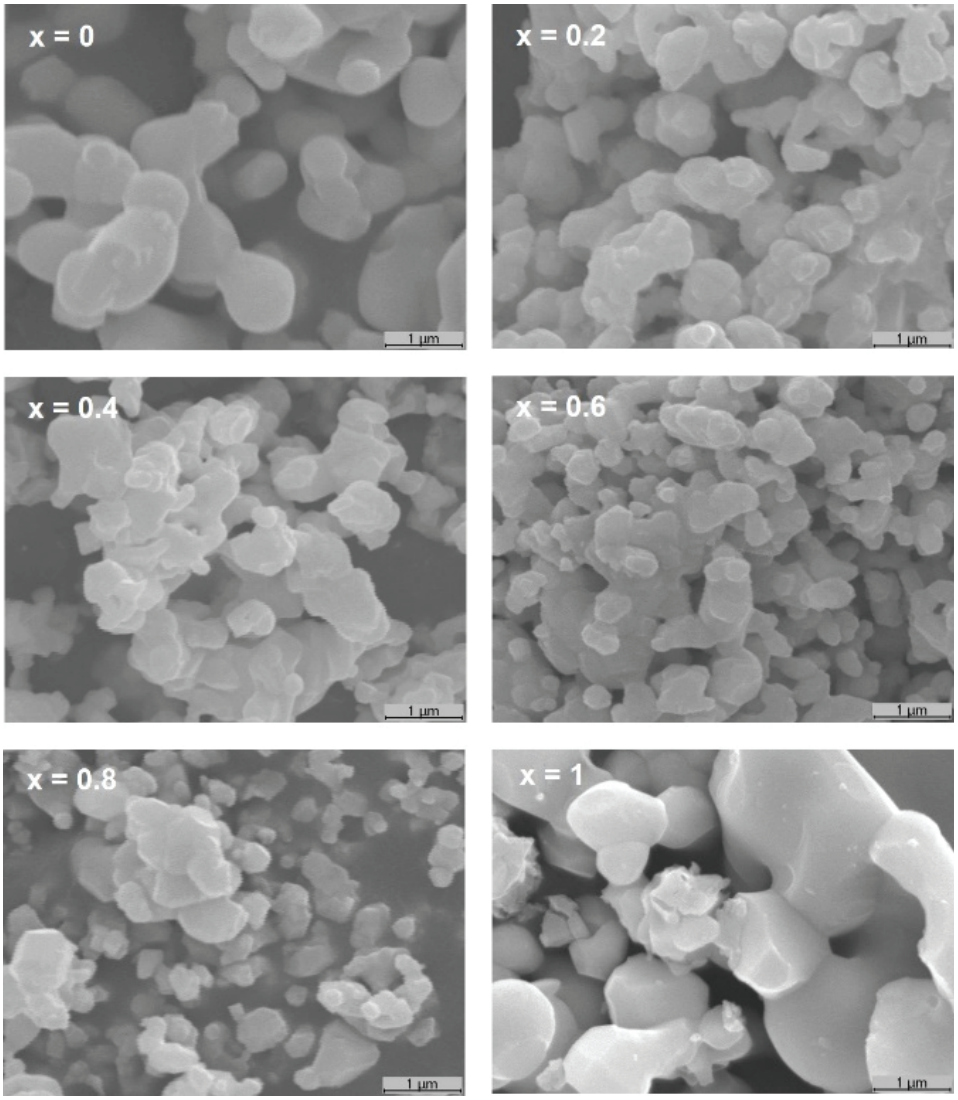

Figure 3: SEM micrographies of all powder samples (×20000).

TABLE 1: E_g values and color of the $LaTi_{1-x}Fe_xO_3$ oxides.

x	E_g / eV	Color
0	3.97	
0.2	3.42; 3.90	
0.4	3.31; 3.72	
0.6	2.65	
0.8	2.50	
1	2.20	

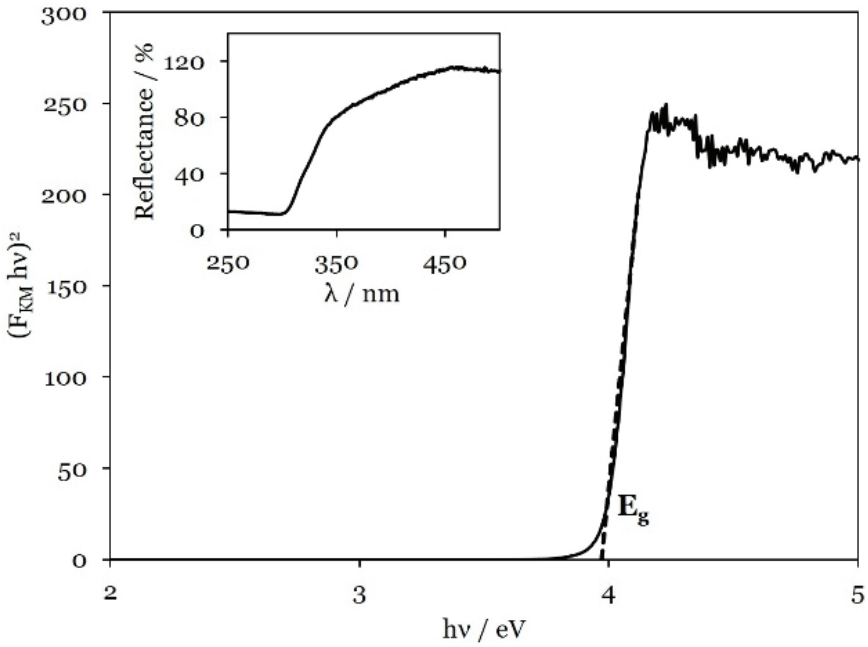

Figure 4: UV-Vi diffuse reflectance spectrum for the $La_2Ti_2O_7$ oxide. Inset – band gap energy determination.

Abs_{484nm} removal of 71.1% after 2 h, indicating that, if enough time is employed, complete decolorization, of the AO7 dye solution, could be achieved.

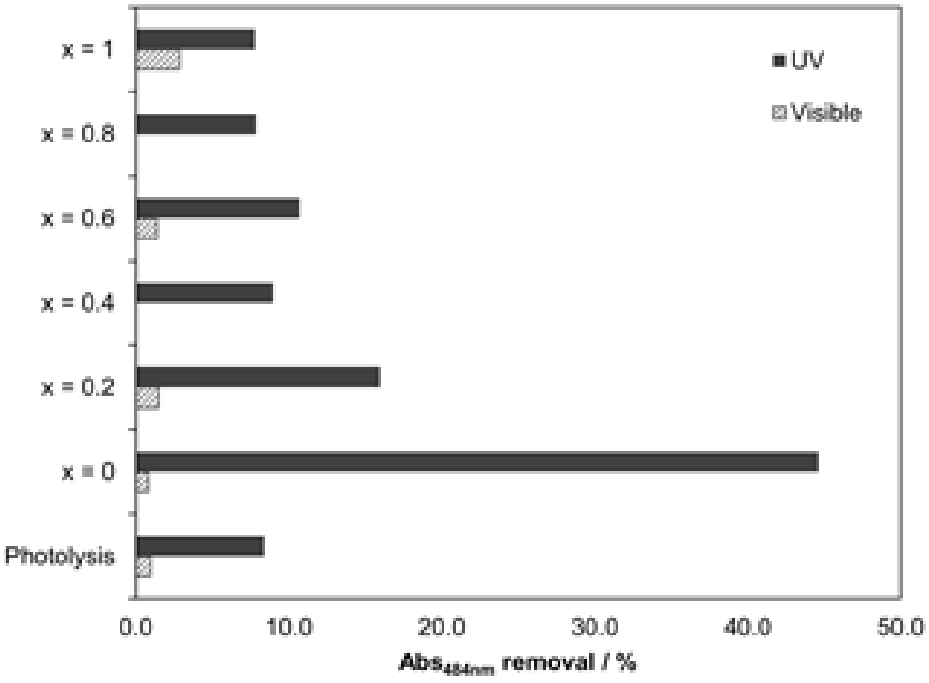

Figure 5: Absorbance removal of the AO7 solutions (C_i = 10 mg L^{-1}) obtained with the photocatalyst powder suspensions (C = 0.5 g L^{-1}) under UV and visible light, after 1 h.

4. Conclusions

All powder samples were successfully synthesized and displayed a phase change with the increase in Fe content, from monoclinic, at x = 0, to orthorhombic at x = 1. All partially substituted perovskite oxides exhibited smaller average grain size. With the increase in Fe content the E_g decreased, from 3.97 to 2.20 eV and the powders color darkened. All samples exhibited better photocatalytic activity under UV light, with an Abs_{484nm} removal of 47% achieved by the $La_2Ti_2O_7$ sample, after 1 h.

Acknowledgements

The authors acknowledge the financial support from Fundação para a Ciência e a Tecnologia, FCT, for the project UIDB/00195/2020 of the FibEnTech-UBI Research Unit and for the PhD grant awarded to Maria João Nunes (SFRH/BD/132436/2017 and COVID/BD/151965/2021).

References

[1] Yang Y, Sun Y, Jiang Y. Structure and photocatalytic property of perovskite and perovskite-related compounds. Materials Chemistry and Physics. 2006;96(2-3):234-239. https://doi.org/10.1016/j.matchemphys.2005.07.007

[2] Zhu J, Li H, Zhong L, Xiao P, Xu X, Yang X, Zhao Z, Li J. Perovskite oxides: Preparation, characterizations, and applications in heterogeneous catalysis. ACS Catalysis. 2014;4(9):2917-2940. https://doi.org/10.1021/cs500606g

[3] Wang W, Tadé MO, Shao Z. Research progress of perovskite materials in photocatalysis- and photovoltaics-related energy conversion and environmental treatment. Chemical Society Reviews. 2004;44:5371-5408. https://doi.org/10.1039/c5cs00113g

[4] Hou L, Sun G, Liu K, Li Y, Gao F. Preparation, characterization and investigation of catalytic activity of Li-doped $LaFeO_3$. Journal of Sol-Gel Science and Technology. 2006;40:9-14. https://doi.org/10.1007/s10971-006-8368-9

[5] Hu R, Li C, Wang X, Sun Y, Jia H, Su H, Zhang Y. Photocatalytic activities of $LaFeO_3$ and La_2FeTiO_6 in p-chlorophenol degradation under visible light. Catalysis Communications. 2012;29:35-39. https://doi.org/10.1016/j.catcom.2012.09.012

KnE Materials Science

FibEnTech21
1st International FibEnTech Congress (FibEnTech21) New opportunities for fibrous materials in the ecological transition
Volume 2022

Knowledge E
enriching | engaging | empowering

Research article

Use of Vetiver Zizinioides Floating Beds to Improve the Quality of Surface Water in a Mediterranean Climate

José Correia[1], Adelaide Almeida[1,2], Anabela Durão[3], Ana Pardal[1,2] and Teresa Borralho[1,B]*

[1]Polytechnic Institute of Beja- Higher School of Agriculture, Department of Technologies and Applied Sciences, Rua Pedro Soares - Campus do IPBeja, 7800-295 Beja, Portugal
[2]FibEnTech-Fibrous Materials and Environmental Technologies, University of Beira Interior, Rua Marquês de Ávila e Bolama- 6201 Covilhã, Portugal
[3]Polytechnic Institute of Beja- Higher School of Technology and Management, Rua Pedro Soares Campus do IPBeja, 7800-295 Beja, Portugal

Abstract.
Due to the negative effects of its main inflows, the water quality of Roxo stream, located in southern Portugal, an area characterized by Mediterranean climate, is degraded, causing consequences in irrigated agricultural activity. The eco technology of floating beds was used to improve the quality of this water. Three *Vetiver zizinioides* floating beds (3.3 m^2/unit; density 40.5 plants/m^2) were placed on the Roxo stream in May 2020 and the water quality was monitored until December 2020 in two places: at the floating beds location and 100 m higher up in the stream. The load mass was calculated for both sampling points and the removal rate for each parameter was monitored. The average removal rates obtained were: (i) TN = 33%; (ii) TP = 43%; (iii) COD = 44%; and (iv) Cl- = 15%. The DO level increased slightly, and the pH remained neutral. Although the water quality improved, the quality was still not high enough to be able to use the water for irrigation and to achieve good ecological status.

Keywords: Roxo stream, surface water quality, real scale, floating beds; *Vetiver zizinioides*

Corresponding Author: Teresa Borralho; email: ?????

Dates
?????

Publishing services provided by Knowledge E

© José Correia et al. This article is distributed under the terms of the Creative Commons Attribution License, which permits unrestricted use and redistribution provided that the original author and source are credited.

Selection and Peer-review under the responsibility of the FibEnTech21 Conference Committee.

OPEN ACCESS

1. Introduction

The water bodies of Southern Portugal are subject to a great seasonal variability of strong and localized events [1]. This variability can lead to prolonged droughts, which severity has increased in recent decades as a result of temperature rise due to climate change [1]. The quantity and quality reduction of water induces destructive and often irreparable impacts on crop production, soil quality, increased risk of desertification and decreased biodiversity [2].

The Roxo stream, located on the right bank of the Sado river (Southern Portugal), near the city of Aljustrel, is a perennial water course and has been heavily influenced by mining and agricultural activity of the region. As a result, the quality of water for

irrigation is bad [3], according Portuguese Law [4] and presents poor ecological state, when evaluated only for the physicochemical parameters [5]. Thus, solving this problem by using an effective and environmentally sustainable pollutant removal solution is considered relevant.

The use of Floating Beds (FB) is one of rivers Eco-rehabilitation strategies [6]. FB are floating matrices, which are associated with ecological communities such as macrophytes and microorganisms [6]. They have the ability to degrade pollutants by taking advantage of the benefits that ecosystems have, so they can be used to improve the surface water bodies quality [7].

Plants play a key role in this issue due having a dense root system, providing: (i) the creation of the necessary conditions for the circulation of water; (ii) the creation of laminar flow between the surface and bottom of the water column; (iii) the fixation of micro-organisms; (iv) the transport of atmospheric air through its upper organs to the roots; (v) nutrient assimilation; (vi) the occurrence of solid sedimentation processes and (vii) sediment storage capacity without causing excessive damage to the system [8].

Previous studies regarding artificial floating wetland technology have been focusing on the application of this treatment on standing or stagnant water such as wetlands, lakes and ponds [9]. However, in this study, the FB system is applied for the treatment of running water (dynamic system) (i.e., river, stream or channel), to which use there are a very few information [10].

The macrophyte *Vetiver zizinioides* has been widely studied for the reduction of environmental contamination. The main plant features are, among others: large and deep root system, resistance of a wide pH range (3,3 a 9,5), tolerance air temperatures between -20°C e 60°C, high efficiency to removing nutrients, resistance of high saturation levels of Al, Mn and heavy metals and is effective in herbicide retention [11].

The main aim of this work is to test, at real scale, the floating bed technology (FB) using floating matrix with the macrophyte *Vetiver zizinioides*, with the purpose to improve water quality of Roxo stream, contributing to it ecological improvement and also, in order to be possible to be used in irrigation proposes.

2. Material and methods

2.1. Meteorological data 2020

It was obtained the meteorological data of 2020 on region of Aljustrel, [12], to study its possible influence on the influx of pollutants into the water.

2.2. Field Installation

The FB are constituted by a floating system and a support system for plants (Network in PEAD and organic blanket), (Fig.1) on which were planted the macrophyte *Vetiver Zizinioides* (Density 40.5 plants/m^2) and tied to the borders of the watercourse. The choice of this macrophyte was based in previous studies, on pilot scale, where were tested several macrophythes and this one presented the best results in terms of production of biomass and without severe damage on its external and anatomical morphology [13].

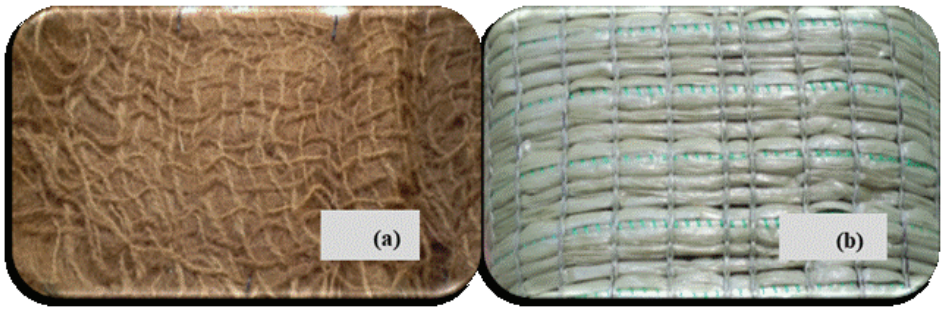

Figure 1: (a) Support System for Plants (organic blanket); (b) Floating System (PEAD Network).

Three floating beds with the dimensions of 3.3 m^2/unit were placed on Roxo stream (location: coordinates GPS: *37.944685-8.153876*), on May 2020, (Fig.2). They were placed in a water section, that presented the depth of 0,9 ± 0,3 m, the wide of 10.0 ± 1.3 m and a flow rate of 0.11 ± 0.10 m^3/s.

Figure 2: Field Installation of floating beds.

2.3. Experimental Procedure

The sampling collection was made in two points, namely after floating beds location (Outlet) and around 100 m before them at Roxo stream (Inlet). They were carried out by May 2020 to December 2020 according to Standard Methods of Analysis [14].

In *situ,* physical-chemical monitoring was performed bimonthly, for the parameters: pH, Temperature (ºC), Potential redox (Eh); Electrical conductivity (ECw) and Total Dissolved Solids (TDS), using multiparametric portable probe (HI9829 HANNA).

The remaining parameters were monitored monthly *in lab*, and were determined according to Standard Methods for the Examination of Water and Wastewater [13]: Sodium (Na^+); Potassium (K^+); Magnesium (Mg^{2+}); Calcium (Ca^{2+}); Total Suspended Solids (TSS); Chlorides (Cl^-); Ammoniacal Nitrogen (NH_4^+); Total Nitrogen (TN); Nitrates (NO_3^-); Nitrites (NO_2^-); Total Phosphorus (TP); Phosphate ($P_2O_5^{2-}$); Boron (B^{3+}); Chemical Oxygen Demand (COD) and Sulphates (SO_4^{2-}).

- The assays were made in duplicate.

2.4. Data Treatment

- It was calculated the load mass, for the parameters analysed, with the exception of the pH and Electrical Conductivity, in both sampling points.

- It was calculated the removal rate for each parameter using the Eq.1.

-It was calculated the average of removal rates, for each parameter, for the period of monitorization.

-The data was grouped by parameter, for both sampling points, and represented using the software *Excel 2016.*

3. Results and discussion

The Fig.3 shows the mean temperature, precipitation and wind velocity occurred on Aljustrel for the year of 2020.

On the Mediterranean climate the influent pollutants to the rivers are very closely related to the hydrological behaviour [1]. So, in 2020, precipitation on Aljustrel, occurred mainly in the Spring months of March (60 mm) and April (90 mm) and October (60mm), November (130 mm) and December (50mm). On June, July and August there was no precipitation. The temperature ranged between, approximately, 5ºC in January and above 35ºC in July.

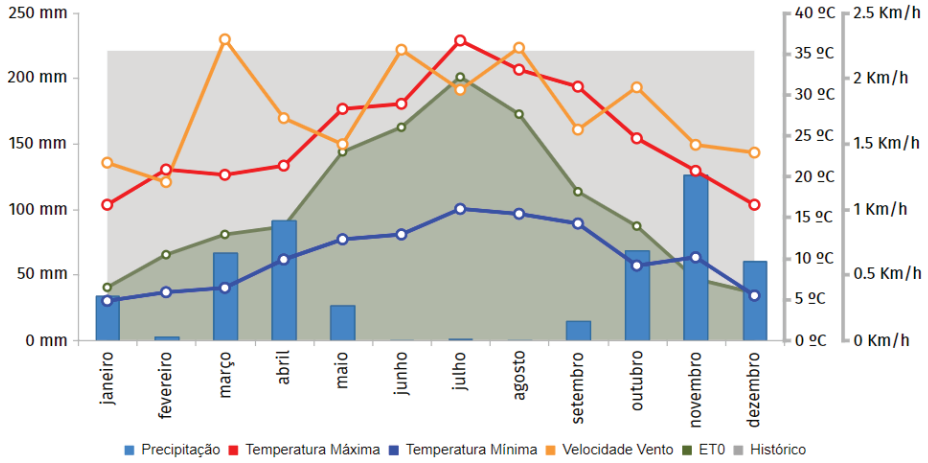

Figure 3: Meteorological data 2020 at Aljustrel, Portugal (Adapted from [12]).

Table 1. summarises the main results obtained in this work. They show some chemical physical characteristics of the Roxo stream water; i) high chemical oxygen demand (COD); ii) low dissolved oxygen (DO) levels; iii) high values of chlorides (Cl^-) and iv) low concentrations of nitrogen and phosphorous nutrients.

Also shows the importance of the precipitation on the increase of pollutants into the stream. In fact, with the rains of autumn, in October and especially in November, it can be observed an increase of concentration in almost all parameters. This may happened due to the soils drainage processes, which were very dry due to high summer temperatures.

On the other hand, the removal rates obtained for each parameter suffers large variations (ranges between 0%-90%) over monitoring period. It seems to be no relationship between the efficiency of the treatment with FB and the inlet mass load to the river bed.

In Fig. 4 is represented the results obtained for Electrical Conductivity (Ecw) and pH.

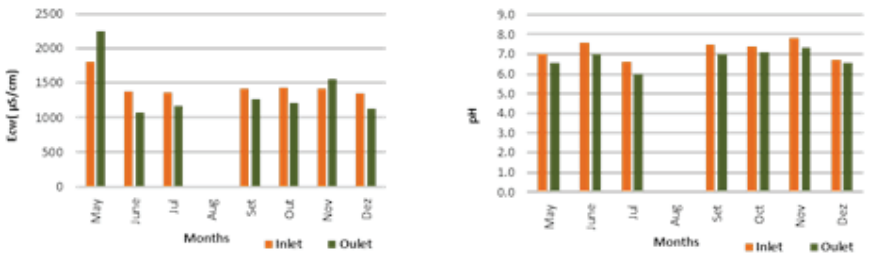

Figure 4: Representation of the values of Electrical Conductivity (ECw) and pH at inlet and outlet of FB obtained along the monitored period.

Table 1: Presentation of concentrations and mass load (ML) obtained on the two sampling points (inlet and outlet) for the main parameters studied along the monitored period of time.

Months Parameters	May	June	July	Aug.	Set.	Oct.	Nov	Dec.
DO (Inlet)								
[DO] (mg/L)	7	8	7	-	5	8	7	8
ML (kg/m^2.day)	4.8	3.9	1.0	-	5.0	3.4	29.3	1.8
DO (Outlet)								
[DO] (mg/L)	7	8	7	-	6	8	8	12
ML (kg/m^2.day)	4.8	3.9	1.8	-	6.0	3.4	33.5	2.7
R (%)	-	-	-	-	-	-	-	-
COD (Inlet)								
[COD] (mg/L O_2)	13	45	29	-	52	65	36	40
ML (kg/m^2.day)	8.9	22.2	7.6	-	52.1	27.6	150.5	8.8
COD (Outlet)								
[COD] (mg/L O_2)	13	15	13	-	14	27	30	140
ML (kg/m^2.day)	8.9	7.4	3.4	-	14..0	11.5	125.5	30.9
R (%)	0	66	55	-	73	58	17	0
Cl^-(Inlet)								
[Cl^-] (mg/L)	264	368	374	-	429	950	1250	1000
ML (kg/m^2.day)	180.4	181.2	98.4	-	430.2	406.3	5227.2	221.2
Cl^- (Outlet)								
[Cl^-] (mg/L)	264	178	500	-	310	950	1300	770
ML (kg/m^2.day)	180.4	87.4	131.5	-	310.7	406.3	5436.3	170.3
R (%)	0	52	0	-	23	0	0	23
TP (Inlet)								
[TP] (mg/L)	0.02	0.5	0.03	-	0.1	0.2	0.3	0.2
ML (kg/m^2.day)	0.01	0.25	0.01	-	0.10	0.09	1.25	0.04
TP (Outlet)								
[TP] (mg/L)	0.02	0.05	0.05	-	0.04	0.06	0.06	0.5
ML (kg/m^2.day)	0.01	0.025	0.01	-	0.04	0.025	0.26	0.11
R (%)	0	90	0	-	61	71	78	0
TN (Inlet)								
[TN] (mg/L)	3	3	2	-	2	1	7	4
ML (kg/m^2.day)	2.1	1.5	0.8	-	2.0	0.4	29.3	1.0
TN (Outlet)								
[TN] (mg/L)	3	6	0.7	-	0.5	0.5	5	4
ML (kg/m^2.day)	2.1	2,9	0.2	-	0.5	0.2	20.1	1,0
R (%)	0	0	77	-	74	50	31	0

Electrical conductivity (ECw) is associated to dissolved ions content in waters, and is often used as a reference of salinity.

The values obtained from ECw, in both sampling points, were always high and indicate that this water body presents mild to moderate risk of salinity (Ce=700-3000 µS/cm) [15]. The treatment of FB seems to promote a slighted decrease of ECw against the inlet values during almost every month.

The parameter pH remains neutral. According [7] the macrophytes don't promote significant pH changes in medium.

The results related to the inflows and outflows loads for the parameter DO are presented in Fig.5.

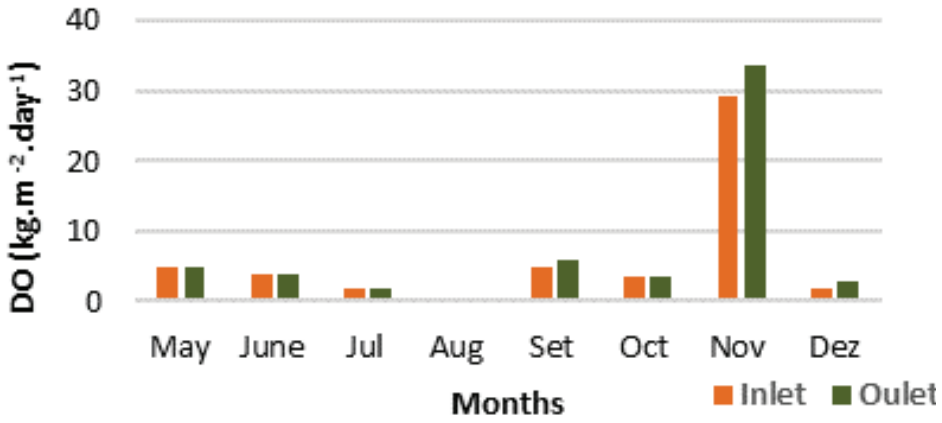

Figure 5: Representation of dissolved oxygen, DO, loads at inlet and outlet of FB obtained along the monitored period.

Dissolved oxygen (OD) is an important indicator of the ecological status of the bodies of water and in FBs interferes in some pollutant removal mechanisms [7].

The DO level depends largely on the mass loads applied. So, it can be observed that the OD loads were low with the exception in the month of November in which an unexpected increase occurred. This was due to the great rainfall that occurred in this month that promoted the great oxygenation of the water masses. In any case, it seems that exists a trend of a gradual increase in values of OD at the exit of FB compared to the inlet. In fact, *Vetiver zizinioides*, with their long roots can improve the levels of oxygen of water [11].

The inflow of organic matter, monitored by the parameter chemical organic demand, COD, (Fig.6) shows that it is always high (ranged between 8.8-150 $kg.m^2.day^{-1}$), with November month standing out remarkably due to the precipitation conditions recorded. The FB allowed significant load removals rates and the average of removal rate obtained was 44%.

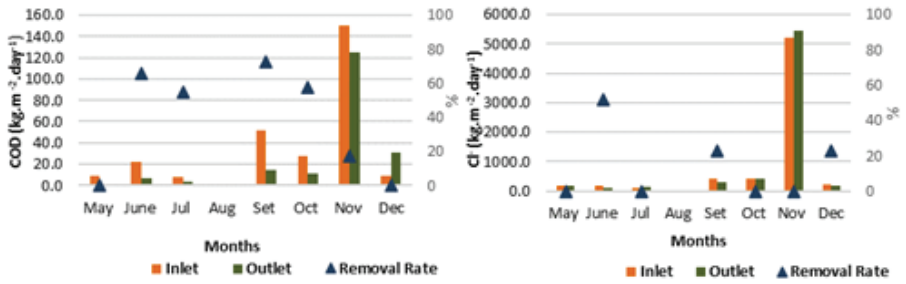

Figure 6: Representation of load rates of chemical organic matter, COD, and chlorides (Cl^-) at inlet and outlet of FB obtained along the monitored period and removal rates obtained.

The continuous use of waters with high salt content (e.g. Cl^-), can lead to soil salinization, making it impossible for agricultural use. Depending on the salt content, the salinity of the water may also affect the availability of water to crops, and may restrict its use [15]. The inflow loads of chlorides are very high (ranged between 98-5227 $kg.m^2.day^{-1}$), (Fig. 6), and the treatment by FB allowed an average removal rate of 15%.

The evolution of the nutrients phosphorus and nitrogen measured by total phosphorous parameter (TP) and total nitrogen (TN) during the monitoring period is presented in Fig.7.

Figure 7: Representation of load rates of total phosphorus (TP) and total nitrogen (TN) at inlet and outlet of FB obtained along the monitorization period and removal rates obtained.

The low levels of these two macro nutrients are characteristic of Roxo stream [3]. Phosphorus constitutes an important limiting factor of eutrophication processes and even in low concentrations could foster the growth of algae, causing problems of eutrophication.

The inflows range of load rate were 0.01 -1.30 $kg.m^2.day^{-1}$ and outflows were 0.01-0.26 $kg.m^2.day^{-1}$. The FB system showed capacity to remove this parameter, reaching

the average of removal efficiency of 43%. This result is in line with those referred in [11] that indicates, for treatments with *Vetiver zizinioides*, high removal load rates.

For total nitrogen, (TN), the inflows are lows too and FB has showed a capacity to reach an average of removal efficiency of 33%.

4. Conclusions

The influent pollutants to the river are very closely related to the hydrological behaviour;

The main results obtained had shown that the average removal rates obtained were: (i)TN=33%; (ii)TP=43%; (iii) COD=44% and (iv) Cl-=15%;

Ecw presents always high values. The FB treatment promotes a slighted decrease of ECw, but not enough to avoid the slight-moderate risk of salinity;

DO level increased slightly and the pH remained neutral;

The capacity of removal of the treatment with FB seems to be not dependent of the concentration of the pollutants and

Although the study carried out was short-lived, the results suggest that the use of FB may constitute a long-term, ecological and economical system for the treatment of the Roxo stream water. Further work is needed to consolidate the results, to determining hydraulic and kinetic parameters relevant to the possible dissemination of this technology.

Acknowledgements

The authors are very grateful for the support given by research unit Fiber Materials and Environmental Technologies (FibEnTech-UBI) through the project UIDB/00195/2020, funded by the Fundação para a Ciência e a Tecnologia (FCT).

References

[1] European Environment Agency. Climate change impacts and vulnerability in Europe. EEA:.Copanhgen; Denmark, 2012.

[2] Iglesias A, Santillán D, Garrote L. On the barriers to adaption to less water under climate change: Policy choices in Mediterranean countries. Water Resources Management. 2018, 32(15) 4819–4832. https://doi.org/10.1007/s11269-018-2043-0.

[3] Borralho T, Durão A. Qualidade da água da albufeira do roxo na dinâmica dos solos e culturas agrícolas (QARSC). Associação de Regantes do Roxo, Instituto Politécnico de Beja, Universidade de Évora. Aljustrel; Portugal, 2016.

[4] Decree Law n^{o}. 236/98. Ministry of the Environment; 1998 Aug 1.

[5] Instituto da Água, Instituto Público. Critérios para a classificação do estado das massas de água superficiais. Ministério do Ambiente, Ordenamento do Território e do Desenvolvimento Regional. Lisboa; Portugal, 2009.

[6] Durão ACR. Estratégias para a melhoria da qualidade da água na Bacia Hidrográfica do Rio Ardila [thesis, doutor em Ciências da Engenharia do Território e Ambiente]. Évora: Universidade de Évora; Portugal, 2013.

[7] Billore SK, Prashant, Sharma, JK. Treatment performance of artificial floating reed beds in an experimental mesocosm to improve the water quality of river Kshipra. Water Science and Technology. 2009;60 (11):2851-2859. https://doi.org/10.2166/wst.2009.731

[8] Kadlec RH, Wallace SD (2009). Treatment wetlands. 2nd ed. CRC PressTaylor & Francis Group; United States of America, 2009.

[9] Walker C, Tondera K, Lucke, T. Stormwater treatment evaluation of a constructed floating wetland after two years operation in an urban catchment. Sustainability (Switzerland). 2017;9(10):1–10. https://doi.org/10.3390/su9101687

[10] Kusin FM, Has SN, Nordin NA, Mohamat- Yusuff F, Ibraim ZZ. Floating vetiver island (FVI) and implication for treatment system design of polluted running water. Applied Ecology and Environmental Research. 2019;17(1):497-510.http://dx.doi.org/10.15666/aeer/1701_497510

[11] Brix H. Plants used in constructed wetlands and their functions. Paper presented at: 1st International Seminar on the Use of Aquatic Macrophytes for Wastewater Treatment in Constructed Wetlands; 5–10 May, Lisbon, Portugal, 2003.

[12] s/n Meteorologia - Home - EDIA. Regante alqueva – Metreorologia; Empresa de Desenvolvimento e Infraestruturas do Alqueva, november, 2^{sd}, 2021. Available from: https://regante.edia.pt/suporteaatividade/meteorologia/SitePages/Home.aspx

[13] Carvalhos T, Durão A, Almeida A, Pardal A, Parente I, Parreira A, Marques C. Utilização de leitos flutuantes para melhoria da qualidade de massa de água superficial -O caso da Ribeira do Roxo. Paper presented at: 15° Congresso da Água. 22-26 março, Lisboa, Portugal, 2021.

[14] American Public Health Association. Standard methods for examination of water and wastewater. Washington, DC: American Public Health Association; 2012.

[15] Vargas R, Pankova EI, Balyuk SA, Khasankhanova PV, editors. Handbook for saline soil management. 1st ed. Food and Agriculture Organization of the United Nations and Lomonosov Moscow State University; Rome, Italy, 2018.

KnE Materials Science

FibEnTech21
1st International FibEnTech Congress (FibEnTech21) New opportunities for fibrous materials in the ecological transition
Volume 2022

Knowledge E
enriching | engaging | empowering

Research article

Treatment of Industrial Effluents by the Microalgae Selenastrum Sp.

Bruno Escobar*, André Cunha, and Rogério Simões

FibEnTech and Departament of Chemistry, University of Beira Interior, Rua Marquês d'Ávila e Bolama, 6201-001, Covilhã, Portugal

Abstract.

High consumption of clean water results in the generation of effluents that need to be treated and then safely discarded. Conventional methods for such treatment often do not offer an economical and sustainable result; therefore, new methods are needed, such as microalgae usage. Microalgae are unicellular beings capable of rapid adaptation, growth, and production of compounds of interest (pharmaceuticals, biofuels and others). This work aimed to study the effectiveness of the microalgae *Selenastrum sp.* in the treatment of effluents from the textile and pulp & paper industries, as well as the respective effects on its biomass development and accumulation of compounds. Four types of culture were carried out (for each type of effluent, a control, and a control with addition of glucose) lasting eight days, in duplicate, all with the addition of a standard culture medium and controlled abiotic factors. Analyses for compound removal (chemical oxygen demand and colour readings on the 200–800nm range) and biomass development (cell number, its dimensions, and weight) were performed four times during the process. At the end of the experiments, the average removal in effluents for COD and colour were 56.6% and 32.7% respectively, in addition to a biomass accumulation of 0.45 g/L. These results were comparable to those obtained for the control cultivation using glucose as a carbon source (70.0% COD removal and 0.51 g/L biomass accumulation). These results demonstrate the effectiveness of *Selenastrum sp.* in the treatment of industrial effluents, its resilience in stressful environments and the potential use of its accumulated compounds for biotechnological purposes.

Keywords: microalgae, *Selenastrum sp.*, industrial effluent, textile effluent, pulp effluent, effluent treatment

Corresponding Author: Bruno Escobar; email: bruno.p.escobar@ubi.pt

Dates

?????

Publishing services provided by Knowledge E

© Bruno Escobar et al.. This article is distributed under the terms of the Creative Commons Attribution License, which permits unrestricted use and redistribution provided that the original author and source are credited.

Selection and Peer-review under the responsibility of the FibEnTech21 Conference Committee.

OPEN ACCESS

1. Introduction

In 09/2015, the United Nations approved the 2030 Agenda for global sustainable development, with some of its main prerogatives being access to efficient and sustainable water sources for all and decrease in water pollution **[1]**. With the energy and clean water needs, growing continually, the environmental impact generated and the need to reverse them, to find alternatives that are ecological, efficient, and low cost have been sought, being microalgae one of those alternatives. Microalgae are unicellular microorganisms found in almost all types of aqueous media, capable of adapt and

change their environment, to reproduce quickly and are sources of various compounds of interest for a myriad of different sectors and industries **[2]**.

Water is essential in large volumes in the industry mainly to be used in manufacturing processes or washing and with such function and degree of consumption an appropriated method for cleaning and discharge of the effluent generated needs to be applied. Nowadays, conventional systems used for treatment of industrial effluents are effective if well implemented and operated, but are often expensive, complex, and sometimes doesn't eliminate all its contaminants, therefore not achieving the minimum conditions appropriated for discharge. The use of microalgae for the treatment of industrial effluents can be an effective, economical, and simple solution for such situations since its effectiveness has been extensively studied and applied **[3-10]**.

The present work aims to analyse the acclimatization of the microalgae *Selenastrum sp.* in effluents derived from the textile and paper pulp industry, evaluate the treatment and elimination of biodegradable organic matter, and observe the microalgae accumulation of compounds of interest.

2. Material and methods

Cultures were carried out in 1L reactors for 8 days, with control of light intensity (195 $\mu mol.m^{-2}.s^{-1}$, 12h/day), temperature (23ºC) and filtered air flow (0.4L/L/min). Cultures with 90% (v/v) of filtered effluent from the textile and pulp industries, and control (with and without glucose) assays were carried out. Control cultures consisted in 900mL of distilled water, 60mL of microalgae and 40mL of standard nutrients (and 0,5g of glucose for the control with glucose). Due to the low inorganic nutrient content in the effluents, 40mL of GoldMedium Fresh-Water Species were added to all cultures. Samples for cell counting, chemical oxygen demand (COD) analysis, dry weight, spectrophotometer colour reading (200 – 800nm) and cell dimensions (through microscopic observation coupled with specialized software for image processing and analysis) were taken at 4 different times of cultivation.

The Figure 1 illustrates how the dimensions were considered for microalgae cell volume determination (volume was estimated considering the sum of the volumes of two semi-spheres and one cylinder).

For the characterization of the effluents, measurements were made utilizing a multiparameter sensor for the determination of pH, dissolved O_2 and redox potential, along with a nutrient test kit for determination of nitrate and phosphate, standard methods for the COD calculation and spectrophotometer for colour readings of filtered samples in

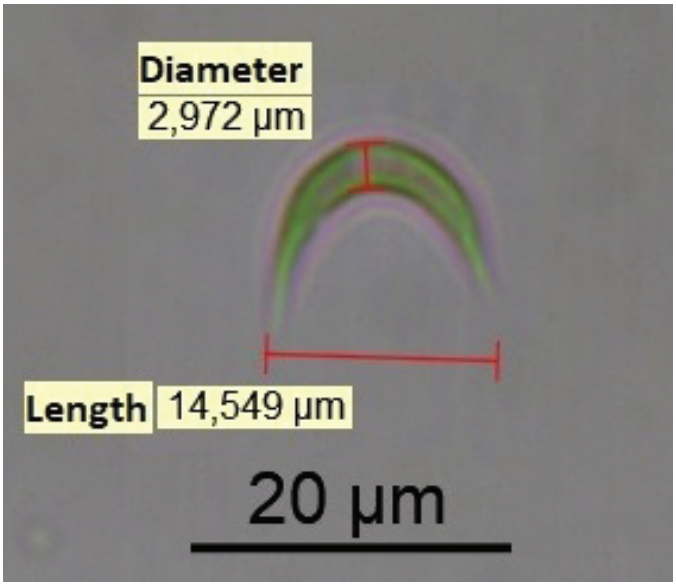

Figure 1: *Selenastrum spp.* dimensions.

the UV-Visible spectrum (200-800nm range). The COD standard method chosen was the closed reflux, titrimetric method.

The characteristics of both industrial effluents (as well as commonly dissolved constituents found in such effluents) are indicated in the table 1.

TABLE 1: Characteristics measured for both industrial effluents.

	Textile effluent	Paper pulp effluent
pH	8.4	7.0
Dissolved O_2 (mg/mL)	4.1	1.5
Nitrate (mg/L)	2.9	4.1
Phosphate (mg/L)	3.0	7.0
Redox potential (mV)	163	-433
Integral of the UV-Visible spectrum	785.5	836.6
COD (mgO_2/L)	434	462
BOD (mgO_2/L)*	103	178
BOD/COD*	0.238	0.385
Other common constituents**	chlorinated compounds, heavy metals, dyes, sulphates, nitrogen oxides, amines	Resins, fatty acids, sterols (□-sitosterol), waxes, adsorbable organic halides

* COD/BOD ratio for both effluents were based on previous works with similar effluents (BODs values were also acquired through this ratio) [3] [4]. ** Common constituents found in both effluents [5] [6].

3. Results and discussion

Figures 2, 3, 4 and 5 demonstrate the COD variation, the integral of spectrophotometer colour readings, cell growth and dry biomass accumulation values for all the tests respectively (time periods for all results shown are the 2h, 24h, 96h and 196h of culture respectively).

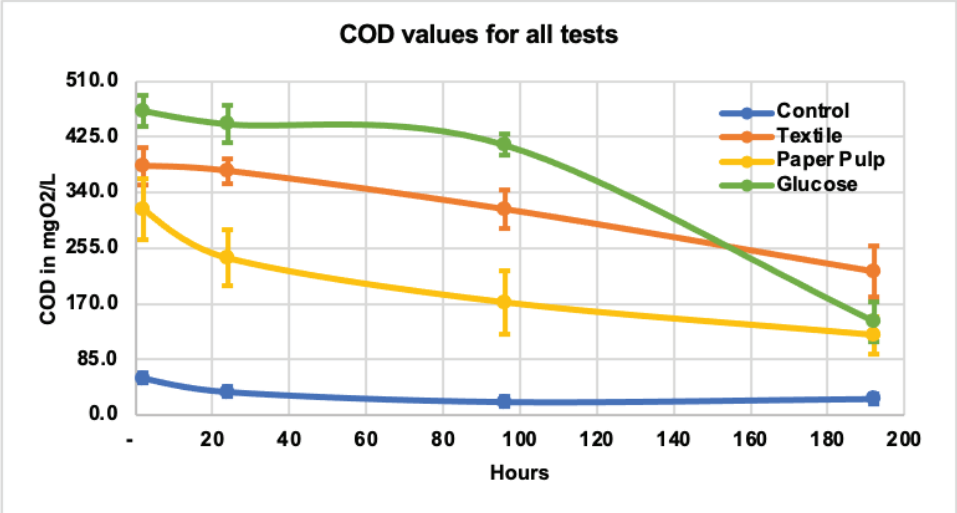

Figure 2: COD removal rate and extent for all cultures.

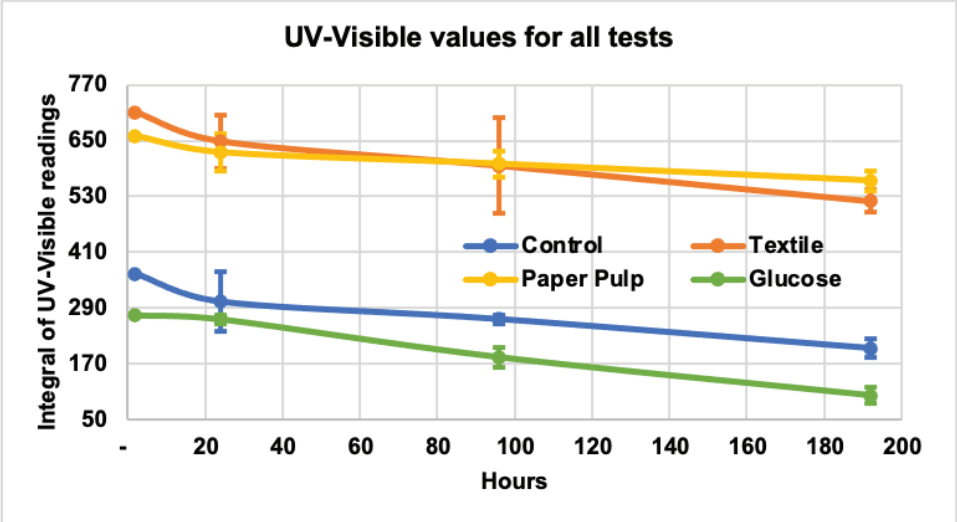

Figure 3: Results for the integral of UV-Visible colour readings for all cultures.

Regarding COD, it is important to comment that the COD values in control culture comes from the organic compounds present in the microalgae inoculum themselves. It is also interesting to observe that in the glucose culture, the organic matter only started to be consumed after about 80 hours, suggesting that the microalgae shifted from a

metabolic state to another, possibly from an autotrophic regime to a heterotopic one **[11]**. On the other hand, considering that both effluents (paper pulp and textile) had approximately the same initial COD, the microalgae assimilation of the two industrial effluents was significantly different; the COD removal for the paper pulp effluent is higher than for the textile effluents, which is in good agreement with the higher biodegradability (BOD/COD ratio) of the pulp effluent (table 1). However, the rapid decrease in COD concentrations in pulp effluents after 2 h is somewhat unexpected and can tentatively explained by the adsorption of these compounds on the surfaces of microalgae, thus, removing them suddenly as the microalgae are introduced in the medium.

Regarding the COD removal, there was a reduction in COD levels of 70.0%, 64.3% and 49.2% for cultures with glucose, pulp effluent and textile effluent respectively, after 8 days of cultivation. On the other hand, considering the both the colour removal (400-800 nm) and other aromatic compounds (200-400 nm) (Figure 3), an average reduction of 31.7% was observed for the industrial effluents, which indicates a reduction of colour in both effluents and the removal of dyes in the textile effluent. Such values demonstrate the potential of *Selenastrum sp.* microalgae to degrade both the pulp and textile effluents. In addition, these results are in good agreement with it was observed by other authors working with effluents derived from the same kind of industries and other species of microalgae. Working with textile effluent, El-Kassas & Mohamed (2014) **[7]** reported a mean value of COD removal around 61.6% in a 14-day culture with *Chlorella vulgaris,* whereas Lim et al. (2010) **[8]**, obtained a mean value of 50.3% for the COD removal in a 12-day culture with the same microalgae. In relation to the microalgae grown in the paper pulp effluents, Gentili (2014) **[9]**, obtained a mean value of 79.8% for the COD removal in a 6-day culture in a paper pulp effluent mixed with other effluents (dairy and municipal) using 3 different microalgae (2 *Scenedesmus* and *Selenastrum*) and Usha et al. (2016) **[10]**, had a 75.0% of COD removal in an outdoor open pound culture (28 days) using two species of *Scenedesmus sp*.

The biochemical reaction conditions resulted in the highest cell production for the controlled cultures (with and without glucose) with an average of 12.3 million cells per mL in contrast with the 7.4 million cells per mL in the cultures with industrial effluents. However, regarding the weight of accumulated biomass, the cultures with dissolved organic carbon (effluents and control with glucose) resulted in higher biomass concentration when compared with the control culture (0.29mg/mL), obtaining 0.42mg/mL in the textile effluent (46.5% higher than the control without glucose), 0.47mg/mL for the pulp effluent (62.8% higher) and 0.51mg/mL for the glucose culture (76.7% higher than the control without glucose).

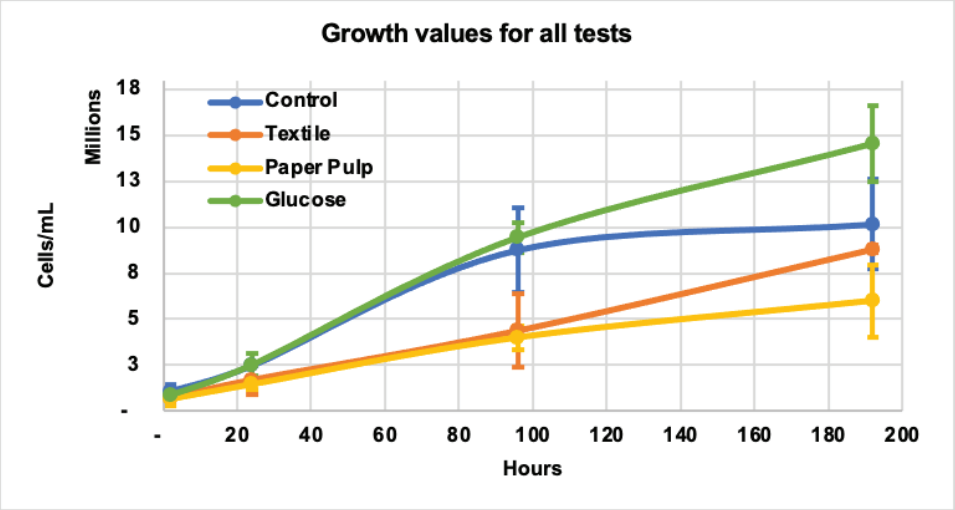

Figure 4: Growth rate for all cultures.

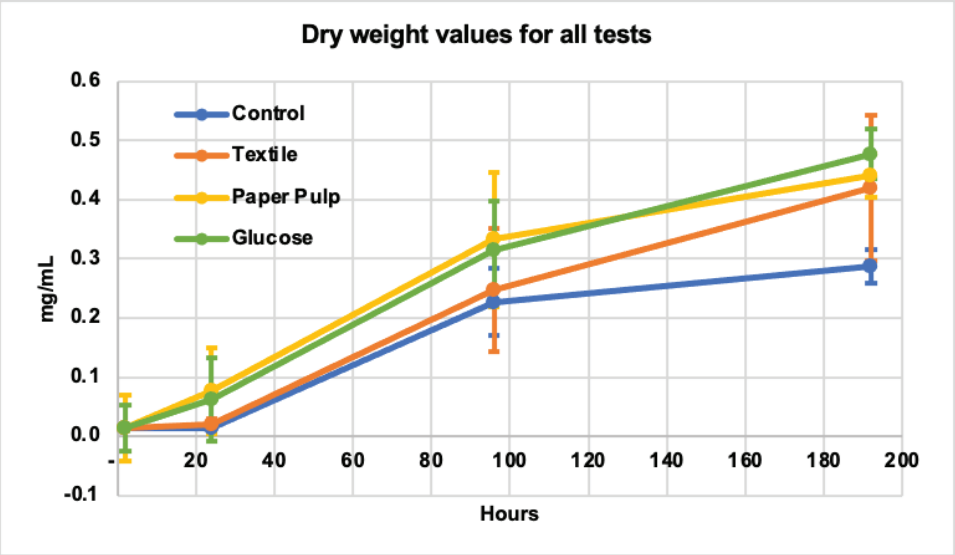

Figure 5: Dry biomass values for all cultures.

Overall, it is noticed that the more controlled and less stressful the environment, the greater the number of cells, while the more stressful environments or those with higher COD content determine a greater dry biomass. Such growth of microalgae biomass in industrial effluents was also observed by Lim et al. (2010) **[8]** and El-Kassas & Mohamed (2014) **[7]** in textile effluents, obtaining the mean values of 0.155 mg/mL (12 days) and 1.325mg/mL (14 days and addition of sodium bicarbonate) of dry weight respectively, both using the microalga *Chlorella vulgaris*. For paper pulp effluent, Gentili (2014) **[9]** reported a mean value of biomass concentration of 0.93mg/mL (mix of effluents, lasting 6 days) using 3 different microalgae (2 *Scenedesmus* and *Selenastrum*).

The contrast between cell number and dry biomass weight can be observed in Figure 6, which shows the value of the mass per cell. A clear difference is revealed, suggesting that stressed cells growing in effluent show higher values. The time profile of this parameter is also very interesting and deserves further studies, namely, to investigate the metabolites accumulated. Based on the results, we can speculate that 4 days culture maximise the metabolites production, namely for culture in the pulp effluent.

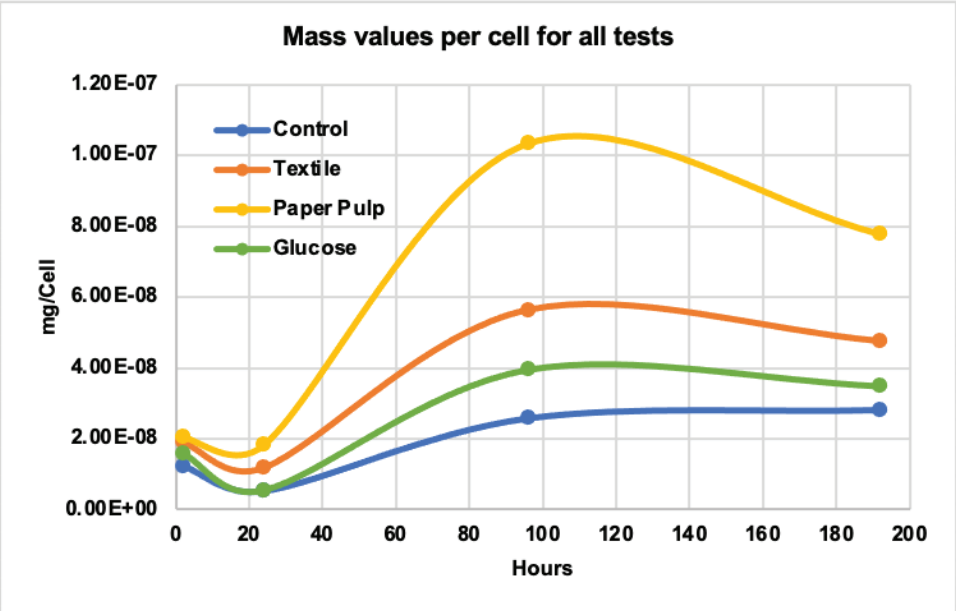

Figure 6: Mass per cell values for all cultures (time periods shown are the 2h, 24h, 96h and 196h respectively).

Figure 7 shows the estimated cell volume. Comparing the control essays with and without glucose, we can conclude the cell with glucose are bigger than the corresponding cell cultivated with inorganic carbon only. On the other hand, comparing the cell cultivated with glucose and effluents, the cell volume is of the same magnitude, but the mass of each cell is much higher in the effluents (Figure 6), suggesting higher accumulation of compounds inside the cell. Figure 7 also shows the cell volume significantly increase along the culture period. Comparing the estimated cell volume variation from the beginning to the end of culture period, the control essays had an increase of 31.9% (from 82.01 to 108.24μm^3), the textile effluent essay an increase of 149% (from 123.18 to 149.05μm^3), the pulp effluent essay an increase of 167.8% (115.09 to 167.82μm^3) and an increase of 201.2% was observed for the microalgae grown in the controlled culture with glucose (127.61 to 201.24μm^3).

The obtained results put in evidence the effect of the carbon source (organic vs inorganic; glucose vs complex molecules from effluents) and the culture condition, namely the stress environment, on the cell characteristics (dimensions and accumulated

metabolites). This phenomenon was also observed by Chioccioli et al. (2014) **[12]**, where addition of organic carbon (glucose) resulted in an increase of 0.25mg/mL in dry weight of microalgae cultures using the species of *Chlorella vulgaris* and *Chlamydomonas reinhardtii*.

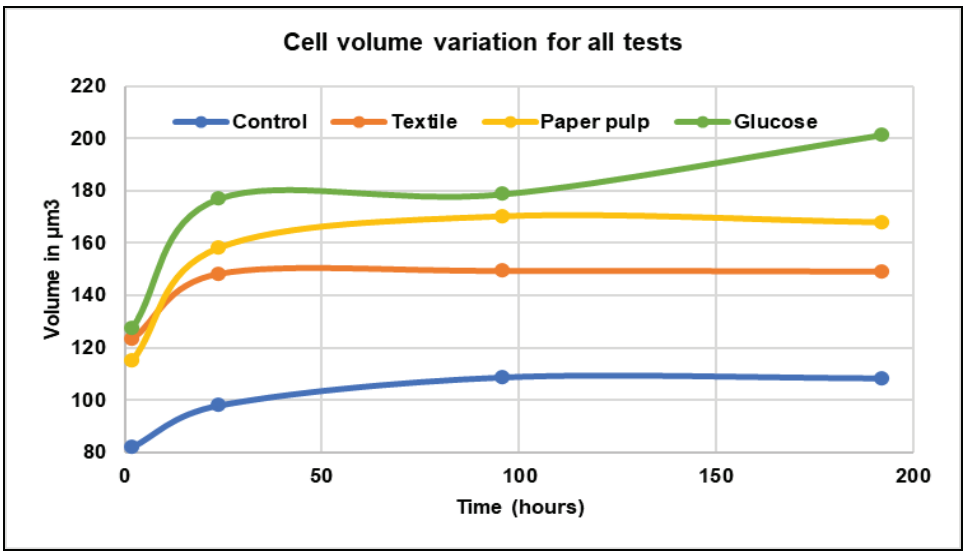

Figure 7: Cell volume values for all cultures (time periods shown are the 2h, 24h, 96h and 196h respectively).

Considering the results for dry biomass obtained in this work and the biomass lipid content reported (14%) by Chakravarty & Mallick in 2019 **[13]**, it is expected that this biomass has higher potential for lipid production. Although other species can provide better lipid results **[14]**, it is possible that changing a few parameters on the cultures **[15]** (like temperature or salt concentration) or mixing effluent with more nutrients **[9]** (like dairy or food effluents), even better results in lipid concentrations can be achieved.

4. Conclusions

The study demonstrates the microalgae *Selenastrum sp* has the potential to treat effluents from the pulp and textile industries. For these effluents, the average COD and colour removal were 56.7% and 32.7%, respectively. In addition, the biochemical conversion of the effluent compounds resulted in a biomass accumulation of 0.45 g/L, comparable with the obtained in the control essay using glucose as carbon source. These experimental results demonstrated that *Selenastrum sp*. is an efficient alternative for the treatment of industrial effluents. Its growth and high biomass accumulation suggest high potential for reusing its compounds for biotechnological purposes.

5. Acknowledgements

The authors are very grateful for the support given by research unit Fiber Materials and Environmental Technologies (FibEnTech-UBI) through the project UIDB/00195/2020, funded by the Fundação para a Ciência e a Tecnologia (FCT).

References

[1] General Assembly resolution 70/1, Transforming our world: the 2030 Agenda for Sustainable Development, A/RES/70/1 (25 September 2015), available from undocs.org/A/RES/70/1.

[2] Sudhakar MP, Kumar BR, Mathimani T, Arunkumar K. A review on bioenergy and bioactive compounds from microalgae and macroalgae-sustainable energy perspective. Journal of Cleaner Production. 2019;228:1320–1333.

[3] Silva A. Valorização do efluente tratado da indústria papeleira em usos compatíveis [Dissertation for obtaining the master's degree in Environmental Engineering - Sanitary Engineering Profile]. Portugal: Universidade Nova de Lisboa, Caparica; 2019.

[4] Batista M. Tratamento eletroquímico de efluentes têxteis reutilização de efluentes têxteis em novos tingimentos [Dissertation for obtaining the master's degree in industrial chemistry]. Portugal: Universidade da Beira Interior; 2015.

[5] Kamali M, Khodaparast Z. Review on recent developments on pulp and paper mill wastewater treatment. Ecotoxicology and Environmental Safety. 2015;114:326–342.

[6] Yaseen DA, Scholz M. Textile dye wastewater characteristics and constituents of synthetic effluents: A critical review. International Journal of Environmental Science and Technology. 2019;16:1193–1226.

[7] El-Kassas HY, Mohamed LA. Bioremediation of the textile waste effluent by *Chlorella vulgaris*. Egyptian Journal of Aquatic Research. 2014;40:301–308.

[8] Lim SL, Chu WL, Phang SM. Use of *Chlorella vulgaris* for bioremediation of textile wastewater. Bioresource Technology. 2010;101:7314–7322.

[9] Gentili FG. Microalgal biomass and lipid production in mixed municipal, dairy, pulp and paper wastewater together with added flue gases. Bioresource Technology. 2014;169:27-32.

[10] Usha MT, Chandra TS, Sarada R, Chauhan VS. Removal of nutrients and organic pollution load from pulp and paper mill effluent by microalgae in outdoor open pond. Bioresource Technology. 2016;14:856–860.

[11] Daneshvar E, Ok YS, Tavakoli S et al. Insights into upstream processing of microalgae: A review. Bioresource Technology. 2021;329: Article 124870.

[12] Chioccioli M, Hankamer B, Ross IL. Flow cytometry pulse width data enables rapid and sensitive estimation of biomass dry weight in the microalgae *Chlamydomonas reinhardtii* and *Chlorella vulgaris*. PLoS One. 2014;9(5): Article e97269.

[13] Chakravarty S, Mallick N. Biomass and bioenergy optimization of lipid accumulation in an aboriginal green microalga *Selenastrum* sp. GA66 for biodiesel production. Biomass and Bioenergy. 2019;126:1–13.

[14] Aratboni AH, Rafiei N, Garcia-Granados R, Alemzadeh A, Morones-Ramírez JR. Biomass and lipid induction strategies in microalgae for biofuel production and other applications. Microbial Cell Factories. 2019;18:1–17.

[15] Ananthi V, Brindhadevi K, Pugazhendhi A, Arun A. Impact of abiotic factors on biodiesel production by microalgae. Fuel. 2021;284: Article 118962.

KnE Materials Science

FibEnTech21
1st International FibEnTech Congress (FibEnTech21) New opportunities for fibrous materials in the ecological transition
Volume 2022

Knowledge E
enriching | engaging | empowering

Research article

Influence of Hydraulic Conditions on Reclaimed Water Polishing Using Soil and Sand Columns

Flora Silva[1,5,6]*, Ana Maria Antão-Geraldes[2,5], Paulo Scalize[3,5], Victor Cavaleiro[4,6] and António Albuquerque[4,5,6]

[1]ESTiG, Instituto Politécnico de Bragança, Campus de Santa Apolónia, 5300-253, Bragança, Portugal
[2]Centro de Investigação de Montanha (CIMO), Instituto Politécnico de Bragança, Campus de Santa Apolónia, 5300-253, Bragança, Portugal
[3]School of Civil and Environmental Engineering, Federal University of Goiás, Av. Universitária, 1488, Setor Universitário, CEP 74605-220 Goiânia-GO, Brazil
[4]Department of Civil Engineering and Architecture, University of Beira Interior, Calçada Fonte do Lameiro, 6201-001, Covilhã, Portugal
[5]Fiber Materials and Environmental Technologies (FibEnTech-UBI), University of Beira Interior, R. Marquês D'Ávila e Bolama, 6201-001 Covilhã, Portugal
[6]GeoBioTec-UBI, University of Beira Interior, Calçada Fonte do Lameiro, 6201-001 Covilhã, Portugal

Corresponding Author: Flora Silva; email: flora@ipb.pt

Dates

?????

Publishing services provided by Knowledge E

© Flora Silva et al. This article is distributed under the terms of the Creative Commons Attribution License, which permits unrestricted use and redistribution provided that the original author and source are credited.

Selection and Peer-review under the responsibility of the FibEnTech21 Conference Committee.

Abstract.

The removal of residual pollutants from a synthetic effluent with a composition similar to that of urban effluent from secondary treatment was evaluated in vertical downflow columns. These were filled with soil, the fine fraction of the soil, and sand, and operated in discontinuous and continuous mode. The results showed high removal rates of organic matter, ammonium, nitrate and phosphate in the discontinuous and continuous experiments, especially for the fine fraction. Therefore, the soil is suitable for removing organic matter and nutrients ($N\text{-}NH_4$, $N\text{-}NO_3$, and $P\text{-}PO_4$), and can be used for polishing wastewater before its infiltration.

Keywords: wastewater reuse, organics removal, nutrient removal, residual soil, river sand

1. Introduction

Adaptation and mitigation of climate change through water management are essential for sustainable development. Therefore, it is increasingly necessary to consider "unconventional" water resources in future planning [1]. Reclaimed water is a reliable alternative to conventional water resources for many uses [1-2]. Indeed, there are several successful cases of water reuse worldwide [3], including the artificial recharge of aquifers with treated wastewater. The complementary treatment of secondary effluents through the soil (Soil aquifer treatment - SAT), before its inclusion in the aquifers, has been gaining increased attention in several countries around the world [4-5], with studies pointing to the advantage of its application [4,6]. However, if the soil does

OPEN ACCESS

not present favourable conditions for infiltration of treated wastewater, the residual loads of that water, characterized by an organic matter of difficult biodegradability (e.g. hydrocarbons, pesticides and several contaminants of emerging concern), forms of nitrogen (ammonium, nitrite, and nitrate), and phosphorus (orthophosphates and polyphosphates), heavy metals and pathogenic microorganisms, can be a disadvantage for groundwater quality.

Thus, the purpose of this research was to evaluate the influence of the hydraulic conditions on the removal of organic matter and nutrients (nitrogen and phosphorus forms), using laboratory columns filled with soil, the fine fraction of the soil and river sand, and verify the main mechanisms responsible for removing these pollutants.

2. Material and methods

2.1. Characterization tests of soil, fine soil, and sand

A granitic residual soil was collected at the Quinta de Gonçalo Martins (Guarda, Portugal) [7]. A component less than 0.075 mm (fine soil) was extracted from the soil, as this is where the most reactive soil fractions are found, namely silt and clay. In addition, river sand was also used [8].

To understand the importance of soil properties in the removal of pollutants, soil granulometric analysis was performed using the sieving method [9] and the fine soil analysis using the sedimentation method [10]. The specific surface was determined by laser diffraction, using the Coulter LS200 equipment. The density of solid particles was determined by the pycnometer method [11] and the porosity using the procedures described in [6]. The qualitative mineralogical composition of the soil was determined by X-Ray Diffraction (XRD) with a Rigaku diffractometer, DMAX III/C, USA. For the morphological and microstructural analysis, the Scanning Electron Microscope (SEM), Hitachi S-2700, USA, was used. The chemical composition (analysis in oxides) was determined with the Energy Dispersive Spectrometer (EDS), which is coupled to the SEM. Organic matter was determined by the Walkley-Black method [12], and soil pH was determined in H_2O and KCl by the potentiometric method, in suspension (soil: water, 1:2.5), described by [13].

2.2. Columns experiments

Experiments were set up in three acrylic circular columns with vertical and downflow flux, with a height of 42 cm and 14 cm in diameter (Figure 1), and a synthetic effluent. Water samples were collected at column top (C_T, influent), P_1, P_2, and C_B points (the C_B point was considered for the effluent at the column base). The three columns were filled with soil, fine soil, and river sand. The filling media had a height of 25 cm. The first column had 20 cm of soil (mass = 4467.4 g) and 5 cm of sand (mass = 891.4 g) at the bottom. The second column had 20 cm of fine soil (mass = 3588.1 g) and 5 cm of sand (mass = 891.4 g) at the bottom. The third column had 25 cm of sand (mass = 5912.1 g). All columns were filled with synthetic wastewater until the media was submerged with a water level of $\pm$ 2 mm above the C_T point. The lower sand layer was provided to protect the upper layers of soil and fine soil against the exit of fine particles and disturbance of the flow.

The synthetic effluent was similar to those used by [14-15], which included a carbon source (sodium acetate trihydrate, $CH_3COONa*3H_2O$), two nitrogen sources (ammonium chloride, NH_4Cl; and potassium nitrate, KNO_3), a phosphorus source (di-potassium hydrogen phosphate trihydrate, $K_2HPO_4*3H_2O$), and a trace element solution (iron chloride, magnesium sulphate, and calcium chloride), according to the compositions and C/N/P ratios indicated in [6]. The solutions of sodium acetate, ammonium chloride, potassium nitrate, and di-potassium hydrogen phosphate were prepared in a concentrated form and diluted according to the desired loads. The loads used were similar to those observed by [15], approximately 150 mg L^{-1} of COD, 30 mg L^{-1} of $N\text{-}NH_4$, 10 mg L^{-1} of $N\text{-}NO_3$, and 10 mg L^{-1} of $P\text{-}PO_4$, which are typical of urban effluents from secondary treatment. In the analysis and discussion of results, the following terms will be used: organic matter (for COD values), ammonium or ammonia nitrogen (for $N\text{-}NH_4$ values), nitrate or nitric nitrogen (for $N\text{-}NO_3$ values), and phosphate (for $P\text{-}PO_4$ values).

Experiments were run in two phases. In the first phase, the columns were operated in a discontinuous mode, including filling with the feed solution, reaction for 3.5 days (totalling 35 days, 10 cycles), drainage, and sampling, as suggested by [16]. In the second phase, the columns were operated in a continuous mode, also for 35 days, with a feeding system composed of an ISMATEC MCP CA4 peristaltic pump (Switzerland) for pumping the influent to the inlet of the column, with a flow rate of 0.36 L d^{-1} and a hydraulic load of 2.34 cm d^{-1}, values previously tested in the laboratory and in agreement with those observed by [17-19], on similar filling materials. At the beginning and end of each cycle, in the first phase, water samples were collected at the influent (C_T point), P_1, P_2, and C_B

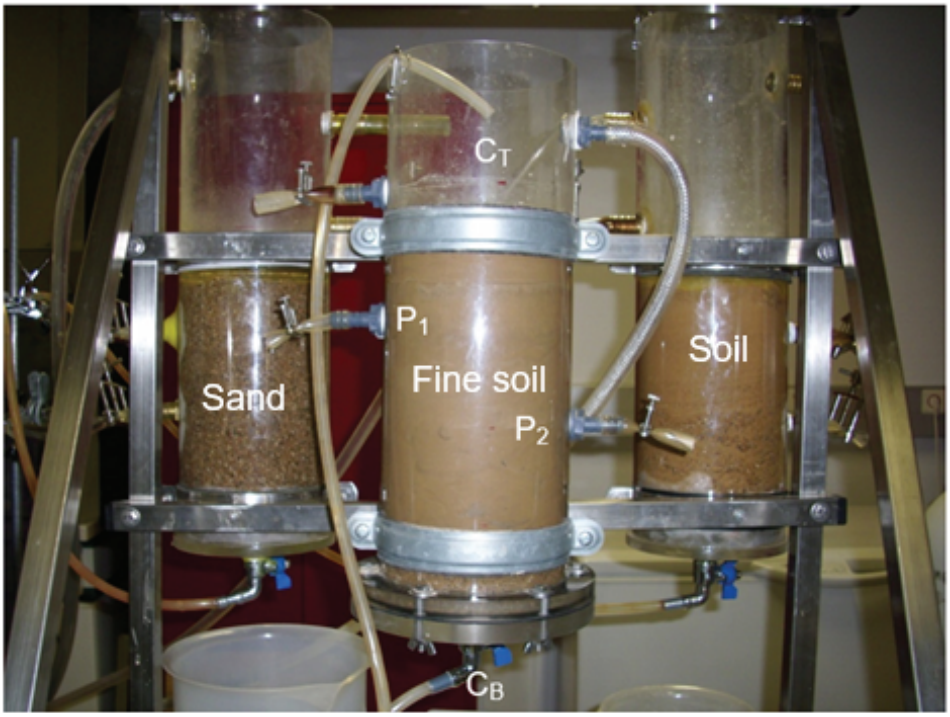

Figure 1: Column tests.

for measuring pH, temperature, COD, N-NH_4, N-NO_3, and P-PO_4. For the second phase, water samples were collected at the same points every 3.5 days for determining the same parameters. A SenTix 41 probe connected to a Multi 340i meter (WTW, Germany) was used for determining pH and temperature. COD, N-NH_4, N-NO_3, and P-PO_4 were determined according to [20].

3. Results and discussion

3.1. Characterization of soil, fine soil, and sand

The soil used in the study has a low clay fraction (particle size less than 2 µm) of approximately 5% (Figure 2), which means that most of the fines are essentially silty. According to [21], to prevent soil clogging and ensure wastewater treatment, the soil should not contain more than 10% clay. Figures 3-(a) to 3-(c) show the morphology of soil, fine soil, and sand particles.

Table 1 presents the physicochemical characteristics of the three materials, most relevant to the study. For fine soil (Table 1), the permeability (k) is low (k = 3.72 x 10^{-6} m s^{-1}). However, soils with permeability in the order of 6.94 x 10^{-6} m s^{-1} are suitable for controlled infiltration of treated effluents [2]. It essentially contains silica (60.44%) and

alumina (31.76%), with lower levels of iron (3.99%) and potassium (3.81%) oxides. The organic matter content is very low (0.45%), and the soil is very acidic (pH = 4.44). The mineralogical composition consists of quartz, muscovite, illite, kaolinite, and smectite (identified in the fraction below 2 µm). Kaolinite constitutes about 60% of the clay mineral present in the soil.

This soil has a specific surface area suitable for the development of biofilm capable of removing pollutants and pathogens and the clay-colloidal complex of this soil also has reactive properties that allow the removal of pollutants by sorption mechanisms [6].

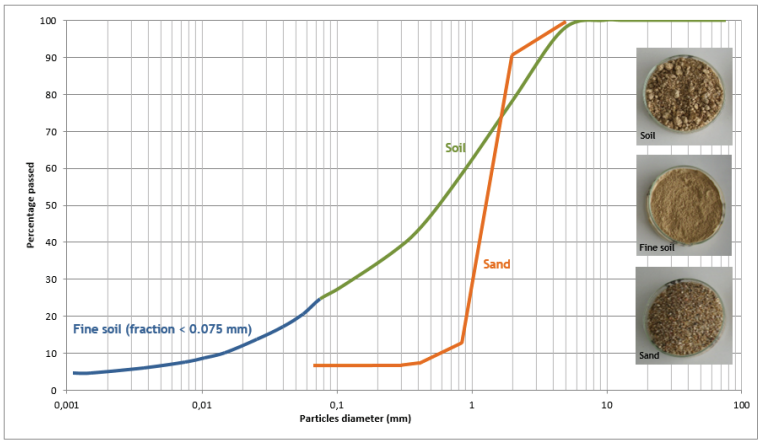

Figure 2: Particle size of soil, fine soil and sand.

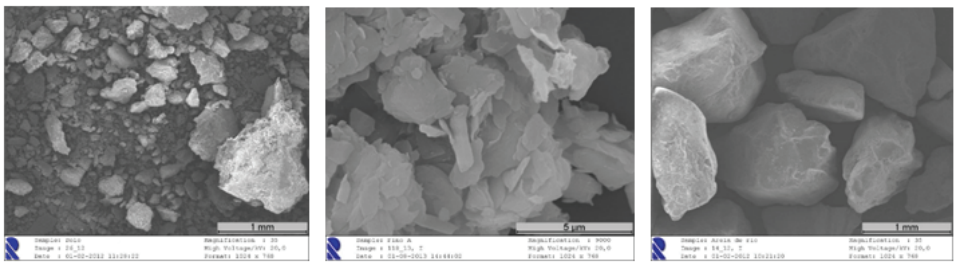

Figure 3: SEM images: (a) Soil, (b) Fine soil, and (c) Sand, with a magnification of 35x, 9000x, and 35x, respectively.

3.2. Evaluation of the removal of organic matter and nutrients

Table 2 and Table 3 show the variation of pH, temperature, COD, N-NH_4, N-NO_3, and P-PO_4, for the sampling points C_T and C_B in the first and second phases.

Assuming a 95% confidence level, for the following sample sizes:

[1]10 (CQO); 10 (N-NH_4); 9 (N-NO_3); 8 (P-PO_4); [2]9 (CQO); 8 (N-NH_4); 6 (N-NO_3); 8 (P-PO_4);

Table 1: Physicochemical characteristics of the materials.

Parameters	Soil	Fine soil (< 0.075 mm)	Sand
Effective diameter D_{50} (mm)	0.59	0.027	1.28
Porosity (%)	38.5	48.0	41.0
Solid particle density (G_s)	2.65	2.65	2.65
Permeability (k) (m s^{-1})	3.23 x 10^{-5}	3.72 x 10^{-6}	8.98 x 10^{-4}
Specific surface area (m^2 g^{-1})	-	0.29	-
Oxides (%): SiO_2; Al_2O_3; Fe_2O_3; K_2O	58.64; 33.17; 3.96; 4.23	60.44; 31.76; 3.99; 3.81	86.44; 7.99; 1.54; 4.03
Organic matter content (%)	0.25	0.45	0.03
pH (1:2.5) H_2O; KCl	4.91; 3.84	4.44; 3.48	6.32; 5.26

Table 2: Results of the first phase in discontinuous feeding.

Parameters	Column top[1]	Soil[2]	Fine soil[3] (< 0.075 mm)	Sand[4]
		Column base		
pH	6.67 - 7.32	4.90 - 6.78	6.32 - 7.12	6.67 - 7.28
Temp. (°C)	21.96 ± 0.37	21.8 ± 0.23	22.35 ± 0.51	21.90 ± 0.15
COD (mg L^{-1})	154.70 ± 11.57	36.01 ± 10.84	29.11 ± 6.66	51.12 ± 32.11
$N\text{-}NH_4$ (mg L^{-1})	33.73 ± 2.31	2.20 ± 1.13	1.15 ± 0.78	16.95 ± 3.09
$N\text{-}NO_3$ (mg L^{-1})	9.95 ± 0.59	1.61 ± 0.82	0.31 ± 0.08	6.50 ± 1.59
$P\text{-}PO_4$ (mg L^{-1})	10.28 ± 0.22	0.33 ± 0.29	0.13 ± 0.10	9.83 ± 0.37

[3]10 (CQO); 8 ($N\text{-}NH_4$); 6 ($N\text{-}NO_3$); 4 ($P\text{-}PO_4$); [4]10 (CQO); 9 ($N\text{-}NH_4$); 9 ($N\text{-}NO_3$); 8 ($P\text{-}PO_4$).

Table 3: Results of the second phase in continuous feeding.

Parameters	Column top[1]	Soil[2]	Fine soil[3] (< 0.075 mm)	Sand[4]
		Column base		
pH	7.31 - 8.17	5.38 - 6.97	5.12 - 6.40	7.37 - 7.85
Temp. (°C)	22.38 ± 0.40	22.07 ± 0.41	22.12 ± 0.45	22.08 ± 0.38
COD (mg L^{-1})	93.78 ± 13.89	24.69 ± 4.54	18.18 ± 4.07	47.15 ± 6.45
$N\text{-}NH_4$ (mg L^{-1})	26.84 ± 1.12	5.64 ± 2.48	0.41 ± 0.06	21.81 ± 3.55
$N\text{-}NO_3$ (mg L^{-1})	10.94 ± 0.49	2.24 ± 0.63	0.14 ± 0.04	9.66 ± 0.43
$P\text{-}PO_4$ (mg L^{-1})	10.51 ± 0.40	3.05 ± 0.88	1.16 ± 0.59	10.25 ± 0.30

Assuming a 95% confidence level, for the following sample sizes:

[1]10 (CQO); 10 ($N\text{-}NH_4$); 10 ($N\text{-}NO_3$); 10 ($P\text{-}PO_4$); [2]10 (CQO); 10 ($N\text{-}NH_4$); 10 ($N\text{-}NO_3$); 10 ($P\text{-}PO_4$);

[3]10 (CQO); 10 ($N\text{-}NH_4$); 10 ($N\text{-}NO_3$); 10 ($P\text{-}PO_4$); [4]10 (CQO); 10 ($N\text{-}NH_4$); 10 ($N\text{-}NO_3$); 10 ($P\text{-}PO_4$).

Table 2 and Table 3 show a drop in pH from C_T to C_B. The average temperature remains practically constant throughout all cycles. The best removal rates were obtained for fine soil, and, therefore, the analysis will only be focused on the fine soil results.

The results for the first phase (Table 2) show average concentration removals of 125.59 mg COD L^{-1}, 32.57 mg N-NH_4 L^{-1}, 9.52 N-NO_3 L^{-1}, and 10.24 mg P-PO_4 L^{-1}, which correspond to mass removals rates of 232.0 mg of COD, 60.17 mg of N-NH_4, 17.59 mg of N-NO_3 and 18.91 mg of P-PO_4, and removal efficiencies of 80.78% COD, 96.55% N-NH_4, 96.81% N-NO_3 and 98.73% P-PO_4. For the second phase (Table 3), the average concentration removals were 75.60 mg COD L^{-1}, 26.43 mg N-NH_4 L^{-1}, 10.80 N-NO_3 L^{-1}, and 9.35 mg P-PO_4 L^{-1}, corresponding to mass removals rates of 139.65 mg of COD, 48.82 mg of N-NH_4, 19.95 mg of N-NO_3 and 17.28 mg of P-PO_4 and removal efficiencies of 80.43% COD, 98.45% N-NH_4, 98.70% N-NO_3 and 88.95% P-PO_4.

In the first phase (discontinuous feeding), the removal of organic matter starts to be significant in the 4th cycle, because the biofilm was already stable and well developed to be able to continuously remove acetate, as was also observed by [22]. In the second phase (continuous feeding), the higher removal efficiency (86.27%) was observed on the 8th day. In both experiments, carbonaceous removal has occurred, either in the presence of oxygen (closer to the surface of the column), by aerobic removal mechanisms such as aerobic respiration and nitrification, or in the absence of oxygen, by anaerobic removal mechanisms, such as anaerobic respiration, denitrification and fermentation processes.

Ammonium reached a higher removal efficiency of 98.66% (7th cycle), for the discontinuous feeding, and higher removal efficiency (99.46%) for the 3rd day, for the continuous feeding. This means that nitrification was present. Therefore, ammonium oxidation may have occurred closer to the surface, where oxygen is able to dissolve in the water mass by diffusion, as admitted by [23].

In both phases (discontinuous and continuous experiments), the removal of nitrate was very significant, which have occurred through denitrification at the lower layers where oxygen was low. Nitrate was present through the feeding solution and also produced due to the ammonia oxidation (nitrification). The decrease in pH indicates that there was more alkalinity consumption, which is characteristic of the nitrification mechanism, than production, which is characteristic of the denitrification mechanism, as mentioned by [24]. The pH variation observed (from around 7 to around 5) is also favourable to the presence of unconventional removal mechanisms, as mentioned by [25].

Phosphate removal was also significant and reached a higher removal efficiency of 99.54% in the 5th cycle, for discontinuous experiments, and higher removal efficiency of 94.62% on the 15th day, for continuous experiments. However, contrary to what would have happened with organic matter, ammonium, and nitrate, the biological removal of phosphate is low [26] and usually occurs by biosorption (i.e. it is adsorbed on the polymers that make up the biofilm) and by complexation and precipitation at low pH (usually complexes with aluminium and iron, precipitating in the form of phosphates), as reported by [27-28].

4. Conclusions

The soil and its fine fraction have reactive properties that allow a good capability for removing organic matter, ammonium, and nitrate by biodegradation mechanisms and phosphate by sorption mechanisms, either in discontinuous or continuous mode experiments, allowing it to act as a barrier to the contamination of groundwater during infiltration with reclaimed water. However, fine soil has showed to be a better media for residual pollutant removal.

5. Acknowledgments

The authors are grateful to the Foundation for Science and Technology (FCT, Portugal) for financial support by national funds FCT/MCTES to CIMO (UIDB/00690/2020), FibEnTech (UIDB/00195/2020) and GeoBioTec-UBI (UIDB/04035/2020).

References

[1] UNESCO WWAP (World Water Assessment Programme). The United Nations world water development report 2020: Water and climate change, executive summary. Perugia, Italy: UNESCO; 2020. Available from: https://unesdoc.unesco.org/ark:/48223/pf0000372882

[2] do Monte MH, Albuquerque A. Reutilização de águas residuais: Guia Técnico no. 14. Lisboa: Entidade Reguladora dos Serviços de Águas e Resíduos (ERSAR); 2010.

[3] Lazarova V, Asano T, Bahri A, Anderson J, editors. Milestones in water reuse - The best success stories. London: IWA Publishing; 2013.

[4] Sharma SK, Kennedy MD. Soil aquifer treatment for wastewater treatment and reuse. International Biodeterioration & Biodegradation. 2017;119:671–677.

https://doi.org/10.1016/j.ibiod.2016.09.013

[5] Dillon P, Stuyfzand P, Grischek T et al. Sixty years of global progress in managed aquifer recharge. Hydrogeology Journal. 2019;27:1–30. https://doi.org/10.1007/s10040-018-1841-z

[6] Silva F. Avaliação da capacidade reativa de solos residuais destinados à infiltração de águas residuais tratadas [PhD thesis in Civil Engineering]. Covilhã, Portugal: Universidade da Beira Interior; 2015.

[7] Silva F, Scalize P, Cruvinel K, Albuquerque A. Caracterização de solos residuais para infiltração de efluente de estação de tratamento de esgoto. Engenharia Sanitária e Ambiental. 2017;22(1):95-102. https://doi.org/10.1590/S1413-41522016141677

[8] Fael C. Erosões localizadas junto de encontros de pontes e respetivas medidas de proteção [PhD thesis in Civil Engineering]. Covilhã, Portugal: Universidade da Beira Interior; 2007.

[9] Especificação LNEC E 239. Solos. Análise granulométrica por peneiração húmida. Lisboa: Laboratório Nacional de Engenharia Civil; 1970.

[10] Especificação LNEC E 196. Solos. Análise granulométrica. Lisboa: Laboratório Nacional de Engenharia Civil; 1966.

[11] Norma Portuguesa definitiva NP 83. Solos. Determinação da densidade das partículas. Lisboa: Inspeção Geral dos Produtos Agrícolas e Industriais (IGPAI) – Repartição de Normalização; 1965.

[12] Nelson D. W, Sommers L. E. Total carbon, organic carbon and organic matter. In: D. L. Sparks, A. L. Page, P. A. Helmke, R. H. Loeppert, P.N. Soltanpour, M.A. Tabatabai, C.T. Johnston, M.E. Sumner (Eds.). Methods of soil analysis: Part 3. Chemical methods. Madison, Wisconsin, USA: Soil Science Society of America, Inc., American Society of Agronomy, Inc.. 1996;961– 1010.

[13] Van Reeuwijk L. Procedures for soil analysis. 6th ed. ISRIC, FAO, Wageningen; 2002.

[14] Albuquerque A. Contribuição para o estudo da remoção de residuais de carbono em filtros fiológicos de leito imerso e fluxo descendente [PhD thesis in Civil Engineering]. Covilhã, Portugal: Universidade da Beira Interior; 2003.

[15] Amado L. Sistemas de tratamento de águas residuais por zonas húmidas artificiais em Portugal Continental [MSc thesis]. Coimbra, Portugal: Universidade de Coimbra; 2007.

[16] Opoku B. Suitability of different reactive filter media for onsite wastewater [MSc thesis]. Suécia: KTH Royal Institute of Technology, Estocolmo; 2007.

[17] Eliasson J. Rule development commitee issue research report-draft: Hidraulic loading. Washington, DC: Washington State Department of Health; 2002.

[18] Jellali S, Sediri T, Kallali H, Anane M, Jedidi N. Analysis of hydraulic conditions and HRT on the basis of experiments and simulations on soil column. Desalination. 2009;246(1-3):435-443. https://doi.org/10.1016/j.desal.2008.03.065

[19] Pavelic P, Dillon P, Mucha M, Nakai T, Barry K, Bestland E. Laboratory assessment of factors affecting soil clogging of soil aquifer treatment systems. Water Research. 2011;45(10):3153-3163. https://doi.org/10.1016/j.watres.2011.03.027

[20] APHA-AWWA-WEF. Standard methods for the examination of water and wastewater. 20th ed. Washington, DC: American Public Health Association, American Water Works Association, Water Environmental Federation; 2005.

[21] Kallali H, Anane M, Jellali S, Tarhouni J. GIS-Based multi-criteria analysis for potencial wastewater aquifer recharge sites. Desalination. 2007;215:111-119. https://doi.org/10.1016/j.desal.2006.11.016

[22] Silva I. Desenvolvimento de agregados artificiais por ativação alcalina de lamas residuais para utilização no tratamento de águas residuais [PhD thesis in Civil Engineering]. Covilhã, Portugal: Universidade da Beira Interior; 2013.

[23] Tchobanoglous G, Burton F, Stensel H. Wastewater engineering: Treatment and reuse. 4th ed. Nova Iorque: McGraw-Hill; 2003.

[24] Grady Jr W, Daigger G, Lim H. Biological wastewater treatment. 2nd ed. Basel: Marcel Decker; 1999.

[25] Paredes D, Kuschk P, Mbwette T, Stange F, Mueller R, Koeser H. New aspects of microbial nitrogen transformations in the context of wastewater treatment - A review. Engineering in Life Sciences. 2007;7(1):13-25. https://doi.org/10.1002/elsc.200620170

[26] Asano T, Burton F, Leverenz H, Tsuchihashi RE, Tchobanoglous G. Water reuse: Issues, technologies and applications. New York: McGraw-Hill; 2007.

[27] Costa J. Caracterização e constituição do solo. 8th ed. Lisboa: Fundação Calouste Gulbenkian; 2011.

[28] Ruan H, Gilkes R. Kinetics of phosphate sorption and desorption by synthetic aluminous goethite before and after thermal transformation to hematite. Clay Minerals. 1996;31(1):63-74. https://doi.org/10.1180/claymin.1996.031.1.06

KnE Materials Science

FibEnTech21
1st International FibEnTech Congress (FibEnTech21) New opportunities for fibrous materials in the ecological transition
Volume 2022

Knowledge E
enriching | engaging | empowering

Research article

Investigation of Agricultural Waste as Economical and Effective Bio-Inhibitors for Inhibiting Scaling in Natural Hard Water

Faléstine Souiad[1,2]*, Yasmina Bendaoud-Boulahlib[1], Wafa Kerkatou[3], Annabel Fernandes[2], Chibani Aissa[1] and Ana Lopes[2]

[1]Unité de recherche CHEMS, Département de Chimie, Faculté des Sciences Exactes, Université Constantine 1, 25000, Constantine, Algérie
[2]FibEnTech and Departament of Chemistry, University of Beira Interior, Rua Marquês d'Ávila e Bolama, 6201-001, Covilhã, Portugal [3]Unité de Recherche Valorisation des Ressources Naturelles, Molécules Bioactives et Analyses Physicochimiques et Biologiques. Université Constantine 1, 25000, Constantine, Algérie

Abstract.
In this study, agricultural waste was utilized as new bio-inhibitors to prevent scale formation in hard waters. Aqueous extracts of strawberry and tomato leaves were utilized for reducing the scale deposits formed on metallic surfaces by Bounouara ground hard water, which supplies Constantine city in Algeria. Anti-scaling properties were evaluated by chronoamperometry and impedancemetry techniques. The effect of temperature and concentration on the efficiency of the bio-inhibitors was assessed. The results showed that the anti-scaling effect of strawberry leaf extracts started at the very low concentration of 1 ppm, with 31% efficiency, reaching complete scaling inhibition at 15 ppm (20°C), whereas the inhibitory effect of tomato leaf extracts was noticed at 2.5 ppm, with 36% efficiency, and total inhibition at 20 ppm (20°C). The efficiency of strawberry and tomato leaf extracts at 40°C was also confirmed, although total inhibition was attained at a higher concentration.

Keywords: hard water, agricultural waste, strawberry leaves, tomato leaves, bio-inhibitors, scaling inhibition

Corresponding Author: Faléstine Souiad; email: falastine.souiad@umc.edu.dz

Dates
?????

Publishing services provided by Knowledge E

© Faléstine Souiad et al. This article is distributed under the terms of the Creative Commons Attribution License, which permits unrestricted use and redistribution provided that the original author and source are credited.

Selection and Peer-review under the responsibility of the FibEnTech21 Conference Committee.

OPEN ACCESS

1. Introduction

In natural aquatic ecosystems, ground waters present high concentrations of calcium and magnesium, which leads to a natural, spontaneous formation of undesirable scaling deposits on surfaces. These scaling deposits are mainly due from the precipitation of calcium carbonate [1–3], which causes various undesirable effects, such as the formation of those insoluble mineral salts that almost totally block the water distribution pipelines or the cooling water tubes [4,5], reducing the flow rate. Moreover, the scale formation significantly reduces the water treatment technology's efficiency, and of the desalination and water softening systems [6–8].

During decades, many researchers have investigated the scale deposits from natural, industrial, or synthetic waters [9–12], to hinder or control scaling process. The most common method that was investigated to avoid scale formation was the addition of chemical substances to the hard waters, that are known as chemical inhibitors [13–16]. Researchers proved that a small amount of these substances can highly reduce the scale precipitation and change the kinetics of the scale formation process. Despite the high efficiency of these inhibitors, they may be toxic to the environment and dangereous to the human health.

Recently, research to find new inhibitors compatible with the environment is underway, using the so-called green inhibitors, according to three criteria: Toxicity, bioaccumulation, and biodegradation [17-19]. To go further with this aim, this work focuses on new bio-inhibitors, for reducing the scaling deposits formed by Bounouara ground water, which supplies the entire southern region of the Constantine city in Algeria and is characterized by 60°f hardness. The bio-inhibitors utilized are aqueous extracts of strawberry and tomato waste, since a large amount of these waste accumulates annually, having a negative impact on the environment. To our knowledge, no study has so far being performed on the anti-scaling effect of strawberry and tomato leaves. Chronoamperometry combined with impedancemetry were used to investigate the efficiency of strawberry and tomato leaves aqueous extract on the inhibition of calcium carbonate deposition on metallic surface. The effect of water temperature and inhibitor concentration was studied in detail.

The chronoamperometry and impedancemetry methods have been widely used to study the scaling power of water and the inhibitors efficiency [9-11]. They are based on the controlled precipitation of calcium carbonate on a metal surface, by applying a negative cathodic potential (-1 V versus SCE) to reduce the oxygen, leading to the production of hydroxyl ions (Eq. 1). The hydroxyl ions increase the pH value near the electrode's surface, which forces the calcium carbonate to precipitate on the surface of the working electrode (Eqs. 2 and 3).

$$O_2 + 2H_2O + 4e^- \; 4OH^- \quad (1)$$

$$HCO_3^- + OH^- \; CO_3^{2-} + H_2O \quad (2)$$

$$Ca^{2+} + CO_3^{2-} \; CaCO_3 \quad (3)$$

2. Material and methods

Preparation of extracts. Strawberry and tomato leaves were collected from a greenhouse in Jijel city, Algeria. After collection, they were washed, dried, and crushed, to be

ready for use. The extraction was performed by adding 100 ml of boiling distilled water to 5 g of leaves and leaving them for 15-20 min, to infusion. After that, they were filtered, with a paper filter of 0.5 mm of porosity, thus obtaining an extract of 5% (mass/volume). The filtrate was evaporated, and the residue was weighed.

3. Electrochemical experiments

The electrochemical tests (chronoamperometry and impedancemetry) were carried out in a thermostated double-walled conventional three-electrode cell, in pyrex glass, with a capacity of 500 mL (Fig. 1). Before each experiment, the cell was cleaned with ethanol, rinsed with distilled water, and dried. A saturated calomel electrode (SCE), was used as the reference electrode, having a platinum wire as the auxiliary electrode. The working electrode was a stainless-steel electrode (SS) made of XC10, with 1 cm^2 active area, embedded in inert resin. The surface of SS electrode was polished before every assay with abrasive papers (first P#400, and then P#800), cleaned with acetone, and rinsed with distilled water.

For the chronoamperometric tests, the electrodes were centred in the electrochemical glass cell at a constant distance, connected to a Potentiostat-Galvanostat ZRA (Reference 3000), controlled by Gamery analysis software. The experiments were operated in batch mode, for 60 minutes, applying a potential of -1V vs SCE. Tests were run at 20 and 40°C, utilizing 400 mL of Bounouara raw water, in the absence or in the presence of strawberry or tomato leaves extract. Solutions were continuously stirred during the experiments, at 500 rpm.

The electrochemical impedance diagrams were recorded with the operating system utilized for chronoamperometry, at a scaling potential of -1V vs SCE, after 60 min polarisation. The measurements were carried out in the frequency range 100 kHz - 10 mHz, with 10 points per decade, and an amplitude of 10 mV. The disturbance amplitude parameter had already been optimized in a previous study.

4. Results and discussion

Chronoamperometric study. Figure 2 presents the chronoamperometric curves of Bounouara water in the absence of the inhibitors, at different temperatures. The curve represents the resulting current density as a function of time during scaling deposition. According to Ledion [20], the scaling power of water can be characterized by the scaling time and the scaling index values obtained from the chronoamperometric curve

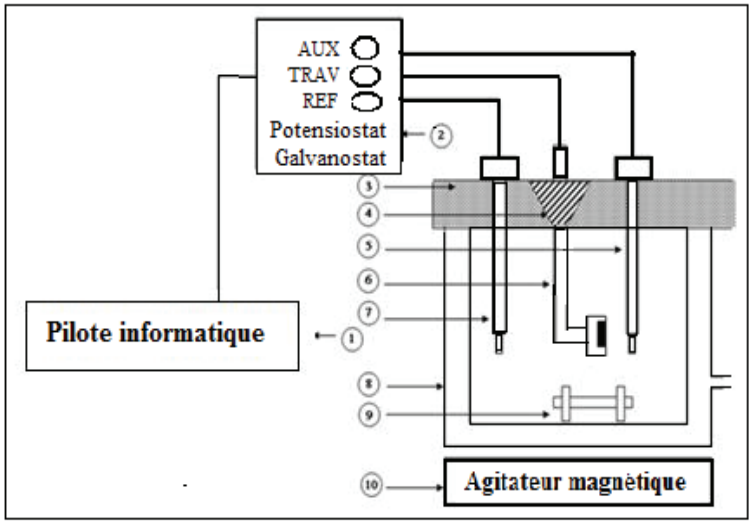

Figure 1: Experimental set-up.

of this water: the scaling time, t_s, corresponds to the minimum time needed to obtain a residual current, which remains stable after that time; the scaling index, I_s, is calculated from the scaling time, according to Eq. 4.

$$I_s = \frac{1000}{t_s} \quad (4)$$

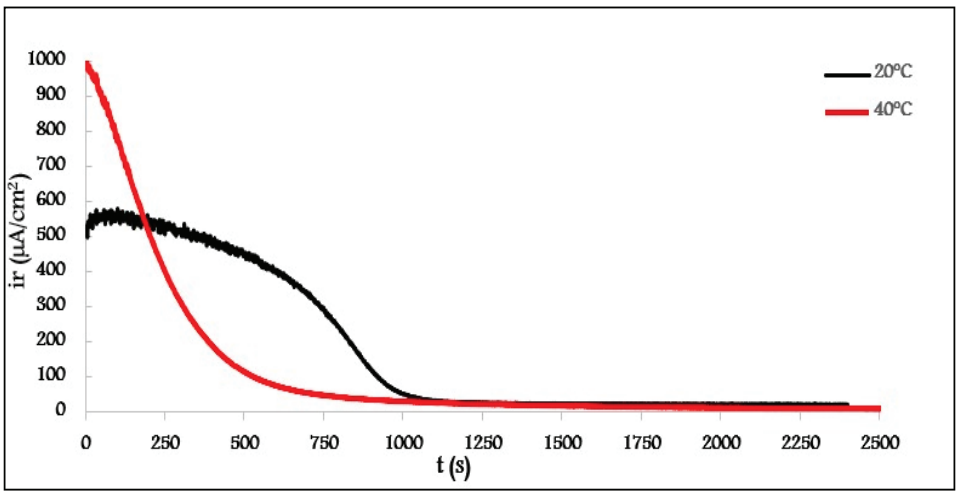

Figure 2: Chronoamperometric curves of Bounouara raw water at 20°C and 40°C on a SS electrode at -1 V (vs SCE), Ω= 500 rpm .

From the slope of the linear part of Bounouara water curve at 20°C (Fig. 2), it can be seen that Bounouara water has a scaling time of around 16 minutes, with a scaling index of approximately 64 min^{-1}. According to this I_s, Ledion [20] classifies Bounouara water as very hard scaling forming water. Comparing the curves shape of Bounouara water at 20 and 40°C, it can be observed that temperature has a favourable role upon

scaling deposition, as expected. The scaling rate increases when the temperature was raised from 20 to 40°C, the scaling time decreases from 16 min to 8 min, the residual current also decreases, and Bounouara water becomes more scale-forming at high temperature. The explanation for this fact is described in the literature [21,22], since the temperature decreases the solubility of dissolved oxygen and increases the diffusion coefficient [22], which leads to an increase of cathodic current of oxygen reduction (Eq. 1) [23]. As observed in Fig.2, the initial current increases when temperature raises from 20 to 40°C.

To study the effectiveness of tomato and strawberry leaves in inhibiting the formation of calcium carbonate, the chronoamperometric assays were carried out for Bounouara water in presence of various concentration of inhibitors extracts, at 20°C and 40°C (Figs. 3 to 6). Figures 3 and 4 present the chronoamperometric experiments realized at different concentration of strawberry leaves extracts for inhibition calcium carbonate formation. The efficiency of the inhibitors, I_{eff}, is calculated according to Eq.5 [9]. The scaling time and residual current increases with inhibitors concentration, and 1 ppm of strawberry extract was sufficient to change the shape of Bounouara raw water curve (Fig. 3a). The scaling time increased from 16 min to 24 min with efficiency of 31%, and the residual current increases from 20 to 31 µA. The scaling time and residual current keep increasing with the strawberry leaves extract concentration. For 15 ppm, at 20 °C, and 30 ppm, at 40 °C, no current reduction was observed, and the scaling time became undetermined (Fig. 4).

$$I_{eff}(\%) = 200\ x\ \frac{t_s\,(treated\ water) - t_s\,(raw\ water)}{t_s\,(treated\ water) + t_s(raw\ water)} \quad (5)$$

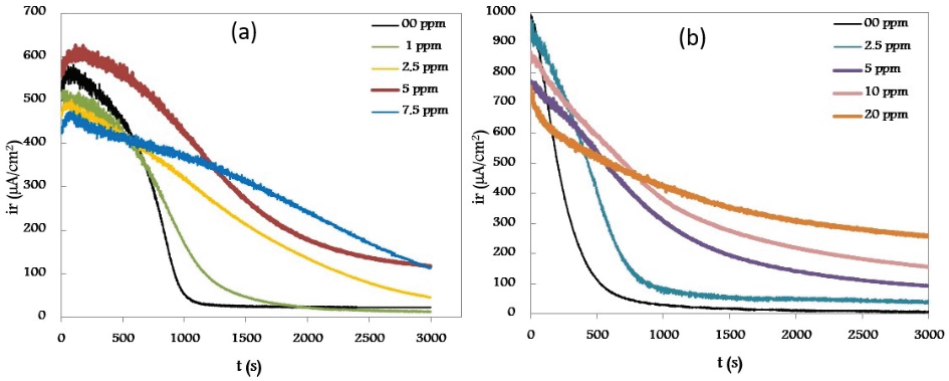

Figure 3: Chronoamperometric curves of Bounouara water in presence of different concentrations of strawberry leaves aqueous extract at 20°C (a) and 40°C (b) on a SS electrode at -1 V (vs SCE), Ω= 500 rpm.

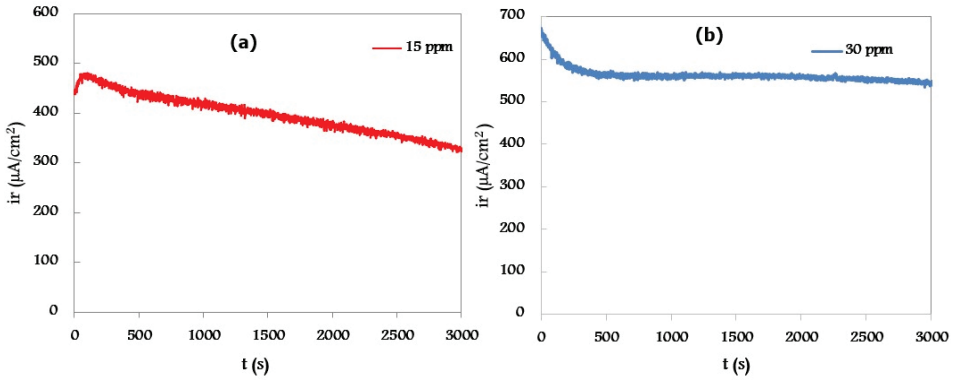

Figure 4: Chronoamperometric curves of optimum concentration of strawberry leaves aqueous extracts, at 20°C (a) and 40°C (b) on a SS electrode at -1 V (vs SCE), Ω= 500 rpm.

Tomato leaves extract has a similar effect on the scaling time and residual current as showing in (Fig 5). However, its efficient in calcium carbonate inhibition is lower, since it reacts with higher concentrations when compared to strawberry leaves extract, and the total inhibition (almost no reduction in current during the assay) was obtained at 20 ppm (Fig. 6a). At 40°C, similar behaviour is observed, i.e., the residual current increases with the inhibitors extract concentration, until reaching a constant value of optimum concentrations. Since Bounouara becomes more scale-forming at 40°C, the extract seems to be less efficient at higher temperature, where higher concentrations were necessary to attain the same rate of inhibition obtained at 20°C (Fig. 6b).

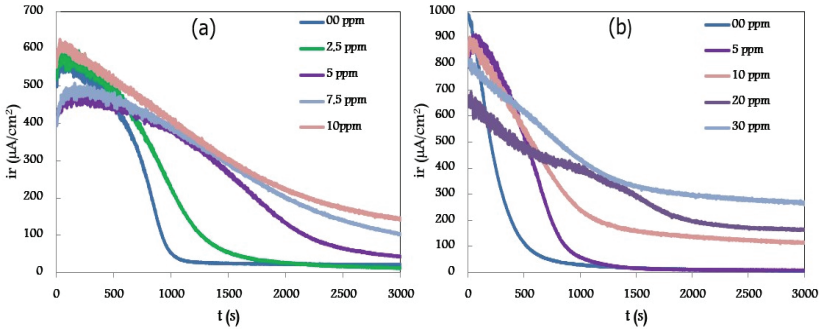

Figure 5: Chronoamperometric curves of Bounouara water in presence of different concentrations of aqueous extract of Tomato leaves at 20°C (a) and 40°C (b) on a SS electrode at -1 V (vs SCE), Ω= 500 rpm.

Impedancemetry study. The effect of strawberry and tomato leaves using impedancemetry was characterized by charge transfer resistance (R_{ct}) values, which were obtained after polarization of the SS electrode in the absence and in the presence of the bio-inhibitors strawberry or tomato leaves extracts (Figs. 7 and 8, respectively). A higher transfer resistance indicates that the formed scale is more compact, and the surface of SS electrode is highly covered by the calcium carbonate crystals. The rate

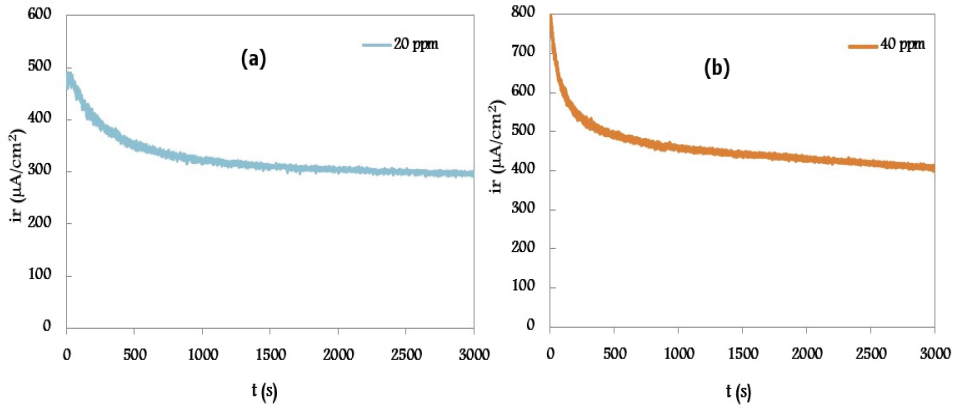

Figure 6: Chronoamperometric curves of optimum concentration of aqueous extract of Tomato leaves at 20°C (a) and 40°C (b) on a SS electrode at -1 V (vs SCE), Ω= 500 rpm.

efficiency (E) is calculated from (Eq.6), where $R_{ct(0)}$ and $R_{ct(inh)}$ refer to the charge transfer resistance for the solutions without and with plant leaves extract, respectively.

$$E(\%) = \frac{R_{ct(0)} - R_{ct(inh)}}{R_{ct(0)}} \times 100 (6)$$

In the absence of the inhibitors, the impedance diagram consists of two loops with real impedances ranging from 0 to 2000 Ω/cm^2 and from 2000 to 8980 Ω/cm^2 at 20°C, from 0 to 4000 Ω/cm^2 and from 4000 to 13850 Ω/cm^2 at 40°C, compared with curves obtained in the presence of strawberry and tomato leaves extracts, where the first loop completely disappears. According Gabrielli et al. [10], the existence of two capacitive loops indicates the presence of the calcite crystals on surface of the electrode. It can also be clearly observed that the diameter of the diagrams loop is decreasing as extracts concentration increases, due to charge transfer resistance decreasing. In fact, R_{ct} of Bounouara raw water is 8980 Ω/cm^2, and this value decreases more than 58% in the presence of 5 ppm of strawberry leaves extract, to become 3815 Ω/cm^2. The addition of similar concentration of tomato leaves extract (Fig. 8) decreases the R_{ct} value to 4175 Ω/cm^2, with an inhibition of 52%. The minimum values of charge transfer resistance were obtained in the presence of 15 ppm at 20°C in the case of strawberry leaves extract and at 20 ppm for tomato leaves extract. These concentrations were also the optimum concentration in chronoamperometry curves. So, the results of impedancemetry are in agreement with those from chronoamperometry. The effect of temperature is noticed on the impedance diagrams, being the R_{ct}decrease, at 40°C, observed for higher concentrations.

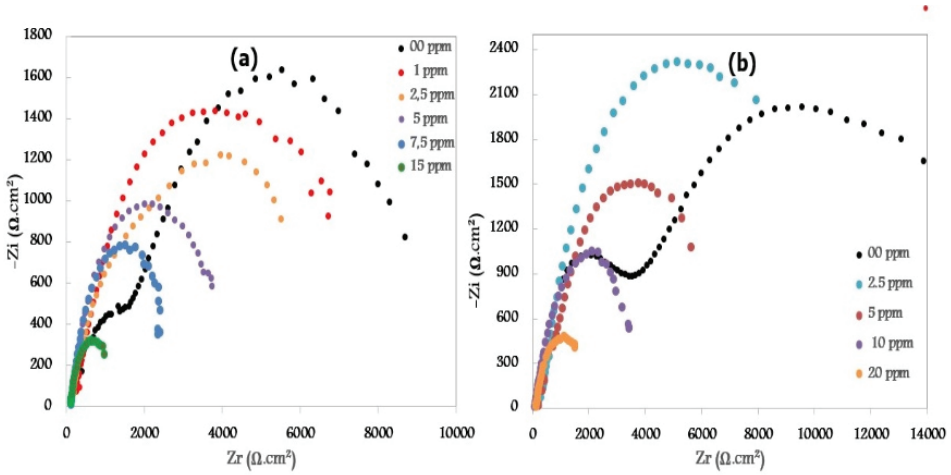

Figure 7: Impedance diagrams of Bounouara water in presence of various concentrations of strawberry leaves aqueous extract at 20°C (a) and 40°C (b), 500 rpm, on: SS at -1VvsSCE.

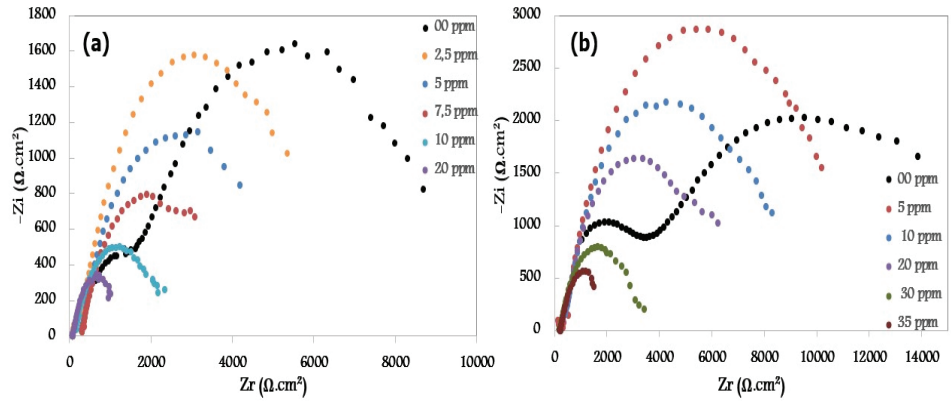

Figure 8: Impedance diagrams of Bounouara water in presence of various concentrations of Tomato leaves aqueous extract at 20°C (a) and 40°C (b), 500 rpm, on SS at -1VvsSCE.

5. Conclusions

The inhibition of scaling formation on a stainless-steel electrode from Bounouara water using agricultural waste was accomplished with success. The electrode's surface is uncovered with the scale particles in the presence of strawberry or tomato leaves extracts at an appropriate concentration. The results obtained show that the aqueous extract of strawberry leaves is more effective than the aqueous extract of tomato leaves because it acts at lower concentrations. The anti-scale capacity of tomato or leaves extracts are higher at lower temperature. Thus, the temperature and the inhibitor concentration influence the kinetics of the scale deposition. The inhibitory effect of natural products, which differs from one product to another, depends on its composition and therefore of its mode of action. Recovery and valorization of agricultural waste in the treatment of hard water is a good solution to clean and protect the environment.

6. Acknowledgements

The authors are very grateful for the support given by research unit Fiber Materials and Environmental Technologies (FibEnTech-UBI) through the project UIDB/00195/2020, funded by the Fundação para a Ciência e a Tecnologia (FCT).

References

[1] Rosset R, Sok P, Poindessous G, Amor MB, Walha K. Caractérisation de la compacité des dépôts de carbonate de calcium d'eaux géothermales du Sud tunisien par impédancemétrie. Comptes Rendus De L'académie Des Scinces.-Serie IIC-Chemestry. 1998;1:751–759. https://doi.org/10.1016/S1251-8069(99)80041-3

[2] Bouchkima B. L'eau de la nappe albienne du sud algérien. Paper presented at: Journées Technique et Scientifique sur la Qualité Des Eaux du Sud; 2003 Mai 19–20; El-Oued, Algerie.

[3] Rakitin AR, Kichigin VI. Electrochemical study of calcium carbonate deposition on iron. Effect anion. Electrochimica Acta. 2009;54(9):2647–2654. https://doi.org/10.1016/j.electacta.2008.10.064

[4] Wang C, Shu-ping L, Tian-duo L. Calcium carbonate inhibition by a phosphonate-terminated poly(maleic-co-sulfonate). Desalination. 2009;(1)249:1–4. https://doi.org/10.1016/j.desal.2009.06.006

[5] Chauhan K, Kumar R, Kumar M, Sharma P, Chauhan GS. Modified pectin-based polymers as green antiscalants for calcium sulfate. Desalination. 2012;305:31–37. https://doi.org/10.1016/j.desal.2012.07.042

[6] Asif M, Faizur R, Hafiz ZS, Syed MZ. Scaling of reverse osmosis membranes used in water desalination: Phenomena, impact, and control; future directions. Desalination. 2019;455:135–157. https://doi.org/10.1016/j.desal.2018.12.009

[7] Goh PS, Lau WJ, Othman MHD, Ismail AF. Membrane fouling in desalination and its mitigation strategies. Desalination. 2018;425:130–155. https://doi.org/10.1016/j.desal.2017.10.018

[8] Demadis KD, Neofotist E, Mavredaki E, Tsiknakis M, Sarigiannidou E-M, Katarachia SD. Inorganic foulants in membrane systems: Chemical control strategies and the contribution of green chemistry. Desalination. 2005;179:281–295. https://doi.org/10.1016/j.desal.2004.11.074

[9] Lin W, Colin C, Rosset R. Caractérisation du pouvoir incrustant d'une eau par chronoampérométrie au potentiel optimal d'entartrage. TSM-L'eau; 1990.France.

[10] Gabrielli C, Keddam M, Khalil A, Rosset R, Zidoune M. Study of calcium carbonate scales by electrochemical impedance spectroscopy. Electrochimica Acta. 1997;42(8):1207–1218. https://doi.org/10.1016/S0013-4686(96)0028-7

[11] Ketrane R, Leleyter L, Baraud F, Jeannin M, Gil O, Saidani B. Characterization of natural scale deposits formed in southern Algeria groundwater. Effect of its major ions on calcium carbonate precipitation. Desalination. 2010;262(1–3):21–30https://doi.org/10.1016/j.desal.2010.05.019

[12] Ben-aazza S, Hadfi A, Mohareb S et al. Geochemical characterization and thermodynamic study of water scaling phenomenon at Tiznit Region in Southern Morocco, Groundwater for Sustainable Development. 2020;11:100379 (1-6). https://doi.org/10.1016/j.gsd.2020.100379

[13] Zeppenfeld K. Prevention of $CaCO_3$ scale formation by trace amounts of copper (II) in comparison to zinc (II). Desalination. 2010;252:60–65. https://doi.org/10.1016/j.desal.2009.10.025

[14] Gu X, Qiu F, Zhou X et al. Synthesis and application of terpolymer scale inhibitor in the presence of β-cyclodextrins. Journal of Petroleum Science and Engineering. 2013;109:177–186. https://doi.org/10.1016/j.petrol.2013.08.021

[15] Boulahlib-Bendaoud Y, Ghizellaoui S, Tlili M. Inhibition of $CaCO_3$ scale formation in ground waters using mineral phosphates. Desalination and Water Treatment. 2012;38:271–277. https://doi.org/10/5004/dwt.2012.1430

[16] Belattar M, Hadfi A, Ben-Aazza S et al. Efficiency of one scale inhibitor on calcium carbonate precipitation from hot water sanitary: Effect of temperature and concentration. Heliyon. 2021;7:e06152 (1-6). https://doi.org/10.1016/j.heliyon.2021.e06152

[17] Anastas PT, Warner JC. Green chemistry: Theory and practice. New York: Oxford University Press; 1998.

[18] Darling D, Rakshpal R. Green chemistry applied to corrosion and scale inhibitors. Materials Performance. 1998;37:42–45.

[19] Thatcher M, Payne G. Impact of the OSPAR decision on the harmonised mandatory control scheme on the offshore chemical supply industry. Manchester: RSC &EOSCA; 2005.

[20] Ledion J, Leroy P, Labbe JP. Détermination du pouvoir incrustant d'une eau par un essai d'entartrage accéléré. Techniques Sciences Méthode(TSM) -L'eau. 1985:323-328.

[21] Ras HS, Ghizellaoui S. Determination of anti-scale effect of hard water by test of electrodeposition. Procedia Engineering. 2012;33:357–365. https://doi.org/10.1016/j.proeng.2012.01.1215

[22] Ketrane R, Saidani B, Gil O, Leleyter L, Baraud F. Efficiency of five scale inhibitors on calcium carbonate precipitation from hard water: Effect of temperature and concentration. Desalination. 2009;249(3):1397–1404. https://doi.org/10.1016/j.desal.2009.06.013

[23] Zidoune M, Khalil A, Sakya P, Colin C, Rosset R. Mise en évidence de l'effet anti-incrustant de l'acide aminotris (méthylènephosphonique) par chronoampérométrie et chronoélectrogravimétrie. Electrochimie. C.R. Academy of Science. 1992;315(2):795–799.

KnE Materials Science

FibEnTech21
1st International FibEnTech Congress (FibEnTech21) New opportunities for fibrous materials in the ecological transition
Volume 2022

Knowledge E
enriching | engaging | empowering

Research article

Opportunities for Microalgae-Bacteria Consortium Application to the Treatment of Effluents Generated in Fiber-Waste-Based Recycling Processes

Josivaldo Sátiro[1,2]*, Sanderson Leitão[1], Arlindo Gomes[2], Rogério Simões[2] and António Albuquerque[1,2]

[1]FibEnTech, GeoBioTec and Department of Civil Engineering and Architecture, University of Beira Interior, Calçada Fonte do Lameiro, 6201-001, Covilhã, Portugal
[2]FibEnTech and Department of Chemistry, University of Beira Interior, Rua Marquês d'Ávila e Bolama, 6201-001, Covilhã, Portugal

Abstract.
Technologies based on microalgae-bacteria seem to be sustainable options for wastewater treatment and reuse, with lower costs than conventional biological treatment technologies. Furthermore, they can generate added-value products produced from algae biomass. Among other advantages, the consortium bacteria-algae produce photosynthetic oxygen through the microalgae, which can be used by aerobic bacteria for oxidizing organic matter and nitrogen, thus reducing the need for introducing artificial oxygen. In this review paper, the main systems that use microalgae-bacteria consortium are discussed. Microalgae-bacteria present advantages in the removal of organics, nitrogen and phosphorus, when compared with conventional biological treatment systems (e.g., activated sludge, percolating filters and ponds), and are able to produce final effluents for reuse (e.g., in agricultural irrigation, industry or aquifer recharge) and excess of microalgae that can be converted to added-value products such as biogas and biofuels. Attention is given to the innovative aspects of applying photobioreators to the treatment and reuse of pulp and paper effluents and fiber-waste-based recycling wastewaters, which seems to open a new opportunity for the pulp, paper and recycling paper industries.

Keywords: fiber-waste-based industry, microalgae-bacteria consortium, removal of nutrients, wastewater treatment

Corresponding Author: Josivaldo Sátiro; email: josivaldo.satiro@ubi.pt

Dates
?????

Publishing services provided by Knowledge E

© Josivaldo Sátiro et al. This article is distributed under the terms of the Creative Commons Attribution License, which permits unrestricted use and redistribution provided that the original author and source are credited.

Selection and Peer-review under the responsibility of the FibEnTech21 Conference Committee.

OPEN ACCESS

1. Introduction

Anthropic activities and water pollution have intensified, due to population growth and the increase in the industrial process in the last decades. Water pollution has been thus caused by inadequate domestic, industrial and agricultural effluent discharge, which provides increases concentrations of nutrients in the environment [1], [2]. The application of biological processes is widely used in the world scenario for the treatment of domestic and industrial wastewater aiming at reducing the generated impacts [3]. However, conventional wastewater treatment plants face technical limitations, with

a high operational cost to obtain nutrient removals [4]. Besides being sustainable, systems that use microalgae-bacteria aggregate and promote more efficient and less costly techniques for the effluents treatment [5]. The great advantage of this system is the production of photosynthetic oxygen, which is used by aerobic bacteria to oxidize organic matter, reducing the need for introducing artificial oxygen into the system. According Ashrafi et al. (2015) [6], wastewater generated in the processes of the paper and cellulose industry is a result of the processes of debarking wood, paper manufacturing, fiber recycling, pulp manufacturing, among others. In general, the operational processes present in this type of industry are chemical, mechanical, thermo- mechanical and chemical-mechanical, so these processes generate a large volume of effluents with a range of pollutants. It seems that the use of microalgae-bacteria consortium (MABA) for wastewater treatment would lead less costly operation with greater efficiency in removal of nutrients. Therefore, the main objective of this article is to analyse the opportunity in using the consortium microalgae-bacteria for wastewater treatment from paper pulp and used paper recycling.

2. Use of microalgae-bacteria consortium in wastewater treatment

Microalgae and bacterial aggregate systems constitute a symbiotic form of the consortium of these elements and can be applied to wastewater treatment [7]. Such systems do not require the addition of artificial oxygen, in contrast to activated sludge or aerobic granular sludge systems, which demand high energy costs, due to the insertion of artificial oxygen and because they are operationally complex processes [8]. In general, the aerobic systems commonly used for wastewater treatment are aerated lagoons, biological filters and activated sludge [9]. However, closed photobioreactors stand out for their better control of operation, as well as in the supply of CO2, temperature, lighting, crop density, pH levels and mixing rates [10]. These photobioreactors are characterized by aerobic decomposition commonly known as fermentation and respiration, biosynthesis and endogenous respiration; and their main feature is the conversion of organic compounds into biomass and CO2 [11]. The operation of photobioreactors can occur in two ways: in sequential batches [12]–[14] and in continuous flow [15]–[17], with anaerobic and anoxic zones [18]. Table 1 presents the characteristics of several photobioreactors in sequential batches (PBSB). It can be seen that the behaviour of the aggregate depends on the species of microalgae attached to the biomass. According to Zhao et al. (2018) [19] and Liu et al. (2018) [20] applied variations of aeration and lighting in the PBSB

and thus found granules with a great abundance of microalgae from the seventh day of operation and particle size larger than 2.5 mm. [14], using synthetic wastewater, obtained removals of 99% of COD and 96% of N-ammonia, due to the good stability and content of extracellular polymeric substances (EPS) found in the MABAs.

Table 2 presents the characteristics of several continuous flow photobioreactors (PBCF), which present low installation and operation costs, when compared to the batch system, and a simpler operation [15]. However, when applied in systems with microalgae-bacteria aggregate, there is greater concern and caution with food control, to ensure the structural integrity of the biomass in its stratified form [21]. Ansari et al. (2017) [22] compared two ways of operating the PBCF with the microalgae-bacteria aggregate and with recirculation. The results showed better performance in the microalgae reactor, reaching 100%, 98% and 64% COD, TN and TP removals, respectively. In addition, the PBCF system showed greater energy efficiency when compared to PBSB with microalgae-bacteria consortium of [23]. Hydraulic retention time (HRT) in the order of 24 hours results in higher operational costs. According to Ahmad et al. (2017) [15] were able to establish MABAs in PBCF with 6-hour HRT, treating effluent with COD: 300mg/L; NH4-N: 100mg/L; PO4-P: 10mg/L). Some studies indicate the need for an internal sedimentation zone in PBCF in order to avoid washing the biomass, and the applied pressure must be associated with the particle sedimentation velocity. There are still few investigations on the behaviour of these aggregates, considering that the use of the microalgae-bacteria consortium for wastewater treatment arises with the objective of filling the gap of costly systems for treatment, thus allowing for a reduction energy consumption, as well as promoting biomass harvesting with greater sedimentability [24], [25]. Biomass generated by the consortium has a high molecular weight, high lipid content and, due to this, has a high potential to produce methane and biofuels [26], [27].

3. Application of microalgae-bacteria consortium fibers-waste-based recycling effluents

Despite the wide applicability for domestic wastewater treatment, in general, the use of microalgae- bacteria consortium can be applied to industrial effluents (Table 3), as an alternative technology for producing final effluents for discharge in watercourses or for reuse (*e.g.* in agricultural irrigation, industry or aquifer recharge). Satisfactory results from aerobic treatment systems were found in the use of high rate activated sludge (pilot scale) treating effluents from pulp and paper industries [9], [29]. These

TABLE 1: Studies that applied the microalgae-bacteria consortium in photobioreactors operated in sequential batches (PBSB).

Type of treatment concentration (mg/L)	Reactor dimensions and operating conditions	Treatment performance	Biomass Characteristics	Microalgae species present	Remarks	References
Synthetic sewage (50% glucose and 50% sodium acetate) COD = 200 mg/L; $NH4^{+}$-N = 20 mg/L; PO_4^{3-}-P = 5 mg/L;	Volume = 3.6L; Natural lighting; HRT = 12h. 300 mL/min flow rate	-	Dark green granules were observed on day 7 of operation	*Diatomea, Chlorophyceae, Chrysophyceae* and *Trebouxioplyceae* (naturally growing algae)	The symbiosis decreased the average size and sedimentation capacity of the granule, but stimulated bioactivity	[12]
Synthetic sewage (sodium acetate) COD = 50-400 mg/L; $NH4^{+}$-N = 50 mg/L; PO_4^{3-}-P = 10 mg/L;	Volume = 0.92 L; Light intensity 7200 lux (12 h light phase and 12 h dark phase; TDH = 7.5 hours; 0.55 cm/s air flow rate through an air pump at the bottom of the reactor	Best performance COD/N = 8 for nutrient and organic matter removal. 96% COD removal; 100% nitrification efficiency;	MLVSS = 3.21 g/L. Well-formed dark green granules, with an average diameter of 2.5 mm.	-	Satisfactory results with COD/N = 1	[19]
Synthetic sewage (glucose) COD = 300 mg/L; $NH4^{+}$-N = 35 mg/L; PO_4^{3-}-P = 10 mg/L;	Volume = 2 L; Light intensity 200-6000 lux (12 h light phase and 12 h dark phase; Introduction of air at the bottom of the reactor	98.4% $NH4^{+}$-N removal; 50.2%PO_4^{3-}-P removal;	MLVSS = 28.9 mg/L; IVL5 = 24 ml/g;	*Chlorella sp. and Scenedesmus sp.* (Targeted algae)	Directed algae maintain dominance during the experiment. The intercropping showed better performance in nutrient removal efficiency.	[20]

processes are also efficient in the removal of pharmaceutical compounds, being applied under ideal operating parameters for the removal of antibiotics, antihypertensives and psychiatric drugs [2], [30]. Additionally, during system operation, the process of gas transfer is also evident, in which the photosynthetic oxygen produced is used by aerobic bacteria to oxidize organic matter, reducing the need for introducing artificial oxygen into the system. On the other hand, bacteria, through the action of the enzyme carbonic

Table 2: Studies that applied the microalgae-bacteria consortium in continuous flow photobioreactors (PBCF).

Type of treatment concentration (mg/L)	Reactor dimensions and operating conditions	Treatment performance	Biomass Characteristics	Microalgae species present	Remarks	References
Synthetic sewage (50% glucose and 50% sodium acetate) R1:COD=300-600 mg/L; $NH4^+$-N =200 mg/L; PO_4^{3-}-P = 20 mg/L; R2: COD = 300 mg/L; $NH4^+$-N = 100 mg/L; PO_4^{3-}-P = 10 mg/L;	HRT = 6 hours; 60 min of aeration and 30 min without aeration. DO=7-8 mg/L Intensity of illumination 900-1100; TRS = 30-70 days. R1 = 1L; H=31cm; D = 6.5 cm R2-1 and R2-2 in series: 1L; H = 23 cm; D = 5.3 cm	R1:(96% COD removal; 94%$NH4^+$-N removal; 46% removal of phosphorus); R2:(95% COD removal; 99%$NH4^+$-N removal; 50% phosphorus	R1 : Average diameter 1.0 – 1.5mm; MLVSS = 4.8 g/L; IVL = 44 mL/g R2 : Average diameter 1.0 – 1.5mm; MLVSS = 4.3 g/L; IVL = 49 mL/g	*Phormidium sp.* (Algae that grow naturally)	Formation of alga- bacteria granules Internal separator made hydraulic selection easier	[22]
Synthetic sewage (sodium acetate) COD = 300 mg/L; $NH4^+$-N = 152 mg/L; PO_4^{3-}-P = 47 mg/L;	Volume = 2L; Light intensity on the surface 200 µmol/(m2·s); HRT = 24 h; No oxygen supply; Use of magnetic mixer;	90% COD removal; 94.5%$NH4^+$-N removal; 9% phosphorus removal;	MLVSS = 4g/L	*Scenedesmus sp.; Closterium sp; Chlorella sp.; Diatoms; Oscillatoria Sp; Chroococcus sp*	Heterotrophic, autotrophic, algae and PAO bacteria coexisted and functioned in the reactor. Stable reactor performance.	[16]
Wastewater with dyes COD = 600-750 mg/L; $NH4^+$-N = 20-30 mg/L; PO_4^{3-}-P = 5-6 mg/L;	Volume = 5L; Rectangular with three phases and sedimentation zone HRT = 16; TRS = 15 days; DO = 2.8 mg/L	78-85% COD removal; 88.6% removal of $NH4^+$-N; 36.6% removal of phosphorus;	MLVSS = 3,4 g/L; IVL = 135 mL/g	*Chlorella; Filamentous algae; Selenastrum bibraianum*	Color reduced 60- 80 times compared to the TEE under study. Best performance with TDH=16h; DO=0.45 mg/L	[17]

anhydrase (CA), release CO2 from the breathing process, in which they are assimilated in the form of HCO3- by microalgae [31]. The great challenge for application in industrial effluents - such as the pulp and paper industry, is related to the composition of the effluent generated, in particular chemical products and heavy metals, which can be toxic and cause negative environmental impacts in aquatic bodies [32]. The effluents produced in industries of pulp and paper and fibers-waste-based recycling processes

are important sources of heavy metals [33] and, therefore, innovative solutions should be looked in order to improve recycling and reuse of wastes.

During paper production, several fibers are produced including wastepaper, and cellulose fibers from plants and trees, which are mixed in aqueous cellulosic suspension through filters or other shear device [34]. The main characteristics of these wastewater may include strong color, due to organic and extractive compounds, tannin resins, synthetic dyes, lignin and the degradation products formed by the action of chlorine on the lignin during the bleaching process [35]. Some researchers have used microalgae for removing high content of nitrogen and phosphorus in pulp and paper effluents [36]. Additively, microalgal species such as *Microcystis, Chlorella, Chlamydomonas,* in good lighting conditions, can remove up to 80% of the color. Table 3 shows some data collected in research works that have used microalgae for treating wastewater from the pulp and paper industry, showing an average total nitrogen removal of 80% and an average total phosphorus removal of around 70% [37], [38]. The most applied microalgae species in the works was *Chlorella vulgaris* and *Scenedesmus sp.* The works indicate good conditions of the algae biomass production, with high protein and lipid content, which could be used for bioenergy and biofuel production [39], [40], such as biodiesel and bioethanol, but also for energy, animal feed, and fertilizers production. In this context, in addition to economic aspects and nutrient removal, the application of microalgae-bacteria consortium to pulp and paper mills and fibers-waste-based recycling effluents shows potential for resource recovery, contributing for the circular economy [41]. Subashchandrabose *et al.,* (2011) [42] indicated that the consortium algae-bacteria can reach high efficiencies in removing heavy metals, organics, nitrate and phosphate.

4. Conclusion

This work has shown that photobioreactors are a viable technology for industrial wastewater treatment and reuse. The consortium microalgae-bacteria may bring several advantages for the treatment of pulp and paper mills and fibers-waste-based recycling effluents, when compared to conventional wastewater treatment technologies. This technology allows producing oxygen, carbon sequestering, removal of water pollutants such as biodegradable organics, refractory organics, nutrients and heavy metals by the industry, and the production of added-value products, which are advantages for the pulp, paper and recycling paper industries.

TABLE 3: Studies that applied microalgae-bacteria consortium to wastewater treatment in the paper industry.

Type of treatment concentration (mg/L)	Reactor dimensions and operating conditions	Treatment performance	Microalgae species present	Remarks	References
Wastewater paper industry $NH4^{+}$-N = 22,35 mg/L PO_4^{3-}-P = 10,1 mg/L	Radiation (PAR) = 130.0 µmol.m-2s-1 Air Pump = 50 L/h Volume = 500mL	96% ammonia removal 91% phosphate removal	*Scenedesmus dimorphus Selenastrum minutum*	Biomass generated with high lipid content.	[40]
Wastewater paper industry NO_3-N = 2,24 mg/L PO_4^{3-}-P = 9,86 mg/L	Outdoor open circular tanks (1m x 1.5m) Volume = 30 L	65% nitrogen removal 71% phosphorus removal	*Scenedesmus sp.*	Obtainment of protein-rich biomass with significant production of linolenic acid.	[43]
Wastewater paper industry COD = 296 mg/L NO_3-N = 8,73 mg/L NO_2-N = 3,42 mg/L PO_4^{3-}-P = 12,3 mg/L	Volume = 950 mL Air Pump = 90 L/h	80% removal of nitrogen (nitrite + nitrate) 54% phosphorus removal	*Chlorella vulgaris*	The microalgae species used showed good adaptation for phosphorus removal.	[37]
Wastewater pulp and paper industry COD = 266 mg/L TN = 3,6 mg/L TP = 3,72 mg/L	Volume = 1 L Variation in effluent concentration 20%, 40%, 60%, 80% and 100%. Radiation = 202,9 µmol.m-2s-1	82% average nitrogen removal 87% average removal of total phosphorus	*Chlorella vulgaris*	Treatment was sustainable based on microalgae, with potential for generating bioenergy.	[38]

5. Acknowledgments

The authors are grateful to the Foundation for Science and Technology (FCT, Portugal) for financial support by national funds through the projects UIDB/00195/2020 (FibEnTech) and UIDB/04035/2020 (GeoBioTec).

References

[1] Chan Y, Chong MF, Law CL. A review on anaerobic-aerobic treatment of industrial and municipal wastewater. Chemical Engineering Journal. 2009;155(1–2):1–18. https://doi.org/10.1016/j.cej.2009.06.041

[2] Gallardo-Altamirano MJ, Maza-Márquez P, Montemurro N, Rodelas B, Osorio F, Pozo C. Linking microbial diversity and population dynamics to

the removal efficiency of pharmaceutically active compounds (PhACs) in an anaerobic/anoxic/aerobic (A2O) system. Chemosphere. 2019;233:828–842. https://doi.org/10.1016/j.chemosphere.2019.06.017

[3] Goli A, Shamiri A, Khosroyar S, Talaiekhozani A, Sanaye R, Azizi K. A review on different aerobic and anaerobic treatment methods in dairy industry wastewater. Journal of Environmental Treatment Techniques. 2019;6(1):113–141.

[4] Godos I. A comparative evaluation of microalgae for the degradation of piggery wastewater under photosynthetic oxygenation. Bioresource Technology. 2010;101(14):5150–5158. https://doi.org/10.1016/j.biortech.2010.02.010

[5] Chandra R, Iqbal H, Vishal G, Lee H, Nagra S. Algal biorefinery: A sustainable approach to valorize algal-based biomass towards multiple product recovery. Bioresource. Technology. 2019;278:346–359. https://doi.org/10.1016/j.biortech.2019.01.104

[6] Ashrafi O, Yerushalmi L, Haghighat F. Wastewater treatment in the pulp-and- paper industry: A review of treatment processes and the associated greenhouse gas emission. Journal Environmental. Management. 2015;158:146–157. https://doi.org/10.1016/j.jenvman.2015.05.010

[7] Lee Y, Lei Z. Microalgal-bacterial aggregates for wastewater treatment: A mini-review. Bioresource Technology Reports. 2019;8:100199. https://doi.org/10.1016/j.biteb.2019.100199

[8] Sun L. Performance and microbial community analysis of an algal-activated sludge symbiotic system: Effect of activated sludge concentration. Journal Environmental Sciences (China). 2019;76:121–132. https://doi.org/10.1016/j.jes.2018.04.010

[9] Show K, Lee D. Anaerobic treatment versus aerobic treatment. Current Developmentss in Biotechnology and Bioengineering. Elsevier. 2017; 205-230.

https://doi.org/10.1016/B978-0-444-63665-2.00008-4

[10] Gupta P, Lee S, Choi H. A mini review: Photobioreactors for large scale algal cultivation. World Journal of Microbiology Biotechnology. 2015;31(9):1409–1417. https://doi.org/10.1007/s11274-015-1892-4

[11] Miao Y. Partial nitrification-anammox (PNA) treating sewage with intermittent aeration mode: Effect of influent C/N ratios. Chemical Engineering Journal. 2018;334:664–672. https://doi.org/10.1016/j.cej.2017.10.072

[12] He Q. Natural sunlight induced rapid formation of water-born algal-bacterial granules in an aerobic bacterial granular photo-sequencing batch reactor. Journal of Hazardous Materials. 2018;359:222–230. https://doi.org/10.1016/j.jhazmat.2018.07.051

[13] Li B. Effect of TiO2 nanoparticles on aerobic granulation of algal-bacterial symbiosis system and nutrients removal from synthetic wastewater. Bioresource Technology. 2015;187:214–220. doi: 10.1016/j.biortech.2015.03.118.

[14] Zhang B. Enhancement of aerobic granulation and nutrient removal by an algal–bacterial consortium in a lab-scale photobioreactor. Chemical Engineering Journal. 2018;334:2373–2382. doi: 10.1016/j.cej.2017.11.151.

[15] Ahmad J. Stability of algal-bacterial granules in continuous-flow reactors to treat varying strength domestic wastewater. Bioresource Technology. 2017;244:225–233. doi: 10.1016/j.biortech.2017.07.134.

[16] Yang J, Gou Y, Fang F, Lu L, Zhou Y. Potential of wastewater treatment using a concentrated and suspended algal-bacterial consortium in a photo membrane bioreactor. Chemical Engineering Journal. 2018;335:154–160. doi: 10.1016/j.cej.2017.10.149.

[17] Lin C, Cao P, Xu X, B Ye. Algal-bacterial symbiosis system treating high-load printing and dyeing wastewater in continuous-flow reactors under natural light. Water (Switzerland). 2019;11, 469. doi: 10.3390/w11030469.

[18] Ji X, Jiang M, Zhang J, Zheng Z. The interactions of algae-bacteria symbiotic system and its effects on nutrients removal from synthetic wastewater. Bioresource Technology. 2017;247:44–50, 2018, doi:10.1016/j.biortech.2017.09.074.

[19] Zhao Z, Yang X, Cai W, Lei Z, Shimizu K. Response of algal-bacterial granular system to low carbon wastewater: Focus on granular stability, nutrients removal and accumulation. Bioresource Technology. 2018;268:221–229. doi: 10.1016/j.biortech.2018.07.114.

[20] Liu L, Zeng Z, Bee M, Gibson V, Wei L, Huang X. Characteristics and performance of aerobic algae-bacteria granular consortia in a photo-sequencing batch reactor. Journal of Hazardous Materials. 2018;349:135–142. doi:10.1016/j.jhazmat.2018.01.059.

[21] Corsino S, Campo R, Di Bella P, Torregrossa M, Viviani G. Study of aerobic granular sludge stability in a continuous-flow membrane bioreactor. Bioresource Technology. 2016;200:1055–1059. doi: 10.1016/j.biortech.2015.10.065.

[22] Ansari F, Shriwastav A, Gupta S, Rawat I, Bux F. Exploration of microalgae biorefinery by optimizing sequential extraction of major metabolites from Scenedesmus obliquus. Industrial & Engineering Chemistry Research. 2017;12:3407-3412. doi:10.1021/acs.iecr.6b04814.

[23] Huang W, Li B, Zhang C, Zhang Z, Lei Z. Effect of algae growth on aerobic granulation and nutrients removal from synthetic wastewater by using sequencing batch reactors. Bioresource Technology. 2015;179:187–192. doi:10.1016/j.biortech.2014.12.024.

[24] Christenson L, Sims R. Production and harvesting of microalgae for wastewater treatment, biofuels, and bioproducts. Biotechnology Advances. 2011;29(6):686–702. Doi:10.1016/j.biotechadv.2011.05.015.

[25] Mata T, Martins A, Caetano N. Microalgae for biodiesel production and other applications: A review. Renewable and Sustainable Energy Reviews. 2010;14(1):217–232. doi:10.1016/j.rser.2009.07.020.

[26] Wang Y et al. Perspectives on the feasibility of using microalgae for industrial wastewater treatment. Bioresource Technology. 2016;222:485–497. doi:10.1016/j.biortech.2016.09.106.

[27] Arcila J, Buitrón G. Microalgae – bacteria aggregates: Effect of the hydraulic retention time on the municipal wastewater treatment, biomass settleability and methane potential. Journal Chemical Technology and Biotechnology. 2016; 2862-2870. doi: 10.1002/jctb.4901.

[28] Wang Y, Guo W, Yen H, Ho S, Lo Y. Cultivation of Chlorella vulgaris JSC-6 with swine wastewater for simultaneous nutrient/COD removal and carbohydrate production. Bioresource Technology. 2015;198:619–625. doi:10.1016/j.biortech.2015.09.067.

[29] Lang X, Li Q, Xu Y, Ji M, Yan G. Aerobic denitrifiers with petroleum metabolizing ability isolated from caprolactam sewage treatment pool. Bioresource Technology. 2019;290:121719. doi: 10.1016/j.biortech.2019.121719.

[30] Xiong J, Kurade M, Shanab R, Ji M, Choi J, Kim J, Jeon B. Biodegradation of carbamazepine using freshwater microalgae Chlamydomonas mexicana and Scenedesmus obliquus and the determination of its metabolic fate. Bioresource Technology. 2016;205:183–190. doi:10.1016/j.biortech.2016.01.038.

[31] Kampschreur M, Temmink H, Kleerebezem R, Jetten M. Nitrous oxide emission during wastewater treatment. Water Resource 2009;43(17):4093–4103. doi:10.1016/j.watres.2009.03.001.

[32] Häder DP. Ecotoxicological monitoring of wastewater. Bioassays Advances Methods Applications. 2018:18,369–386. doi:10.1016/B978-0-12-811861-0.00018-8.

[33] Chia S, Chew K, Leong H, Ho S, Munawaroh H, Show P. CO2 mitigation and phycoremediation of industrial flue gas and wastewater via microalgae-bacteria consortium: Possibilities and challenges. Chemical Engineering Journal. 2021;425:131436. doi:10.1016/j.cej.2021.131436.

[34] Boguniewicz-Zablocka J, Klosok-Bazan I, Naddeo V, Mozejko J. Cost- effective removal of COD in the pre-treatment of wastewater from the paper industry. Water Science Technology. 2020;81(7):1345–1353. doi:10.2166/wst.2019.328.

[35] Buyukkamaci N, Koken E. Economic evaluation of alternative wastewater treatment plant options for pulp and paper industry. Science of The Total Environment 2010;408(24):6070–6078. doi:10.1016/j.scitotenv.2010.08.045.

[36] Gurumoorthy P, Saravanan A. Biofuel production from marine microalgae Nannochloropsis salina using paper mill effluents. International Journal of Mechanical Engineering Technology. 2019;10(1):1471–1477.

[37] Porto B, Gonçalves A, Esteves A, Souza S, Souza A, Vilar V, Pires J. Microalgal growth in paper industry effluent: Coupling biomass production with nutrients removal. Applied sciences. 2020;10,3009. doi:10.3390/app10093009.

[38] Silva M, Gonçalves A, Vilar V, Pires J. Article experimental and techno-economic study on the use of microalgae for paper industry effluents remediation. Sustainability. 2021;13(3):1–29. doi: 10.3390/su13031314.

[39] Kumar A, Srivastava N, Gera P. Removal of color from pulp and paper mill wastewater- methods and techniques- A review. Journal Environmental Management. 2021;298(August):113527.

[40] Gentili FG. Microalgal biomass and lipid production in mixed municipal, dairy, pulp and paper wastewater together with added flue gases. Bioresource Technology. 2014;169:27–32. doi: 10.1016/j.biortech.2014.06.061.

[41] Sutherland D, Park J, Heubeck S, Ralph P, Craggs R. Size matters – Microalgae production and nutrient removal in wastewater treatment high rate algal ponds of three different sizes. Algal Research. 2020;45(July):101734. doi:10.1016/j.algal.2019.101734.

[42] Subashchandrabose S, Ramakrishnan B, Megharaj M. Consortia of cyanobacteria / microalgae and bacteria: Biotechnological potential. Biotechnology Advances. 2011;29:896–907. doi: 10.1016/j.biotechadv.2011.07.009.

[43] Usha M, Sarat C, Sarada R, Chauhan V. Removal of nutrients and organic pollution load from pulp and paper mill effluent by microalgae in outdoor open pond. Bioresource Technology. 2016;214:856–860. doi:10.1016/j.biortech.2016.04.060.

KnE Materials Science

FibEnTech21
1st International FibEnTech Congress (FibEnTech21) New opportunities for fibrous materials in the ecological transition
Volume 2022

Knowledge E
enriching | engaging | empowering

Research article

Phytoremediation of Boron From Wastewater in Vertical Flow Constructed Wetlands

Pedro Correia[1,2,3], Carlos Ribeiro[1], Humberto Chaves[1,4], Fátima Carvalho[1,3,4], and Adelaide Almeida[1,3,4]*

[1]Polytechnic Institute of Beja, Higher School of Agriculture, Department of Technologies and Applied Sciences, Rua Pedro Soares - Campus do IPBeja, 7800-295 Beja, Portugal.
[2]Faculty of Science and Technology, University of Algarve, 7, Campus de Gambelas, 8005-139 Faro, Portugal
[3]CENSE - Center for Enviromental and Sustainability Research, Faculty of Science and Technology, University Nova de Lisboa, 2829-516 Caparica, Portugal
[4]FibEnTech – Fiber Materials and Environmental Technologies, R. Marques de Avila e Bolama, 6201-001, Covilhã, Portugal

Abstract.
The aim of this work was to evaluate the possibility of boron removal from synthetic wastewater using a vertical constructed flow (VFCW) planted with *Vetiveria zizanioides*. Two boron concentrations were used (15 ± 1 and 30 ± 1 mg L^{-1}) and a hydraulic load (H_L) of 191 ± 10 L $m^{-2}d^{-1}$. The wastewater samples were taken and the flow rate in the inlet and outlet of the VFCW were measured. The levels of dissolved oxygen, electrical conductivity, pH and boron were determined in the wastewater. The concentrations of the essential elements and nutrients, namely total Kjeldhal nitrogen, phosphorus, calcium, magnesium, sodium and potassium in above growth biomass composition were measured. The results showed that: boron removal efficiencies depended on the boron concentration, so 60 ± 3% was obtained for the 15 mg L^{-1} concentration and 26 ± 2% for 30 mg L^{-1}; calcium, magnesium, potassium and sodium concentrations in the vegetal biomass decreased to the boron concentration of 30 mg L^{-1}, and boron may have interfered with *Vetiveria zizanioides* growth.

Keywords: biomass composition, boron removal, light expanded clay aggregates, *Vetiveria zizanioides*, vertical flow constructed wetland

Corresponding Author: Adelaide Almeida; email: maalmeida@ipbeja.pt

Dates
?????

Publishing services provided by Knowledge E

© Pedro Correia et al. This article is distributed under the terms of the Creative Commons Attribution License, which permits unrestricted use and redistribution provided that the original author and source are credited.

Selection and Peer-review under the responsibility of the FibEnTech21 Conference Committee.

OPEN ACCESS

1. Introduction

Boron (B) is an inorganic, semi-metallic, water-soluble compound that causes environmental problems, especially in surface waters due to agricultural runoff, since its use is strongly associated with fertilizers and pesticides. The forms in which boron is present in wastewater are quite variable, and the some of the factors that control this are the pH of the water and the concentration of these compounds. That is, at high concentrations, greater than 50 mg L^{-1}, pH $\leq$ 10, boron is found essentially in the forms of triborate ($[B_3O_3(OH)_5]^{2-}$), tetraborate ($[B_4O_5(OH)_4]^{2-}$). However, at low concentrations (less than 4.8 mg L^{-1}), it is essentially found in the form of boric acid (H_3BO_3), borate ion ($[B(OH)_4]^-$) and boron oxide (B_2O_3) [16].The contamination of surface water and

groundwater, derived from excess boron (B), can cause toxicity and chronic effects on crops and plants, and can also contaminate soil and/or sediment, as well as promote problems in the reproduction of some animal species and in humans [17]. Therefore, it is necessary to treat urban or industrial effluents in order to minimize/reduce the presence of this contaminant in water used for irrigation and drinking water production [18]. Effluent treatment is often carried out through electro-coagulation, ion exchange, adsorption, among others [19]. These technologies are known for their efficiency in removing some pollutants, such as heavy metals and organic matter, but are not suitable for boron removal [5, 6]. Vertical flow constructed wetland (VFCW), are environmentally sustainable technologies with characteristics and processes similar to natural wetlands and are used for wastewater treatment [7, 8, 9, 10]. These systems are designed and built with the objective of using the natural processes involving the plants, the substrate and their interaction with the microbial community present to treat effluents in a controlled manner. They have been used to treat various types of effluents, including urban wastewater, industrial wastewater, storm water, acid mine water, and to remove organic and inorganic pollutants, heavy metals, boron compounds, and many other pollutants [18].

This work aimed to study the possibility of using constructed wetlands planted with the *Vetiveria Zizanioides* to treat synthetic urban wastewater with high boron concentration and evaluate the effects of two different and increasing boron concentrations in above grow leaves biomass composition.

2. Methods

2.1. Characteristics of experimental set-up

The experimental work was carried out by 24 weeks in a pilot-scale VFCW with an area of 0.24 m^2 and a depth of 0.70 m filled with light expanded clay aggregates (Leca® NR 10/20) and planted with *Vetiveria zizanioides*. Batches of 125 dm^3 of boric acid (H_3BO_3) in aqueous solution were homogenized by one submersible pumps and VFCWs were fed through a network of equidistant sprinklers. The medium was not saturated due to effluent drainage type and substrate material used, allowing the oxygen diffusion into the beds. The affluent was prepared using H_3BO_3 as a boron source, with a variable concentration. The VFCW was fed with synthetic wastewater, prepared by mixing tap water with KNO_3, Na_2HPO_4, CH_4N_2O, KH_2PO_4, $CaCl_2$, $MgCl_2$, $FeSO_4$ and $C_2H_2NaO_2$ prepared according to Almeida et al. [26].

2.2. Experimental conditions

It was used two different and increasing boron concentrations (15 ± 1 and 30 ± 1 mg L^{-1}) and the flow rate to the VFCW was kept constant, with and hydraulic load (H_L) of 191 ± 10 L $m^{-2}d^{-1}$, as described in Table 1.

2.3. Sampling collection and analysis

The system was monitored at all times during the testing period, from Monday to Friday, around 10 a.m. At the beginning of each test, a value was set for the feed flow rate, depending on the hydraulic load (H_L) with which it was intended to work. The measurements of flow rate, at the influent and effluent of the VFCW, were performed manually, in a valve placed at the inlet of the VFCW and in the liquid outlet siphon, with the aid of a stopwatch. The samples were analyzed for pH, electrical conductivity (EC), redox potential (Eh), dissolved oxygen (DO). To determine the remaining parameters, when it was not possible to analyze them immediately, aliquots were stored and conserved at -20°C for short periods of time, as indicated in *Standard Methods of Analysis* [27].

Visual observation of the system was done in order to detect possible toxicity effects on the plants (tissue). Plant growth was through marking and measurements at the beginning of the trial. The leaf biomass was also sampled for subsequent determination of nitrogen, moisture, chlorophylls (a, b, total) and carotenoids. The mineral and nutrient composition was also determined, namely the calcium (Ca^{2+}), magnesium (Mg^{2+}), sodium (Na^{+}), potassium (K^{+}), phosphorus (P) and nitrogen (N) content according to Horneck & Miller [28].

TABLE 1: Operational condition applied to the VFCW. Values are means ± standard deviation (SD), (n ≥ 10).

Exp	**H_L** (L $m^{-2}d^{-1}$)	**[B]** (mg L^{-1})
1	191 ± 10	30 ± 1
2		15 ± 1

3. Data analysis

Results were statistically verified using software the software ”Statistica 12 ’”(StatSoft Inc. USA) was used. Differences in wastewater quality between influent and effluent of the VFCW bed were tested using ANOVA at the significance level of $p < .05$, Post-hoc (a posteriori) Tukey’s test was used to determine differences between means of specific

variables. All results were presented as means ± standard deviation calculated for n ≥ 10.

4. Results and discussion

Boron removal efficiency up to 60 ± 3% was obtained for a concentration of 15 mg L^{-1}. It can be observed that when the boron concentration increased, the capacity of VFCW to boron removal decreased (Fig 1). Ye et al. [25], in wetland microcosms were obtained B removal efficiency of the 30% to a boron concentration of the 46.5 ± 1.4 mg L^{-1}. Where Gross et al. [29], reported 50% removal for VFCW systems in Israel with an initial concentration of 0.3 ± 0.03 mg L^{-1}. Furthermore, studies from Turkey showed that VFCW systems planted with *T.latifolia* and *P.australis* removed 32% of boron in the effluent at a concentration >1 mg L^{-1} [16]. Rees et al. [30], revealed that B was transported to leaves and stems after being taken up by below-ground parts (roots/rhizomes) in the plants. These findings support the fact that B is transported from roots to stems and leaves into the xylem with the stream of transpiration water. Thus, harvesting could be a viable option for removing of B from CWs when B is efficiently stored into the aboveground biomass.

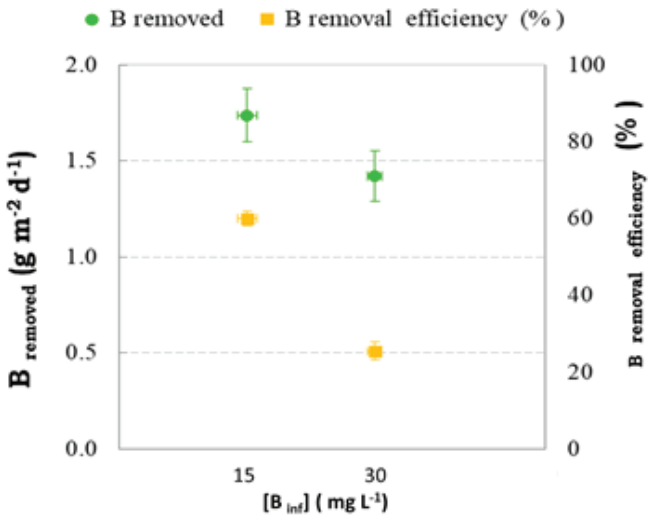

Figure 1: Boron mass load removed and removal efficiencies.

Boron may interfere with the physiological structure of plants or the microorganisms present in the VFCW. When boron concentration was the highest the plants stop growth and leaves chlorosis was observed (Fig. 2).

Dissolved oxygen (DO) and pH (Fig. 3) in effluent were decreased with significantly differences in trial that was done with lower boron concentration (15 mg L^{-1}) or lower

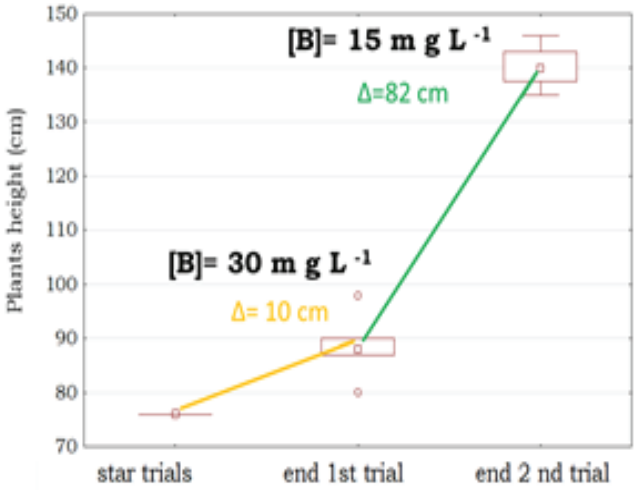

Figure 2: Plants leaf growth during the experimental trials.

boron probably due to the boron phytoremediation processes that can consume oxygen. The pH decreased in effluent because boron removal mechanisms can produce H^+ so pH decreased. The redox potential (Eh) (Fig. 3), like the dissolved oxygen concentration, is a parameter to measure or evaluate the possible occurrence of oxidation-reduction reactions, namely, how degradation or reactions involving oxidation state changes of the boron compounds have occurred.

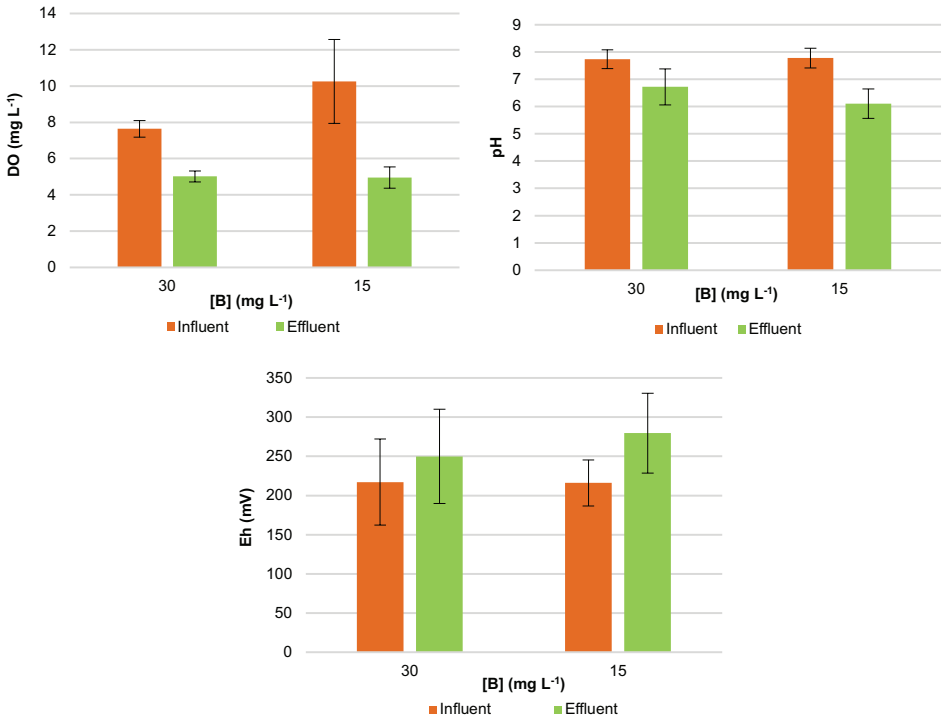

Figure 3: Values of DO, pH and Eh in the influent and effluent.

The micronutrients composition (calcium, magnesium, potassium and sodium in dry biomass (DB)) in vegetal biomass decreased when wastewater boron concentration increased (Table 2).

TABLE 2: Leaf biomass composition at beginning and the end of each trial.

Parameter (mg g^{-1} DB)	**Leaf biomass composition**		
	Start trials	**end**	
		1st trial (30 mg L^{-1} B)	**2nd trial** (15 mg L^{-1} B)
Ca^{2+}	13±1.5	12±4	21±4
Mg^{2+}	22±1	13±1	20±2
Na^{+}	11±4	36±1	45±3
K^{+}	33±41	33±6	68±4
TN	10±1	9±1	11±1
P	1.1±0.1	0.7±0.1	2.6±0.3

The Table 2 it is possible to observe a tendency for an increase, less significant in the test performed with the highest boron concentration (30 mg L^{-1} B). In the analysis of the previous results, boron causes more changes in the cations and nutrients (P and N) present in the leaf biomass of *Vetiveria zizanioides* (Table 2 and Fig. 4).

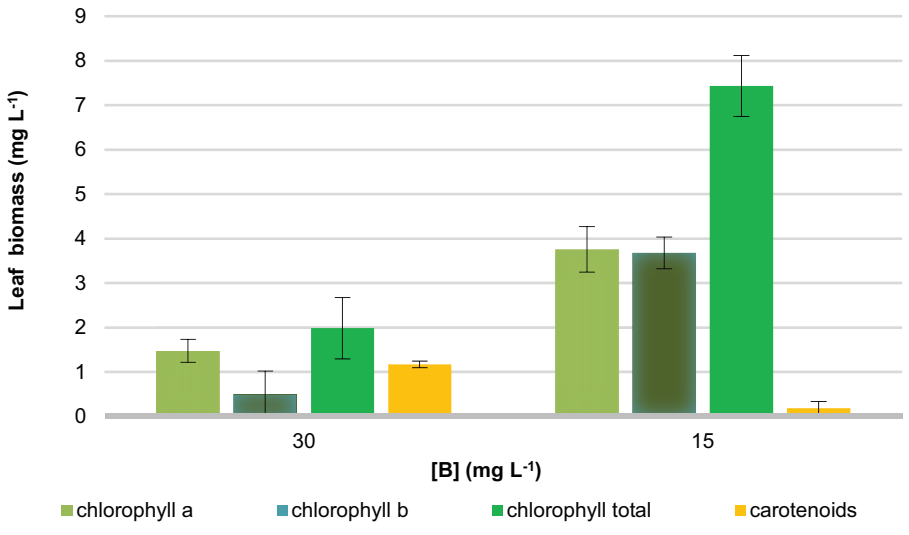

Figure 4: Concentration of chlorophylls a, b, total and carotenoids.

5. Conclusions

Through the analysis of Fig 1, it was found that boron removal occurred by phytoremediation. The main conclusions should be highlighted in this section. So, we can conclude

that Boron removal efficiencies of 60% were obtained for the 15 mg L^{-1} concentration and 26% for 30 mg L^{-1}. Also, Boron may interfere with the *Vetiveria zizanioides* growth and with respectively physiological structure of plants.

6. Acknowledgments

The authors are grateful to the Foundation for Science and Technology (FCT, Portugal) for financial support by national funds through the project UIDB/00195/2020 (FibEnTech).

References

[16] Turker O, Vymazal J, Ture C. Constructed wetlands for boron removal. Ecological Engineering. 2014;64:350-359.

[17] Irawan C, Kuo YL, Liu J. Treatment of boron-containing optoelectronic wastewater by precipitation process. Desalination. 2011;280:146-151.

[18] Correia P. Phytoremediation of effluent with high levels of nitrogen and boron. Beja: Polytechnic Institute of Beja - School of Agriculture; 2019.

[19] Wolska J, Bryjak M. Methods for boron removal from aqueous solutions — A review. Desalination. 2013;310:18–24.

[20] Barth SR. Utilization of boron as a critical parameter in water quality evaluation: Implications for thermal and mineral water resources in SW Germany and N Switzerland. Environmental Geology. 2000;40:73-89.

[21] Kluczka J, Korolewicz T, Zołotajkin M, Adamek J. Boron removal from water and wastewater using. Water Resources and Industry. 2015;11:46-57.

[22] Allende L, Fletcher T, Sun G. The effect of substrate media on the removal of arsenic, boron and iron from an acidic wastewater in planted column reactors. Chemical Engineering Journal. 2012;11:46-57.

[23] Allende L, Eugenia K, Fletcher TD. The influence of media type on removal of arsenic, iron and boron from acidic wastewater in horizontal flow wetland microcosms planted with *Phragmites australis*. Chemical Engineering Journal. 2014;246:217-228.

[24] Kröpfelova L, Vymazal J, Svehla J, Stíchová J. Removal of trace elements in three horizontal sub-surface flow constructed wetlands in the Czech Republic. Environmental Pollution. 2009;157:1186-1194.

[25] Ye Z, Lin Z, Whiting S, de Souza M, Terry N. Possible use of constructed wetland to remove selenocyanate, arsenic, and boron from electric utility wastewater. Chemosphere. 2013;52:1571-1579.

[26] Almeida A, Carvalho F, Imaginário M. Nitrate removal in vertical flow constructed wetland planted with *Vetiveria zizanioides*: Effect of hydraulic load. Ecological Engineering 2017; 99:535–542.

[27] Clesceri L, Greenberg A, Eaton E. Standard methods for the examination of water and wastewater. 19th ed. Washington, DC: American Public Health Association; 1995.

[28] Horneck A, Miller R. Handbook of reference method for plant analysis, Boca Raton. CRC Press; 1998; 57–84.

[29] Gross A, Shmueli O, Ronen Z, Raveh E. Recycled vertical flow constructed wetland (RVFCW)— A novel method of recycling greywater for irrigation in small communities and households. Chemosphere. 2007;66:916–923.

[30] Rees R, Robinson B, Menon M, Lehmann E, Günthardt-Goerg M, Schulin R. Boron accumulation and toxicity in hybrid poplar (*Populus nigra* x euramericana). Environmental Science & Technology. 2011;45:10538–10543.

[16] Turker O, Vymazal J, Ture C. Constructed wetlands for boron removal. Ecological Engineering. 2014;64:350-359.

[17] Irawan C, Kuo YL, Liu J. Treatment of boron-containing optoelectronic wastewater by precipitation process. Desalination. 2011;280:146-151.

[18] Correia P. Phytoremediation of effluent with high levels of nitrogen and boron. Beja: Polytechnic Institute of Beja - School of Agriculture; 2019.

[19] Wolska J, Bryjak M. Methods for boron removal from aqueous solutions — A review. Desalination. 2013;310:18–24.

[20] Barth SR. Utilization of boron as a critical parameter in water quality evaluation: Implications for thermal and mineral water resources in SW Germany and N Switzerland. Environmental Geology. 2000;40:73-89.

[21] Kluczka J, Korolewicz T, Zołotajkin M, Adamek J. Boron removal from water and wastewater using. Water Resources and Industry. 2015;11:46-57.

[22] Allende L, Fletcher T, Sun G. The effect of substrate media on the removal of arsenic, boron and iron from an acidic wastewater in planted column reactors. Chemical Engineering Journal. 2012;11:46-57.

[23] Allende L, Eugenia K, Fletcher TD. The influence of media type on removal of arsenic, iron and boron from acidic wastewater in horizontal flow wetland microcosms planted with *Phragmites australis*. Chemical Engineering Journal. 2014;246:217-228.

[24] Kröpfelova L, Vymazal J, Svehla J, Stíchová J. Removal of trace elements in three horizontal sub-surface flow constructed wetlands in the Czech Republic. Environmental Pollution. 2009;157:1186-1194.

[25] Ye Z, Lin Z, Whiting S, de Souza M, Terry N. Possible use of constructed wetland to remove selenocyanate, arsenic, and boron from electric utility wastewater. Chemosphere. 2013;52:1571-1579.

[26] Almeida A, Carvalho F, Imaginário M. Nitrate removal in vertical flow constructed wetland planted with *Vetiveria zizanioides*: Effect of hydraulic load. Ecological Engineering 2017; 99:535–542.

[27] Clesceri L, Greenberg A, Eaton E. Standard methods for the examination of water and wastewater. 19th ed. Washington, DC: American Public Health Association; 1995.

[28] Horneck A, Miller R. Handbook of reference method for plant analysis, Boca Raton. CRC Press; 1998; 57–84.

[29] Gross A, Shmueli O, Ronen Z, Raveh E. Recycled vertical flow constructed wetland (RVFCW)— A novel method of recycling greywater for irrigation in small communities and households. Chemosphere. 2007;66:916–923.

[30] Rees R, Robinson B, Menon M, Lehmann E, Günthardt-Goerg M, Schulin R. Boron accumulation and toxicity in hybrid poplar (*Populus nigra* x euramericana). Environmental Science & Technology. 2011;45:10538–10543.

KnE Materials Science

FibEnTech21
1st International FibEnTech Congress (FibEnTech21) New opportunities for fibrous materials in the ecological transition
Volume 2022

Knowledge E
enriching | engaging | empowering

Research article

Phytoremediation as a Sustainable Alternative for Organic Matter Removal From Slaughterhouse Wastewater Pretreated by Immediate One-Step Lime Precipitation

Luís Madeira[1,2,3], Fátima Carvalho[2,3,4], Margarida Ribau Teixeira[1,3], and Adelaide Almeida[2,3,4]*

[1]Faculty of Sciences and Technology, University of Algarve, Edifício 7, Campus de Gambelas, 8005-139 Faro, Portugal
[2]Polytechnic Institute of Beja, Higher School of Agriculture, Department of Technologies and Applied Sciences, Rua Pedro Soares - Campus do IPBeja, 7800-295 Beja, Portugal
[3]CENSE, Center for Enviromental and Sustainability Research, Portugal
[4]FibEnTech University of Beira Interior, Rua Marquês d'Ávila e Bolama, 6201-001, Covilhã, Portugal

Abstract.
In this study, slaughterhouse wastewater previously treated by immediate one-step lime precipitation was treated using a vertical flow constructed wetland (VFCW). A VFCW pilot scale planted with *Vetiveria zizanioides* in light expanded clay aggregates was used to study the influence of the organic load applied (3 to 212 g m^{-2} d^{-1}) and the bed depth of the VFCW (0.35 and 0.70 m) on the organic matter removal (COD). Two VFCWs operated in parallel under continuous flow, and a hydraulic load of around 80 L m^{-2} d^{-1} was used. The results indicated that an increase in the organic load decreased COD removal efficiency. The bed depth of the VFCW had a significant influence on the removal of organic matter, with greater removal at high bed depths. For organic loads applied up to 9.5 g m^{-2} d^{-1}, COD removal efficiencies of 71.4 ± 4.0% and 85.2 ± 3.4% were observed for lower and higher VFCW bed depth, respectively, which met the requirements for water reuse for irrigation. Throughout the tests, *Vetiveria zizanioides* did not show signs of toxicity, and its growth was substantial.

Keywords: slaughterhouse wastewater, vertical flow constructed wetlands, *Vetiveria zizanioides,* organic matter removal, immediate one-step lime precipitation

Corresponding Author: Adelaide Almeida; email: maalmeida@ipbeja.pt

Dates
?????

Publishing services provided by Knowledge E

© Luís Madeira et al. This article is distributed under the terms of the Creative Commons Attribution License, which permits unrestricted use and redistribution provided that the original author and source are credited.

Selection and Peer-review under the responsibility of the FibEnTech21 Conference Committee.

OPEN ACCESS

1. Introduction

The wastewater reuse has been strongly driven by the European Commission and also by the United Nations, according to the Sustainable Development Goals (SDGs), as a need to address global water scarcity [1]. Slaughterhouse is one of the sectors in which the treated wastewater recover is practically non-existent, since most industries look at effluent as a waste, choosing to discharge effluent into the municipal collection system or a water line [2]. Depending on the company's productivity, large amounts of slaughterhouse wastewater are expected due to slaughtering process and cleaning

of facilities [3]. These volumes of water could be used for other purposes (e.g., for irrigation). Thus, slaughterhouse should be encouraged for wastewater recover.

Slaughterhouse wastewater (SWW) recover has proved to be a challenge for researchers due to its high organic content (e.g., 5000 and 3000 mg O_2 L^{-1} for chemical oxygen demand (COD) and biochemical oxygen demand (BOD), respectively), nutrients (e.g., 450 and 50 mg L^{-1} for total nitrogen and total phosphorus, respectively), oils and fats, suspended solids (e.g., 3000 mg L^{-1}) and bacterial contamination [3]. Currently, conventional wastewater treatments processes have been used to treat SWW. Despite the high efficacy, these treatment processes have some drawbacks. For example, the coagulation-flocculation process produces sludges rich in Fe^{3+} or Al^{3+} salts, which are difficult to apply on agricultural land and their disposal is landfill [4], presenting a cost to the company. Activated sludges have considerable energy consumption and are poorly tolerant to load and flow variations [5]. In this way, different SWW treatment processes have been investigated, namely chemical (e.g., electrochemical oxidation [6], acid precipitation [7] and lime precipitation [8]) and biological treatments (e.g., wetlands [9]), advanced oxidation processes [10] and combined processes [10].

Lime precipitation and wetlands are low-cost treatment processes. High organic matter removals (ca. 93%) with lime precipitation process have been reported by some authors [8]. However, it is not enough to guarantee legal disposal specifications (e.g., discharge into environment or reuse for irrigation). Constructed wetland (CW) has emerged as a sustainable alternative in the treatment of various types of effluents, including those previously treated by immediate one-step lime precipitation (e.g., explosives [11]), compared to conventional processes, due to its low cost, low maintenance and high efficiency in removing contaminants.

The effectiveness of CW in the treatment of slaughterhouse effluents has been investigated by some authors. Mburu et al. [12] studied the effect of depth, time and substrate variation on organic matter removal from slaughterhouse wastewater, using vertical sub-surface flow constructed wetlands (without plants). These authors observed that vertical sub-surface flow constructed wetlands operated at a longer retention time of 5 days, with intermittent wastewater feeding, facilitated over 50% removal of organic matter in slaughterhouse wastewater. High organic matter removals (>70%) were achieved using constructed wetland planted with *C. papyrus* and *P. mauritianus*, in the slaughterhouse wastewater treatment [9]. Manh et al. [13] used constructed wetlands planted *Vetiveria zizanioides L* to treat slaughterhouse wastewater from a biodigester. The results showed that the concentrations of BOD_5 and COD can be reduced by 59.8% and 60%, respectively. Recently, the interest in *Vetiveria zizanioides* plant in

constructed wetlands to treat effluents has increased [11,14], however, studies of its use in slaughterhouse wastewater treatment are still few.

Thus, this work aims to understand the effect of the organic load applied and the bed depth from vertical flow constructed wetland (VFCW) planted with *Vetiveria zizanioides* on the organic matter removal from a slaughterhouse wastewater pretreated by immediate one-step lime precipitation process.

2. Material and methods

SWW was collected from a slaughterhouse (with a production capacity of 700 m^3/day of wastewater) located in Portugal. This SWW include effluents from the slaughtering process (cattle, pigs, goats, sheep and ratite) and the cleaning facilities. SWW composition was pH 7.2±0.2, conductivity 3.1±0.3 mS cm^{-1}, COD 5430±1646 mg O_2 L^{-1}, BOD_5 2813±208 mg O_2 L^{-1} and ammonium nitrogen (NH_4^+) 88±1 mg N-NH_4^+ L^{-1}. Before constructed wetland treatment, SWW was previously pretreated by immediate one-step lime precipitation process, according to Madeira et al. [15].

From February to April, two VFCW (Figure 1), VFCW 1 (0.40m x 0.60m x 0.35m) and VFCW 2 (0.40m x 0.60m x 0.70m), planted with *Vetiveria zizanioides* in light expanded clay aggregates (Leca®NR 10/20), were used in continuous mode. Table 1 shows the applied operation to the VFCW. For each VFCW, three types of SWW were tested (trials A to C in Table 1). Hydraulic retention times used were 3.6±0.5 and 7.1±0.9 hours, for VFCW 1 and VFCW 2, respectively.

During this experiment, wastewater samples were collected daily from the inlet and outlet of the bed. The influent and effluent of both VFCW were analysed to pH, dissolved oxygen (DO), redox potential, electrical conductivity, ammonium nitrogen, COD, and flow rate. Physical-chemical parameters were analysed according to the standard analytical methods defined by Baird et al. [16]. Air and bed temperature were also monitored.

Vetiveria zizaniodes plants were visually inspected on a weekly basis for toxicity signals. The biomass composition was analysed at the beginning and at the end of the experiments, in terms of calcium, magnesium, sodium, potassium, total nitrogen and phosphorus [17-19].

Two-Way ANOVA was used to compare the means, using the Least Significance Difference (LSD) test, at 95% confidence level.

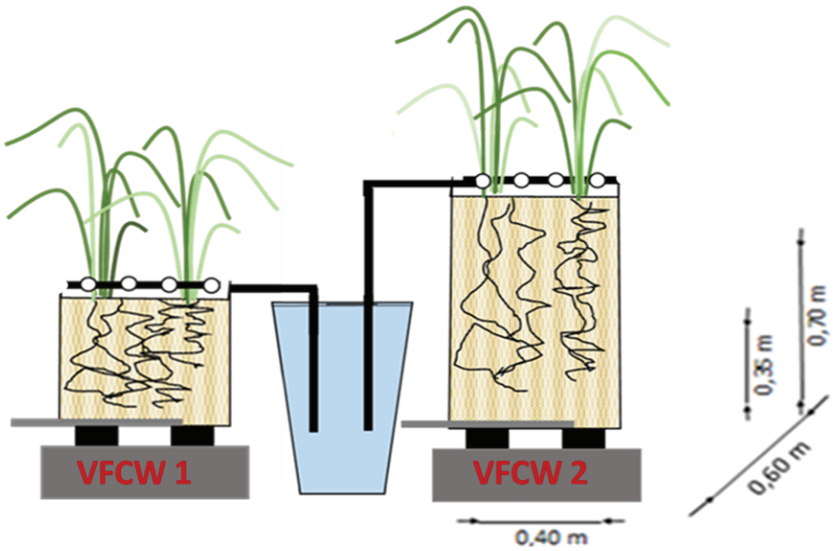

Figure 1: Schematic representation of the VFCW.

TABLE 1: Conditions applied to VFCW 1 and VFCW 2. Mean ± Standard Deviation, calculated for a 95% confidence level and number of determinations (n≥10).

		VFCW 1			VFCW 2		
Parameters / Trials		A1	B1	C1	A2	B2	C2
COD	(g m^{-2} d^{-1})	4.1±0.5	9.5±2.2	211.8±26.4	3.2±1.1	9.4±2.5	211.8±26.4
NH_4^+-N load	(g m^{-2} d^{-1})	0.3±0.1	0.5±0.05	3.9±0.5	0.3±0.1	0.5±0.06	3.9±0.5
Hydraulic load	(L m^{-2} d^{-1})	81±10			80±10		

3. Results and discussion

Figure ?? shows the inlet and outlet results for pH, redox potential, conductivity and DO, in VFCW 1 and VFCW 2 for the three trials.

Fig. 2. pH, redox potential, conductivity and DO results, in inlet and outlet of VFCW 1 (a, b, c and d, respectively) and VFCW 2 (e, f, g and h, respectively), for the different trials (A, B and C). Box and whisker plots showing median, 25th and 75th percentile (box), and range (whiskers).

No significant difference ($p<0.05$) between VFCW and inlet and outlet were observed for pH (Figure ?? a and e), indicating that the wastewater had sufficient alkalinity to act as a buffer. The same behavior was observed for redox potential (Figure ?? b and

f), conductivity (Figure ?? c and g) and DO (Figure ?? d and h), without significant differences ($p<0.05$). However, an increase in COD load from 9.5 to 211 g m^{-2} d^{-1} and ammonium nitrogen load from 0.5 to 3.9 g m^{-2} d^{-1} (trials B to C), provided a significant oxygen consumption ($p<0.05$), reaching zero values of DO in the effluent of both VFCWs (Figure ?? d and h). Dissolved oxygen consumption is mainly due to aerobic degradation of organic matter rather than nitrification.

Figure ?? shows the COD and ammonium nitrogen removal efficiencies obtained with different organic loads in the two VFCW, VFCW 1 (Figure ??a and 3b) and VFCW 2 (Figure ??c and 3d). This figure shows that the highest COD removal efficiencies were obtained with the smallest COD loads applied, in both VFCW. When the COD load was 211.8 g m^{-2} d^{-1}, COD removal did not occur in VFCW 1, and decreased a lot in VFCW 2, reaching values between 60 and 70%. In fact, an increase in the depth of the bed allows for a greater distribution of plant roots and, consequently, a greater distribution of microorganisms in the bed, contributing to a greater removal of organic matter.

Ammonium nitrogen removal efficiency was highest for the lower loads (0.3±0.1 g m^{-2} d^{-1}) and occurred in presence of organic matter and with low dissolved oxygen, reaching a maximum value of 86% for both VFCWs (Figure ??b) and d)). However, this value decreased to 58 % (trial C) in VFCW 2 when a maximum load removed is reached, since this occurred with very low dissolved oxygen. Like COD, deeper VFCW had greater removal of ammonium nitrogen. Almeida et al. [20] also obtained greater ammonium nitrogen removal in deeper VFCW when the authors used VFCW planted with *Vetiveria zizanioides* in the treatment of synthetic effluent (68± 3 to 290± 8 mg L^{-1} NH_4^+-N). In this way, deep root system seems to favor the creation of zones with different oxidations conditions that allow the ammonium nitrogen and organic matter removals [20].

Fig. 3. Organic and ammonium load values in inlet and outlet of VFCW 1(a and b, respectively) and VFCW 2 (c and d, respectively), and the respective COD and ammonium removal efficiencies for the different trials (A, B and C). Box and whisker plots showing median, 25th and 75th percentile (box), and range (whiskers).

Regarding the leaves biomass composition (Table 2), the deeper VFCW had a significative ($p<0.05$) greater accumulation of nutrients (calcium, potassium, total nitrogen, and phosphorus) compared to the less deep VFCW, since the beginning of the experiments. Signs of toxicity or chlorosis in the leaves were never detected in *Vetiveria zizanioides*.

Table 2: Leaves biomass composition.

Parameter (mg g^{-1} DW)	**Leaves biomass composition**		
	Beginning	**Ending**	
		VFCW 1	**VFCW 2**
Ca^{2+}	1.20±0.05	2.00±0.09	2.30±0.01
Mg^{2+}	0.04±0.01	0.06±0.01	0.07±0.02
Na^{+}	0.45±0.01	0.30±0.01	0.36±0.02
K^{+}	0.47±0.02	3.14±0.02	4.0±0.02
TN	10.5±0.5	15.9±0.2	17.6±0.2
P	1.02±0.01	0.20±0.03	0.44±0.03

4. Conclusions

The organic matter and ammonium nitrogen removal efficiencies are influenced by VFCW depth as well as the applied ammonium nitrogen and organic load. For organic loads applied up to 9.5 g m^{-2} d^{-1}, removal efficiencies of 71.4±4 and 85.2±3.4 % were obtained respectively for the lowest and highest depth VFCW studied. For both VFCW, the COD concentrations (about 33.5 mg L^{-1} and 17.36 mg L^{-1} for the lowest and highest depth VFCW) obtained by these removals meet the requirements for water reuse for irrigation (≤40 CBO_5 (mg/L O_2[21]). In this way**,** immediate one-step lime precipitation followed by VFCW is a good solution for slaughterhouse wastewater reuse.

5. Acknowledgments

The authors are grateful to the Foundation for Science and Technology (FCT, Portugal) for financial support by national funds through the project UIDB/00195/2020 (FibEnTech). The authors thank the slaughterhouse for providing the effluent. Luís Madeira also thanks FCT e Fundação para a Ciência e a Tecnologia for granting a PhD scholarship (SFRH/BD/137209/2018).

References

[1] Boretti A, Rosa L. Reassessing the projections of the world water development report. Clean Water. 2019;2:1–6. https://doi.org/10.1038/s41545-019-0039-9

[2] Norsyahariati N, Daud N, Anijiofor SC. Chicken slaughterhouse wastewater disposal: The challenges ahead. Asian Journal of Agriculture and Biology. 2018; 6 (Special issue):42-45.

[3] Bustillo-Lecompte C, Mehrvar M. ”Slaughterhouse Wastewater: Treatment, Management and Resource Recovery”, in Physico-Chemical Wastewater Treatment and Resource Recovery. London, United Kingdom: IntechOpen, 2017. https://doi.org/10.5772/65499

[4] Mahedi M, Cetin B, Dayioglu AY. Leaching behavior of aluminum, copper, iron and zinc from cement activated fly ash and slag stabilized soils. Waste Management. 2019;95:334–355. https://doi.org/10.1016/j.wasman.2019.06.018

[5] Lin SD. Water and Wastewater Calculations Manual. (McGraw-Hill, Ed.) Chemistry & biodiversity, vol. 1; New York, 2007. http://doi.org/10.1036/0071476245

[6] Martínez-Cruz A, Fernandes A, Ciríaco L et al. Electrochemical oxidation of effluents from food processing industries: A short review and a case-study. Water. 2020;12(3546):1-16. https://doi.org/10.3390/w12123546

[7] Prazeres AR, Fernandes F, Madeira L et al. Treatment of slaughterhouse wastewater by acid precipitation (H_2SO_4, HCl and HNO_3) and oxidation ($Ca(ClO)_2$, H_2O_2 and CaO_2). Journal of Environmental Management. 2019;250(109558):1-14. https://doi.org/10.1016/j.jenvman.2019.109558

[8] Hossaini H, Fatehizadeh A, Yousefi N et al. Application of enhanced softening process in slaughterhouse. Indian Journal of Chemical Technology. 2013;20(3):217–221.

[9] Odong R, Kansiime F, Omara J, Kyambadde J. The potential of four tropical wetland plants for the treatment of abattoir effluent. International Journal of Environmental Technology and Management. 2013;16(3):203-222. https://doi.org/10.1504/IJETM.2013.053640

[10] Lecompte CFB, Mehrvar M, Bolaños EQ. Cost-effectiveness analysis of TOC removal from slaughterhouse wastewater using combined anaerobic-aerobic and UV/H2O2 processes. Journal of Environmental Management. 2014;134:145-152. https://doi.org/10.1016/j.jenvman.2013.12.035

[11] Madeira L, Carvalho F, Teixeira MR, Ribeiro C, Almeida A. Vertical flow constructed wetland as a green solution for low biodegradable and high nitrogen wastewater: A case study of explosives industry. Chemosphere. 2021;272(129871):1-10. https://doi.org/10.1016/j.chemosphere.2021.129871

[12] Mburu C, Kipkemboi J, Kimwaga R. Impact of substrate type, depth and retention time on organic matter removal in vertical subsurface flow constructed wetland mesocosms for treating slaughterhouse wastewater. Physics and Chemistry of the Earth. 2019;114:102792. https://doi.org/10.1016/J.PCE.2019.07.005

[13] Manh LH, Dung NNX, Am LV, Minh BTL. Treatment of wastewater from slaughterhouse by biodigester and *Vetiveria zizanioides*. Livestock Research for Rural Development. 2014, volume 26, *Article #68*. ISSN 0121-3784

[14] Almeida A, Ribeiro C, Carvalho F et al. Phytoremediation potential of *Vetiveria zizanioides* and *Oryza sativa* to nitrate and organic substance removal in vertical flow constructed wetland systems. Ecological engineering. 2019;138:19-27. https://doi.org/10.1016/j.ecoleng.2019.06.020

[15] Madeira L, Almeida A, Teixeira RM, Prazeres A, e Carvalho FCH. Immediate one-step lime precipitation and atmospheric carbonation as pre-treatment for low biodegradable and high nitrogen wastewaters: A case study of explosives industry. Journal of Environmental Chemical Engineering. 2020;8(103808):1-10. https://doi.org/10.1016/j.jece.2020.103808

[16] Baird R, Eaton AD, Rice EW, Bridgewater L. Standard methods for the examination of water and wastewater. 23rd ed. American Public Health Association, American Water Works Association, Water Environment Federation; 2017.

[17] Campbell CR, Plank CO. Handbook of reference method for plant analysis. Kalra YP, editor. Boca Raton: CRC Press; 1998.

[18] Miller RO. Handbook of reference method for plant analysis. Kalra YP, editor. Boca Raton (FL): CRC Press; 1998.

[19] Horneck A, Miller RO. Handbook of reference method for plant analysis. Kalra YP, editor. Boca Raton (FL): CRC Press; 1998.

[20] Almeida A, Jozwiakowski K, Kowalczyk-Jusko A et al. Nitrogen removal in vertical flow constructed wetlands: Influence of bed depth and high nitrogen loadings. Environmental Technology. 2018;41(17):2196-2209. https://doi.org/10.1080/09593330.2018.1557749

[21] Decree-Law no. 119/2019, Diário da República, 1.ª série, N.º 159, 21 de agosto de 2019.

KnE Materials Science

FibEnTech21
1st International FibEnTech Congress (FibEnTech21) New opportunities for fibrous materials in the ecological transition
Volume 2022

Knowledge E
enriching | engaging | empowering

Research article

Removal of Emergent Pollutants by a Vertical Constructed Wetland with Vetiveria Zizanioides: A Case Study for Caffeine

Adelaide Almeida[1], Júlio Oliveira[1], Flávia Matias[1], Carlos Ribeiro[1], Daniele Silveira[2], and Jorge Tavares[1]*

[1]Department of Technologies and Applied Sciences, School of Agriculture (ESA), Polytechnic Institute of Beja (IPBeja), Beja, Portugal
[2]Department of Sanitary and Environmental Engineering (ENS), Federal University of Santa Catarina (UFSC), Florianopolis, Brazil

Abstract.
This work evaluated caffeine removal in a vertical flow constructed wetland (VFCW), planted with *Vetiveria zizanioides*. The feeding was continuous (synthetic influent: mineral medium and caffeine) to reduce the concentration variations in the bed. Two influent concentrations (0.75 ± 1.0 mg·L^{-1} and 1.5 ± 1.0 mg·L^{-1}) were used with a constant hydraulic load (100 ± 10 L·m^{-2}·d^{-1}). Plant growth was monitored weekly, and characterization was carried out to determine the levels of chlorophyll *a* and *b*, pigments and carotenoids, and nutrients (nitrogen, phosphorus, magnesium, calcium, sodium and potassium). HPLC-MS was used to determine the caffeine concentration. The caffeine removal efficiency reached averages of 93 ± 1% and 87 ± 1% (retention time: 6.23 ± 0.23 hours). The caffeine contents in the influent did not affect chlorophyll *a*, total chlorophyll or carotenoids, and an increasing trend throughout the tests was observed. Sodium and potassium contents also showed an increase with higher caffeine concentration. This preliminary study showed that removing caffeine from wastewater using a VFCW is promising.

Keywords: wastewater, emergent pollutants, caffeine, vertical flow constructed wetlands, *Vetiveria zizanioides*

Corresponding Author: Jorge Tavares; email: jorge.tavares@ipbeja.pt

Dates
?????

Publishing services provided by Knowledge E

© Adelaide Almeida et al. This article is distributed under the terms of the Creative Commons Attribution License, which permits unrestricted use and redistribution provided that the original author and source are credited.

Selection and Peer-review under the responsibility of the FibEnTech21 Conference Committee.

OPEN ACCESS

1. Introduction

Most pharmaceutical products are not completely metabolized after human ingestion resulting in the metabolites excretion and other similar compounds that reach wastewater treatment plants (WWTPs) [1]. Since these plants are not designed with the specific purpose of removing pharmaceutical compounds, their detection is often found in effluents and surface water [2]. Among the pharmaceuticals, caffeine has been widely studied in wastewater treatment systems. As an alkaloid, a psychoactive substance, legal is one of the most consumed in the world, being present in different drinks, such as coke soft drinks, coffee, tea, and energy drinks. In humans, caffeine acts on the central nervous system, stimulating the body's alertness and consequently preventing

sleepiness. In developed countries, for example, 90% of the adults consume caffeine in a daily basis. Thus, caffeine is present both in domestic wastewater and in some industrial effluents. Due to their high solubility and low volatility, caffeine is quite persistent in water bodies [3]. These characteristics allow caffeine detection in the environment which are essential to correlate the risk it may offer to humans and ecosystems [4-7], and its presence in environmental matrices were confirm in recent studies [8]. Per example, wastewater from two WWTPs in Barbados, a city with about 300,000 inhabitants, were analyzed and it was obtained a range of caffeine concentrations from 0.10 to 6.90 µg L^{-1} [9]; in Italy, 13 WWTPs located in northern, central, and southern (responsible for the collection and treatment of effluents from 50 to 500,000 inhabitants) were evaluated and the results showed caffeine concentrations between 17.6 and 67.6 µg L^{-1} [10].

Constructed wetlands are considered economical compared to other types of wastewater treatment systems like ozonation, chlorination, membrane filtration or the use of activated carbon (high cost, energy demand, and maintenance and therefore only economical for large plants). The complex processes that occur in these systems are conducted through the filter material, plants, and mainly by microorganisms [4]. Treatment wetlands are nature-based technologies with a porous substrate and typically planted with macrophytes. The water passes through the system horizontally or vertically in a certain time, also known as nominal hydraulic retention time [11]. The substrate, as well as the roots of the plants, serve here as a filter and a natural growth body for the microbial community. These engineered wetlands thus mimic natural processes to ultimately improve water quality [12]. In recent years, several studies have deal with the removal of micropollutants through constructed wetlands. A wide range of wetland projects, operational conditions, and influent compositions to efficiently remove micropollutants were examined and intensified wetlands showed a great potential [2; 13-14]. Currently, the use of vertical flow has been increasing to remove both organic matter and nitrogen forms due to the aerobic conditions in this system. [15].

Among a wide range of macrophytes used in these types of projects stands out *Vetiveria Zizanioides*, with specific characteristics such as its high resistance to variations of pH (from 3 to 10.5) and temperature of the soil (-10 to 60°C), and to high concentrations of heavy metals (As, Cd, Pb, Hg, Ni, Se and Zn) [16]. Other features that may stand out are its asexual mode of reproduction and its long root system [17]. Studies carried out to assess the removal mechanisms of pharmaceutical compounds in VFCWs have been shown that this kind of compound, as caffeine, is partially accumulated by plants [18]. However, it is necessary to understand the main mechanisms involved in caffeine removal and its effect of increasing concentrations on plant biomass and system

performance in general. This work aimed to evaluate the caffeine removal capacity (under two different concentrations) in vertical flow constructed wetlands planted with *Vetiveria zizanioides* in expanded clay aggregates as filter material to understand the removal of this type of pollutant.

2. Material and methods

The experimental work was carried out in a well-established 8-year-old pilot-scale vertical flow constructed wetland (VFCW) (0.24 m^2 × 0.70 m), planted with *Vetiveria zizanioides* (plant density higher than 120 plants m^{-2}), filled with light expanded clay aggregates (Filtralite® NR 10/20), with a bottom slope of 2%, applied to enable the hydraulic collection of the effluent. A layer of gravel (diameter 10–50 mm) was placed around the outlet valve to prevent clogging by fine particles. The flooding levels were maintained at 14% through a siphon in the outlet. The pilot bed was fed in continuous mode, through network sprinklers, equidistantly located over the whole VFCW using a submersible pump (Eheim- 1250, Deizisan, Germany) in feeding tank (Fig. 1). A synthetic wastewater was prepared with mineral medium composed by 28 mg·dm^{-3}$CaCl_2$, 52 mg·dm^{-3}MgSO4·7H_2O, 17.40 mg·dm^{-3}KH_2PO_4, 11 mg·dm^{-3}K_2SO_4, 0.03 mg·dm^{-3}$CuCl_2$·2H_2O, 0.18 mg·dm^{-3}$MnCl_2$.4H_2O, 0.08 mg·dm^{-3} $ZnCl_2$, 1.7 mg·dm^{-3} $FeSO_4$·7H_2O diluted in tap water [19], and caffeine to minimize variations in concentration of effluent in the batch's reservoirs [Caffeine (>99%) was purchased from Sigma–Aldrich (Germany)].

The VFCW was acclimatized during one month before the beginning of trials by the application of 0.75 mg·L^{-1} of caffeine and hydraulic load (C_h) was kept constant at 100±10 L·m^{-2}·d^{-1}. The experiment was designed to rise caffeine concentration at two different concentrations (0.75 mg·L^{-1} and 1.5 mg·L^{-1}), ignoring any ordinary low levels occurring in wastewater [3]. Each trial occurs approximately during one month for each caffeine concentration (from April till July). Each new trial was initiated by increasing the caffeine concentration. Wastewater samples were collected at the inlet and outlet of the VFCW from Monday to Friday, at 10:00 a.m, wherefore a minimum of ten samples were taken from influent and effluent wastewater in each trial. The electrical conductivity (EC), pH, redox potential (Eh) and dissolved oxygen (DO) were immediately measured *in situ*, using a portable probe multiparameter (HI9829 HANNA). Aliquots were frozen (-20^{o}C) to determine the caffeine. The studied caffeine concentration at the inlet (0.75±1 mg·L^{-1}; 1.5±1 mg·L^{-1}) and outlet, as well as in the plant biomass after leaves extraction, was determined using a HPLC-MS *UltiMate 3000 HPLC series* da *Thermo Scientific* (Thermo

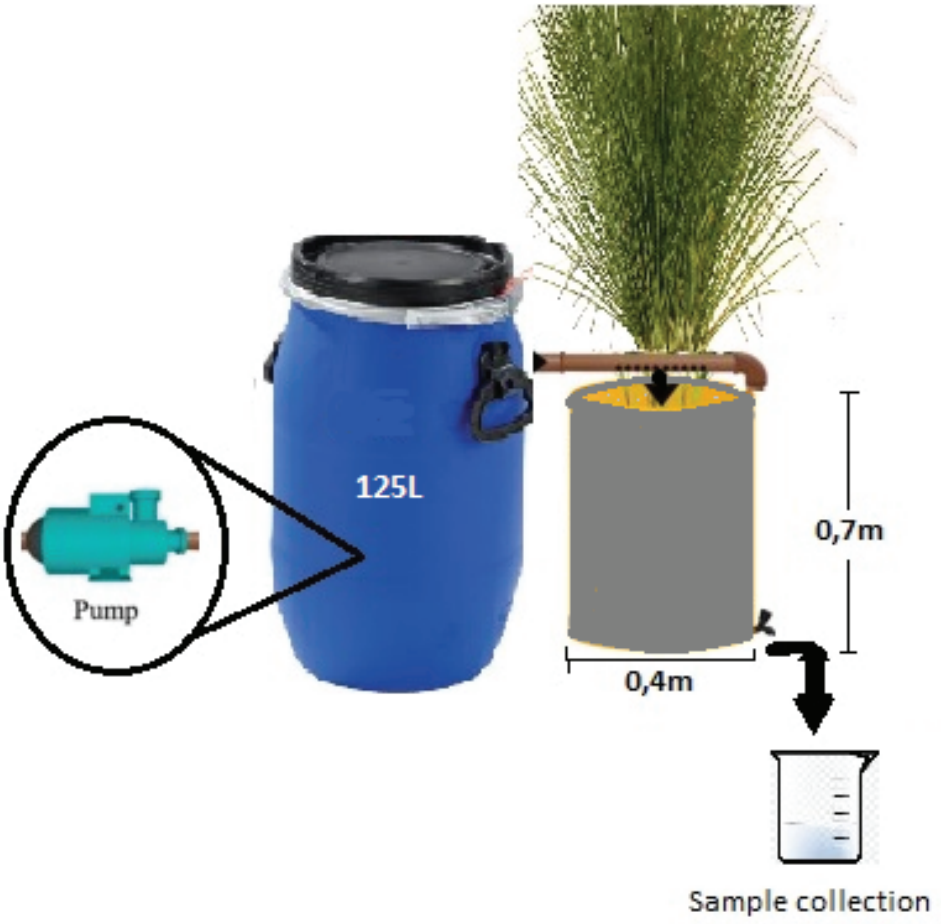

Figure 1: Schematic representation (not at scale) of the VFCW (0.24 m^2× 0.70 m).

Scientific, EUA) with ionization source (ESI), [3; 20]. The reverse phase analytical column used was an Accucore aQ C18 de 100 x 2,1 mm, at 25 ^{o}C. Separation was performed in isocratic mode, and the mobile phase used was using a linear composed by 30:70 acetonitrile:water, acidified with 0.1% formic acid (v:v), with a flow of 0.25 mL·min^{-1} and the infection volume was 25 µL. Three replicate of injections were made for each sample. HPLC-grade acetonitrile, water and formic acid a were obtained from Fisher Scientific (USA). All chemicals used were analytical grade.

Vetiveria zizanioides plants were visually inspected on a weekly basis for toxicity signals. The plant biomass growth (leaves) was monitored at beginning and at the end of each trial, with different caffein concentration, being determined the levels of chlorophyll *a* and *b* (Chl *a* and Chl *b*), carotenoids, the concentrations of nutrients (nitrogen, phosphorus, magnesium, calcium, sodium, and potassium) [21-22].

Results were statistically verified using software “Statistica 12.0” (StatSoft, Inc., USA). Differences in wastewater quality between influent and effluent of the VFCW were determined using ANOVA at the significance level of $p<0.05$. Tukey’s test was used

to determine differences between means of specific variables. The means and the standard deviation (S.D.) were calculated with n≥10.

3. Results and discussion

The biomass growth was not negatively influenced by the presence of caffeine in the influent. There was an increment in the growth of biomass during the second trial (caffeine concentration: 1.5±1 mg·L^{-1}).

The level of Chl *a*, and carotenoids showed an increased tendency due to the feeding of plants with caffeine (Fig. 2a). However, the Chl *b* level showed a very strong tendency to decrease during the trials.

Sodium (Na) and potassium (K) levels showed an increasing trend due to increased caffeine level in the influent of the VFCWs (Fig. 2b).

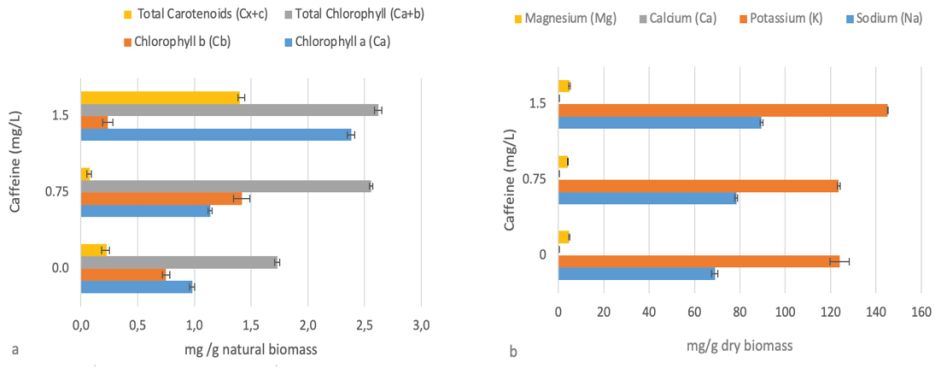

Figure 2: (a) Chlorophyll level [a, b and total], and (b) biomass composition [Mg, Ca, K, and Na] determined at beginning and at the end of each trial.

The results obtained for potential redox, dissolved oxygen and pH are presented at Figure 3.

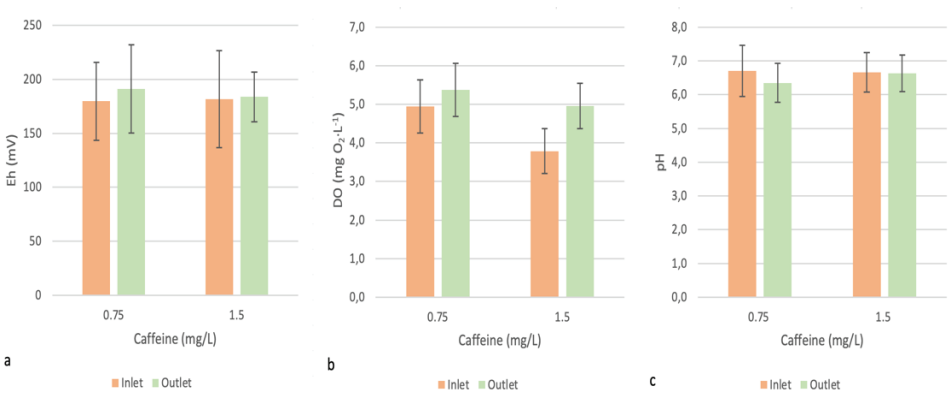

Figure 3: Evolution of Eh (a), Dissolved oxygen (b), and pH (c) during experiment.

The potential redox measured in the inlet and outlet of the VFCWs was always positive. There was not significant difference when compared the average values obtained for the influent and effluent ($p>0.05$) (Fig.3a). The dissolved oxygen of the effluent increased in both trials (Fig.3b), possibly due to the capacity of the plants or the type of flow that allowed the replacement of oxygen consumed by the microbial presented in the beds. The outlet pH decreased, without statistical significance at both trials ($p>0.05$), when compared with inlet synthetic wastewater (Fig.3c). Additionally, it was not observed significative difference at electrical conductivity between the influent and effluent at the beds monitored ($p>0.05$). It this sense, it was deduced that TSS concentration remained constant over the trials and did not occur precipitation of salts during the experiment.

Regarding efficiency and effective monitoring of beds (HRT=6.23±0.23 hours), it was obtained, considering the different and increasing concentrations of caffeine (0.75±1 mg·L^{-1}; 1.5±1 mg·L-1), an average removal of 93±1% and 87±1%, respectively (Fig. 4).

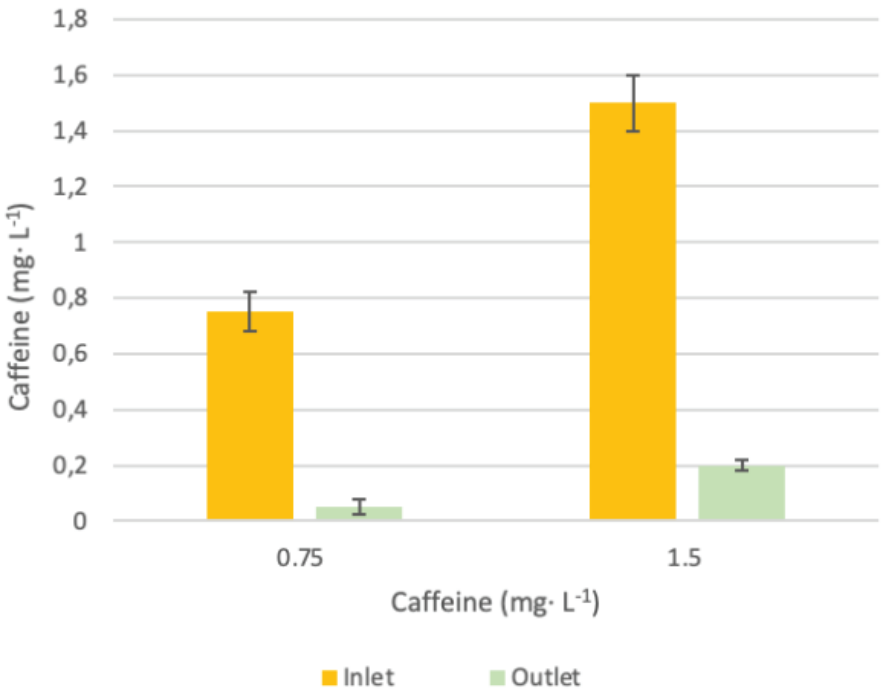

Figure 4: Caffeine concentration at VFCW (inlet and outlet), in each trial.

As mentioned before, although our HRT was 6.23±0.23 hours, the results obtained in our study were like others presented at literature [24]. Performing lab trials with a VFWC with an HRT of 7 days, it was achieved removal efficiencies of 97%. Other authors [3] using a retention time of 21 days obtained a removal efficiency in hydroponic conditions until 99 % [3].

The caffeine content in the leaves of *Vetiveria zizanioides* suggested that the plant assimilated during the experiment about 10 $\mu g \cdot g^{-1}$ of natural biomass. Therefore, it was also observed that with the increase in the caffeine concentration, the pollutant mass load input increased, leading to a reduction in the plant's capacity to removal the emergent pollutant in the system evaluated.

4. Conclusions

The results obtained showed a removal efficiency up to 93% of caffeine using vertical flow constructed wetlands with *Vetiveria zizanioides*, suggesting an assimilation of 10 µg·g-1 by plants. However, given the high caffeine removed content, this was not the main removal mechanism, pointing to the possible formation of metabolites and their assimilation by plants. In this sense, it will be important consider for future research, the internal sampling and analysis of the microbiota involved in the removal mechanism. This preliminary study showed that removing caffeine from wastewater using VFCW is promising.

5. Acknowledgments

The authors are very grateful for the support given by research unit Fiber Materials and Environmental Technologies (FibEnTech-UBI), on the extent of the project reference UIDB/00195/2020, funded by the Fundação para a Ciência e a Tecnologia.

References

[1] Zhang D, Luo J, Lee ZM, et al. Characterization of microbial communities in wetland mesocosms receiving caffeine-enriched wastewater. Environmental Science and Pollution Research. 2016;23(14):14526-39. https://doi.org/10.1007/s11356-016-6586-4

[2] Hijosa-Valsero M, Reyes-Contreras C, Domínguez C, Bécares E, Bayona JM. Behaviour of pharmaceuticals and personal care products in constructed wetland compartments: Influent, effluent, pore water, substrate, and plant roots. Chemosphere. 2016;145:508-517. https://doi.org/10.1016/j.chemosphere.2015.11.090

[3] Zhang DQ, Hua T, Gersberg RM, Zhu J, Ng WJ, Tan SK. Fate of caffeine in mesocosms wetland planted with *Scirpus validus*. Chemosphere. 2013;90(4):1568–1572. https://doi.org/10.1016/j.chemosphere.2012.09.059

[4] Montagner CC, Vidal C, Acayaba RD. Contaminantes emergentes em matrizes aquáticas do Brasil: Cenário atual e aspectos analíticos, ecotoxicológicos e regulatórios. Química Nova. 2017;40(9):1094-1110. https://doi.org/10.21577/0100-4042.20170091

[5] Wu J, Yue J, Hu R, Yang Z, Zhang L. Use of caffeine and human pharmaceutical compounds to identify sewage contamination. International Journal of Civil and Environmental Engineering. 2010;2(2):98-102. https://doi.org/10.5281/zenodo.1070943

[6] Gracia-Lor E, Castiglioni S, Bade R et al. Measuring biomarkers in wastewater as a new source of epidemiological information: Current state and future perspectives. Environment International. 2017;99:131-150. https://doi.org/10.1016/j.envint.2016.12.016

[7] Ferreira AP. Caffeine as an environmental indicator for assessing urban aquatic ecosystems. Cadernos de Saúde Pública. 2005;21(6):1884-1892. https://doi.org/10.1590/S0102-311X2005000600038

[8] Marasco Júnior CA, Luchiari NC, Gomes PCFL. Occurrence of caffeine in wastewater and sewage and applied techniques for analysis: A review. Eclética Química Journal. 2019;44(4):11-26. https://doi.org/10.26850/1678-4618eqj.v44.4.p11-26

[9] Edwards QA, Kulikov SM, Garner-O'neale LD. Caffeine in surface and wastewaters in Barbados. West Indies Springer Plus. 2015;4(57):1-12. https://doi.org/10.1186/s40064-015-0809-x

[10] Senta I, Gracia-Lor E, Borsotti A, Zuccato E, Castiglioni S. Wastewater analysis to monitor use of caffeine and nicotine and evaluation of their metabolites as biomarkers for population size assessment. Water Research. 2015;74:23-33. https://doi.org/10.1016/j.watres.2015.02.002

[11] Sossalla NA. Characterization, resilience, and optimization of micropollutant and biological effect removal by treatment wetlands treating municipal wastewater [Thesis to obtain the academic degree Doctor of natural sciences]. Germany; 2021.

[12] Nivala J, Boog J, Headley T et al. Side-by-side comparison of 15 pilot-scale conventional and intensified subsurface flow wetlands for treatment of domestic wastewater. Science of the Total Environment. 2019;658:1500–1513. https://doi.org/10.1016/j.scitotenv.2018.12.165

[13] Matamoros V, Arias CA, Brix H, Bayona JM. Removal of pharmaceuticals and personal care products (PPCPs) from urban wastewater in a pilot vertical flow constructed wetland and a sand filter. Environment Science Technology. 2007;41:8171–8177. https://doi.org/10.1021/es071594+

[14] Nivala J, Kahl S, Boog J, van Afferden M, Reemtsma T, Müller RA. Dynamics of emerging organic contaminant removal in conventional and intensified subsurface flow treatment wetlands. Science of the Total Environment. 2019;649:1144–1156. https://doi.org/10.1016/j.scitotenv.2018.08.339

[15] Vymazal J. Proc. conf. The use of aquatic macrophytes for wastewater treatment in constructed wetlands. Dias V, Vymazal J, editors. Lisboa: ICN e INAG; 2003.

[16] Truong P, Hart B. Vetiver system for wastewater treatment. Queensland; 2001. Available from: https://www.vetiver.org/PRVN_wastewater_bul.pdf

[17] The World Bank. Vetiver grass: The hedge against erosion. 4^{th} ed. Washington DC: The World Bank; 1993. Available from: http://www.vetiver.org/PUBLICATIONS/TVN_greenEng.pdf

[18] Kadlec RH, Wallace S. Treatment wetlands. 2^{nd} ed. Boca Raton: Taylor & Francis; 2008.

[19] Dordio AV, Belo M, Teixeira DM et al. Evaluation of carbamazepine uptake and metabolization by *Typha* spp., a plant with potential use in phytotreatment. Bioresource Technology. 2011;102(17):7827–7834. https://doi.org/10.1016/j.biortech.2011.06.050

[20] Hunter RG, Combs DL, George DB. Nitrogen, phosphorous and organic carbon removal in simulated wetland treatment systems. Archives of Environmental Contamination and Toxicology. 2001;41(3):274–281. https://doi.org/10.1007/s002440010249

[21] APAH. Standard methods for the examination of water and wastewater. 22nd ed. Washington DC: American Public Health Association/American Water Works Association/Water Environment Federation; 2013.

[22] Campbell CR, Plank CO. Handbook of reference method for plant analysis. Kalra YP, editor. Boca Raton: CRC Press; 1998.

[23] Lichtenthaler HK. Chlorophylls and carotenoids: Pigments of photosynthetic biomembranes. Methods In Enzymology. 1987:350-382.

[24] Oliveira M, Atalla AA, Frihling BEF, Cavalheri PS, Migliolo L, Filho FJCM. Ibuprofen and caffeine removal in vertical flow and free-floating macrophyte constructed wetlands with *Heliconia rostrata* and *Eichornia crassipes*. Chemical Engineering Journal. 2019;373:458-467. https://doi.org/10.1016/j.cej.2019.05.064

KnE Materials Science

FibEnTech21
1st International FibEnTech Congress (FibEnTech21) New opportunities for fibrous materials in the ecological transition
Volume 2022

Knowledge E
enriching | engaging | empowering

Research article

Water Reuse: A Risk Assessment Model for Water Resources

Anabela Rebelo[1]*, Albertina Bento Amaro[2], and Felisbina Quadrado[1]

[1]Portuguese Environment Agency, Water Resources Department, 2610-124, Amadora, Portugal
[2]FibEnTech and Department of Chemistry, University of Beira Interior, Rua Marquês d'Ávila e Bolama, 6201-001, Covilhã, Portugal

Abstract.
The increasing demands for water for multiple purposes combined with climate change challenges are leading to water scarcity and quality deterioration. Portugal is vulnerable to the impacts of climate change and therefore, the use of reclaimed waters has been identified as a suitable alternative water source for non-potable uses, such as irrigation, to overcome water shortages. In the last two years, new policies for water reuse have been approved at the Portuguese and European levels. The legal frameworks are supported in the international guidelines developed by the International Organization for Standardization, namely for irrigation, urban uses and health risk assessment. In this way, all reuse projects must follow a fit-for-purpose approach, i.e., the water quality needs to meet the requirements of its specific end-uses without compromising public health or the surrounding environment, and all reuse projects must conduct a risk assessment for health and the environment. Quantitative, qualitative or semi-quantitative models can be used. Although a quantitative assessment may be desirable, these models tend to be complex and present high uncertainty. Furthermore, these usually require extensive data which are often not available. Accordingly, this study intended to develop a conceptual model to deal with the risk assessment for water resources, namely surface and ground waters. A semi-quantitative approach was employed for the risk characterization, using empirical qualitative judgment to assess the relative importance of hazards, exposure routes, scenarios and barriers in place. The use of a strategic assessment allows the quality standards that meet the needs of each project to be validated. The developed model was applied to a case study to illustrate its applicability.

Keywords: water reuse, water resources, risk assessment, semi-quantitative model, compounds of emerging concern

Corresponding Author: Anabela Rebelo; email: anabela.rebelo@apambiente.pt

Dates
?????

Publishing services provided by Knowledge E

© Anabela Rebelo et al. This article is distributed under the terms of the Creative Commons Attribution License, which permits unrestricted use and redistribution provided that the original author and source are credited.

Selection and Peer-review under the responsibility of the FibEnTech21 Conference Committee.

OPEN ACCESS

1. Introduction

The increasing demands for water resources for multiple purposes such as public water supply, agriculture, industry, recreational uses and others are leading to water scarcity and quality deterioration. The intensification of severe weather conditions due to climate change, such as droughts, and urban development has put a significant strain on freshwater supplies [1]. Therefore, the search for new alternative water sources like reclaimed waters is rising in several countries, such as the United States of America,

Singapore, Australia, Spain, Malta, Cyprus, and even in Portugal [1-3]. However, the use of treated wastewaters may pose some risks, where microbial risks are usually the main focus to protect human health, but other aspects are also catching attention, in particular, disinfection by-products (DBP) and compounds of emerging concern (CoC) which can pose risk to water resources and aquatic ecosystems and through these to humans [2-4].

The current policies in the European Union for the use of reclaimed water for agriculture irrigation (Regulation EU 741/2020) and in Portugal for multiple uses (Decree-Law 119/2019, 21st August) emphases on the adoption of projects supported on a risk management framework and in quality standards defined according to a fit-for-purpose approach, based on ISO standards 16075. This approach is supported on the production of water quality that meets the needs of the intended end-users. Accordingly, the European and Portuguese policies establish that all projects shall follow a risk assessment for human health and to the environment, which includes water resources. This type of appraisal will allow to select the quality standards applicable to each reuse project and the risk management conditions that should be followed to ensure an associated minimum risk value [3]. For health risk assessment were already developed several qualitative, semi-quantitative and quantitative methods, but for water resources, the most popular methods are based on complex mathematical models to assess pollutants fate and transport on environmental compartments or to evaluate hydrological conditions [5]. In the quantitative methods, the risk characterization is usually based on the ratio between the predicted environmental concentrations (PEC) and the predicted no-effect concentration (PNEC) for water, sediment, and biota. However, this type of methodology presents several limitations, such as the use of standardized bioassays involving single species and unique substances, without taking into account the real routes of exposure and the effects of mixtures and large uncertainties in extrapolating data across doses, species, and life stages, namely due to the lack of data on dose-response relationships [6]. Hence, these type of approaches requires the existence of a significant number of monitoring data from reuse projects to establish the predicted concentrations associated with each exposure scenario, since in this practice no direct discharge to water occurs, which limits the applicability of these methodologies to water reuse projects. Consequently, the quality criteria applied to a certain project are usual flat legal requirements without taking into account local conditions, such as water bodies characteristics, status, and uses of surface and groundwaters.

However, the use of knowledge-based models already showed its feasibility and applicability with simple outputs that may provide support for environmental authorities

on the decision-making process [5, 7]. Taking into account these considerations, this study aims to propose the development of a semi-quantitative model to perform water reuse risk characterization for water resources, including surface and groundwater, and demonstrate its suitability to validate the quality standards for chemical parameters, like nutrients (N and P), DBP and CoC, to be applied to a water reuse project and to be noted in the water reuse permits issued by environmental authorities [5, 7-9]. The proposed model is a site-specific assessment, supported on the typical tier approach including hazard identification, exposure and pathway assessment, and risk characterization [6].

2. Methodology

The proposed model was supported on a previous conceptual model developed by Rebelo et al., named Risk Assessment Model for Water Resources (RAMWR) and the ISO 16075-2:2020 and all factors are measured according to an importance scale from 1 to 9 [3,7]. The model proposed the risk determination by the product between hazard, the vulnerability of water resources and damage.

The hazard identification, within the scope of the current study, is nutrients (nitrogen and phosphorous) and chemicals, such as DBP, CoC, and priority substances/priority hazardous substances or specific pollutants classified according to the Directive 2000/60/EC, usually known as Water Framework Directive (WFD). The classification of hazards, as can be seen in table 1, is made according to its characteristics, treatment level, and expected concentrations in reclaimed waters. For nutrients the used criteria are the treatment level, the legal classification of water bodies in terms of sensibility to eutrophication (Directive 91/27/EEC) and vulnerability due to nitrates pollution (91/676/EEC) and the ecological status of water bodies (when the concern parameters are N or P). For chemicals, the classification is made according to expected concentration, which can derive from monitoring data or from a proposal of a quality standard to write on a permit.

[1] In vulnerable areas to nitrate pollution or when water body status is less than “Good” due to parameter N, consider Hazard for N equal to 7 and for P equal to 5; In sensitive areas to eutrophication or when water body status is less than “Good” for parameter P, consider .Hazard for N equal to 5 and for P equal to 7.

[2] EQS – Environmental quality standard (legal value) applicable to water bodies according to its status or uses

[3] LoQ – Limit of quantification of the applicable analytical method

[4]Relationship established according to [10]

TABLE 1: Hazard level.

Nutrients		Chemicals in water bodies	Hazard
Treatment level	N & P ($mg{\cdot}L^{-1}$)	Units of concentration	H_z
Without N and P removal[1]	N > 15 and P > 3	>EQS[2] or >30·LoQ[3,4]	9
With partial removal of N or P[2]	N ≤ 15 or P ≤ 3	>10·LoQ[4]	7
With partial removal of N or P	N ≤ 15 or P ≤ 3	>LoQ	5
With partial removal of N and P	N ≤ 10 and P ≤ 3	>LoD[5]	3
With advance removal of N and P	N ≤ 5 and P ≤ 0,5	<LoD	1

[5] LoD – Limit of detection of the applicable analytical method

The pathway assessment considers runoff to surface waters and infiltration, leaching and percolation to groundwaters. The vulnerability of water resources (V_{WR}) is given by equation 1:

$$V_{WR}=Vp_{GW}\times fp_{GW}+Vp_{SW}\times fp_{SW} \quad (1)$$

Where Vp_{GW} and Vp_{SW} are partial vulnerabilities directly achieved by Figure 1 and $f_p$are partial factors equal to $fp_{SW}=Vp_{SW}/(Vp_{SW} + Vp_{GW})$ and $fp_{GW}=Vp_{GW}/(Vp_{SW} + Vp_{GW})$, developed according to the same principles proposed by other authors [7]. From equation 1 is possible to obtain four different values which are prioritized through the importance scale according to table 2.

TABLE 2: Water resources vulnerably expressed in importance factors.

Values for V_{WR} given by equation 1	N & P ($mg{\cdot}L^{-1}$)
5,2	9
5,0	7
4,0	5
3,3	3

From the exposure evaluation of water resources is possible to determine trough equation 2, the global vulnerability (V_G).

$$V_G= V_{WR}\times\frac{\sum f_{i\ barrier}}{f_{max}\times n_{Scen}} \quad (2)$$

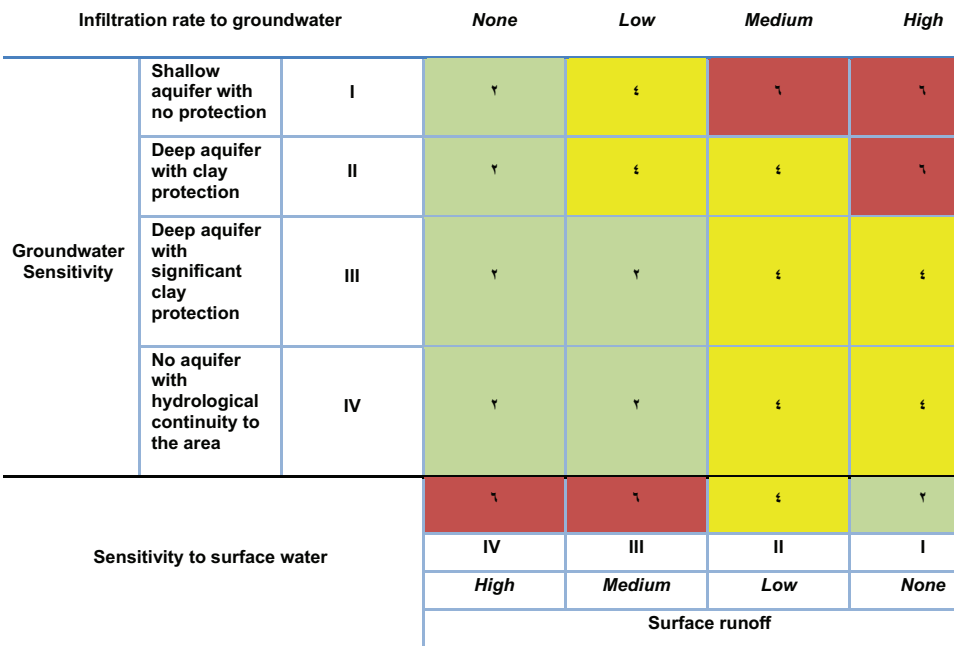

Figure 1: Matrix for surface and groundwater vulnerability assessment (adapted from ISO 16075-1:2020).

Where $f_{ibarrier}$ is the factor applicable to barriers according to table 3, where $f_{max} x n_{Scen}$ is a normalization factor, to adjust the scale to a common range [11], where n_{scen} is the number of scenarios given by table 4 and f_{max} is the maximum value of the used importance scale (9). The number of exposure scenarios depends on the barriers in place since a barrier is a mean that reduces or prevents the exposure of the receiving waters to the reclaimed waters [8,9]. In this study, the proposed barriers were adopted from Rebelo et al. and the number of exposure scenarios is displayed in table 4 [3,7],

TABLE 3: Applicable barriers for water resources protection

Type of barrier	Importance factor
Absence of barriers	9
Leak detection system	7
Partial retention capacity/irrigation system according to water crop needs	5
Total retention capacity	3

The final step to determine the risk is the definition of damage which can be attained by the severity of damage *versus* the likelihood of occurrence of failure in barriers (which also translates the likelihood of exposure occurrence). According to the ISO 20426:2018, a certain likelihood of exposure occurrence can be defined depending on data availability as can be seen in table 5.

Table 4: Number of exposure scenarios according to barriers in place.

Type of barrier	Number of exposure scenarios (n_{Scen})
Absence of barriers	1
Leak detection system	1
Partial retention capacity/irrigation system according to water crop needs	1
Total retention capacity	1
Leak detection system Partial retention capacity and irrigation system according to water crop needs	2
Leak detection system and total retention capacity	2

Table 5: Likelihood of occurrence of water resources exposure to contamination (adapted from ISO 20426:2018).

Likelihood of occurrence	Observations according to evidence (from other irrigation projects) and/or literature	Value
Unlikely	Has not happened in the past but may occur in exceptional circumstances in the reasonable period	2
Possible	May have happened in the past and/or may occur under regular circumstances in the reasonable period	3
Likely	Has been observed in the past and/or is likely to occur in the reasonable period	4
Almost certain	Has often been observed in the past and/or will almost certainly occur in most circumstances in the reasonable	5

The reasonable period is defined according to the validity period of reuse permits as mentioned in the Portuguese legislation, i.e., 10 years (Decree-Law 119/2019, 21st August). The severity of damage depends on the characteristics of the receiving water resources, namely its classification according to existent legislation (e.g., sensitive areas according to the Directive 91/271/EEC), status of the water body according to the WFD and the respective existing uses (e.g., drinking waters). This correlation is presented in table 6:

The partial damage (d_i) associated with the exposure routes and exposure scenarios considered is given by the matrix presented in Figure 2, by combining the values

Table 6: The severity of damage for water resources from exposure to contamination.

Severity of damage	Observations according to water resources evidence	Value
Severe	Water body with status less than good	5
Major	Water body in good status, with defined use and classification (vulnerable to nitrate pollution or sensitive area)	4
Moderate	Water body in good status, with defined use or classification (vulnerable to nitrate pollution or sensitive area)	3
Minor	Water body in good status, without defined use or classification (vulnerable to nitrate pollution or sensitive area)	2

obtained in table 5 with the data from table 6. The global damage (D) can be calculated by equation 3:

$$D = \frac{\sum d_i \times n_{Scen}}{f_{max} \times n_{Scen}} \quad (3)$$

			Unlikely	Possible	Likely	Almost certain
			Likelihood of occurrence of barrier failure			
			2	3	4	5
Minor	Severety of damage	2	2	4	4	5
Moderate		3	4	4	6	7
Major		4	4	6	8	9
Severe		5	5	7	9	9

Figure 2: Expression of partial damage (di) associated with the barrier failure (adapted from Rebelo et al. [3]).

Where n_{Scen} is the number of exposure scenarios from table 4 and f_{max}xn_{Scen} is a normalization factor similar to equation 2.

The risk for water resources (R_{WR}) is achieved by the product between the hazard (Hz), the global vulnerability (V_G), and associated damage (D), normalized to the maximum value of importance scale (9), i.e.:

$$R_{WR} = \frac{H_z \times V_G \times D}{f_{max}} = \frac{H_z \times V_G \times D}{9} \quad (3)$$

The R_{WR} value varies from a minimum value above zero (0) to nine (9) depending on the number of scenarios, barriers and the characteristics of water bodies. The prioritisation is accomplished by conversion of the R_{WR} results into a three-level qualitative scale as follows: Despicable Risk (R_{WR} <3), Acceptable Risk (3≤R_{WR} <7), and Unacceptable Risk (R_{WR}≥7), similar to descriptions used by other authors [3, 7]. When the risk presents an unacceptable, the process should be repeated considering additional minimization measures, such as additional barriers or increase of treatment level and as a result a lower level of hazard (Hz), which means a proposal for a quality standard more restricted. Nevertheless, a project may not be viable if it is not possible to below the R_{WR} at least to an acceptable level. Similar to other risk management options, the proposed methodology follows a strategic appraisal where a reassessment will allow defining the best management options [3, 7,12]. Whenever possible, the risk level should be despicable although some projects may be approved with an acceptable risk if supported on the evidence that further reduction would be highly disproportionate to the benefit gained.

3. Results and discussion

The model was applied to a casestudy, a golf course that intends to reuse water for irrigation. The course is located in an area classified as vulnerable to nitrate pollution. The hydrogeological conditions determine that is a local with a high infiltration rate for groundwater and there is an aquifer with some clay protection, in the area of the sports field. The aquifer is also classified as a strategic reserve for public water supply. Both surface and groundwater present Good Status according to the River Basin Management in force. The effluents treatment level in place is a secondary plus disinfection (UV), and according the monitoring data, from the European Pollutant Release and Transfer Register, the treated wastewaters also present an annual average below the limit of quantification for Di(2-ethylhexyl)phthalate (DEHP). The methodology was used to define the quality standards to be applied to nitrogen and DEHP and the possible needs of additional treatment, taking into account that no barriers are in place.

From the above description is possible to define Hazard (Hz) level for DEHP, which is equal to three (3), and for nitrogen, since no nutrient removal is in place, the H_z level is nine (9), The hydrogeological description allows to understand that partial vulnerabilities for surface and groundwaters (Vp_{SW} and Vp_{GW}) are 2 and 6, respectively. By the application of equation 1 and table 2, is possible to obtain a value of seven (7) to the V_{WR}. The absence of barriers determines a f_{ibarr} that matches the maximum level of

importance (9) and a single scenario of exposure, leading to a global vulnerability value equal to seven (7). In the same way, the absence of barriers determines an "almost certain" likelihood of exposure occurrence, which translates to a value of five (5). The water body as mentioned presents a good status, has a defined use since is a reserve for drinking waters, and is also classified as vulnerable to nitrate pollution, which determines the severity of damage with a major level with a value of four (4). Therefore, the partial damage (d_i) reveals a value of nine (9) and the global damage will then be equal to one (1). All results are presented in table 7 where is possible to see that for the considered hazards (DEHP and N), the risk assessment reveals a despicable level for DEHP (2,3) and an unacceptable level for nitrogen (7,0). Consequently, in terms of DEHP the risk level defines that there is no need to establish a quality standard for this parameter. However, for nitrogen, an increase of treatment level could be desirable. A definition of a quality standard level equal to or below 5 mg L^{-1} will result in a despicable risk while standard equal to or below 15 mg L^{-1} will promote an acceptable risk. However, the final solution should be adopted based on a nitrogen balance study, since not all the nitrogen in the reclaimed waters is immediately available for consumption by the crop, namely the organic fraction will only be accessible after the mineralization process, which not only depends on the treatment level but also the retention time in the storage system. Hence, besides the previous risk assessment, the final quality standard to be defined should take into account the maximum amount of nitrogen from reclaimed waters that can be adsorbed by the crop (grass and other ornamental crops on the golf course) to minimize the use of synthetic fertilizers [13].

TABLE 7: Risk assessment results

	Hazard	V_{WR}	Damage	Risk	Risk Level
Nitrogen	9	7	1	7,0	Unacceptable
Nitrogen (reassessment option 1)	7			5,4	Acceptable
Nitrogen (reassessment option 2)	1			0,8	Despicable
DEHP	3			2,3	Despicable

If a post-chlorination is proposed, the use of DBP formation models can also be used to predict possible risk levels for these types of pollutants [14]. For instance, using the model developed by other authors [14], the use of a typical chloride dose of 5 mg·L^{-1} and a reaction time between 5 to 15 min will induce a formation of trichloromethane from 3,7 a 4,6 µg·L^{-1}, above the EQS of 2,5 µg·L^{-1}, previewed on the Directive 2008/105/EC and 2013/39/UE. These results reflect a Hz of maximum level and, thus, an unacceptable

risk. However, is quite common the use of a LoQ for this substance below 5 $\mu g \cdot L^{-1}$, and real sampling results may result in a despicable risk. Thus, special attention should be paid to LoQ and EQS when results are displayed as below LoQ and further research could be useful to improve the model for this type of pollutants, namely, to apply to centralized systems for a more sustainable urban water management [15].

4. Conclusions

To promote and increase water reuse practices in Europe and Portugal, new policies, supported on the international guidelines, such as ISO standards, were adopted and one of its most critical features is the application of a flexible approach without jeopardizing the health and environmental safety. The main strength of the proposed model is its simplicity. The application of the methodology to a case study allowed to demonstrate its applicability and respective strengths, such as the use of a strategic assessment, that allows to evaluate the risks involved in each water reuse project for surface and groundwater and helps authorities, with simple outputs, on the validation process of the appropriate quality standards to be noted on water reuse permits and, subsequently, helps them on the decision-making process namely on the imposition of minimization measures. Although the model allows the determine the quality standards for reclaimed waters, these results should always be seen with other management options, namely for nutrients to minimize the use of synthetic fertilisers.

5. Acknowledgments

The authors are grateful to the Foundation for Science and Technology (FCT, Portugal) for financial support by national funds through the project UIDB/00195/2020 (FibEnTech).

References

[1] Lazarova V, Asano T, Bahri A, Anderson J. Milestones in water reuse: The best success stories. New York: IWA Publishing; 2013.

[2] Chen Z, Wu G, Wu Y et al. Water eco-nexus cycle system (WaterEcoNet) as a key solution for water shortage and water environment problems in urban areas. Water Cycle. 2020;1:71-77. https://doi.org/10.1016/j.watcyc.2020.05.004

[3] Rebelo A, Quadrado M, Franco A, Lacasta N, Machado P. Water reuse in Portugal: New legislation trends to support the definition of water quality standards based on risk characterization. Water Cycle. 2020;1:41-53. https://doi.org/10.1016/j.watcyc.2020.05.006

[4] Wilcox J, Nasiri F, Bell S, Rahaman MS. Urban water reuse: A triple bottom line assessment framework and review. Sustainable Cities and Society. 2016;27:448-456. https://doi.org/10.1016/j.scs.2016.06.021

[5] H. Shakeri SN. Development of an algorithm for risk-based management of wastewater reuse alternatives. Journal of Water Reuse and Desalination. 2018;8(1):38–57.

[6] Amiard J, Amiard-Triquet C. Chapter 2 – Conventional Risk Assessment of Environmental Contaminants. In Aquatic ecotoxicology - Advancing tools for dealing with emerging risks. Amiard-Triquet C, Amiard J, Mouneyrac C, editors. London: Academic Press; 2015. https://doi.org/10.1016/B978-0-12-800949-9.00002-4

[7] Rebelo A, Ferra I, Gonçalves I, Marques AM. A risk assessment model for water resources: Releases of dangerous and hazardous substances. Journal of Environmental Management. 2014;140:51-59. https://doi.org/10.1016/j.jenvman.2014.02.025

[8] Shakir E, Zahraw Z, Al-Obaidy AHMJ. Environmental and health risks associated with reuse of wastewater for irrigation. Egyptian Journal of Petroleum. 2017;26(1):95–102.

[9] Shakir E, Zahraw Z, Al-Obaidy AHMJ. Environmental and health risks associated with reuse of wastewater for irrigation. Egyptian Journal of Petroleum. 2017;26(1):95-102. https://doi.org/10.1016/j.ejpe.2016.01.003

[10] Jirka GH, Bleninger T, Burrows R, Larsen T. Management of point source discharges into rivers: Where do environmental quality standards in the new EC-water framework directive apply? International Journal of River Basin Management. 2004;2(3):225-233. https://doi.org/10.1080/15715124.2004.9635234

[11] Ishizaka A, Markus L. How to derive priorities in AHP: A comparative study. Central European Journal of Operations Research. 2006;14(4):387–400. https://doi.org/10.1007/s10100-006-0012-9

[12] Gormley S. Pollard R, Black E. Guidelines for environmental risk assessment and management - Green leaves III. London: Department for Environment, Food & Rural Affairs; 2011.

[13] Kafkafi U, Tarchitzky J. Fertigation: A tool for efficient fertilizer and water management. 1st ed. Paris: International Fertilizer Industry Association; 2011.

[14] Rebelo A, Ferra I, Marques A, Silva MM. Wastewater reuse: Modeling chloroform formation. Environmental Science and Pollution Research. 2016;23:24560-24566. https://doi.org/10.1007/s11356-016-7749-z

[15] Chen Z, Wu Q, Wu G, Hu H-Y. Centralized water reuse system with multiple applications in urban areas: Lessons from China's experience. Resources, Conservation and Recycling. 2017;117:125–136. https://doi.org/10.1016/j.resconrec.2016.11.008

KnE Materials Science

FibEnTech21
1st International FibEnTech Congress (FibEnTech21) New opportunities for fibrous materials in the ecological transition
Volume 2022

Knowledge E
enriching | engaging | empowering

Research article

Water Reuse in a Municipal Sports Center

Flora Silva[1,4,5]*, Ana Maria Antão-Geraldes[2,4] and António Albuquerque[3,4,5]

[1]ESTiG, Instituto Politécnico de Bragança, Campus de Santa Apolónia, 5300-253, Bragança, Portugal
[2]Centro de Investigação de Montanha (CIMO), Instituto Politécnico de Bragança, Campus de Santa Apolónia, 5300-253, Bragança, Portugal
[3]Department of Civil Engineering and Architecture, University of Beira Interior, Calçada Fonte do Lameiro, 6201-001, Covilhã, Portugal
[4]Fiber Materials and Environmental Technologies (FibEnTech-UBI), University of Beira Interior, R. Marquês D'Ávila e Bolama, 6201-001, Covilhã, Portugal
[5]GeoBioTec-UBI, University of Beira Interior, Calçada Fonte do Lameiro, 6201-001, Covilhã, Portugal

Abstract.
Two potential measures for increasing water use efficiency in a municipal sports center were evaluated: (1) the reuse of water originating from showers in the flushing toilets in the indoor football court building; and (2) the reuse of water from swimming pool filter backwashing for irrigation. In the indoor football court building the total annual water consumption is around 3,500.5 m^3 and from the showers is approximately 1,785.26 m^3. Therefore, the greywater generated in showers can be reused in toilet flushing, which consumes about 840.12 m^3 per year. The estimated annual water consumption for filter backwashing is 4,197.6 m^3. The annual amount of water necessary for irrigating the lawn of the local football stadium is around 7,200 m^3. Thus, the filter backwashed water, after being subjected to a sedimentation process, could be fully reused for this purpose.

Keywords: water efficiency, water reuse, swimming pools filter backwashing reuse, sports center, sustainability

Corresponding Author: Flora Silva; email: flora@ipb.pt

Dates
?????

Publishing services provided by Knowledge E

© Flora Silva et al. This article is distributed under the terms of the Creative Commons Attribution License, which permits unrestricted use and redistribution provided that the original author and source are credited.

Selection and Peer-review under the responsibility of the FibEnTech21 Conference Committee.

OPEN ACCESS

1. Introduction

Water scarcity is one of the leading social and environmental problems faced by society. Consequently, there is a need to preserve water and search for alternative sources. The reuse of greywater (water flow originated from showers, hand basins, laundry, dish-washing) can be one of the solutions to achieve one of the major goals of urban sustainability: the water [1-4] and energy efficiency [5]. It has been estimated that about 41–91% of the domestic water use turns into greywater. In Europe, around 35–150 L/(person.day) of greywater is produced [1]. Greywater from laundry and kitchen are considered to have a high pollutant load [1], whereas the water from showers and hand basins has a low pollutant load [6]. Thus, the latter can be reused for flushing cisterns or gardening after simple treatments (e.g., filtration, sedimentation, and disinfection) since the water used for the mentioned purposes does not require potable quality water

standards. In sports centers, around 72% of the water is used in showers (51%) and hand basins (21%) [7]. Therefore, it is of paramount importance to implement management measures to promote the reuse of this water in these large-area facilities where water consumption is usually high [4]. If these have simultaneously swimming pools, the pool filters backwashing also generate large amounts of water, which can, in turn, be reused [8]. Indeed, this process is required to remove contaminants accumulated during the pool filtration process. The filters are cleaned by flushing them with water in the reverse direction to normal flow (backwashing) [9]. The resulting backwash water is characterized by high contents of suspension and dissolved substances and, depending on the future application, requires differentiated treatment before being reused [8,10-11]. The Bragança municipal sports center has the following facilities (Fig.1): an indoor football court (building A), two indoor swimming pools (building B), and the local football stadium (C). In the present approach, two potential measures for increasing water use efficiency in this building were evaluated: (1) the reuse of water originated from showers in the flushing toilets in building A, and (2) the reuse of water from swimming pools filters cleaning for irrigation.

Figure 1: Plan of the Bragança municipal sports center: indoor football court (A) pools (B) and football stadium (C) (source: Google Earth).

2. Material and methods

According to the information provided by the municipality, the average number of users/year in building A was 36,873 (128 users per day) from 2016-2018. In the present approach, because of the COVID-19 pandemic, it was impossible to measure ”in-situ” the different water uses. Therefore, these were estimated based on audits carried out by ANQIP (Portuguese Association for Quality and Efficiency in Building Services) for water use in sports centers [7]. The amount of water necessary to backwash the swimming

pool sand filters (Table 1) was quantified by registering the values of the water flow meter immediately before and after the backwashing process. Swimming pool filters are rinsed every two days for five minutes. After, the backwashed water is discharged into the wastewater drainage network.

To evaluate the quality of backwashed water and, therefore, the possibility of its reuse for irrigating the lawn of the local football stadium (Figure 1), samples from filter washings were collected in the first and the third minute after the cleaning was started. In the Lab were submitted to differing sedimentation periods (0, 2, and 15 hours). Afterward, samples were analyzed for total suspended solids (TSS), pH, turbidity, and total coliforms, fecal coliforms, and streptococci colonies were enumerated. Further information concerning methodology can be found in [12].

TABLE 1: Swimming pools/filter characteristics and water consumption in filters backwashing process.

Characteristics	Competition Pool	Learning Pool
Pools		
Dimensions (L x W) (m)	25 x 17	16.6 x 10
Base area (m^2)	425.0	166.6
Minimum depth (m)	1.8	0.7
Maximum depth (m)	2.0	1.3
Water volume (m^3)	890.0	160.0
Filters		
Number	2	2
Diameter (mm)	2,000	1,400
Filtration surface (m^2/ft^2)	3.1/33.8	1.5/16.6
Filtration speed ($L/min/m^2$)	500	500
Flow rate (L/min)	1,566.7	766.7
Water consumption: filter backwashing (m^3/year)	2,818.8	1,378.8

3. Results and discussion

The average annual water consumption in building A is around 3,500.5 m^3. The estimated annual water consumption for showers is 1,785.26 m^3 (51% of the total water

consumption) (Table 2). Therefore, the greywater generated by showers can be reused in the flushing cisterns, whose predicted consumption is about 840.12 m^3/ year.

Table 2: Water consumption estimation by use category in building A.

Equipment	Consumption			%
	(m^3/year)	(m^3/month	(m^3/day)	
Flushing cisterns	840.12	70.01	2.92	24
Urinals	70.01	5.83	0.24	2
Washing basins	735.11	61.26	2.55	21
Showers	1,785.26	148.77	6.20	51
Other uses	70.01	5.83	0.24	2
Total	3,500.50	291.71	12.15	100

The daily consumption for the flushing cisterns is around 2.92 m^3/day, and the daily greywater produced by showers is 6.20 m^3/day (Table 2). Therefore, it is recommended the acquisition of a water recycler dimensioned for the observed water flux to minimize the gap between the inflow of greywater and its consumption. Indeed, raw/untreated greywater shall only be stored temporarily in a tank for less than 24 hours [13] to avoid bad odors and good conditions for pathogens proliferation [14], to reduce turbidity and TSS to admissible values [15-18].

The predicted water consumption reduction can reach 24% (from 3,500.5 to 2,660.4 m^3/year), and the annual water bill cutback would be € 4,594.22 [19].

The average daily water consumption for swimming pool filters backwashing was 15.7 m^3 (competition pool) and 7.7 m^3 (learning pool). Therefore, the estimated annual water consumption for filter washing were 2,818.8 m^3 and 1,378.8 m^3, respectively, totaling 4,197.6 m^3 (Table 1). TSS and turbidity showed higher values in the samples collected during the first minute of the filter backwashing (first flux). In those collected in the third minute, a reduction between 10% and 20% occurred in the studied parameters. Concerning TSS, the two and the fifteen-hour sedimentation reduced the amounts of suspended solids by 60 and 80 %, respectively. Turbidity showed a similar trend. Nevertheless, TSS and turbidity values exceeded the permissible values [15-18], except those submitted to fifteen-hour sedimentation (Table 3). pH values were always in the admissible range. Total coliforms, fecal coliforms, and fecal streptococci were not detected.

[1]Flushing cistern quality requirement: TSS 10 mg/L; Turbidity 2 NUT [15].

[2]Irrigation quality requirement: TSS 10 mg/L; Turbidity 2 NUT [15]. Irrigation of private gardens. For lawn irrigation, the same requirements were adopted.

[3]Recommended limit: Free residual chlorine 0.2 - 0.6 mg/L [16,17]; pH: 6.5-9.0 [16].

Table 3: TSS, turbidity, free chlorine, and pH values observed in 1 and 3 minutes samples submitted to different sedimentation times.

Parameter	Sample sedimentation time	Values [1,2,3]
TSS (mg/L)	No sedimentation (1 min)	61.5
	Sedimentation 2 h (1 min)	24.5
	Sedimentation 15 h (1 min)	9.0
	No sedimentation (3 min)	49.5
	Sedimentation 2h (3 min)	21.5
	Sedimentation 15 h (3 min)	10.0
	No sedimentation (1 min)	36.1
	Sedimentation 2 h (1 min)	5.0
Turbidity (NTU)	Sedimentation 15 h (1 min)	1.7
	No sedimentation (3 min)	25.5
	Sedimentation 2h (3 min)	5.9
	Sedimentation 15 h (3 min)	1.9
Free residual chlorine (mg/L)	No sedimentation (1 min) Sedimentation 2 h (1 min) Sedimentation 15 h (1 min) No sedimentation (3 min) Sedimentation 2h (3 min) Sedimentation 15 h (3 min)	0.58 0.12 0.02 0.42 0.11 0.02
	No sedimentation (1 min)	6.7
	Sedimentation 2 h (1 min)	7.1
pH	Sedimentation 15 h (1 min)	7.8
	No sedimentation (3 min)	6.8
	Sedimentation 2h (3 min)	6.4
	Sedimentation 15 h (3 min)	7.8

The regular swimming pool filters backwashing is unavoidable. Nevertheless, this process generates large amounts of water, usually discharged into the sewage contributing to the water (and energy) use inefficiencies. Therefore, it is crucial to promote the sustainable management of filter washings. The preliminary results showed that this water could not be directly reused because it does not fulfill the regulation requisites. However, the sedimentation process seemed to effectively reduce these parameters to permissible values, allowing the reuse of this water for irrigation or flushing toilets system. Similar results were found by Łaskawiec et al. (2016) [8] and by Wyczarska-Kokot and Lempart (2018) [10]. Furthermore, these authors also verified that the sedimentation process was effective in removing nitrogen and phosphorus. Therefore, considering these results, it is plausible to assume that the management of filter washings is possible after installing a relatively simple system for their treatment, such as a settler or a settling tank [8,10]. The annual amount of water necessary for irrigating the lawn of

the local football stadium, located in the surroundings of the swimming pool complex, is around 7,200 m^3 (data provided by Bragança Municipality). Therefore, in the future, filter backwashing could be fully reused for this purpose. Nevertheless, the treated backwashing could also be used in the flushing cisterns or, after a broader treatment, reintroduced back into the swimming pool [20]. However, due to the lack of specific legislation for backwashing monitoring and quality control, other indicators such as nutrients, micropollutants, and other chlorine forms [11, 20] should be determined and monitored before deciding on the best reuse for the water from the filter backwashing.

4. Conclusions

In a scenario of increasing water demand and scarcity, implementing measures leading to greywater reuse when quality drinking water is not required for water supply is paramount. The present study showed that it is possible to promote a substantial increase in water use efficiency in the municipal sports center, promoting water reuse measures, which contribute to the financial burden reduction and increasing environmental benefits. Indeed, sports centers have substantial operational costs due to extensive water consumption, indirectly implying significant energy consumption levels. Herein, the evaluation of the energy consumption under the scope of water-energy nexus was not evaluated. Consequently, the earnings for implementing the suggested measures are monetarily and environmentally much higher than the estimates obtained herein. In short, the current approach indicates that the reuse of greywater and filter backwashing is not only feasible but can lead to a significant reduction of water consumption in the municipal sports center, reducing the environmental impacts associated with urban water demand. Nevertheless, future approaches are needed to fully evaluate the feasibility of water reusing for irrigation and, eventually, for other purposes, in terms of the water–energy nexus, water quality, and investment turnover.

Acknowledgments

The authors are very grateful for the support given by research unit Fiber Materials and Environmental Technologies (FibEnTech-UBI), on the extent of the project reference UIDB/00195/2020, funded by the Fundação para a Ciência e a Tecnologia, IP/MCTES through national funds (PIDDAC). AMAG is also very grateful to the Foundation for Science and Technology (FCT, Portugal) for financial support by national funds FCT/MCTES to CIMO (UIDB/00690/2020). The authors thank CMB for providing data for this study.

References

[1] Vuppaladadiyam AK, Merayo N, Prinsen P et al. A review on greywater reuse: Quality, risks, barriers and global scenarios. Reviews in Environmental Science and Bio/Technology. 2019;18:77-99. https://doi.org/10.1007/s11157-018-9487-9

[2] Gabarró J, Batchelli L, Balaguer MD, Puig S, Colprim J. Grey water treatment at a sports centre for reuse in irrigation: A case study. Environmental Technology. 2013;34(9-12):1385-1392. https://doi.org/10.1080/09593330.2012.750382

[3] Shanableh A, Mohamad AK, Abdallah M et al. Assessment and reform of greywater reuse policies and practice: a case study from Sharjah, United Arab Emirates. Water Policy. 2021;23(2):376-396. https://doi.org/10.2166/wp.2021.205

[4] Burszta-Adamiak E, Spychalski P. Water savings and reduction of costs through the use of a dual water supply system in a sports facility. Sustainable Cities and Society. 2021;66:102620. https://doi.org/10.1016/j.scs.2020.102620

[5] Knutsson J, Knutsson P. Water and energy savings from greywater reuse: A modelling scheme using disaggregated consumption data. International Journal of Energy and Water Resources. 2021;5:13-24. https://doi.org/10.1007/s42108-020-00096-z

[6] Chaillou K, Gérente C, Andrès Y et al. Bathroom greywater characterization and potential treatments for reuse. Water Air Soil Pollution. 2011;215:31-42. https://doi.org/10.1007/s11270-010-0454-5

[7] Silva-Afonso A, Pimentel-Rodrigues C. Manual de eficiência hídrica em edifícios. Aveiro: Associação Nacional para a Qualidade nas Instalações Prediais (ANQIP); 2017.

[8] Łaskawiec E, Dudziak M, Wyczarska-Kokot J. Assessment of the possibility of recycling backwashing water from the swimming pool water treatment system. Ecological Chemistry and Engineering A. 2016 ;23:401-410. https://doi.org/10.2428/ecea.2016.23(4)30

[9] Doménech-Sánchez A, Laso E, Berrocal CI. Water loss in swimming pool filter backwashing processes in the Balearic Islands (Spain). Water Policy. 2021;23:1314-1328. https://doi.org/10.2166/wp.2021.217

[10] Wyczarska-Kokot J, Lempart A. The reuse of washings from pool filtration plants after the use of simple purification processes. Architecture, Civil Engineering, Environment. 2018;11:163-170. https://doi.org/10.21307/ACEE-2018-049

[11] Lempart A, Kudlek E, Dudziak M, Zawadzka A. The source of toxicity of backwash water from a swimming pool filter bed washings. Architecture, Civil Engineering, Environment. 2018;11:139-146. https://doi.org/10.21307/ACEE-2018-046

[12] Silva F, Antão-Geraldes AM, Zavattieri C, Afonso MJ, Freire F, Albuquerque A. Improving water efficiency in a municipal indoor swimming-pool complex: A case study. Applied. Sciences. 2021;11:10530. https://doi.org/10.3390/app112210530

[13] Singapure's Water National Agency. Technical guide for greywater recycling system. 1st ed. Singapure. Singapure Government; 2014. Available from: https://www.pub.gov.sg/Documents/greywaterTech.pdf

[14] World Health Organization. Overview of greywater management - Health considerations. Amman-Jordan. WHO-EM/CEH/125/E document. WHO; 2006.Available from : https://applications.emro.who.int/dsaf/dsa1203.pdf

[15] Associação Nacional para a Qualidade nas Instalações Prediais (ANQIP). ETA 0905 - Sistemas prediais de reutilização e reciclagem de águas cinzentas. Aveiro: Associação Nacional para a Qualidade nas Instalações Prediais (ANQIP); 2011-2016. Available from: https://anqip.pt/index.php/pt/comissoes-tecnicas/98-comissao-tecnica-0905.

[16] Decreto-Lei n.º 306/2007. Estabelece o regime da qualidade da água destinada ao consumo humano; Diário da República 1.ª série. 27 de agosto de 2007.

[17] Decreto-Lei n.º 152/2017. Altera o regime da qualidade da água para consumo humano, transpondo as Diretivas n.^{os} 2013/51/EURATOM e 2015/1787; Diário da República 1.ª série. 7 de dezembro de 2017.

[18] Agência Portuguesa do Ambiente (APA). Guia para a reutilização de água-usos não potáveis. 1st ed. Agência Portuguesa do Ambiente. Lisboa; 2019. Available from: https://apambiente.pt/sites/default/files/_Agua/DRH/Licenciamento/ApR/APA_Guia_Reutilizacao_v1.pdf

[19] CMB. Edital n.º 63/2018. Tarifário de abastecimento de água do Município de Bragança, 2018. Available from: https://www.apfn.com.pt/estudoagua/2018/ficha59.pdf

[20] Doménech-Sánchez A, Laso E, Berrocal CI. Water loss in swimming pool filter backwashing processes in the Balearic Islands (Spain). Water Policy. 2021;23:1314–1328. https://doi.org/10.2166/wp.2021.217

KnE Materials Science

FibEnTech21
1st International FibEnTech Congress (FibEnTech21) New opportunities for fibrous materials in the ecological transition
Volume 2022

Knowledge E
enriching | engaging | empowering

Research article

Chemical and Mineralogical Characterization of Biomass Ashes for Soil Reinforcement and Liner Material

André Studart[1,2,3]*, Leonardo Marchiori[1,2,3], Maria Vitoria Morais[1,2,3], António Albuquerque[1,2,3], Pedro Gabriel Almeida[1,3], and Victor Cavaleiro[1,3]

[1]Department of Civil Engineering and Architecture, University of Beira Interior, Calçada Fonte do Lameiro, 6201-001, Covilhã, Portugal
[2] FibEnTech, University of Beira Interior, Calçada Fonte do Lameiro, 6201-001, Covilhã, Portugal
[3] GeoBioTec, University of Beira Interior, Calçada Fonte do Lameiro, 6201-001, Covilhã, Portugal

Abstract.
Mineralogical and chemical evaluations are necessary to investigate the background and origins of materials. In terms of residues commonly produced around the world, ashes biomass stands out for its high calorific capacity and use for energy production at thermoelectrical facilities. Given current sustainability issues and new demands from society, ashes and soil from pine biomass in the Castelo Branco region were investigated to research possible anthropogenic contaminations, heavy metals among their composition, and their physic-chemical characteristics. These properties can be used to define possible valorisation methods through residue introduction into the soil for its reinforcement and liner application. The results indicated that ashes biomass could help achieve these objectives and could be introduced into the soil, due to its enrichment with pozzolanic minerals and fine granulometry, while having a low-density, which could reduce final weight; however it was considerably different from the original biomass, and contained anthropogenic contaminations and high concentrations of heavy metals.

Keywords: biomass ashes, chemical and mineralogical properties, residue valorisation, soil reinforcement, liner material

Corresponding Author: André Studart; email: andre.studart@ubi.pt

Dates
?????

Publishing services provided by Knowledge E

© André Studart et al. This article is distributed under the terms of the Creative Commons Attribution License, which permits unrestricted use and redistribution provided that the original author and source are credited.

Selection and Peer-review under the responsibility of the FibEnTech21 Conference Committee.

OPEN ACCESS

1. Introduction

Soils and residues throughout the world can be classified in varied forms, characteristics, and specifications. Based on these properties, investigating their mineralogy can provide background origins and possible anthropogenic contaminations, providing a deeper investigation surrounding the material's origin and its properties. Therefore, fully understanding the background of soils and residues can provide the right tools to understand how to integrate them and ameliorate specific properties, possibly making them successfully appliable to larger applications, such as soft soil reinforcement and liners materials while addressing sustainability issues. Some of these residues, such as biomass ashes, are rich in organic matter gathered from the decomposition of

vegetables or animals, hence making it feasible for use at thermoelectrical facilities for energy production due to their high calorific value. Although feasible for this activity, these facilities can alter biomass' properties as they suffer burns with temperatures up to 1400°C while being also co-fired with coal [1], which is a highly calorific material that is contaminant itself. Therefore, it is important to investigate anthropogenic contamination on these residues, as they can present contamination properties, which are necessary to be evaluated through X-Ray diffraction (XRD) and X-Ray fluorescence (XRF) tests.

Thus, this paper aims to investigate the chemical and mineralogical backgrounds of a soil sample and biomass ashes, in order to research their background and origins for a possible integration and stabilization of this residue within the analysed soil for soils reinforcement and liners materials.

2. Methods

The biomass ashes (BA) were collected at the industrial park of VALAMB - Grupo Razão, located in Castelo Branco (Portugal). The soil for reinforcement was collected at Castelo Branco (Portugal). Both materials were characterized to evaluate their chemical and mineralogical characteristics, as follows: optimum dry density ($\rho_{d,opt)}$ and water content, according to standards [2–4]; energy-dispersive X-ray spectroscopy (EDS) for elemental analysis determination, according to equipment S-2700 Hitachi; and X-ray diffraction (XRD) for mineralogical characterization, according to equipment Phillips Analytical X-Ray B.V.

3. Results and discussion

EDS results are presented in Table 1, while Figure 1 and Figure 2 show XRD results for soil and BA, respectively. Both figures use relative intensity in the y-axis in order to obtain the peaks of the minerals.

TABLE 1: EDS elemental analysis of soil and BA

Concentration levels	Soil	BA	Oxides	Soil	BA
Na_2O (%)	0.58	1.22	K_2O (%)	4.45	7.08
MgO (%)	2.28	4.24	SO_3 (%)	-	1.84
Al_2O_3 (%)	27.37	17.82	Fe_2O_3 (%)	8.30	5.80
SiO_2 (%)	56.09	44.87	TiO_2 (%)	0.93	0.66
CaO (%)	-	14.80	Cd (ppm)		5.07
As (ppm)	-	33.87	Cu (ppm)		63.43

The analysed soil is characterized by having a silty sand granulometry with a 10.5% clay portion, $\rho_{d,opt}$ of 1.92 g/cm^3 related to an optimum water content of 19.40%, which were obtained through granulometry and proctor standards. Its mineralogical composition is characterized by quartz, muscovite, and kaolinite clay, which are characteristic of the Castelo Branco region, where the soil was collected. This region is characterized by an erosive geological episode that flattened a large portion of this area, consisting of K-feldspars, granites, and schists formations [5]. Non-eroded quartzites crests and granites mineral can be found, providing kaolinite clay matrix, which is also evidenced by the sample's whitish colour.

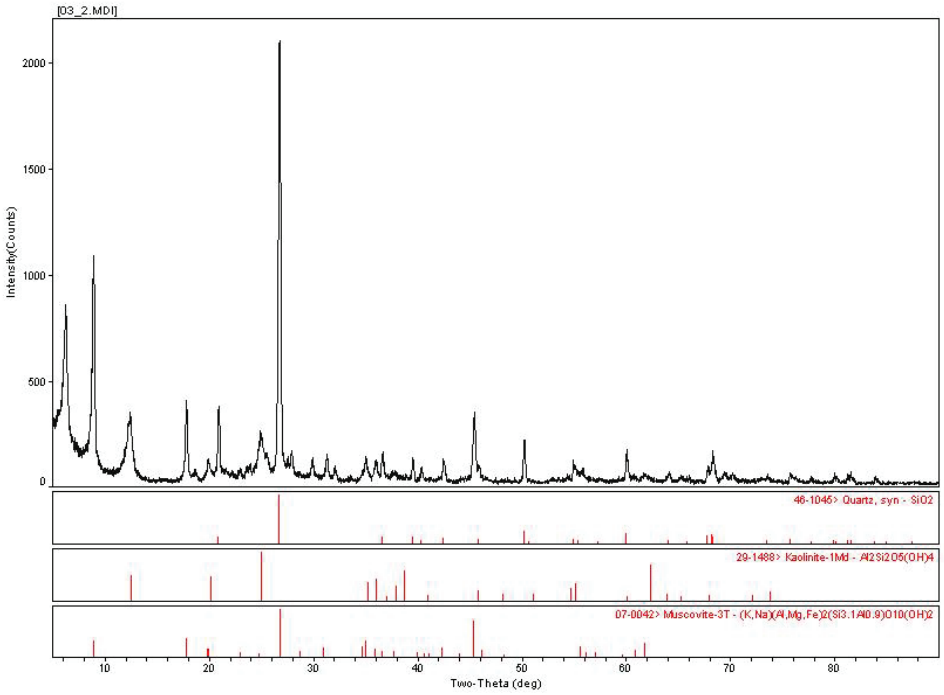

Figure 1: XRD mineralogical characterization of the soil.

The analysed biomass ashes have a finer silty granulometry, proving to be mainly a silty material associated with a $\rho_{d,opt}$ of 1.12 g/cm^3 related to an optimum water content of 25.80%. In addition, it has exposed a heterogenic and highly crystalline composition, which is the result of physical and chemical processes that occur during its combustion, altering BA's structure due to high temperatures - ranging from 500°C up to more than 1000°C - that end up removing most of the organic matter [6]. Quartz, muscovite, orthoclase, and calcite were detected during XRD tests. Quartz is due to the silicious sand used within the biomass combustion process while also typically found, along with the other minerals, in the analysed region. Although the soil provides different minerals to the local vegetation, biomass will also present different composition depending on

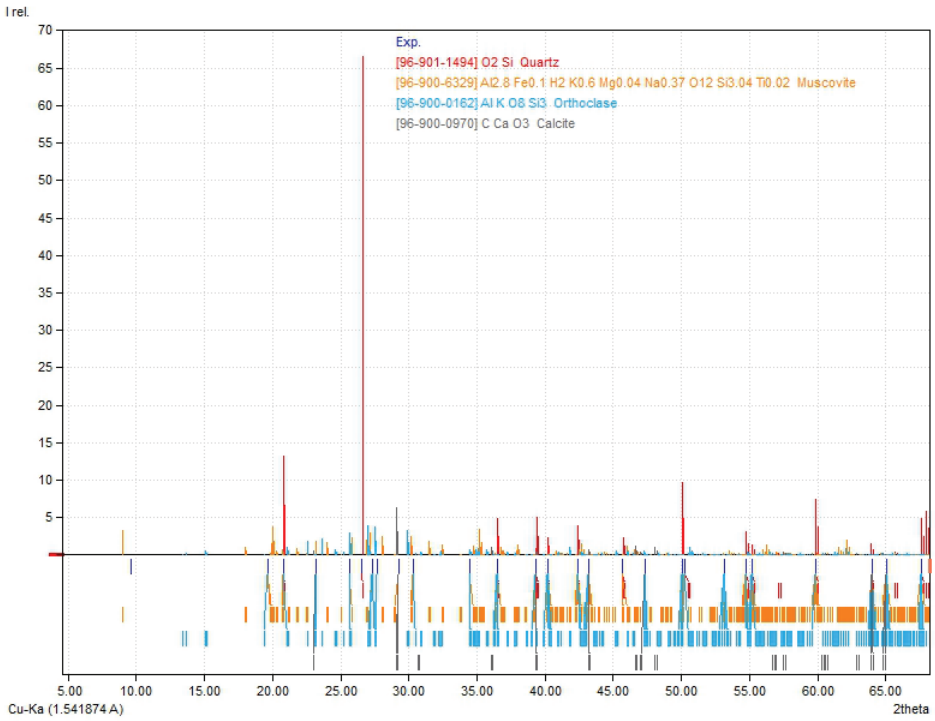

Figure 2: XRD mineralogical characterization of the BA.

the plant species and within different portions of the plant – branches, leaves, or stems – as each one store and concentrate minerals on different levels through different processes [7].

Thus, the used biomass in thermoelectrical facilities is partially understood by the soil and type of vegetation, as it suffers physical-chemical alterations during the combustion due to high temperatures – up to 1400°C - and to the type of used char, which interfere in biomass ashes' composition, deeply altering the original biomass' composition and structure [1]. In addition, during combustion, minerals can suffer enrichment due to thermal-conversions, happening mostly on carbonated minerals [8,9], such as Calcite's ($CCaO_3$) disintegration to CaO and CO_2, explaining some high minerals' concentration that is not easily explained by the local soil' chemical composition. Calcium, for example, would be an example of the retaining capacity through oxalate calcium precipitation that plants have, being this element stored in their different portions (branches, trunks, and stems) on different levels, as this is a major element for their development, besides animals' decomposition and bones fragmentation that could also provide calcium concentration for plants [10,11].

When analysing the region where it was first collected, pines are among the most common species in this region, raising suspicion about the biomass' origins. Therefore, the analysed biomass ash is considered here as an aluminosilicate associated with the

original biomass' vegetation – Pines - and to the used char during its combustion. Pines tend to contain high SiO_2 values, and a considerable amount of calcium and aluminium along with accessory elements. In addition, although the exact used char type during the combustion is not known, [12] has shown chars' varied composition, which affects BA composition. All these natural and artificial processes will completely change the final product – BA – compared to the original biomass. As [13,14] have exposed, the belief that biomass itself is sustainable, as it returns to the atmosphere the already used CO_2 value during its incineration, is not fully correct due to these contamination and alteration processes that occur in such facilities, which could lead to a final product that is highly contaminant, as fly ashes are produced in high temperatures up to 1600°C, due to inherent ash particles that retain heavy metals [1,14]. These heavy metals are mostly present due to inherent geological processes that occur during the formation of the above-mentioned minerals. Heavy metals presented in Table 1 on the analysed biomass ashes have shown the materials' susceptibility for contaminating properties, as its Arsenic (As) concentration would not pass Poland's and US New Jersey regulatory limits [15,16] while Cd (Cadmium) concentration would not pass UE's regulatory limits [17]. Thus, this states their contamination potential, although important to reiterate that these values correspond to the full biomass and its introduction in lower percentages into the soil could imply concentrations low enough to attend countries' directives for regulatory limits.

4. Conclusions

Biomass ashes' high variability is a challenge as it is difficult to trace exact patterns due to varied anthropogenic and natural conditions that alter the original biomass, producing new material at the end of the biomass combustion. Apart from this, their granulometry indicates possible soils' void-filling property while its chemical composition shows possible pozzolanic activity due to high Si, Al, and Fe content. Therefore, their background research has indicated anthropogenic contamination plays considerable role in altering biomass' properties and characteristics while also interesting possibilities for soft soils reinforcement due to the above-mentioned properties, although necessary to keep evaluating their contamination potential with leachability tests. Further geomechanical studies are necessary to confirm these characteristics.

Acknowledgments

The authors are grateful to the Foundation for Science and Technology (FCT, Portugal) for financial support by national funds through the projects UIDB/00195/2020 (FibEnTech) and UIDB/04035/2020 (GeoBioTec). The authors are also grateful to João Dias das Neves (VALAMB - Grupo Razão), who provided the samples of biomass ashes.

References

[1] S. van Loo, J. Koppejan, The Handbook of Biomass Combustion and Co-Firing, Earthscan; United Kingdom, 2008.

[2] ISO17892-1, Geotechnical investigation and testing - Laboratory testing of soil - Part 1: Determination of water content, 2014.

[3] ISO17892-2, Geotechnical investigation and testing - Laboratory testing of soil - Part 2 : Determination of bulk density, 2014.

[4] ISO17892-3, Geotechnical investigation and testing - Laboratory testing of soil - Part 3: Determination of particle density, 2015.

[5] P.P. Cunha, Evolução Tectono-Sedimentar Terciária da Região de Sarzedas (Portugal), Comunicações dos Serviços Geológicos de Portugal (1987) 67–84.

[6] S. V Vassilev, D. Baxter, L.K. Andersen, C.G. Vassileva, An overview of the composition and application of biomass ash. Part 1. Phase–mineral and chemical composition and classification, Fuel. 105 (2013) 40–76. https://doi.org/10.1016/j.fuel.2012.09.041.

[7] S. V. Vassilev, D. Baxter, L.K. Andersen, C.G. Vassileva, An overview of the chemical composition of biomass, Fuel. 89 (2010) 913–933. https://doi.org/10.1016/j.fuel.2009.10.022.

[8] D. Vamvuka, D. Zografos, Predicting the behaviour of ash from agricultural wastes during combustion, Fuel. 83 (2004) 2051–2057. https://doi.org/10.1016/j.fuel.2004.04.012.

[9] D. Vamvuka, M. Pitharoulis, G. Alevizos, E. Repouskou, D. Pentari, Ash effects during combustion of lignite/biomass blends in fluidized bed, Renew. Energy. 34 (2009) 2662–2671. https://doi.org/10.1016/j.renene.2009.05.005.

[10] D. Krutul, T. Zielenkiewicz, A. Radomski, J. Zawadzki, A. Antczak, M. Drozdzek, T. Makowski, Metals accumulation in Scots Pine (Pinus Sylvestris L.) wood and bark affected with environmental pollution, Wood Res. 62 (2017) 353–364.

[11] J. Fromm, Wood formation of trees in relation to potassium and calcium nutrition, Tree Physiol. 30 (2010) 1140–1147. https://doi.org/10.1093/treephys/tpq024.

[12] S. V. Vassilev, C.G. Vassileva, A new approach for the classification of coal fly ashes based on their origin, composition, properties, and behaviour, Fuel. 86 (2007) 1490–1512. https://doi.org/10.1016/j.fuel.2006.11.020.

[13] M. Sami, K. Annamalai, M. Wooldridge, Co-firing of coal and biomass fuel blends, Progress in Energy Combustion Science. 27 (2001) 171–214. https://doi.org/10.1016/S0360-1285(00)00020-4.

[14] S. V. Vassilev, D. Baxter, L.K. Andersen, C.G. Vassileva, An overview of the composition and application of biomass ash., Fuel. 105 (2013) 19–39. https://doi.org/10.1016/j.fuel.2012.10.001.

[15] United States Enviromental Agency Protection, Hazardous Wastes, 2020.https://www.nj.gov/dep/srp/guidance/scc/#q

[16] A. Kabata-pendias, H. Pendias, Trace Elements in Soils and Plants, 3rd ed., CRC Press, 2001.

[17] Official Journal of The European Communities, Directive 86/278/EEC, 1986.

KnE Materials Science

FibEnTech21
1st International FibEnTech Congress (FibEnTech21) New opportunities for fibrous materials in the ecological transition
Volume 2022

Knowledge E
enriching | engaging | empowering

Research article

Geotechnical Characterization of Biomass Ashes for Soil Reinforcement and Liner Material

Leonardo Marchiori[1,2,3]*, André Studart[1,2,3], Maria Vitoria Morais[1,2,3], António Albuquerque[1,2,3], Luis Andrade Pais[1,3], Maria Eugênia Boscov[4], and Victor Cavaleiro[1,3]

[1]Department of Civil Engineering and Architecture, University of Beira Interior, Calçada Fonte do Lameiro, 6201-001, Covilhã, Portugal.
[2]FibEnTech, University of Beira Interior, Calçada Fonte do Lameiro, 6201-001, Covilhã, Portugal.
[3]GeoBioTec, University of Beira Interior, Calçada Fonte do Lameiro, 6201-001, Covilhã, Portugal.
[4]Department of Structural and Geotechnical Engineering, University of São Paulo (USP), Av. Prof. Almeida Prado – TRAV. 2, 83, 05508-900, São Paulo, Brazil.

Abstract.
Biomass ashes (BA) have been intensively studied as amendments for soil in earthworks. This paper aimed to geotechnically characterize BA from pines and olive trees compared to the soil from Castelo Branco, Portugal. Namely, granulometry, specific gravity, Atterberg limits and optimal compaction values were obtained and analyzed in order to valorize the residue incorporated into soils. This work is part of broader efforts to develop an alternative material that can be used in hydraulic barriers as liners and for soil reinforcement. Thus, BA can contribute to reductions in weight and plasticity, and filling properties. Further studies are needed, particularly mechanical and hydraulic performances tests.

Keywords: biomass ashes, geotechnical and mechanical properties, residue valorization, soil reinforcement, liner material

Corresponding Author: Leonardo Marchiori; email: leonardo.marchiori@ubi.pt

Dates
?????

Publishing services provided by Knowledge E

© Leonardo Marchiori et al. This article is distributed under the terms of the Creative Commons Attribution License, which permits unrestricted use and redistribution provided that the original author and source are credited.

Selection and Peer-review under the responsibility of the FibEnTech21 Conference Committee.

OPEN ACCESS

1. Introduction

BA are the by-product produced mostly in co-fired thermoelectrical facilities for energy production. Several processes are involved in such facilities, such as combustion, pyrolysis, and incineration, generating filter and fly biomass ashes, which are considerably different from the original biomass, as they are mixed with other products and suffer physical and chemical processes [1-2]. Therefore, as a residue that could cause contamination, BA waste has received attention due to its possible pozzolanic properties, which could indicate their use as cementitious material after alkali content reduction [3] or substituting gravel in road construction while possibly replacing fine-grained clays and soils in the construction of landfill liners due to its latent hydraulic properties [4]. Bagasse ash, rice husk ash, and palm oil fuel ash are prominent examples

of such residues [5], like the, already studied cellulose and paper mill sludge which consist mainly of fibers, fillers, clays, and several other minor impurities that can have low hydraulic conductivity (k) when properly compacted, the geotechnical characteristics of the sludge in the paper mill are very different from typical clays, but in general they behave similarly. [6] analyzed the industrial potential for BA and concluded the main advantages: the concentration and recovery of valuable components - SiO_2, Al_2O_3, CaO. These components could indicate their feasibility for soft soil reinforcements, increasing friction angle while reducing the number of voids and settlements, even though BA properties vary when dealing with different types of biomasses.

As biomass ashes are originated from different natural and anthropogenic processes that take place within combustion units, they are a highly variable residue, principally when considering its large and varied origin possibilities. In addition, several types of BA, such as pines BA are not yet fully understood, requiring further investigation to understand their properties within soils. Different geotechnical characteristics can be seen among literature, which some of them have stated biomass ashes' successful approach for reinforcing soft soils, as stated in [7-8].

Thus, this paper aims to investigate and characterize biomass pine and olive ashes geotechnically searching its feasibility for soils' reinforcement and alternative liner material incorporating or substituting usual material in earthworks due to geotechnical parameters.

2. Materials and methods

The BA were collected at the industrial park of Valamb - Grupo Razão, located in Castelo Branco (Portugal), and the soil for reinforcement was collected at Castelo Branco (Portugal). Both materials were characterized to evaluate their geomechanical characteristics, as follows: specific gravity (G_S) and water content (w), according to standards [9–11]; granulometry and specific surface (SS), according to the equipment CoulterLS200 procedure, and based on standard [12]; Atterberg limits and plastic index (PI) according to standard [13]; and compaction characteristics with Normal Proctor, according to standard [14].

3. Results and discussion

The granulometry curves are presented in Figure 1 and the geotechnical parameters are presented in Table 1.

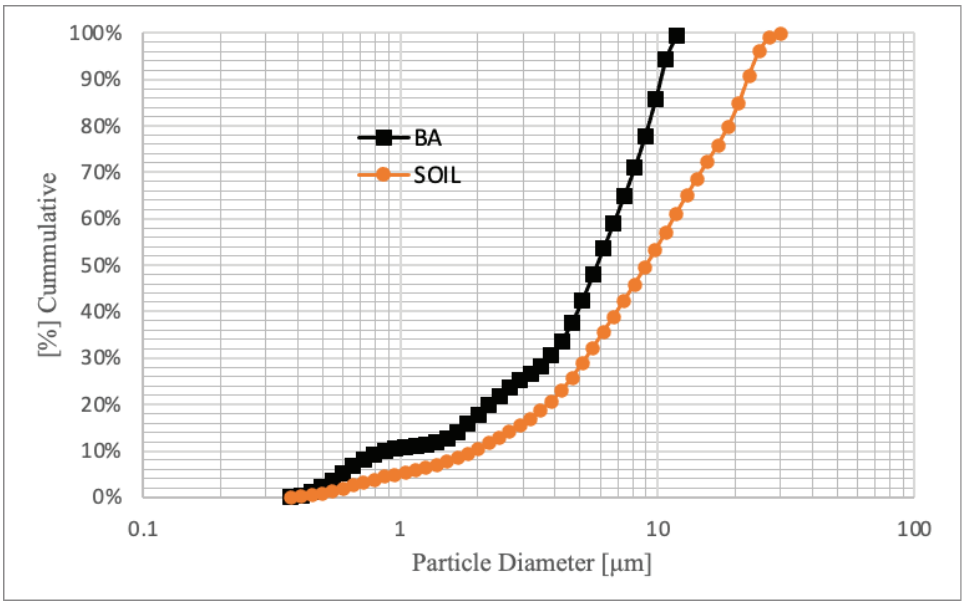

Figure 1: Particle size distribution of soil and BA.

Exposed geotechnical parameters in Table 1 have shown BA finer granulometry, non-liquid (NL), and non-plastic (NP) behavior, which could imply that their introduction into soils could reduce the mixture's plasticity, number of voids, and possibly their settlement. Also, a lower G_S value indicates weight-reduction property. Other parameters, such as mechanical and hydraulic values have yet to be investigated, although varied published studies, such as [15], have exposed BA successful introduction into residual compacted granite soil, resulting in lower soil plasticity and weight reduction while also increasing k value at higher BA rates. Thus, currently published results state BA feasibility for improving geotechnical parameters, indicating that these enhancements could be similar to the analyzed pine's BA, being required further investigation to confirm geomechanical parameters – k value, friction angle, and cohesion – and the above-mentioned important characteristics for successfully reinforcing soft soils and possibly application as liners. One possibility for BA valorization is its incorporation into the soil, based on percentages by mass, whether dry or wet and increasing the amounts of this residue in the mixtures, evaluating its characteristics and geotechnical performance analyzing above-mentioned parameters.

BA's literature [18] for hydraulic parameters found k values between 6×10^{-10}-1×10^{-9} m/s [15-16-17] meeting well the required 1×10^{-11}-1×10^{-9} m/s for a geological barrier at the base or top landfill's layer, additionally c' = 20–25 kPa and φ' = 30-45° found by [19-20] make possible soil's reinforcement while incorporating biomass ashes into soils.

Table 1: Geotechnical characterization for soil and BA.

	G_S (-)	W_L (%)	W_P(%)	PI (%)	W_{opt} (%)	$\rho_{d,opt}$ (g/cm^3)
Soil	2.7	38	34	4	20	1.9
BA	1.9	NL	NP	NP	26	1.2
[15]	2.3	35	25	10	20	1.6
[16]	2.5	88	NP	NP	24	1.6
[17]	1.7	41	25	16	80	1.7

4. Conclusions

Biomass ashes are a new focus of attention for clay substitutes in landfills, as studies are beginning to discover their physicochemical, mechanical, and hydraulic properties. Their characteristics and composition are highly variable and dependent on the plant's species, origin location, and collect, while combustion processes and used products/accessory materials, such as char, transform the original biomass into basically a new material. Some of the studied biomasses are bagasse ash, rice husk ash, and palm oil fuel ash, although there is a lack of research for soils reinforcement and liners application. This indicates the necessity of further investigating pines' BA into soils to test long-term performance, compaction, and strength characteristics. Primary results are optimistic and could indicate a solid path towards using this residue for the named applications, principally for weight-reduction due to lower G_s and $\rho_{d,opt}$, non-plastic behaviour, decreasing plasticity and filling properties caused by finer granulometry.

5. Acknowledgments

The authors are grateful to the Foundation for Science and Technology (FCT, Portugal) for financial support by national funds through the projects UIDB/00195/2020 (FibEnTech) and UIDB/04035/2020 (GeoBioTec). The authors are also grateful to João Dias das Neves (VALAMB - Grupo Razão), who provided the samples of biomass ashes.

References

[1] Vassilev SV, Baxter D, Andersen LK, Vassileva CG. An overview of the composition and application of biomass ash. Fuel. 2013;105:19–39. https://doi.org/10.1016/j.fuel.2012.10.001

[2] Loo S, Koppejan J. The handbook of biomass combustion and co-firing. Earthscan; Routledge, 2007.

[3] Salvo M, Rizzo S, Caldirola M et al. Biomass ash as supplementary cementitious material (SCM). Advances in Applied Ceramics. 2015;114(1):3-10. https://doi.org/10.1179/1743676115Y.0000000043

[4] Obernberger I, Supancic K. Possibilities of ash utilisation from biomass combustion plants. Paper presented at: Proceedings of the 17th European Biomass Conference; 2009 29 Jun – 3 Jul; Hamburg, Germany.

[5] Rubinos DA, Spagnoli G. Utilization of waste products as alternative landfill liner and cover materials – A critical review. Critical Reviews in Environmental Science and Technology 2018;48(4):376–438. https://doi.org/10.1080/10643389.2018.1461495

[6] Vassilev SV, Baxter D, Andersen LK, Vassileva CG. An overview of the composition and application of biomass ash: Part 2. Potential utilisation, technological and ecological advantages and challenges. Fuel. 2013;105:19–39. https://doi.org/10.1016/j.fuel.2012.10.001

[7] Galvín AP, López-Uceda A, Cabrera M, Rosales J, Ayuso J. Stabilization of expansive soils with biomass bottom ashes for an eco-efficient construction. Environmental Science and Pollution Research. 2020; 28:24441-24454. https://doi.org/10.1007/s11356-020-08768-3

[8] Cabrera M, Rosales J, Ayuso J, Estaire J, Agrela F. Feasibility of using olive biomass bottom ash in the sub-bases of roads and rural paths. Construction Building Materials 2018;181:266–275. https://doi.org/10.1016/j.conbuildmat.2018.06.035

[9] ISO 17892-1. Geotechnical investigation and testing - Laboratory testing of soil - Part 1: Determination of water content; 2014.

[10] ISO 17892-2. Geotechnical investigation and testing - Laboratory testing of soil - Part 2: Determination of bulk density; 2014.

[11] ISO 17892-3. Geotechnical investigation and testing - Laboratory testing of soil - Part 3: Determination of particle density; 2015.

[12] ISO 17892-4. Geotechnical investigation and testing - Laboratory testing of soil - Part 4: Determination of particle size distribution; 2016.

[13] ISO 17892-12. Geotechnical investigation and testing - Laboratory testing of soil - Part 12: Determination of liquid and plastic limits; 2018.

[14] BS 1377-4. Methods of test for soils for civil engineering purposes - Part 4: Compaction-related tests; UK: British Standards Institution; 1990.

[15] Osinubi KJ, Eberemu AO. Hydraulic conductivity of compacted lateritic soil treated with bagasse ash. International Journal of Environmental Waste Management. 2013;11(1):38–58. https://doi.org/10.1504/IJEWM.2013.050522

[16] Daud NN, Muhammed AS, Kundiri AM. Hydraulic conductivity of compacted granite residual soil mixed with palm oil fuel ash in landfill application. Geotechnical and Geological Engineering. 2017;35(5):1967-1976. https://doi.org/10.1007/s10706-017-0220-1

[17] Bajwa TM, Fall M. Mechanical characteristics and behavior of compost-based landfill cover. Paper presented at: Proceedings of 2011 Pan-AM CGS Geotechnical Conference; 2011 Oct 2– 6; Toronto, Canada.

[18] Marchiori L, Alburquerque A. Critical review of industrial solid wastes as barrier material for impermeabilization of storage waste facilities. Paper presented at: Proceedings of 5^{th} Symposium on Urban Mining and Circular Economy – SUM2020; 2020 Nov 18-20; Sardinia, Italy.

[19] Kuokkanen T, Nurmesniemi H, Pöykiö R, Kujala K, Kaakine J, Kuokkanen M. Chemical and leaching properties of paper mill sludge. Chemical Speciation Bioavailability 2008;20(2):111-122. https://doi.org/10.3184/095422908X324480

[20] Slim GI, Morales M, Alrumaidhin L et al. Optimization of polymer-amended fly ash and paper pulp millings mixture for alternative landfill liner.Procedia engineering. International Conference on Sustainable Design, Engineering and Construction. 2016 May 18-20; Tempe, Arizona, USA ; 145:312-318. https://doi.org/10.1016/j.proeng.2016.04.079

KnE Materials Science

FibEnTech21
1st International FibEnTech Congress (FibEnTech21) New opportunities for fibrous materials in the ecological transition
Volume 2022

Knowledge E
enriching | engaging | empowering

Research article

Biopolymer Geogrids for Geotechnics

Gabriel Oliveira*, and Isabel Falorca

University of Beira Interior, Centre of Materials and Building Technologies (C•MADE-UBI), Faculty of Engineering, Calçada Fonte do Lameiro, 6200-358 Covilhã, Portuga

Abstract.

This study focused on the mechanical characterisation of 3D printed biopolymer geogrids for civil and geotechnical engineering applications. The polylactic acid specimens were designed based on first-order similitude conditions and were produced by fused deposition modelling techniques. An experimental programme was carried out to investigate the mechanical behaviour of 1:2 scale model geogrids undergoing tensile loading conditions, in order to explore their use in soil reinforcement and stabilisation of geomaterials. The secant stiffness at 2.0% of strain and the ultimate tensile strength were used for this purpose. The results showed an average tensile strength of 4.5 ± 0.5 kN/m, which is in good agreement with that of fossil oil-derived polymer prototypes, while presenting a significantly lower elongation at failure. The printing process appeared stable and replicable. The influence of degradation on the tensile properties of 3D printed polylactic acid geogrids over time still needs to be studied.

Keywords: geogrid, additive manufacturing, biopolymer, tensile strength, geotechnics

Corresponding Author: Gabriel Oliveira; email: gabriel.marchi.oliveira@ubi.pt

Dates

?????

Publishing services provided by Knowledge E

© Gabriel Oliveira, and Isabel Falorca. This article is distributed under the terms of the Creative Commons Attribution License, which permits unrestricted use and redistribution provided that the original author and source are credited.

Selection and Peer-review under the responsibility of the FibEnTech21 Conference Committee.

OPEN ACCESS

1. Introduction

A geogrid is a planar mesh structure that can be used to reinforce and stabilise soil [1] and has apertures into which soil particles can be locked, in order to make construction more efficient. Figure 1 illustrates the component elements of a geogrid, where ribs and junctions are the tensile load-bearing parts that interact with the environment in which they are inserted. According to [2] when the load-bearing parts have high tensile strength in only one direction, the geogrid is considered uniaxial and biaxial when it has high tensile strength in the two main directions. Triaxial geogrids exhibit high tensile strength in multi-directions of the geogrid plane. So, the most significant characteristics include the suitable aperture size to interact with the surrounding soil particles and the sufficient tensile strength in the short- and long-term. Over the last four decades, much geogrid types have been developed, using a variety of different technologies, considering environmental and economic factors. Geogrids can be manufactured by stitch bonding fabrics made of polymer filaments followed by coating, or by knitting, or

by welding oriented polymer strips. They can also be formed by extruding a polymer sheet material that is provided with a defined pattern of holes and then stretched in a controlled orientation [3]. Most geogrids are produced from fossil oil-derived polymers. To offset the negative impact of using synthetic materials, biopolymer geogrids are increasingly being explored for civil and geotechnical engineering applications. Among the natural-derived and renewable biopolymers, the polylactic acid (PLA) can ensure several advantages in terms of sustainability and eco-compatibility [4].

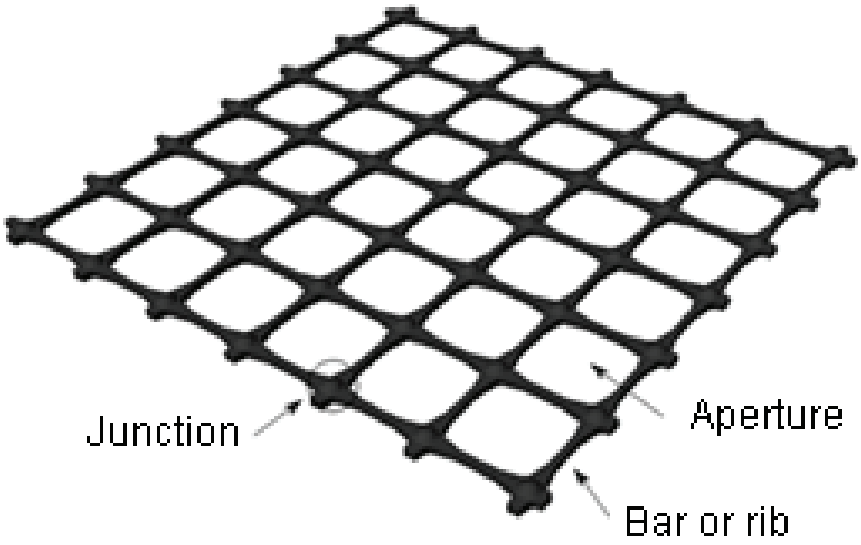

Figure 1: Extruded biaxial geogrid made up of ribs and junction knobs.

A common practice in geotechnical research studies is to use physical modelling techniques in order to infer the prototype behaviour. Therefore, the properties of geogrids (e.g., geometry and tensile strength) must be properly scaled [5] when preparing a small-scale version of geogrids. Recently, model geogrids were successfully produced by a 3D printing process [6]. The 3D printing is an additive manufacturing process to make objects from digital models through the successive layer-by-layer deposition of digital materials. Among several 3D printing methods, fused deposition modelling (FDM) is the most used. Typically, the polymer materials are melted and extruded in the form of filaments and then deposited over the bed where the parts are built, solidifying, and integrating with the surrounding filaments until the product is finished. There are many parameter settings that can be selected for the FDM process, which will affect the mechanical properties of the final product [7]. Hence, mechanical properties of the printed materials are important measures of product quality, thus relying strongly on experiments.

In this study, the procedure to prepare model geogrids with properly scaled tensile behaviour for small-scale laboratory tests are presented. Further, the 3D printed specimens made of PLA and the proposed testing programme are described. The main objective was to evaluate the tensile properties of model geogrids such as the secant stiffness and the ultimate tensile strength in order to explore its use in soil reinforcement and stabilisation of geomaterials.

2. Material and methods

Specimens were designed by scaling down the dimensions of commercially available biaxial geogrids, so that they could be used to investigate the mechanical behaviour of layered geomaterials in the follow-up experimental study [8]. The tensile strength of the model geogrid was $1/N^2$ times of that of the prototype (were N is the scale factor), assuming identical material characteristics and identical geogrid strains in model and prototype. Table 1 presents the geometric characteristics of the model geogrids that were derived using a scale factor of 2. Using PLA white filament, the biaxial geogrids were produced by a high precision open-source FDM printer (Fig.2). Table 2 shows the 3D printing parameters considered in this study. The printing plane was XY, and the layers were summed along the Z direction. Therefore, the printing was in X direction with a raster angle orientation sequence of $\pm 45^{o}$ in order to have a criss-cross sequence with rectilinear infill. The nominal specimen dimensions were 100 mm in width and 100 mm in length, considering the recommendations of NP EN ISO 10319 [9] for the preparation of test specimens. To ensure the repeatability of the results, two specimens were printed and one of them was cut into longitudinal rib pieces with 100 mm length.

Table 1: Summary of characteristics of model geogrids.

Parameter	Value
Grid opening size (mm)	17.9
Rib width (mm)	1.55
Rib thickness (mm)	1.20
Rib cross sectional area, (mm^2)	1.86
Percentage of open area (%)	80.2
Junction thickness (mm)	2.0

The uniaxial tensile tests were carried out at a controlled strain rate, in a universal testing machine at the Department of Textile Science and Technology of the University of Beira Interior as shown in Fig.3. Since a standardised tensile test method for FDM printed geogrids has not yet been developed, the procedure specified in NP EN ISO

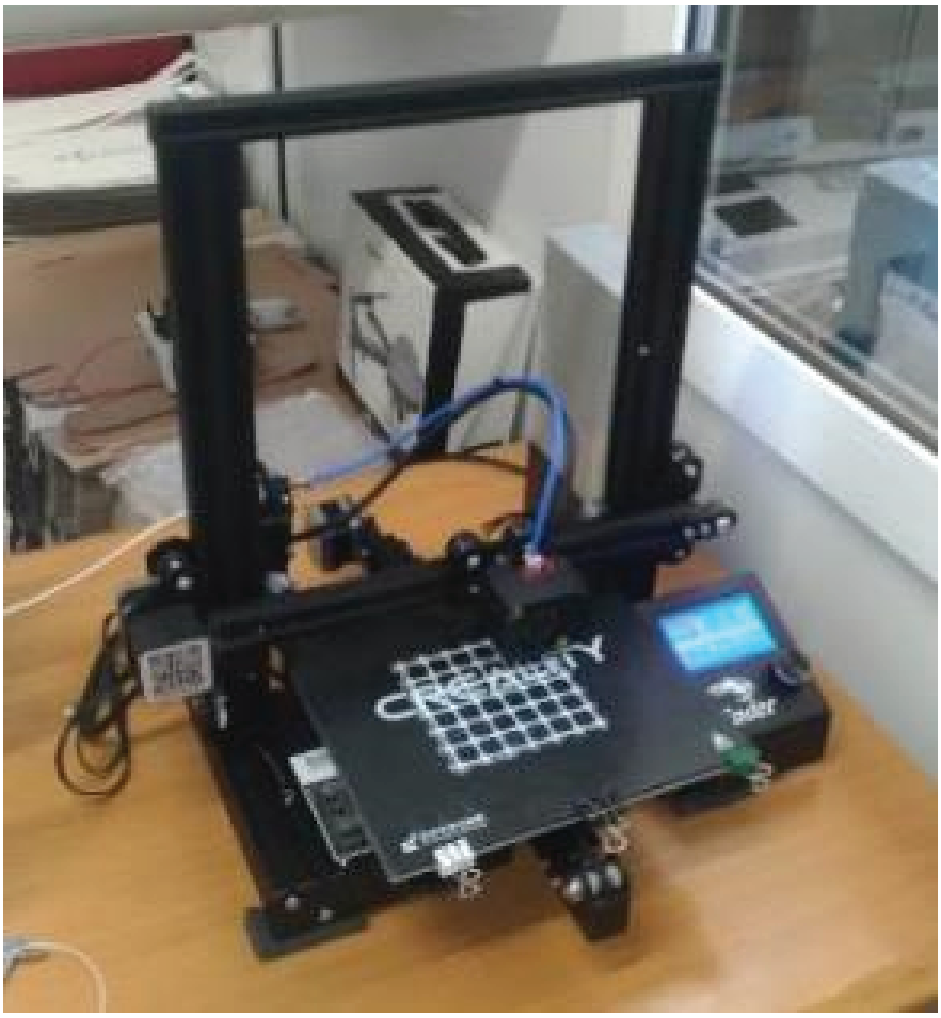

Figure 2: 3D printer used in this study.

Table 2: FDM process parameters during 3D printing of specimens.

Parameter	Value	Parameter	Value
Nozzle diameter (mm)	0.4	Printing speed (mm/s)	55
Extrusion temperature (°C)	220	Layer thickness (mm)	0.1
Infill density (%)	100	Raster width (mm)	0.5
Raster angle (°)	45	Fill pattern	rectilinear
Number of perimeters	1	Bed temperature (°C)	N/A

10319 [9] for geosynthetics testing was used, considering the details described below. The distance between the jaws at the start of the test was adjusted to give an effective length of 50 $\pm$ 1 mm and then both ends of the specimen were clamped in order to prevent both the specimen damage and the slippage during the progress of the test. The load cell was attached to the movable compressive block jaw in a rigid and perpendicular position, and its force range was selected such that the specimen failure

occurs between 30% and 90% of full-scale force. The specimens were stretched at a constant strain rate of 1.0 mm/min, at room temperature of 20 ˚C and 50% RH, until a sudden drop associated with the failure of the specimen was recorded. In this study, experiments were conducted on two test specimens, as summarised in Table 3.

Figure 3: Experimental setup during tensile testing of the model geogrid.

TABLE 3: Details of the tensile testing program.

Test specimen	Geogrid	Longitudinal geogrid rib
Test code	grid#18	rib#18
Number of tensile elements within the test specimen	5	1
Load cell capacity (N)	1000	200

The data obtained from the tests were analysed to calculate the tensile strength, strain at maximum load, and the secant stiffness of the test specimens. The tensile force was calculated directly from the recorded maximum load, and the secant stiffness at a specified strain was calculated by applying the Equation 1, where F is the load determined at the specified strain ε, $N_m$is the minimum number of tensile elements

within a one metre width of geogrid, and N_s is the number of tensile elements within the test specimen.

$$J_{sec} = \frac{F \times N_m}{\varepsilon \times N_s} (1)$$

3. Results and discussion

The test results were represented as tensile strength-strain relationships that showed the usual behaviour of polymer materials with brittle failure. Figure 4 shows the engineering tensile curves of the 3D printed PLA specimens. As can be observed, the behaviour is characterised by a noticeable elastic deformation stage, where the tensile strength is proportional to the strain up to a strain of about 2%. It was verified that engineering tensile curves were similar to each other, indicating that tensile properties would not be changed using different test specimens. Such results demonstrate the repeatability of the results. Grid specimens exhibited a very variable behaviour after the peak strength, due to the progressive failure of the longitudinal ribs.

The tensile properties that arise from the analysis of the results are summarised in Table 4. In terms of ultimate tensile strength, model geogrids were characterised by an average tensile strength of 4.5 ± 0.5 kN/m. Similar results were reported by [4].

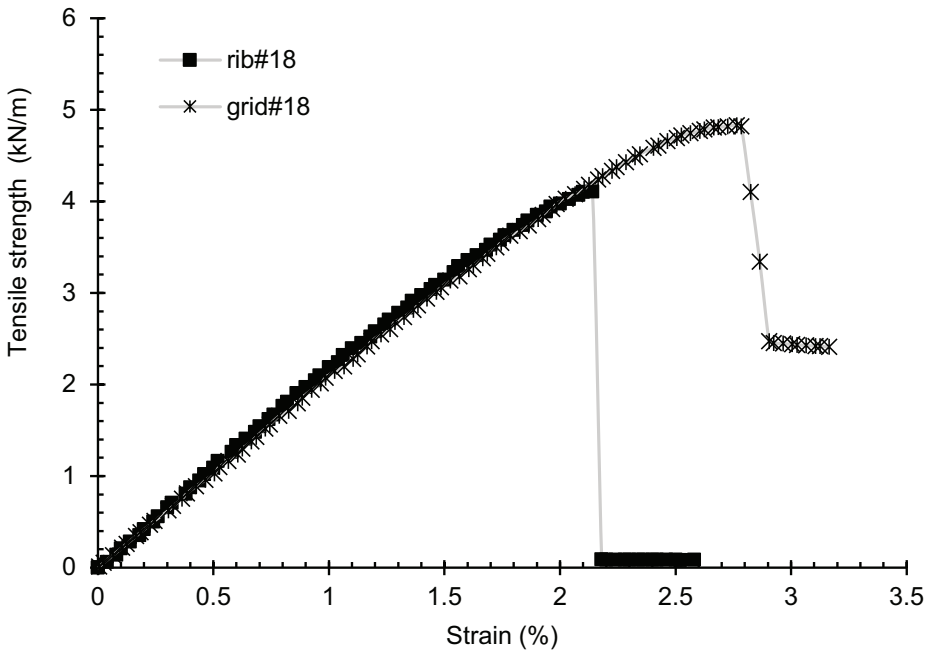

Figure 4: Tensile strength-strain curves of grid and rib PLA specimens.

Table 4: Mechanical properties of 3D printed PLA model geogrids.

Properties	grid#18	rib#18
Elongation at ultimate tensile strength (%)	2.8	2.1
Ultimate tensile strength (kN/m)	4.8	4.1
Secant stiffness at 2.0% strain (kN/m)	199.0	198.7

Table 5 presents the parameter values to be considered with the downscaling of the prototype geogrids with a scale factor of 2 (N = 2) under 1-g conditions for geogrids with 18 mm aperture size.

Table 5: Parameters of prototype geogrid with 36 mm aperture size at 1-g and N =2.

Parameters	PLA geogrid prototype
Elongation at ultimate tensile strength, ε_g (%)	2.8
Rib cross sectional area, A_r (mm^2)	2.88
Ultimate tensile strength, T_u (kN/m)	18
Elements to be tested, N_s	5
Elements to be tested in one meter of width, N_m	48
Secant stiffness at 2.0% of strain, J_{sec} (kN/m)	796
Percentage of open area, f (%)	78

The principles of physical modelling with model geogrids [5] to quantify the effect on the parameters in the prototype geogrids, identified that the elongation at ultimate tensile strength and percentage of open area is unchanged between the model geogrid and prototype geogrid. Furthermore, for 1-g conditions the rib cross sectional area of the geogrid prototype has a ratio of 1/N to the model geogrid and the secant stiffness at 2.0% of strain and ultimate tensile strength of the prototype geogrid has a ratio of $1/N^2$ to the model geogrid. The ultimate tensile strength and secant stiffness at 2.0% of strain of the prototype PLA geogrid showed in this study values within the range of values of commercial geogrids. However, the elongation at ultimate tensile strength (2.8%) is very low compared to commercial geogrids.

4. Conclusions

This study presented the design and tensile testing of 1:2 model geogrids made of PLA and produced by the FDM process. A practical method to derive the uniaxial tensile

properties of geogrids using longitudinal rib specimens was proposed, which proven to be an accurate technique to predict the secant stiffness. In general, the results encourage the development of 3D printed PLA geogrids for civil and geotechnical engineering applications, in line with the recent emphasis on the sustainable economy. The following findings were made:

1. After applying the modelling physic techniques the PLA prototype geogrid show relatively good results of tensile strength about 18 kN/m, which was found to be comparable to that of fossil oil-derived polymer strip and geogrid;
2. lower elongation at failure (about 2.8%) than that of fossil oil-derived polymer geogrid, which would not affect geogrid's performance in geomaterial stabilisation;
3. printing process appears stable and replicable, and the influence of degradation of material tensile properties over time still need to be studied.

Acknowledgements

The scholarship BID/UBI - Santander Universidades/2018 is acknowledged. The authors thank Fabric Laboratory at Department of Textile Science and Technology for the assistance during the tensile testing.

References

[1] NP EN ISO 10318-1:2016. Geossintéticos; Parte 1: Termos e definições (ISO 10318-1:2015). Instituto Português da Qualidade, 2016.

[2] Vertematti JC. Brazilian manual of geosynthetics. Brazilian Association of Nonwoven and Technical Fabrics Industries; São Paulo, Brazil,2004.

[3] Walsh AT. Multi-axial grid or mesh structures with high aspect ratio ribs. United States patent. US 11,149,386. 31th January, 2017. Available from: https://patft.uspto.gov/netahtml/PTO/

[4] Cislaghi A, Sala P, Borgonovo G, Gandolfi C, Bischetti GB. Towards more sustainable materials for geo-environmental engineering: The case of geogrids. Sustainability. 2021;13(5):2585. https://doi.org/10.3390/su13052585

[5] Viswanadham BVS, König D. Studies on scaling and instrumentation of a geogrid. Geotextiles and Geomembranes. 2004;22(5):307–328. https://doi.org/10.1016/s0266-1144(03)00045-1

[6] Stathas D, Wang JP, Ling HI. Model geogrids and 3D printing. Geotextiles and Geomembranes. 2017;45(6):688–696. https://doi.org/10.1016/j.geotexmem.2017.07

[7] Wang S, Ma Y, Deng Z, Zhang S, Cai J. Effects of fused deposition modeling process parameters on tensile, dynamic mechanical properties of 3D printed polylactic acid materials. Polymer Testing. 2020;86:106483. https://doi.org/10.1016/j.polymertesting.2020.106483

[8] Oliveira G, Falorca I. Stress-strain relationship in homogeneous and two-layered triaxial test specimens. KnE Engineering. 2020;5(5):88-99. https://doi.org/10.18502/keg.v5i5.6923

[9] NP EN ISO 10319:2016. Geossintéticos: Ensaios de tração em tiras largas (ISO 10319:2015). Instituto Português da Qualidade, 2016.

KnE Materials Science

FibEnTech21
1st International FibEnTech Congress (FibEnTech21) New opportunities for fibrous materials in the ecological transition
Volume 2022

Knowledge E
enriching | engaging | empowering

Research article

Evaluation of Entre-os-Rios Thermal Aquifer Vulnerability Using DRASTIC Index

Vanessa Gonçalves[1,2,3]*, António Albuquerque[1,2,3], and Victor Cavaleiro[1,3]

[1]Department of Civil Engineering and Architecture, University of Beira Interior, Calçada Fonte do Lameiro, 6201-001, Covilhã, Portugal.
[2]FibEnTech, University of Beira Interior, Calçada Fonte do Lameiro, 6201-001, Covilhã, Portugal.
[3]GeoBioTec, University of Beira Interior, Calçada Fonte do Lameiro, 6201-001, Covilhã, Portugal.

Abstract.
The "Entre-os-Rios" thermal aquifer has a protection perimeter buffer zone for avoiding water contamination. A vulnerability map was generated, using geographic information systems (GIS) tools and the DRASTIC index, to evaluate the risk of contamination of the perimeter area. The results showed that the protection perimeter buffer zone has an insignificant to moderate risk of pollution, with the DRASTIC index's values ranging from 47 to 127 points, and an average pollution vulnerability of 79 points. The alluvium-covered land is vulnerable to moderate contamination but is located far from the catchment point. Areas of minimal risk correspond to locations where the granitic massif has not been altered significantly.

Keywords: geographic information systems, vulnerability map, protection perimeter buffer zone, DRASTIC index

Corresponding Author: Vanessa Gonçalves; email: vanessa_alvane@hotmail.com

Dates
?????

Publishing services provided by Knowledge E

© Vanessa Gonçalves et al. This article is distributed under the terms of the Creative Commons Attribution License, which permits unrestricted use and redistribution provided that the original author and source are credited.

Selection and Peer-review under the responsibility of the FibEnTech21 Conference Committee.

OPEN ACCESS

1. Introduction

The abundance of natural mineral waters and spring waters in Portugal has a high ecological heritage value. The undeniable added value that they have allowed, since 1928, Portuguese legislation established protection perimeter buffer zone. The delimitation of these zones integrates a resource management tool, with a view to its quantitative, qualitative, and ecological preservation. The importance of the "Entre-os-Rios" thermal aquifer in the life and economy of this area goes back to the 1920s when the thermal complex was raised. The current agreement for the exploration of natural mineral water has been signed with the "Instituto Nacional para o Aproveitamento dos Tempos Livres dos Trabalhadores" (INATEL) in 1997 [1]. In 2003, the Decree order n.º 203/2003 has defined the protection perimeter buffer zone for the "Barbeitos" borehole (immediate, closed, and distant zone), based on parameters that support a sustainable exploration of the resource [2]. Given the significance of this Thermal Complex to the local and regional economies, is essential to implement protective and planning measures adapted to the reality under consideration. By establishing a protection perimeter buffer zone, the risk of groundwater contamination is reduced [3].

The need to protect groundwater involves considering an aquifer's vulnerability to pollution, which is determined by the continuous and diffuse pollutant loads that put pressure on its catchment area as well as its intrinsic characteristics [4]. Within this concept, there are two types of vulnerability concepts [5]: intrinsic vulnerability, which is determined by the aquifer's hydrogeological characteristics, and specific vulnerability, which includes a few outside variables in addition to the hydrogeological characteristics (e.g., land occupation, sort of contaminant). It is possible that aquifers with a high vulnerability, but a low pollution risk exist due to the absence of polluting loads, or that aquifers with a high pollution risk exist despite their low vulnerability [6].

The study of groundwater vulnerability allows the identification of areas with the highest potential for contamination, as well as the creation of the aquifer pollution vulnerability map [7]. Despite existing methodologies, there is no satisfactory way to represent aquifer vulnerability due to the difficulty in integrating all parameters that influence contaminant behavior [8]. The DRASTIC index is one of the most commonly used methodologies in this evaluation. Despite the varied amount of information available, its application is relatively simple, and it produces excellent results in areas with varying characteristics. The vulnerability of an aquifer with DRASTIC methodology is determined by seven parameters [4]: depth (D), recharge (R), material typology of the aquifer (A), soil type (S), topography (T), the impact of unsaturated/vadose zone (I) and hydraulic conductivity (C). Each parameter is subdivided into representative classes, which are assigned an index (i), ranging from 1 and 10 to order to correspond with the local hydrogeological characteristics (higher values correspond to greater vulnerability). The product of these values by a relative weight (p) of each parameter gives the value of the DRASTIC index (DI).

$$DI = DixDp + RixRp + AixAp + SixSp + TixTp + IixIp + CixCp \quad (1)$$

The use of Geographic Information Systems (GIS) has simplified the acquisition, processing, analysis, and manipulation of georeferenced data. GIS-based model development has become critical for studies of groundwater vulnerability and quality using hydrogeological parameters and anthropogenic activities [9]. The creation of thematic maps allows for better planning and management, both in terms of sustainable water use and the demarcation of places with the ability (or not) to implement various activities based on their potential impact on aquifers [10]. Map algebra operations enable mathematical operations to be performed between several thematic charts, resulting in composite charts, typically of vulnerability or susceptibility of a spatial nature.

Therefore, the main objective of this work was to create a vulnerability map for the "Entre-os-Rios" thermal aquifer using GIS interpolation tools based on the DRASTIC index.

2. Material and methods

The thermal aquifer is located in "Eja (Penafiel)" and the main point of the study was the "Barbeitos" borehole, which is located in the "Maciço Antigo", in the Douro River Basin, where rivers converge (Figure 1-a) and 1-b)). The mineral water exploration exploitation concession has the registration number HM-23 and the name is named as "Entre-os-Rios (Quinta da Torre)", with a surface area of 96.6 ha, coincident with the closed protection zone area of the protection perimeter buffer zone. The extended protection zone covers an area of 241.8 ha (Figure 1-c). The area is characterized by steep slope variations, which are primarily due to the presence of Ordovician quartzite rocks, which gave rise to ridges-oriented NW-SE due to differential erosion. On a local scale, the massif is dominated by discontinuities, which are typically sub-vertical N-S to NNE-SSW but, can also be horizontal to sub-horizontal. The most prevalent lithology is granite however, granites come in a wide range of textures and granularities. The springs appear to occur at the interface of the two types of granite and always in areas of great separation, primarily in the N20°E direction [11]. It appears that are the microgranite veins, installed throughout the area within the granitic masses that influence the emergence of water locally (at least in the "Torre" and "Termas de S. Vicente"). Except in the weathered superficial zones of the eruptive rocks and in the existing colluvium-alluvial patches, formations with secondary permeability due to granite fissures, predominate in the study area [12].

The waters of the thermal springs in "Entre-os-Rios" are cold, have deep circulation, and have a unique chemistry. The interaction with the massif granite rich in silica results in a pH of approximately 8.8. It is weakly mineralized water, sulphurous, fluoridated, with alkaline and soft reaction [13]. The water from the "Barbeitos" borehole has a low temporal fluctuation of its characteristics, allowing continuous monitoring to infer when contamination emerges in the aquifer. The "Entre-os-Rios" hydromineral system distinguishes the following aquifer systems [11]: at the surface, a highly altered and decomposed free aquifer that represents a critical role in the recharge of the underlying aquifers. A free to semi-confined aquifer with normal water circulation in altered zones and in most granite fissure zones (the pH is between 4.1 and 6; the electrical conductivity is less than 150 S/cm; flow rates are typically less than 0.2 L/s). A confined mineral

aquifer, located in depth near the catchment and conditioned by a zone of structural weakness in depth. The ”Barbeitos” borehole, located in the granitic rock near contact with granodiorites at a maximum depth of 114 m, has an exploration flow of about 2.5 L/s, a pH of 8.4 to 8.9, and electrical conductivity of 550 to 620 S/cm. **a)**

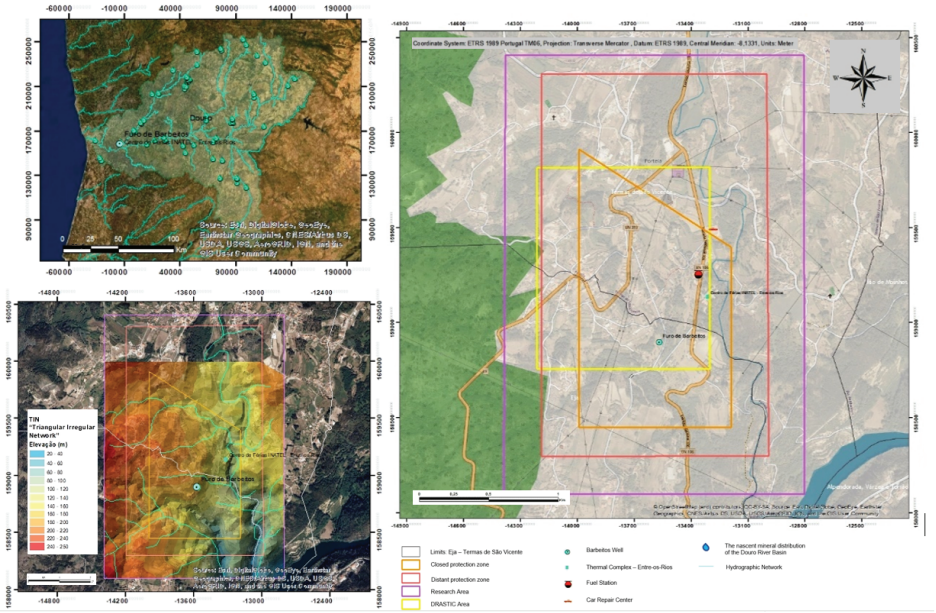

Figure 1: a) Location map of the “Barbeitos” borehole and mineral springs waters in the Douro River Basin [14]; b) Digital Elevation Model (DEM) of the study area surrounding the “Barbeitos” borehole [14]; c) Map of the geographical location of the “Barbeitos” borehole and the protection buffer zones and their conditions [14].

For attribute processing and vulnerability mapping, it was used ArcGIS 10.8 software from ESRI´s, which was based on the ”PT-TM06/ETRS89”. For the construction of the seven thematic maps, a variety of data was collected and processed using ArcGIS tools. The parameter D was calculated using piezometric measurements from a set of 36 georeferenced water points taken in 2008 [11,15]. To interpolate the depth of the aquifer’s top, was applied the Inverse Distance Weighted (IDW) method resulted in mean values of less than 4 m, corresponding to an index of 9. The areas of greater susceptibility correspond to zones with shallower aquifer tops, indicating that it is a very sensitive attribute. The DEM was created using the “Carta Militar de Portugal”, scale 1:25000, N.º 135 of the “Centro de Informação Geoespacial do Exército” (CIGeoE), as shown in Figure 1-b). The Triangulated Irregular Network (TIN) interpolation model was used, which was converted into a matrix structure, allowing create the slope chart, flow direction, and curvature profile. The curvature profile shows the maximum slope direction and has an impact on flow acceleration and deceleration, as well as soil erosion and sediment deposition. The union of slope areas less than or equal to 6%, curvature profiles less

than or equal to 0, and areas that allow infiltration forms the map of infiltration potential zones. A recharge of 40 mm/year [11] was assumed using the precipitation values [11], resulting in an index value of 1. The values for quantifying the partial index A, I, and C were collected from the National Laboratory of Energy and Geology (LNEG) from the Geological Map of Portugal [16]. Parameters A and I assumed the prevalence of indexes 2 and 3, which are features of magmatic rocks in the research area. The attribution of greater susceptibility to microgranite outcrops, on the other hand, is cautious, because fissural percolation can endanger the aquifer. The partial index S was calculated using the Land Use and Occupation Map of Portugal (Cos2018) [17], from the Directorate General for Territory (DGT). Forest soil, as well as temporary crops and bushes, are more likely to be affected by pollution. The partial index T was obtained by considering the DEM and slopes map. The Slopes chart (%) confirmed that the study site ranges in altitude between 20 m and 250 m, with significant slope variations. In low-density areas, where pollutant infiltration is promoted, the vulnerability index is higher. The index C was created using an abacus that relates representative values of hydraulic conductivity for various types of rock [15,18], as well as values of effective porosity and porosity for certain types of rocks [19].

3. Results and discussion

Except in the weathered superficial areas of the eruptive rocks and in the current colluvium-alluvial patches, formations with secondary permeability due to cracking prevail in the study area. Underground water is circulated through fractures, and the greater the degree of fracture and the smaller the filling, especially with clay elements, the more interesting it is. The alteration can reach considerable thicknesses of several tens of meters in the most heavily weathered locations [11]. The vulnerability map for “Barbeitos” borehole (Figure 2-c) was generated by calculating the DRASTIC index (Eq. (1)), for each 5x5 m square, using the data of Table 1.

The cartography of intrinsic vulnerability in the study area was obtained as a result of the weighted sum, according to the DRASTIC methodology, of the various maps relating to each of the attributes. The risk of pollution includes the vulnerability and presence of pollution sources, and the environmental framework is reasonable in the study site where the catchment is located. The DRASTIC index’s values ranged from 47 to 127 points, ranging from insignificant to moderate, with an average pollution vulnerability of 79 points for ”normal” pollutants. The alluvium-covered land is vulnerable to moderate contamination, however, it is located far from the catchment. Because of

Table 1: Values and weights used for calculating the DRASTIC index [4, 14].

Paramete	Characteristics	(i)	(p)	Range
D	3,9 m (average)	5 - 10	5	25 - 50
R	Deep recharge	0 - 1	4	0 - 4
A	Permeability	2 - 7	3	6 - 21
S	Change areas (< 2m)	1 - 6	2	2 - 12
T	Slopes map	1 - 10	1	1 - 10
I	Unsaturated zone lithology	2 - 6	5	10 - 30
C	Capacity to transmit water	1 - 2	3	3 - 6
Drastic Index (DI)				47 - 127

the conditions to which they are subject, the areas occupied by microgranites and where meteoric water infiltrates along with preferential recharge sectors hydraulically linked to deep fracturing represent a moderate vulnerability. Areas of minimal risk, on the other hand, could correspond to locations where the granitic massif has not been altered significantly.

The study location is situated in a sloping terrain (Figure 2-a) bounded by granitic outcrops, indicating a low vulnerability to contamination. However, as previously stated, fracturing can transport pollutants to great depths and/or distances (Figure 2-b).

The mineral water is of meteoric origin, with a long time of permanence in the deep system, classifying these waters among the slowest in the set of sulfuric waters in the country [19]. The pH value is around 8.8 being of basic character, resulting from the interaction with the granitic massif rich in silica. The temperature has an average value of 20.5 ºC, which belongs to the class of hypothermal waters. According to [13,20] and to the traditional classification of the Lisbon Hydrology Institute, the water from the “Barbeitos” borehole is weakly mineralized, sulphureous, fluoridated water, with alkaline and soft reaction.

The use of several approaches to defining protection perimeters buffer zones allows for the long-term preservation of the quality of the hydromineral resource. For the immediate zone, a radius of 50 m is proposed, with the center of the circle representing the mineral water catchment. This is justified by the fact that it is an aquifer system whose lithological support is made up of igneous formations that range in the alteration from highly altered to little altered [21]. It has a total area of 0.785 ha and must be completely closed to any intrusion and always kept clean. The closed zone is defined by geological-structural, hydrogeological, and pollution vulnerability parameters. It coincides with the concession area, occupying an area of 96.6 ha. Its purpose is to protect the use of direct

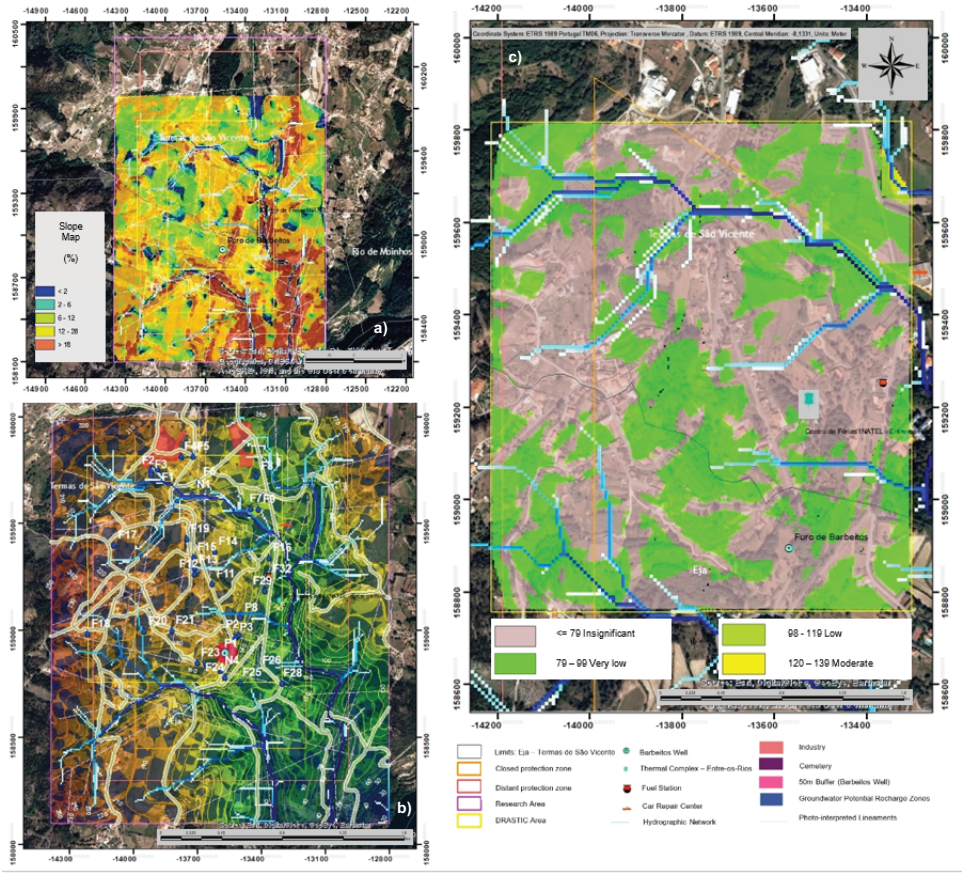

Figure 2: a) Slope map of the area around the “Barbeitos” borehole [14]; b) Map of areas with higher susceptibility to pollution around the “Barbeitos” borehole [14]; c) Map of the “Entre-os-Rios” Aquifer’s Pollution Vulnerability within DRASTIC methodology [14].

interference on the local emergency mechanism, particularly N-oriented fracturing and potentially ENE and NNE fracturing. The limits of the distant zone, which covers 241.8 ha, were established to include preferred recharge sectors that are hydraulically related to deep fracture. The favorable circulation of the aqueous system under study is related to the fracture N-S and NE-SW. The purpose of this area is to prevent contamination zones from developing, preventing further surface runoff and subsurface pollution.

4. Conclusion

This work allowed the determination of the intrinsic vulnerability of groundwater in the surroundings of the “Barbeitos” borehole through the calculation of a pollution vulnerability map, by applying the DRASTIC index. The vulnerability map shows that the protection perimeter buffer zone has a low vulnerability to pollution, which is partly related to the geological characteristics of the region, which tend to prevent polluting compounds from infiltrating. Although the areas are oversized, it is important

to consider the heterogeneity of the underground environment in the study area, the possibility of preferential flow through fractures to areas surrounding the catchment, and the uncertainty associated with method application due to the indeterminacy of some hydraulic parameters.

Acknowledgments

The authors are grateful to the Foundation for Science and Technology (FCT, Portugal) for financial support by national funds through the projects UIDB/00195/2020 (FibEnTech) and UIDB/04035/2020 (GeoBioTec).

References

[1] Ferreira MRN. Evolução hidrogeoquímica das águas sulfúreas de Entre-os-Rios: Avaliação preliminar [Tese de Mestrado]. Instituto Superior de Engenharia do Porto; Porto, 2013.

[2] Diário da República. Portaria n.º 203/2003 de 7 de março do diário da República n.º 56/2003, Série I-B. Fixa o perímetro de protecção da água mineral natural a que corresponde o número HM-23 de cadastro e a denominação de Entre-os-Rios (Quinta da Torre).

[3] Lopo de Mendonça J, Cabral, J. Identificação de falhas na Bacia Cenozóica do Tejo através de técnicas de investigação hidrogeológica. Comunicação Instituto Geológico e Mineiro. 2003; 90:91-102.

[4] Aller L, Bennet T, Lehr J, Petty R. DRASTIC: A standardized system for evaluating groundwater pollution potential using hydrogeologic settings. US EPA US EPA Report, 600/2–87/035, Robert S. Kerr Environmental Research Laboratory, Ada, OK, 1987.

[5] Gómez M. Caracterização da vulnerabilidade dos aquíferos à contaminação dos aquíferos. Aplicação dos índices DRASTIC e GOD. Madrid: Centro de Estudos e Experimentação de Obras Públicas; 1998.

[6] Lobo-Ferreira JPC. Vulnerabilidade à poluição de águas subterrâneas: Fundamentos e conceitos para uma melhor gestão e protecção dos aquíferos de Portugal. 4.º Lisboa: Congresso da Água; 1998.

[7] Al-Zabet T. Evaluation of aquifer vulnerability to contamination potential using the DRASTIC method. Environmental Geology, 2002;43:203-208.

[8] Paralta EA, Francés AP, Ribeiro LF. Avaliação da vulnerabilidade do sistema aquífero dos Grabos de Beja e análise crítica das redes de monitorização no contexto da directiva da água. Paper presented at: VII Simpósio de Hidráulica e Recursos Hídricos dos Países de Língua Oficial Portuguesa - SILUSBA; 2005; Évora, 30 de Maio a 2 de Junho de 2005.

[9] Mejuto MF, Castaño S, Vela A. Utilidad de las ténicas de observación de la tierra a lá elaboración de mapas de vulnerabilidad y riesgo de contaminación de aguas subtrerráneas. Paper presented at: VIII Congresso Nacional de Teledetección; 22-24 Setiembre 1999; Albacete, Espanha.

[10] Xavier J, Gagliardi S, Vidal H, Montano M, Lucena L. Evaluación de la vulnerabilidad a la contaminación del acuífero Mercedes en el área metropolitana de la Ciudad de Paysandú – Comparación de los Métodos GOD y DRASTIC. Revista Latino-Americana de Hidrogeologia. 2004; 4:35-45.

[11] Teixeira J. Hidrogeomorfologia e sustentabilidade de recursos hídricos subterrâneos [Tese de Doutoramento]. Universidade de Aveiro e Universidade do Porto; Aveiro e Porto, 2011.

[12] Carvalho PEM, Cavaleiro VMP. Área de protecção do recurso hidromineral das termas de entre-os-rios. Paper presented at: 1st Joint World Congresso on Groundwater; 31-07 to 04-08, 2000. Fortaleza, Ceará, Brasil.

[13] Laboratório de Análises do Instituto Superior Técnico. Relatório de análise físico-química completa – Fundação inatel, furo dos barbeitos, situado em quinta da torre, entre-os-rios. Instituto Superior Técnico de Lisboa, Lisboa; 2018.

[14] Gonçalves V. Elaboração de perímetros de proteção de captações de águas subterrâneas com recurso a SIG [MSc thesis]. Covilhã: Universidade da Beira Interior ; 2020.

[15] Laboratório nacional de Engenharia Civil. Análise e parecer sobre a situação originada pelo derrame de hidrocarbonetos em Entre□os□Rios. Lisboa: Laboratório Nacional de Engenharia Civil; 2008.

[16] Laboratório Nacional de Energia e Geologia. Carta Geológica de Portugal, escala 1:500.000. Serviços Geológicos de Portugal, Amadora, 1992. Available from: https://sig.lneg.pt/server/services/CGP500k/MapServer/WMSServer

[17] Direcção Geral do Território. Carta de Uso e Ocupação do Solo para 2018. Lisboa, 2019. Available from: http://mapas.dgterritorio.pt/wms-inspire/cos2018v1?service=WMS&REQUEST=GetCapabilities&VERSION=1.3.0

[18] Singhal BBS, Gupta RP. Applied hydrogeology of fractured rocks. 2nd ed. Dordrecht: Springer; 2010.

[19] Lencastre A, Franco FM. Lições de hidrologia. 2nd ed. Universidade Nova de Lisboa; Lisboa, 1992.

[20] Calado C. A ocorrência de água sulfúrea alcalina no Maciço Hespérico: Quadro hidrogeológico e quimiogénese [PhD thesis]. Lisbon: Universidade de Lisboa; 2001.

[21] Diário da República. Decreto-Lei n.º 382/99 de 22 de Setembro do diário da República n.º 222, I série. Delimitação de perímetros de protecção de captações de águas subterrâneas destinadas ao abastecimento público; 1999.

KnE Materials Science

FibEnTech21
1st International FibEnTech Congress (FibEnTech21) New opportunities for fibrous materials in the ecological transition
Volume 2022

Knowledge E
enriching | engaging | empowering

Research article

Dynamic Penetration Profile of Starch Betainate, Pluronics and PCC Coated Papers

Mohit Sharma[1]*, Roberto Aguado[2], Artur J. M. Valente[2], Dina Murtinho[2], and Paulo J. T. Ferreira[1]

[1]University of Coimbra, CIEPQPF, Department of Chemical Engineering, Rua Sílvio Lima, Pólo II – Pinhal de Marrocos, 3030-790 Coimbra, Portugal
[2]University of Coimbra, CQC, Department of Chemistry, Rua Larga, PT - 3004-535 Coimbra, Portugal

Abstract.
Despite changes in optical and printing properties, the applied coating components on the paper surface have a significant impact on the surface chemistry of office paper. Depending on the use, such as ink penetration for printing and writing papers, an optimal hydrophobic and hydrophilic balance may be beneficial. In this study, several coating components including starch betainate, Pluronics, and precipitated calcium carbonate were employed to coat base paper (paper without any surface treatment). The influence of these components on water penetration was investigated using dynamic penetration profiles. When compared to native starch coated papers, paper coated with starch betainate (a cationic starch ester) had reduced hydrophobicity and increased water penetration. Moreover, this effect was further enhanced with the use of Pluronics. Likewise, hydrophobicity decreased as the concentration of starch betainate, precipitated calcium carbonate and Pluronics increased. Furthermore, water penetrated even more quickly when the combination of these components compared with the individual component coatings.

Keywords: hydrophobicity, PCC, Pluronics, starch betainate, water penetration

Corresponding Author: Mohit Sharma; email: mohit@eq.uc.pt

Dates
?????

Publishing services provided by Knowledge E

© Mohit Sharma et al. This article is distributed under the terms of the Creative Commons Attribution License, which permits unrestricted use and redistribution provided that the original author and source are credited.

Selection and Peer-review under the responsibility of the FibEnTech21 Conference Committee.

OPEN ACCESS

1. Introduction

Papers are generally coated with starch to, among other purposes, enhance the surface hydrophobicity, and thus to exhibit controlled water absorption in high moisture environment. Nevertheless, certain paper properties, such as the printing quality, often demand a quick penetration of carrier solvents for water-based inks [1]. Some other factors such as sufficient positive charge on the surface and a more closed surface can also help to improve the printing quality by retaining the ink pigments on the paper surface [2–4] . In this sense, starch betainate (a cationic starch ester), Pluronics (triblock co-polymers) and precipitated calcium carbonate (PCC) were identified as good coating components to produce papers with superior printing quality [5,6] .

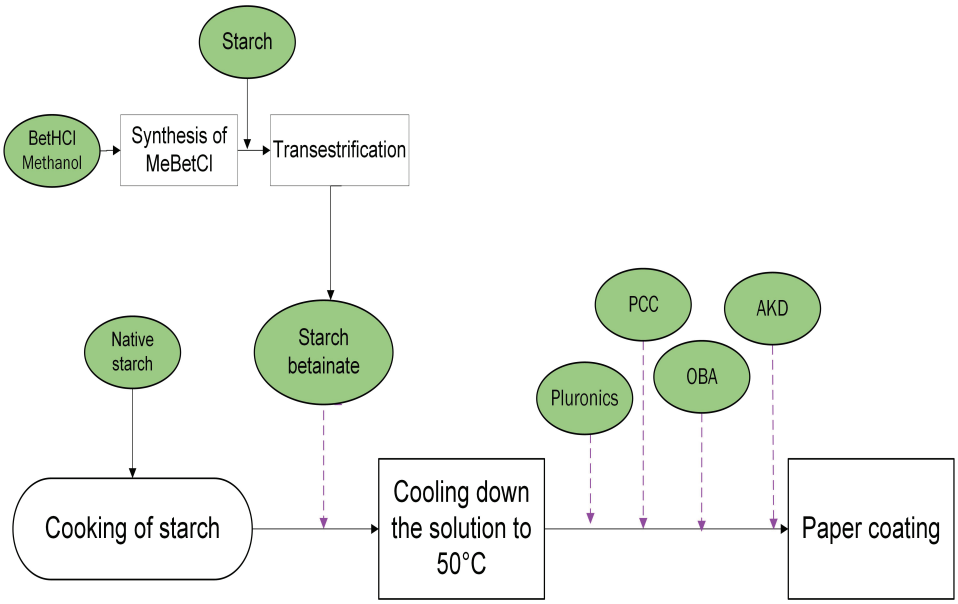

Figure 1: Outline of the experimental methodology.

In this study, paper sheets were coated with different concentrations of coating components, namely starch betainate, Pluronics and PCC. The effect of these components on the surface hydrophobicity and water absorption of coated papers were measured by water penetration profiles.

2. Methods

An industrial calendered uncoated paper (base paper, BP), produced from bleached eucalyptus kraft pulp with a basis weight of ~ 78 g m^{-2}, was used as substrate for performing surface coating. A laboratory coater from Mathis AG was used to coat the base papers. An applicator roll (coupled with the coater) was used to achieve 1.5 to 3 g m^{-2} per side, on the basis of dry coating weight (ISO standard 536:1995). Predrying was performed using a pre-installed infrared system. Besides native starch (NS, used as reference), base papers were coated with starch betainate (SB), Pluronics with different degrees of hydrophilicity (P123, F127), PCC, and combinations thereof. The concentrations of coating components are shown in Table 1 and Table 2. Starch was used as host component for all coatings and a schematic representation of experimental procedure is shown in Fig. 1.

A Surface & Sizing Tester from Emtec was used to obtain the water penetration profile. This device detects the ultrasound absorption or scattering from the air-water interfaces of small bubbles, since air flows out from the pores of the sheet as water penetrates through it. The dynamic water contact angle (DWCA) was measured over periods of

up to 60 s on an OCA 20 goniometer (Dataphysics, Germany) using the sessile drop method. A droplet of deionized water (10 µL) was automatically poured onto the coated paper surface.

Table 1: Composition of formulations for starch betainate (SB), Pluronics and PCC coatings expressed as %w/w, on the basis of dry coating weight.

Ingredients	Coating formulations				
	SB coatings	P123 coatings	F127 coatings	PCC coatings	Ref. coatings
Starch betainate	8 / 16 / 24	–	–	–	–
Pluronics P123	–	8 / 16 / 24	–	–	–
Pluronics F127	–	–	8 / 16 / 24	–	–
PCC	–	–	–	8 / 16 / 24	–
Native starch	85.6 / 77.6 / 61.6				93.6
OBA / AKD	6 / 0.4				

Table 2: Composition of formulations containing starch betainate (SB), Pluronics and PCC in combination expressed as %w/w, on the basis of dry coating weight.

Ingredients	Coating formulations		
	SB and Pluronics-P123 coatings	SB, Pluronics-F127 and PCC coatings	Ref. coatings
Starch betainate	16	16	–
Pluronics P123	8 / 16 / 24	8 / 16 / 24	–
PCC	–	16	–
Native starch	69.6 / 61.6 / 53.6	53.6 / 45.6 / 37.6	93.6
OBA / AKD	6 / 0.4		

3. Results

It was found that the native starch coating showed the lowest water absorption (highest sizing degree) compared to any other coatings which further increases with the use of PCC, starch betainate (SB), Pluronics (F127 and P123) and the combination thereof. Papers coated using the combination of SB, Pluronics and PCC showed high absorption of water (lowest sizing degree).

Water penetration can also be inversely correlated to the t_{95}, time at which ultrasonic intensity decreases to 95% of the maximum value. This time was higher for native starch-coated paper (0.29 s) than for BP (0.14 s). With the use of 8% (t_{95} = 0.17 s), 16% (t_{95} = 0.21 s) and 24% (t_{95} = 0.24 s) of SB, a negative influence of concentration was observed on the water penetration (Fig. 2A). A similar effect of concentration was also observed when varied concentrations of PCC were used on paper surface (t_{95} = 0.15, 0.15 and 0.19

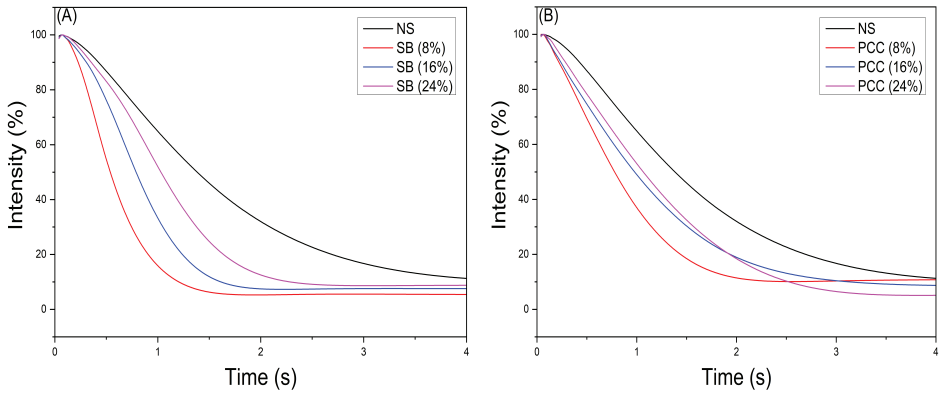

Figure 2: Dynamics of water penetration through paper sheets coated with NS, SB (A) and PCC (B).

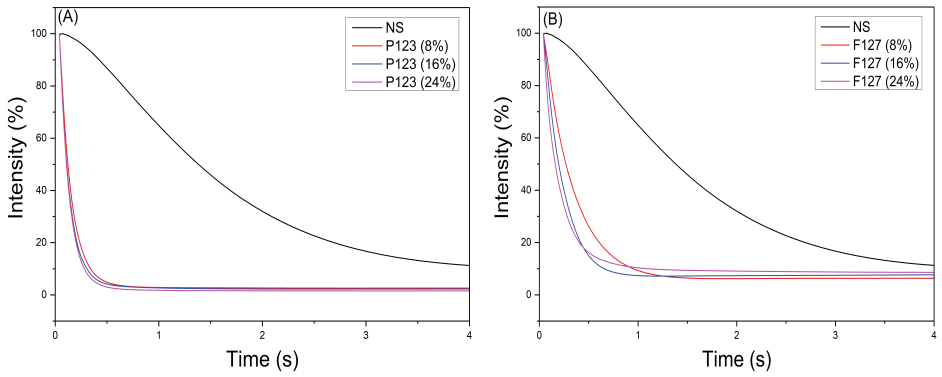

Figure 3: Dynamics of water penetration through paper sheets coated with NS, Pluronics-P127 (A) and Pluronics-F127 (B).

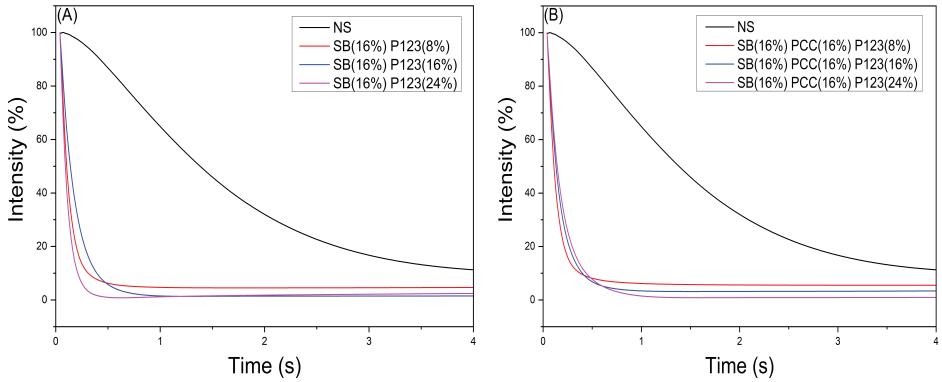

Figure 4: Dynamics of water penetration through paper sheets coated with NS, SB and Pluronics-P123 (A); and NS, SB, Pluronics-P123 and PCC (B).

s for 8, 16, 24 % of PCC in the formulations, respectively) (Fig. 2B). Further, t_{95} was not measurable due to quick absorption for P123 coated papers and it was 0.06 and 0.05 for 8 and 16% of F127, respectively, whereas 24% of F127 showed a quick absorption of water. Also, coating formulation containing combination of SB, P123 and PCC showed non-measurable t_{95} due to quick absorption of water in PDA (Fig. 3A, 3B, 4A and 4B).

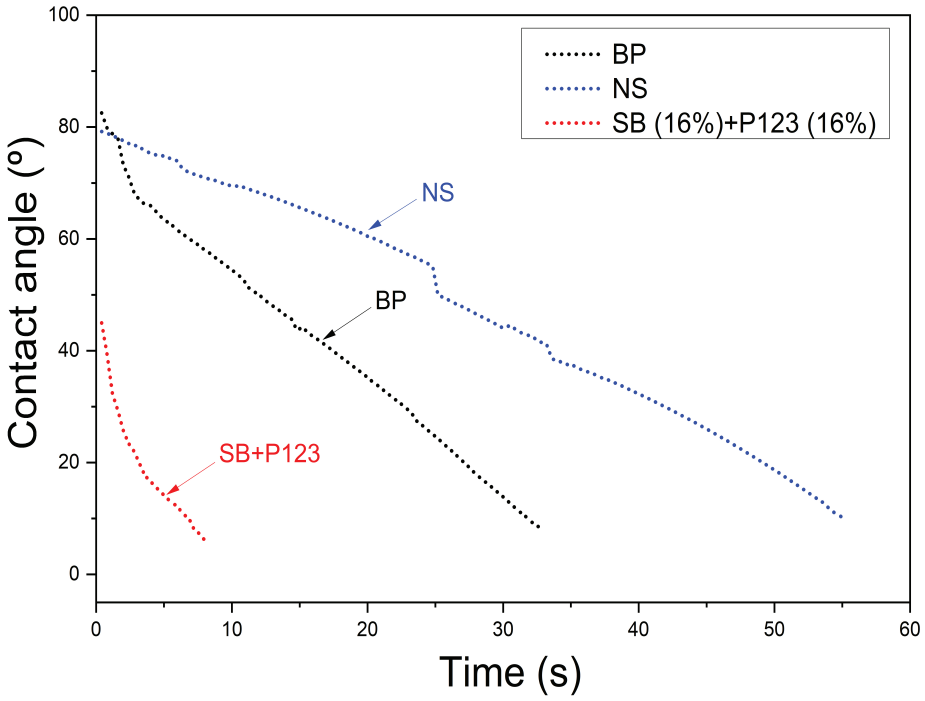

Figure 5: Effect of SB-Pluronics (P123) coating on hydrophobicity of coated paper surface.

As also evidenced by the contact angle, surface of starch coated papers (NS) showed higher time to absorb a water drop, whereas SB (16%) enhanced the static water contact angle (SWCA) from 72 ± 1 (°) (for NS coating) to 77 ± 1 (°). Similar trend was also observed with PCC, increasing SWCA to 83 ± 1 (°). However, Pluronics (P123 and F127) showed remarkably lower SWCA—43 to 63 (°)—compared to NS or SB coated paper. Also, surface of SB and P123 coated papers were also highly hydrophilic with SWCA values of 48 ± 2 for 16% of each component (Fig. 5).

Addition of SB in the coating formulation decreased the presence of hydroxyl groups on the surface of coated papers, thus increased the hydrophobicity of the coated paper surface. The amphiphilic nature of Pluronics, nonionic triblock copolymers of polyethylene oxide (PEO) and polypropylene (PPO), facilitates the absorption of these components on the cellulosic surfaces, additionally, Pluronics forms inclusive complexes with the starches, leading to form self-supporting supramolecular assemblies in formulations, thus enhanced the dispersion of other coating components [7–9]**.** Apart from this, Pluronics also increased the hydrophilicity of the coated surface, as long as their concentration in the coating formulations was higher than the critical micelle concentration.

4. Conclusions.

The delay in water absorption was correlated with the surface hydrophobicity for coated papers. Native starch coated papers take around 60 s to absorb a single drop of water whereas for papers coated with starch betainate, Pluronics and PCC this time was reduced for 5-10 s (Fig. 5). A similar trend of water penetration was observed with a high amount of water in the dynamic penetration analyzer. Coatings with these components can be useful for applications where a proper hydrophilic/hydrophobic balance is desirable, along with good water penetration properties, in order to achieve better printing quality properties.

5. Acknowledgement

This work was carried out under the Project inpactus -innovative products and technologies from eucalyptus, Project N.º 21874 funded by Portugal 2020 through European Regional Development Fund (ERDF) in the frame of COMPETE 2020 nº246/AXIS II/2017. Authors would like to thank the Coimbra Chemical Centre, which is supported by the Fundação para a Ciência e a Tecnologia (FCT), through the projects UID/QUI/00313/2020 and COMPETE. Authors would also like to thank the CIEPQPF - Strategic Research Centre Project UIDB/00102/2020, funded by the Fundação para a Ciência e Tecnologia (FCT). M.S. acknowledges the PhD grant BDE 03|POCI-01-0247-FEDER-021874. R.A. acknowledges the post-doc grant BPD 02|POCI-01-0247-FEDER-021874.

References

[1] Sharma M, Aguado R, Murtinho D, Valente AJM, De Sousa APM, Ferreira PJT. A review on cationic starch and nanocellulose as paper coating components, International Journal of Biological Macromolecules 2020;162:578–598. https://doi.org/10.1016/j.ijbiomac.2020.06.131

[2] Lee HL, Shin JY, Koh C-H, Ryu H, Lee D-J, Sohn C. Surface sizing with cationic starch: Its effect on paper quality and the papermaking process. Tappi Journal 2002;1:34–40.

[3] Lamminmäki TT, Kettle JP, Gane PAC. Absorption and adsorption of dye-based inkjet inks by coating layer components and the implications for print quality. Colloids Surfaces A: Physicochemical. Engineering Aspects 2011;380:79–88.

[4] Gigac J, Stankovská M, Opálená E, Pažitný A. The effect of pigments and binders on inkjet print quality. Wood Research 2016;61:215–226.

[5] Sharma M, Aguado R, Murtinho D, Valente AJM, Ferreira PJT. Novel approach on the synthesis of starch betainate by transestrification, International Journal of Biological Macromolecules 2021;182:1681–1689. https://doi.org/10.1016/j.ijbiomac.2021.05.175

[6] Sharma M, Aguado R, Murtinho D, Valente AJM, Ferreira PJT. Synergetic effect of cationic starch (ether/ester) and Pluronics for improving inkjet printing quality of office papers. Cellulose. 2021;28:10609–10624. https://doi.org/10.1007/s10570-021-04206-w

[7] Liu X, Wu D, Turgman-Cohen S, Genzer J, Theyson TW, Rojas OJ. Adsorption of a nonionic symmetric triblock copolymer on surfaces with different hydrophobicity. Langmuir 2010; 26(12):9565-74. https://doi.org/10.1021/la100156a

[8] Petkova-Olsson Y, Ullsten H, Järnström L. Thermosensitive silica-Pluronic-starch model coating dispersion-part I: The effect of Pluronic block copolymer adsorption on the colloidal stability and rheology. Colloids Surfaces A: Physicochemical Engineering Aspects 2016;506:245–253. https://doi.org/10.1016/j.colsurfa.2016.06.032

[9] Petkova-Olsson Y, Altun S, Ullsten H, Järnström L. Temperature effect on the complex formation between Pluronic F127 and starch. Carbohydrate Polymer 2017;166:264–270.